INVESTIGATION OF THE ROLE OF ETHER GROUPS DURING COAL LIQUEFACTION

J. Youtcheff* and P. H. Given

Department of Material Science and Engineering
The Pennsylvania State University, University Park, PA 16802

A considerable effort has been made in recent years to further the understanding of the structure of coal and to achieve a fundamental understanding of the mechanism of coal liquefaction. Many models have been put forth to explain or correlate data obtained from liquefaction experiments. In most of these studies, species are lumped or grouped by similarity in for example distillation properties (1) or solubility characteristics (2). However, the mechanism of coal liquefaction depends not only on operating parameters such as nature of the donor solvent, temperature and pressure but also on the characteristics and rank of the feed coal. Consequently, kinetic models based on the above lumped parameters may not apply to different processes or for different feed coals.

Neavel's view that the initial chemical reactions involve homolysis to yield free radicals which are capped by hydrogen from the donor solvent or hydroaromatic structures in the coal (3), has been generally accepted. The presence of labile linkages, such as ether groups, in the lattice networks would presumabily hasten the comminution of the coal matrix. However, the importance of ethers in this role has been demonstrated (4-10), but has not been conclusively established. The presence of ether bonds in coal has been inferred from alkali metal reduction studies (11-13) in which the products were considerably more soluble in pyridine, were of a lower molecular weight and were of a higher phenolic content. Siskin and Aczel (9) carried out a parallel study on coal pyrolysates and model compounds. By selectively blocking existing hydroxyl groups, they were able to determine the hydroxyl groups which were generated by ether cleavage during pyrolysis.

We intend to present additional evidence as to the importance of ether cleavage during the early stages of coal liquefaction through a comparison of different kinetic analyses.

EXPERIMENTAL

Detailed information on the experimental procedure were described previously (8). Characteristics of the coals studied are listed in Table 1. The liquefaction experiments were conducted with the use of tubing bomb reactors heated in a fluidized bed sand bath. Basically, coal was heated to temperatures between 350 and 425°C for up to 60 minutes in the presence of tetralin under a hydrogen atmosphere. Following each experiment, the products were dispersed in a large excess of hexane. The hexane - insoluble material was filtered, washed and dried. An aliquot was extracted with THF in a Soxhlet apparatus, and the total conversion to soluble material and gases was calculated from the weight of insoluble residue.

*Presently at M.I.R.L., University of Alaska, Fairbanks, Alaska 99701

Direct oxygen determinations were conducted on the coals and the hexane - insoluble products by using the pyrolysis mode of the Carlo Erba Elemental Analyzer. The measured oxygen contents of the hexane - insolubles were recalculated as a percentage of the dry coal. This total oxygen was subdivided into two components, hydroxyl and unaccounted oxygen, since the amount and changes

$$O_T = O_{OH} + O \text{ unaccounted} \qquad 1)$$

in the carbonyl groups during liquefaction are small (5). Hydroxyl concentrations of the various samples were determined by acetylation. All of the results reported are averages of duplicate values.

BACKGROUND AND THEORETICAL DEVELOPMENT

We had previously noted that the rate of conversion of the western coal (PSOC-521) was slower than those of the Interior (PSOC-767) and Eastern Province (PSOC-757) coals. Sample data are given in Table 2. The Wyoming coal was also inferred to have the highest concentration of ether groups (7.7 O/100 C atoms) for the three coals studied (8). If ether cleavage is an important process in the early stages of liquefaction, this coal should perform well. That it does not could be accounted for if in this coal, the ethers constitute multiple crosslinks, a majority of which have to be cleaved in order to generate soluble products, or if the ether links for this coal are stable and do not react or are relatively slowly cleaved under the conditions used. A more sophisticated kinetic approach will now be presented, which takes account of the complex nature of coal liquefaction.

This approach is an adaptation of that of Szladow and Given (14) in which the theoretical analysis assumes many parallel reactions in a complex reacting mixture. Golikeri and Luss (15) were the first to establish a method for determining the apparent activation energies, E', in systems comprising many parallel first order reactions whose activation energies may be temperature and conversion dependent. Since concentrations are based on molarity rather than mass, the generation of activation energies has little meaning for systems such as coal liquefaction. Szladow and Given (14) extended this treatment for the case where the total mass as opposed to the total number of moles is known for the reacting system. It was shown that E' can be derived at various conversion levels of x using equation 2).

$$\frac{d \ln t_x}{d (1/T)} = \frac{E_a}{R} \qquad 2)$$

t_x = time needed to achieve a specific level of conversion

E_a = the weighted mean of the activation energy at a specific level of conversion.

Using this approach, apparent activation energies were generated for conversion to THF solubles and for removal of unaccounted oxygen.

RESULTS AND DISCUSSION

Since the unaccounted O is determined by difference, all errors incurred throughout the dtermination of total oxygen and O as OH end up in this term. Plots of unaccounted O removal versus time were adjusted to account for the nonisothermality of the first two minutes and for the presence of unconvertible ethers, i.e. benzologues of furan. Shown in figure 1 is a representative plot for the Wyoming coal. The coordinates were adjusted in the following manner:

$$\% \text{ O unaccounted removed} = \frac{O_i - O_o}{O_m - O_o} \times 100 \qquad 3)$$

where

O_i = unaccounted oxygen removed at residence time, t_i

O_o = unaccounted oxygen removed at t_i = 2 minutes

O_m = maximum unaccounted oxygen removed; that is, that part of the unaccounted O that in principle could be removed at infinite reaction time. (Highly unreactive oxygen, as in furans, is excluded).

By defining O_m in this manner, as oppose to O ($t = \infty$), those O functionalities that may be generated by retrogressive reactions, such as condensation reactions, can be ignored. Since unaccounted O removal was found to be linearly related to generation of THF-solubles (8), O_m was obtained from an extrapolation of a least squares fit of the data to C_m. C_m is defined as the sum of the reactive macerals plus one third of the inert macerals less fusinite.

The apparent activation energy, E', for different conversion/removal levels was determined using equation 2 and figure 1. The logarithm of the time needed to attain specific levels of removal of unaccounted O was plotted against the reciprocal of temperature. From the slopes of these lines (E'/R), the activation energies were determined. The values for the three coals are plotted against the level of unaccounted O removed in figure 2. Error bars reported as the standard deviation of the slopes of these plots are also included. It should be noted that E' increases with level of unaccounted O removal. This is consistent with the behavior of reacting mixtures; namely, the more reactive species are preferentially consumed leaving behind the more refractory compounds.

Apparent activation energies were generated in an analogous manner for conversion of the three coals to THF - soluble material. The values for E' are plotted against level of conversion in figure 3. The associated error bars are based on a 90% confidence level. It should be noted that the large errors are reflective in both cases of fewer data points available at higher levels of conversion, as well as the uncertainty in contact time measurement.

It is striking that for any one coal, the plots of conversion against activation energies for production of THF-solubles, and for removal of unaccounted oxygen are closely similar (within the limits of experimental error). The implication seems to be that it is primarily ether cleavage processes that determine the magnitudes of the activation energies for the reactions generating THF-solubles.

In light of the estimates of maximum numbers of ethers cleaved in the three coals (8), as well as their activation energies at different conversion levels, it appears that the basis for the Wyoming coal's slower conversion is the need to cleave a greater number of labile bonds to generate a specific level of conversion to soluble products. The "ethers" in both the Wyoming coal (PSOC-521) and the Ohio coal (PSOC-757) exhibit a wide range of activation energies that are paralleled by their activation energies for conversion to THF-solubles. The Oklahoma coal (PSOC-767) contained the fewest "ethers" (4.1 O/100 C atoms), and also the range of activation energies for cleavage of these was least over the level considered. Furthermore, the change in activation energy for overall conversion was also least for this coal.

In view of previous studies (6, 9, 10, 16, 17) the unaccounted O lost during the early stages of coal liquefaction is probably from structures analogous to phenyl - benzyl and dibenzyl ethers. Under conditions of greater severity additional species may be removed or even added. Phenols present (18) or generated in the products may enhance the cleavage of diaryl ethers. The small magnitudes of the activation energies at low levels of conversion at first sight seem surprising. However, Anthony et al. (19) have shown that in the complex set of parallel reactions occurring during the rapid devolatilization of coal, the overall temperature coefficient for the whole set of reactions can be low, and, in fact, lower than the activation energy for any pure component of the reaction mixture decomposing on its own. In view of the possibility that coals contain a fairly high concentration of physically trapped molecules (20), the processes involved in liquefaction may include activated diffusion out of the macromolecular network. However, this cannot be proven from the activation energy data presented here.

CONCLUSIONS

Since the Wyoming coal (PSOC-521) has a slower conversion in-spite of its higher number of cleavable ethers (8) and its comparably low activation energy for conversion to THF-solubles and for un-accounted O removal, it is inferred that this coal is extensively cross-linked by ether linkages.

Similar changes in activation energies were obtained with level of total conversion and extent of unaccounted O removal for any one coal up to more than 50% conversion. Since the removal of unaccounted O consists of ether cleavage, we infer that ether cleavage continues to be important, not only in the earliest stages of coal liquefaction.

REFERENCES

1. Brunson, R. J., Fuel, 58, 203 (1979).

2. Cronauer, D. C., Shah, Y. T. and Roberts, R. G., Ind. Eng. Chem. Process Des. Dev., 17, 28, (1978).

3. Neavel, R. C., Phil. Trans. Roy. Soc., London, A. 300, 141 (1981).

4. Curran, G. P., Struck, R. T. and Gorin, E., Ind. Eng. Chem., Proc. Des. Dev., 6, 166 (1967).

5. Szladow, A. J. and Given, P. H., Preprint, Amer. Chem. Soc., Fuel Chem. Div., 23, 161 (1978).

6. Carson, D. W. and Ignasiak, B. S., Fuel, 59, 757 (1980).

7. Kuhlmann, E., Boerwinkle, E. and Orchin, M., Fuel, 60, 1002 (1981).

8. Youtcheff, J. S. and Given, P. H., Fuel, 61, 980 (1982).

9. Siskin, M. and Aczel, T., Fuel, 62, 1321 (1983).

10. Cassidy, P. J., Jackson, W. R. and Larkins, F. P., Fuel, 62, 1404 (1983).

11. Sternberg, H. W., Delle Donne, C. L., Pantages, P., Moroni, E. C. and Markby, R. E., Fuel, 50, 432 (1971).

12. Ignasiak, B. S. and Gawlak, M., Fuel, 56, 216 (1977).

13. Wachowska, H. and Pawlak, W., Fuel, 56, 422 (1977).

14. Szladow, A. J. and Given, P. H., Ind. Eng. Chem., Proc. Des. Dev., 20, 27 (1981).

15. Golikeri, S. V. and Luss, D., AICHE J., 18, 277 (1972).

16. Whitehurst, D. D., Farcasiu, M. and Mitchell, T. O., Report prepared for Electric Power Research Institute, Report No. EPRI-AF-480.

17. Benjamin, B. M., Raaen, V. G., Maupin, P. H., Brown, L. L. and Collins, C. J., Fuel, 57, 269 (1978).

18. Kamiya, Y., Sato, H. and Yao, T., Fuel, 57, 681 (1978).

19. Anthony, D. B., Howard J. B., Hottel, H. C. and Meissner, H. P., In: Proceedings of the 15th Symposium on Combustion, pp. 1303-1317 (1975).

20. Bodzek, D. and Marzec, A., Fuel, 60, 47 (1981).

TABLE 1

Characteristics of Coals Used

PSOC No.	757	767	521
State	Ohio	Oklahoma	Wyoming
Seam	Ohio No. 4	(unnamed)	Rock Springs No. 7
ASTM rank class	HVB	HVA	HVC
C (wt.%, dmmf)	81.3	82.1	79.0
H (wt.%, dmmf)	5.3	5.6	5.2
O (wt.%, dmmf)	9.3	8.4	13.8
S, total (wt.%, dry basis)	3.39	3.55	0.78
Maceral composition (%)			
Vitrinites	75.7	91.5	94.2
Exinites	8.0	2.1	1.0
Inertinites	16.4	6.4	4.8
Mean maximum reflectance of vitrinite (%)	0.50	0.54	0.52
Mineral matter (direct by LTA)(wt.%)	7.92	5.69	4.72

[a]Includes 5.4% semifusinite and 7.3% micrinite.

TABLE 2

Time Needed to Attain Specific Level of Conversion

	Level of Conversion	
PSOC No.	50% of dmmf reactive macerals at 400°C	75% of dmmf reactive macerals at 425°C
521	18.6	44
757	8.0	6.6
767	7.5	7.4

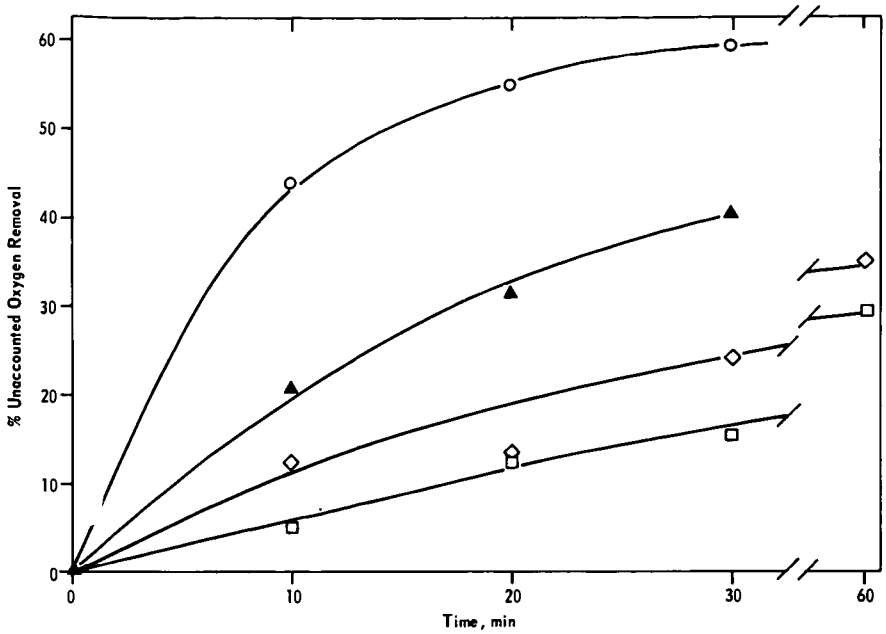

Figure 1. REMOVAL OF UNACCOUNTED OXYGEN FROM WYOMING COAL AS A FUNCTION OF TIME
(with transformed coordinates)
○ 425°C ▲ 400°C ◇ 370°C □ 350°C

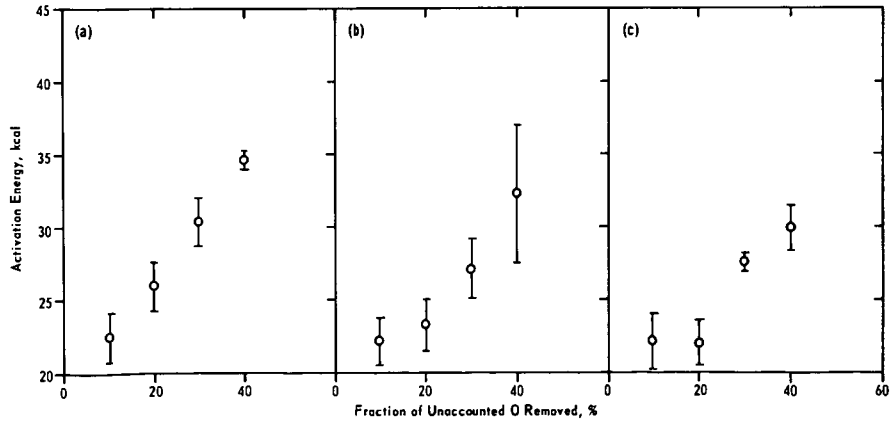

Figure 2. "ACTIVATION" ENERGIES FOR THREE COALS AT DIFFERENT LEVELS OF REMOVAL OF UNACCOUNTED OXYGEN
(a) PSOC-521; (b) PSOC-757; (c) PSOC-767

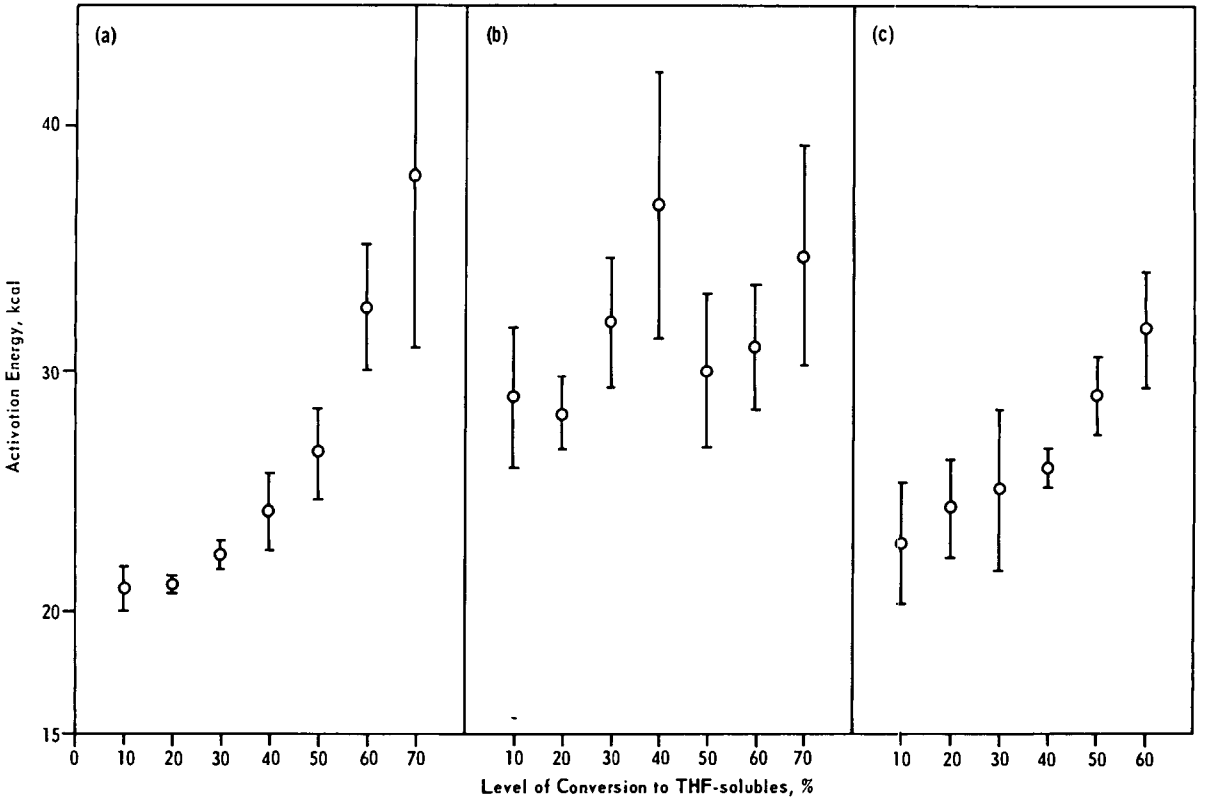

Figure 3. "ACTIVATION" ENERGIES FOR THREE COALS AT DIFFERENT LEVELS OF CONVERSION
(a) PSOC–757; (b) PSOC–767; (c) PSOC–521

CLEAVAGE OF AROMATIC CARBON-CARBON BONDS

Eugene A. Kline and William P. Teichert

Department of Chemistry
Tennessee Technological University
Cookeville, Tennessee 38505

and

Bruce W. Farnum

University of North Dakota Energy Research Center
Box 8213, University Station
Grand Forks, North Dakota 58202

Introduction

The search for a model substrate to use in evaluating relative reactivity of H-donors, under coal liquefaction conditions has led to this study of o-terphenyl.

The stability of biphenyl, terphenyls, quaterphenyls, and polyphenyls in the absence of H-donors has been demonstrated by their high bond dissociation energies between aromatic rings (1, 2). Therefore, they have practical application as coolant moderators in nuclear power plants (3). This stability is gained in part from the orbital overlap of the carbon atoms in the interannular C-C bond. The melting point of p-terphenyl is 208°C, and of hexiphenyl is 469°C. Their UV absorption at 278 and 318 nanometers, respectively, are indications of the increased stability as the number of benzene rings increases and resonance stabilization increases. The thermal temperature (defined as the temperature ±10°C at which decomposition rate is 1 mole % per hour) for m-terphenyl was 485°C and for the p-isomer was 478° (3). The same workers studying the problem of polymerization of polyphenyls and its control in nuclear power plants found one solution to the build up of the high molecular weight polymers. Reclamation by catalytic hydrocracking to reduce molecular weight in every case lowered the decomposition temperature to 320°-400°C due to formation of 20% methylated and ethylated products.

Reaction of polyphenyls under coal liquefaction conditions has been reported (4). The compound o-terphenyl (OTP) was found to couple irreversibly to form the very thermally stable triphenylene in the presence of an H-donor without a catalyst. Formation of different amounts of triphenylene with different H-donors suggested that o-terphenyl was a good candidate as a model substrate for study of the relative abilities of H-donors to react. Two other model substrates, 1,1'-binaphthyl (5) and dibenzo(c,g)phenanthrene (4), were also found to couple at different rates indicating they, too, would be possible substrates which could be used to differentiate the effectiveness of H-donors. Dibenzo(c,g)phenanthrene was difficult to prepare, and it coupled in the absence of H-donor and gave other hydrogenated isomers without coupling. o-Terphenyl formed extremely small amounts of coupled product compared to 1,1'-binaphthyl; consequently, the latter was judged to be the best model substrate of the three compounds to use in studying the effect of H-donors on the coupling reaction.

An unexpected result in the reaction of o-terphenyl and H-donors without catalyst was the large production of biphenyl. As much as 60%

cleavage reaction to yield biphenyl was observed while coupling reaction to yield triphenylene was always less than 5%. The rates of biphenyl formation varied with the particular H-donor used, suggesting that this cleavage reaction can be used to compare reactivity of H-donors at high temperatures. This paper discusses results of cleavage reaction studies with o-terphenyl.

Results and Discussion

All reactions were carried out in 1/2" Gyrolok, Parker, or Swagelok unions. Equimolar amounts of H-donor and o-terphenyl were added to the reaction vessel. It was filled with benzene solvent, and sealed without addition of a gas. The reactor was then placed in a fluidized sand bath controlled at 470±2°C. Analyses of the resulting product mixtures were carried out on a gas chromatograph programmed 75°-300° at 15°/min, 6' x 2 mm ID Dexsil 300 column.

The determination of kinetic rate constants provided some insight into the mechanism of the reaction. Reactions were run for 1, 2, 3, 4, and 5 hours with equimolar amounts of several model H-donors that were able to withstand the severe conditions. Mass balance was obtained in most cases accounting for both H-donor and o-terphenyl. The appearance of triphenylene and biphenyl were fitted to both first order and autocatalytic rate expressions. The best fit for the appearance of triphenylene was the autocatalytic rate expression; however, the first order expression correlated nearly as well. The formation of biphenyl appeared to fit the pseudo first order rate expression. The resulting yields and rate constants for the various H-donors with o-terphenyl to form triphenylene and biphenyl are shown in Table I.

The rate constants for the formation of triphenylene with different H-donors over five hours compared relatively well with the one-hour yield data. Hydrogenated heterocycles such as tetrahydroquinoline were too thermally-unstable to study under these conditions. The fact that triphenylene and biphenyl formation fit different rate expressions was significant. The autocatalytic formation of the coupled product (triphenylene from OTP) suggested that another species (perhaps the hydrogenated intermediate) was involved in the coupling. As this species was generated more coupling occurred.

A radical capping mechanism did not explain the kinetics data. Rather, coupling of the o-terphenyl by induction by a secondary H-donor seemed more justifiable. The 9,10-dihydrophenanthrene decomposed to a very small concentration within one hour (4), yet triphenylene continued to increase. Even in the case of tetralin which decomposed at a constant rate, there appeared to be autocatalytic formation of the coupled product.

Another way to investigate the mechanism was to study the differences and similarities of reactions of the isomeric terphenyls. Since cleavage was involved, the ortho-isomer had no predictable advantage as a model substrate. Two of the isomers, m-terphenyl and o-terphenyl were reacted with one H-donor, tetralin, for 1, 2, 3, 4, and 5 hours, and the products were analyzed by the usual method. p-Terphenyl was found to be quite insoluble in most solvents and reaction times of 1, 3, and 5 hours were selected. The results are summarized in Table II.

One deuterated H-donor 9,9,10,10-d_4-9,10-dihydrophenanthrene was reacted for three hours with o-terphenyl in benzene. The tendency toward random scrambling from the deuterated H-donor to the produced

biphenyl was studied by reacting the deuterated H-donor with biphenyl under the same conditions in a separate experiment. Due to excessive exchange, no clear cut mechanistic information was obtained.

The application of this reaction of o-terphenyl to determine relative reactivity of coal-derived liquids was studied by reacting equal weights of o-terphenyl and various start up and coal-derived recycle solvents produced in the UND Energy Research Center continuous process coal liquefaction pilot plant. The liquids used were from the ends of runs which had undergone several recycle passes in a reducing atmosphere, and which have been well characterized (6). The results of the reactions are summarized in Table III. The values of biphenyl produced were obtained by the difference of the biphenyl after reaction and the initial amount of biphenyl in the coal liquid.

The unique feature in the three hour o-terphenyl reactions was the formation of biphenyl in significant quantities in most cases and in differing amounts showing differences in the ability of the solvents to affect this cleavage. One thing noticeably different in running these reactions was the small amount of gas pressure in the reactor at the end of the reaction compared with the hydrogenated model H-donors.

In summary, o-terphenyl couples in the presence of model H-donors and many coal derived solvents to form triphenylene, and forms biphenyl by cleavage. The latter reaction is of more interest as the yields are substantial, and the yields have application to the study of properties of solvents. Attempts to elucidate the mechanism involved kinetic studies, and reaction with a deuterated H-donor. The best mechanism appears to be that in which the low steady-state concentration of reactive H-donor attacks either ipso position in o-terphenyl followed by cleavage (7). This mechanism is known to occur at high temperatures.

Literature Cited

1. Streitweiser, Jr., Andrew; and Heathcock, Clayton H. "Introduction to Organic Chemistry," 2nd ed., McMillan Publishing Co., Inc., 1194 (1981).
2. Vernon, Lonnie W. Fuel, 59, 102 (1980).
3. Scola, Daniel A.; and Adams, Jr., John S. Ind. Eng. Chem. Prod. Res. Develop., 10, 417 (1971).
4. Kline, Eugene A.; and Farnum, Bruce W. Am. Chem. Soc. Div. Fuel Chem. Preprints, 28, 155 (1983).
5. Kline, Eugene A.; Harrison, Mark E.; and Farnum, Bruce W. Am. Chem. Soc. Div. Fuel Chem. Preprints, 27, 18 (1982).

6a. Farnum, Sylvia A.; Farnum, Bruce W.; Bitzan, Edward F.; Willson, Warrack G. and Baker, Gene G. Fuel 62, 799(1983).

b. Quarterly Technical Progress Report DOE/FC/QTR 82/2 (DE83013383) Grand Forks Energy Technology Center, Grand Forks, ND (1983).

c. Runs 101 and 103, Unpublished Results, UNDERC.

7. McMillan, Donald F.; Ogier, Walter; Chang, Sou-jen; Fleming, Ronald H.; and Malhotra, Ritudamin. Proceedings of International Conference on Coal Science, Pittsburgh, PA, August 15-19, 1983, pp. 199-203.

Table I. Results of Reactions of H-Donors and o-Terphenyl

H-Donor	Triphenylene* Yield	k(/sec) ($\times 10^3$)	Biphenyl** Yield	k(/sec) ($\times 10^3$)
Blank	0.1	--	3%	--
1,2,3,4-detrahydro-naphthalene	2.9%	7.2	60	1.9
1,2-Dihydronaph-thalene	2.7	--	54	1.3
1,4-Dihydronaph-thalene	2.5	6.4	4	1.3
Fluorene	2.9	1.6	60	1.4
Indane	7.1	9.8	30	2.5
Indene	3.7	8.5	46	1.8
9,10-Dihydrophen-anthrene	3.2	7.0	34	2.6
9,10-Dihydroan-thracene	1.0	3.3	47	1.6

*Triphenylene/initial OTP (one hour reaction) (autocatalytic)
**Biphenyl/initial OTP (five hours reaction) (Pseudo first order)

Table II. Results of Reactions of the Terphenyls with Tetralin at 470°C (rate constants - x 10^{3} min^{-1})

o-Terphenyl	m-Terphenyl*	p-Terphenyl*
k=2.0	k=2.4	k=2.0

*Modelled pseudo-first order as best fit.

Table III. Results of Reactions of Coal Derived Liquids with o-Terphenyl at 470°C for 3 Hours

Coal Derived Solvent	Origin of Solvent	Biphenyl (RXN)-Biphenyl (INIT)
101PB21	Zap, ND lignite, pass 12[a]	68%
101PB40	Zap, ND lignite, pass 40[a]	37
67PB23	Wyodak Subbituminous, pass 12[a]	5
64PB25	Big Brown-Texas lignite,[a] pass 13	67
65PB23	Beulah, ND lignite, 12 passes[a]	67
53PB18	Powhatan Bituminous, pass 18[a]	38
Project Lignite Recycle Solvent	Zap, ND lignite, UND PDU	28
Crowley AO4	Typical Anthracene Oil	13
SCR Mid. Dist.	Fort Lewis Pilot Plant (Powhatan coal)	25

a)Recycle solvents from the University of North Dakota Energy Research Center continuous process unit.

ARYLATIONS OF COAL MODEL SYSTEMS

Barbara F. Smith, Clifford G. Venier, and Thomas G. Squires

Applied Organic Chemistry,
Energy and Mineral Resources Research Institute,
Iowa State University, Ames, Iowa 50011

Currently, coal is converted to clean liquids or low melting solids by processes which utilize high temperature, high pressure, or both. These processes occur by thermal bond cleavages and involve the intermediacy of free radicals. In a search for chemistry which could liquefy coal under milder conditions, we have focussed on thermally less demanding ionic reactions.

Of the functional groups which commonly occur in coals, ethers are the easiest to cleave under acid conditions. Depending on the density of these linkages and their importance as crosslinks in the macromolecular structure of coals, solubilization might be greatly enhanced solely by cleaving and capping ether bonds. Benzylic ethers are particularly reactive and have been implicated in the initiation of coal pyrolysis(1) and hydropyrolysis(2). Arylation, the use of acids to cleave bonds in coals in the presence of aromatic rings to trap the consequent incipient carbonium ions, has a long history(3). The most extensively studied system is the Heredy-Neuworth phenol depolymerization(4).

We have chosen to use benzyl phenyl ether and 1-naphthylmethyl phenyl ether and polymers related to them as models to develop and evaluate the chemistry involved in the arylations.

RESULTS

Arylmethyl phenyl ethers undergo competing reactions when treated with Lewis acids. A partitioning of arylmethyl groups between an intramolecular process (a rearrangement) and an intermolecular one can be seen in Table 1. The fact that the rearranged product is overwhelmingly the ortho isomer is consistent with the intramolecular

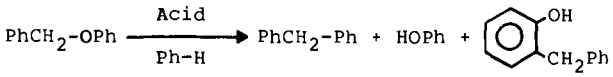

(1)

nature of the rearrangement(5). Regardless of the choice of acid or temperature, essentially one-half of the starting phenylmethyl phenyl ether, 1, ends up as rearranged product. Table 2 shows that generally the same result holds for 1-naphthylmethyl phenyl ether, **4**. However, a previously unrecognized complication shows up in the products of the acid-catalyzed reaction of **4**.

Despite the fact that solvent benzene is in great excess, substrate or product or both, effectively compete for the 1-naphthylmethyl moiety. Capillary gc-ms reveals that at least five products of molecular weight 374 are produced in these reactions. This corresponds to structures containing two 1-naphthylmethyl groups and one phenol. These products can arise by substrate capture of a 1-naphthyl-methyl followed by ether-to-phenol rearrangement or, alternatively, by capture of 1-naphthylmethyl by products **5**. Even under conditions where the molar ratio of benzene to starting material

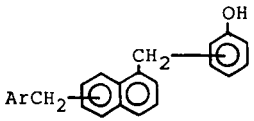

21 isomers possible

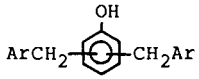

6 isomers possible

exceeds 1000, a significant number of product molecules derive from more than one molecule of starting ether.

If substrate and/or products can trap the electrophilic 1-naphthylmethyl species with such efficiency, it stands to reason that other aromatic compounds will likely be better than benzene also. Table 3 shows data demonstrating that this is the case. The fact that the relative rate constant measured for the naphthalene-benzene competition remains constant over a 100-fold change in naphthalene concentration, confirms that the change in product slate arises by the simple partitioning of an intermediate between the two traps. The straightforward behavior of the system was further checked by allowing diphenylether and 2,6-dimethylphenol to compete directly. The rate constants determined when three traps are present are sensibly the same as those found in binary competition (see last line of Table 3).

One would expect the same sort of behavior for the trapping of intermediates generated from insoluble materials. Naphthalene should be a substantially better capping agent than benzene. The results of the BF_3-catalyzed arylations of polymer **9** with benzene, naphthalene, or phenanthrene as traps in CH_2Cl_2 solvent are given in Table 4, along with the results from some reactions carried out in benzene solvent.

Of particular importance is the fact that the solubilities of products generated in the presence of naphthalene and phenanthrene differ markedly from that produced by BF_3 treatment alone. Infrared spectra clearly establish that the ether functions present in the starting polymer are no longer present in the products. Apparently, in the absence of a trap, polymer **9** is converted to a new polymer, whose structure is best approximated as **10**, equation 2, although we recognize that substantial amounts of interchain crosslinking might occur. The enhanced solubility in the presence of arene, therefore, signals the lowering of molecular weight by capping reactions, equation 3.

(2)

9 10

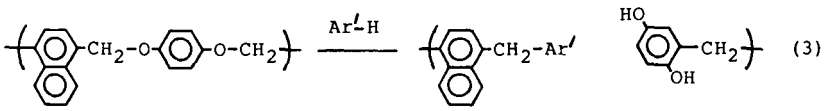

(3)

DISCUSSION

The results reported here are best interpreted on the basis of a model in which carbonium ions generated from arylmethyl phenyl ethers are partitioned between the various nucleophiles present. In this system, aromatic rings are the most nucleophilic functional groups. The 1-naphthylmethyl cation is much more stable than is the simpler

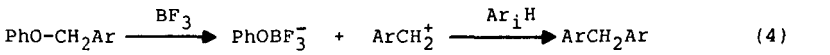

(4)

benzyl cation, and, consequently, much more selective in its reactivity(6). Thus, in the case of benzyl phenyl ether, **1**, solvent benzene effectively traps all generated carbonium ions. However, the more stable 1-naphthylmethyl cation generated from **4**, is sufficiently stable to discriminate between the poorly nucleophilic benzene and the more nucleophilic molecules, **4** and **5**. Naphthalene, on the other hand, is much more nucleophilic than benzene(7), and in sufficient concentration, suppresses "self-trapping".

The same picture emerges from work with polymer **9**. Apparently, benzene is insufficiently reactive to compete with intramolecular (intrapolymer) nucleophiles and, consequently, no increase in solubility accompanies the cleavages of ether links in **9** upon addition of benzene. When better nucleophiles, naphthalene and phenanthene, are provided, carbonium ions generated from ether cleavages are capped and the product is lower in molecular weight and more soluble.

It is worth noting that the naphthalene (k_{rel}=280) is nearly as good a trap as the phenol (k_{rel}=450). Since hydroxylic solvents will level the acid strength of BF_3 to that of $ROBF_3^-H^+$ and hydrocarbons would not, the acid-catalyzed bond cleavages necessary for unlinking coal may in fact be faster in BF_3-arene than in BF_3-phenol. While we have not yet extended these results to coals, we believe that the combination of a relatively mild Lewis acid catalyst, BF_3, with a good carbonium ion trap, naphthalene, will allow selective cleavage and capping of aryl alkyl ether bonds.

EXPERIMENTAL

All gas chromatographic (GC) analyses were performed on a Tracor model 550 gas chromatograph with flame ionization dectector; glass columns were 6'x4mm and 6'x2mm, packed with 3% OV-1 or OV-101 on 80-100 mesh supelcoport, respectively. Columns were held at 80°C for 2 min. and then the temperature raised to 275°C at 25°/min and held for 10 min (benzyl phenyl ether reactions) or initially held at 120° and the temperature raised to 200° at 5°/min and held for 10 min (1-naphthylmethyl phenyl ether reactions). Peak areas were integrated by the "cut and weigh" method. NMR spectra were obtained on a Varian EM 360, IR spectra on a Beckman IR-4230 and GC-Mass Spectra on a Finnigan

4023. Liquid chromatographic analyses were carried out on a Varian 5000 LC with a Varian UV-50 detector at 270 nm.

Benzyl phenyl ether and 1-naphthylmethyl phenyl ether were prepared by reaction of phenoxide ion with the requisite halide, and purified by recrystallization. The polymer 9 has been previously described(8).

Reaction of Arylmethyl Phenyl Ethers with Lewis Acids in Benzene. General Procedure

The arylmethyl phenyl ether, internal standard (hexadecane or dodecane) and trapping agents (naphthalene, 2,6-dimethylphenol or diphenylether) when used, were placed in a dry flask and dissolved in benzene that had been dried by azeotropic distillation and stored over 4A molecular sieves. Lewis Acid (BF_3, BF_3-CH_3OH or $AlBr_3$) was then added as a dilute benzene solution or directly to the reaction mixture at room temperature. Aliquots were removed at timed intervals, quenched with water, and diluted for LC and/or GC analysis.

Reaction of Polymer 9 with Arenes Catalyzed by Lewis Acids

To a dry flask outfitted with a magnetic stirrer was placed polymer, 9, dry solvent (benzene or methylene chloride), and trap (naphthalene or phenanthrene) when used. Lewis acid was added, in most cases, as a dilute solution or, in a few runs with BF_3, as a gas. The heterogeneous mixture was stirred for the indicated time at the required temperature. The resulting blue-green reaction mixture was quenched with water, filtered and washed. The insoluble residue was dried, weighed and analyzed by IR. The organic filtrate was dried and the solvent removed under vacuum.

REFERENCES

1. Siskin, M.; Aczel, T. Fuel **1983**, 62, 1321.
2. Tanner, K.I.; Bell, A.T. Fuel **1981**, 60, 52.
3. Larsen, J.W.; Kuemmerle, E.W. Fuel **1976**, 55, 162.
4. Wender, I.; Heredy, L.A.; Neuworth, M.B.; Dryden, I.G.C. In "Chemistry of Coal Utilization. Second Supplementary Volume"; Elliott, M.A., Ed.; Wiley: New York, 1981; Chapter 8, pp. 447-454; and references therein.
5. Dewar, M.J.S. In "Molecular Rearrangements, Part 1"; de Mayo, P., Ed.; Wiley: New York, 1963; Chapter 5.
6. Streitwieser, A., Jr. Chem. Rev. **1956**, 56, 571.
7. Dewar, M.J.S.; Mole, T.; Warford, E.W.T. J. Chem. Soc. **1956**, 3581, report k(naphthalene)/k(benzene)=350 for nitration.
8. Squires, T.G.; Smith, B.F.; Winans, R.E.; Scott, R.G.; Hayatsu, R. Proc. Intern. Conf. Coal Sci. **1983**, 292.
9. Bunnett, J.F. In "Investigations of Rates and Mechanisms of Reactions"; Lewis, E.S., Ed.; Wiley-Interscience: New York, 1974; Chapter IV, pp. 158 ff.

Table 1. Products of Acid-catalyzed Phenylation of Phenyl Benzyl Ether.[a]

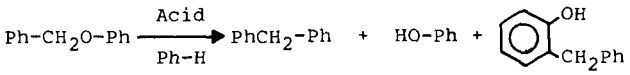

1 2 3

intermolecular intramolecular

ACID	Ph_2CH_2	o-benzylphenol
CF_3SO_3H	44%	48%
$BF_3 \cdot CH_3OH$	47%	40%
$BF_3 \cdot CH_3OH$ (72°)	49%	49%
BF_3	49%	48%
$AlBr_3$	48%	54%

[a]Room temperature, benzene solvent.

Table 2. Products of BF_3-Catalyzed Cleavage of 1-Naphthylmethyl Phenyl Ether.[a]

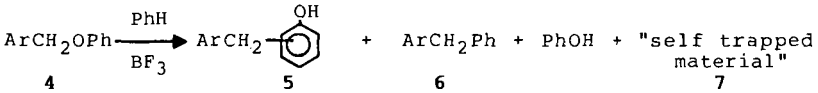

4 5 6 7

ArCH₂OPh	o-5	p-5	6	recovery	7[b]
0.2M	30	12	<1	43%	(1.00)
0.02M	37	15	6	58%	.76
0.002M	50	16	12	78%	.27

[a]Room temperature, benzene solvent

[b]Relative yield of several products from liquid chromatographic analysis.

Table 3. Relative Trapping Ability of Aromatic Compounds in BF_3-Catalyzed Cleavage of 1-Naphthylmethyl Phenyl Ether.[a]

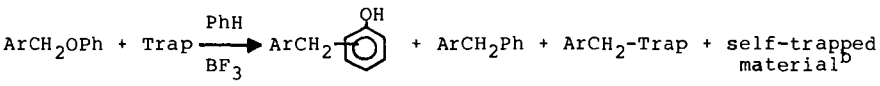

		5		6	8		7
Trap	Trap, M	o-5	p-5	6	8	k_{rel}[c]
Benzene	0	38	13	7	--	(1)
Naphthalene	.020	33	14	7	3	280
Naphthalene	.20	37	14	3	17	310
Naphthalene	2.0	32	8	1	46	260
Diphenyl Ether	.20	41	13	4	4	50
2,6-Dimethylphenol	.20	39	12	2	17	450
Diphenyl Ether	.20	28	9	1.5	15	500
2,6-Dimethylphenol	.20				1.3	45

[a] Room Temperature, benzene solvent.

[b] See Figure 1 for relative yields of self-trapped material.

[c] $\frac{k_{trap}}{k_{PhH}} = \frac{[ArCH_2\text{-Trap}]}{[ArCH_2Ph]} \times \frac{[PhH]}{[Trap]}$, see reference 9.

Table 4. BF_3-Catalyzed Arylation of Polymer 9.

			Product solubilities[a]		
ArH/solvent	Acid	Temp.	CH_2Cl_2	PhH	Acetone
CH_2Cl_2	$BF_3 \cdot H_2O$	23°			0%[b]
CH_2Cl_2	BF_3	20°	<5%		
PhH/CH_2Cl_2[c]	BF_3	20°	<5%		
naphthalene/CH_2Cl_2[c]	BF_3	20°	29%		
phenanthrene/CH_2Cl_2[c]	BF_3	20°	24%		
PhH	$BF_3 \cdot CH_3OH$	80°		11%	39%
PhH	BF_3	23°		19%	76%

[a] Determined by weight of insoluble product.

[b] IR shows complete loss of ether functionality.

[c] 0.4 M Arene.

ACKNOWLEDGEMENT

This material was prepared with the support of the U. S. Department of Energy, Grant No. DE-FG22-82PC50786. However, any opinions, findings, conclusions, or recommendations expressed herein are those of the authors and do not necessarily reflect the views of DOE.

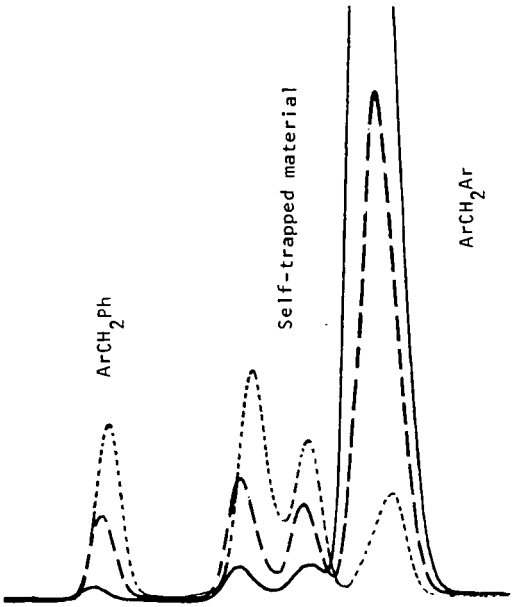

Figure 1. Liquid Chromatograms of the Naphthylation of 1-Naphthylmethyl Phenyl Ether, $ArCH_2OPh$ (see Table 3).

····· 0.020 M Naphthalene (ArH)

-------- 0.20 M Naphthalene (ArH)

———— 2.0 M Naphthalene (ArH)

BENZYLIC FUNCTIONALITY IN COAL DERIVED ASPHALTENES: A CALIFORNIUM-252 PLASMA DESORPTION MASS SPECTROMETRY APPROACH*

R.A. Zingaro, R.D. Macfarlane, J.M. Garcia III, A.G. Vindiola and J.H. Zoeller, Jr.
Department of Chemistry, Texas A&M University, College Station, Texas 77843

INTRODUCTION

The hydroaromatic components embodied in coal molecules strongly influence the thermal behavior of coal in a variety of conversion processes. A body of indirect evidence suggests that effects due to facile bond breaking at benzylic carbon atoms are operative in coal liquefaction (1,2), mesophase development (3,4) and devolatilization behavior (5). In an ongoing study of the structure of coal derived molecules by the technique of Californium-252 Plasma Desorption Mass Spectrometry (CFPDMS), we have found (6) that asphaltenes display positive ion groups of semiregular periodicity in the mass region 150 to 400 amu, and that this pattern is strikingly similar to that of pure hydroaromatic compounds. Such ion groups are also observed (7,8) in Field Ionization Mass Spectrometry (FIMS) spectra of coal derived materials. We wish to present evidence that such ion groups are due to benzylic functionalities and not to families of compound group classes.

The CFPDMS technique involves the use of the nuclide ^{252}Cf, one of whose modes of decay is spontaneous fission. Each fission event ejects two fragments in opposite directions, each with speeds of c/10, and energies of 80 to 150 MeV. Interaction of one of these fission fragments with a thin film of organic substrate generates a highly localized hot spot which devolatilizes positive and negative ions. In the CFPDMS experiment (9,10) these ions are accelerated towards a charged grid and into a time of flight (TOF) mass spectrometer. The TOF clock is triggered by the second, simultaneously ejected fission fragment colliding with a start detector and stopped when an organic ion collides with the TOF detector. Acquisition of the TOF data over many events is managed under computer control. Accumulated data is assembled into a mass spectrum by calibration with known common ions.

Native coal asphaltenes can be isolated from low rank coals by dimethylsulfoxide (DMSO) extraction and solvent fractionation. DMSO extraction of the Wilcox seam lignite lithotype yields almost a quarter of the organic matter present. From this extract is isolated the tetrahydrofuran (THF)-soluble, hexane-insoluble fraction, formally a asphaltene-preasphaltene blend. The positive ion CFPDMS spectrum of this sample displays the ion

* Dedicated to Professor Peter Given, honorable recipient of the 1984 Henry H. Storch Award in coal research.

groups described. Such ions are also seen in the spectra of asphaltenes and preasphaltenes from coal liquefaction products, and in the spectra of hydroaromatic compounds. The CFPDMS fragmentation pattern of 1,2,3,6,7,8 hexahydropyrene (HHP) can be interpreted in rational structural terms and illustrates how the mass distribution and configuration of these ion groups is a function of the type of benzylic methylene functionalities present.

EXPERIMENTAL

Wilcox seam lignite (Martin Lake, Texas) is agitated with sonication in ten times its mass of DMSO for twenty four hours, filtered through a ceramic frit, and the solvent removed by evaporation in vacuo. The tar is digested in THF for twenty four hours and the DMSO-soluble, THF-insoluble solid is removed by filtration. Solvent-free THF-soluble matter is digested in excess hexane. Solids are filtered through a ceramic thimble and extracted with hexane in a Soxhlet apparatus for six hours, then with water for twenty four hours, to remove any DMSO. Upon drying, a five percent yield (DAF basis) of asphaltene-preasphaltene blend is obtained in the form of a fine brown powder.

Liquefaction of Herron seam bituminous coal (Illinois No. 6), Pittsburgh seam bituminous coal (West Virginia) and Wilcox seam lignite (Texas) is carried out in tetralin under hydrogen at 400° C. THF-soluble matter is digested in benzene and filtered to obtain preasphaltenes. Benzene-soluble matter is extracted with hexane to yield oil-free asphaltenes.

CFPDMS spectra are taken by methods described previously (9,10).

CFPDMS SPECTRAL RESULTS

The periodic positive ion groups in the mass range 150 to 400 amu are commonly seen in the CFPDMS spectra of coal derived asphaltenes and preasphaltenes. Representative examples are shown in Figure 1. The groups occur with a mass periodicity of from 12.1 to 14.1 amu, and are most apparent in the region from 200 to 350 amu. Mass centroids of these groups are very nearly the same in all samples examined, including the pure hydroaromatic compounds. Average masses of these centroids are listed in Table 2. These masses are very similar to those of analogous FIMS ions obtained from other coal products (7,8). It is significant that these ion groups usually appear at the top of a broad envelope of ions extending from 200 to 500 amu, the high mass downward slope of which is devoid of ion groups. An additional analogy with the FIMS coal spectra is the more intense ion groups below 200 amu. The composite ions could be interpreted as several families of compound group classes of the form $C_nH_{2n-z}O_y$, the populations of which result in apparent mass periodicities of less than fourteen. The CFPDMS spectra of pure hydroaromatic compounds suggests that an alternate explanation must be considered

Figure 2 shows the 150 to 500 amu range of the positive ion CFPDMS spectrum of HHP (MW 208). Fourteen ion groups appear between 152 and 340 amu. The first five groups are large, consisting of the parent ions and its fragments. Higher mass ions are smaller, and from expansions of the spectrum (Figure 2) it is apparent that the ion groups fall at approximatly the same masses as the asphaltene ions (Table 2). The parent ion group (200-208 amu) consists of a benzyl cation type ion at 207 amu, its unsaturated analogs at 205 and 203 amu, and the pyrene cation radical at 202 amu. Most probable structures are shown in Table 1. The latter ions are derived by facile dehydrogenation, for which hydroaromatic compounds are well known (2). Ion groups at lower masses correspond to the extrusion of carbon and hydrogen from the skeleton, as methylene, methine or carbon chains. Fragment masses imply that the extrusions are accompanied by rearrangement, dehydrogenation and/or intramolecular recombination to produce ions isomeric with the most probable structures shown in Table 1. The apparent periodicity of these ion groups is nearly the same as that of the asphaltene ion groups. The smaller "postparent" ion groups - eight of them between 221 and 325 amu - appear to be recombinant ions, originating from the attack of fragment ions on the parent molecule, or on other fragments.

DISCUSSION

In a preliminary survey of the CFPDMS fragmentation behavior of coal-like compounds (6) we have screened polynuclear aromatic hydrocarbons, aromatic and aliphatic carboxylic acids, phenols, aryl ethers, monoalkylbenzenes and hydroaromatic compounds. Oxygen containing compounds invariably yield parent ions an order of magnitude more intense than their fragment ions. Hydrocarbons, such as phenyl pentadecane, dibenzanthracene and hexahydropyrene, do not fragment in this manner, but give rise to fragment ions typically half as intense as the parent ions. The periodicity of the fragment ions is rational, but quite different from that seen in electron impact ionization mass spectrometry. For example, the positive ion CFPDMS spectrum of behenic acid exhibits a series of ion groups of periodicity 14 amu (Figure 3), reflecting random cleavage along the alkyl chain (11). 1,2,5,6 Dibenzanthracene displays fragments of periodicity 13 amu (Figure 3) corresponding to successive expulsion of from one to eight methine groups from the parent structure. The fragment periodicity of alkylaromatics(including hydroaromatic compounds) is not so regular, and their intensities are of the same magnitude as the parent ions. This is a result of multiple fragmentation modes available to benzylic functionalities, and the formation of very stable benzyl cation structures, exemplefied by the fragment ions of HHP shown in Table 1.

CFPDMS fragmentation resembles that of Pyrolysis-Field Desorption Mass Spectrometry (PFDMS). The PFDMS positive ion groups of German coals (8) fall at the same masses as those shown in Table 2. Schulten attributes some of the principal ions of these groups to several series of compositions C_nH_{2n-z}. An additional similarity between PFDMS and

CFPDMS is the appearance of high molecular weight ions of periodicity 74 amu. We find that monoalkylbenzene compounds, and some coal fractions, show positive CFPDMS ions at m/z = 948 + 74 n , where n is 0 to 14. Such ions appear to be polymeric tris-fused triphenylene structures formed in the pyrolytic environment in which the ions are devolatilized (6). Ions of these same masses have also been seen in Schulten's study (8).

The coincidence of the masses of the asphaltene ions with those of HHP and other hydroaromatics leads us to conclude that the CFPDMS technique is detecting hydroaromatic and other benzylic functionalities among the disparate coal components. A supporting observation is the presence of smaller recombinant ions in the spectrum of HHP which appear at masses above that of the parent. This is a general feature of the CFPDMS spectra of hydroaromatic compounds. In the asphaltene spectra, individual recombinant ions are not seen. The variety of hydroaromatics in the sample gives rise to a broad envelope of ions, superimposed by the larger fragment ions. The feature is very obvious in the FIMS spectra (12) of coal liquids. The configuration of the individual ion groups contains information reflecting the population of extant hydroaromatic molecules.

Organic CFPDMS ions have been detected up to 1200 amu in many coal derived products, yet the ion groups described in this report do not appear at masses above 600 amu. These ion groups have not been detected in the CFPDMS spectra of hexane-soluble coal products, because many other intense ions interfere. They are definitly absent from the CFPDMS spectra of DMSO-soluble, THF-insoluble fractions. A working hypothesis is that as hydroaromatic components condense into high molecular weight crosslinked molecules during coalification metamorphosis, their benzylic character is lost.

ACKNOWLEDGEMENTS

Support from the Gas Research Institute, the Robert A. Welch Foundation, and the Center for Energy and Mineral Resources is gratefully acknowledged.

REFERENCES

1 Derbyshire, F. J.; Varghese, P. and Whitehurst, D. D. "Synergistic Effect between Light and Heavy Solvent Components during Coal Liquefaction": Fuel 61, 859 (1982)

2 Stephens, H. P. and Chapman, R. N. "The Kinetics of Catalytic Hydrogenation of Pyrene - Implications for Direct Coal Liquefaction Processing": Preprints Amer. Chem. Soc. Div. of Fuel Chem. 28 (5), 161 (1983)

3 Mochida, I.; Tamaru, K.; Korai, Y.; Fujitsu, H. and Takashita, K. "Carbonization Properties of Hydrogenated Aromatic Hydrocarbons - III Modifying Activities of Hydrogenated Pyrene and its Oxidized Derivitives in the Co-carbonization of Coals and Coal Liquids": Carbon 21 (1), 535 (1983)

4 Weinberg, V. A. and Yen, T. F. "Mesophase Formation in Coal Liquid Solvent Fractions": Carbon 21 (1), 39 (1983)
5 Institute of Gas Technology "Coal Gasification Support Studies Subtask 1-1, Effect of Process Variables on the Initial Coal Gasification Reactions": Final Report, DOE/MC/14705-T5, May 1982
6 Zingaro, R. A.; Macfarlane, R. D. and Zoeller, J. H., Jr. "Application of Unconventional Solvents and Cf-252 Plasma Desorption Mass Spectrometry in Studies of Coal": Annual Report to the Gas Research Institute, March 1984
7 Bodusynski, M. M.; Hurtubise, R. J. and Silver, H. F. "Relationship between Solvent-Derived and Compound-Class Fractions in Coal Derived Distillates and Vacuum Still Bottoms": Fuel 63(1), 93 (1984)
8 Schulten, H-F "Pyrolysis-Field Desorption Mass Spectrometry of Coal": Fuel 61, 670 (1982)
9 Macfarlane, R. D. "Californium-252 Plasma Desorption Mass Spectrometry, Large Molecules, Software, and the Essence of Time": Anal. Chem. 55(12), 1247A (1983)
10 Macfarlane, R. D. and Torgerson, D. F. "Californium-252 Plasma Desorption Mass Spectrometry": Science 191, 920 (1976)
11 Zingaro, R. A.; Vindiola, A. G. and Zoeller, J. H. , Jr. "Fragmentation in Cf-252 Plasma Desorption Mass Spectrometry 1. Positive Ions of Behenic Acid": Int. J. Mass. Spectrom. Ion Phys. 53, 349 (1983)
12 Chen, C-H B. and Durai-Swami, K. "Characterization of Controlled Flash Pyrolysis Coal Liquids": Preprints Amer. Chem. Soc. Div. Fuel Chem. 27 (3-4), 292 (1982)

Table 1: Most probable structures of the main positive CFPDMS fragment ions of 1,2,3,6,7,8 Hexahydropyrene, shown in Figure 2

MASS		MASS	
207		179	
205		178	
203		176	
202		165	
191		163	
189		152	

Table 2: Mean mass centroids of CFPDMS positive ion groups exhibited by asphaltenes and hexahydropyrene in the mass range 150 to 370 amu.

151	224	299
167	237	311
179	250	323
191	263	337
201	275 (irregular)	349
212	284	361

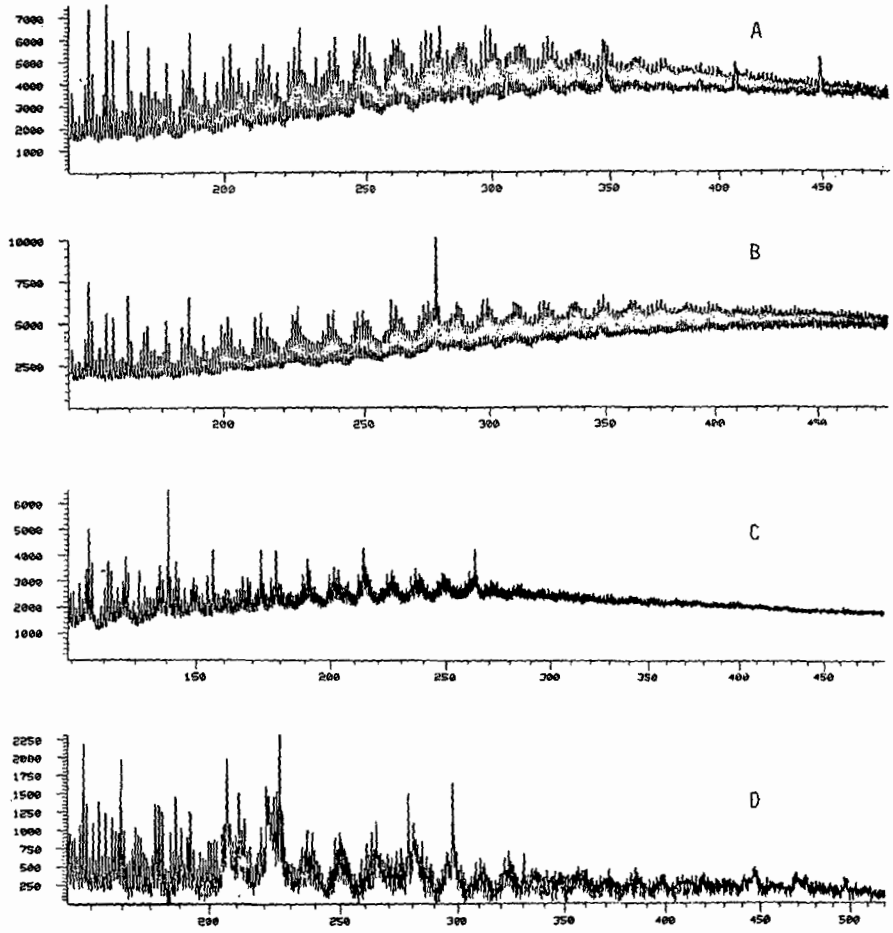

Figure 1: Positive CFPDMS ion groups of Coal derived Asphaltenes in the mass range 150 to 500 amu. A - Illinois No. 6 liquefaction asphaltene, B - Pittsburgh Seam Bituminous Coal liquefaction asphaltene, C - Wilcox Seam Lignite, native asphaltene-pre-asphaltene blend, D - Wilcox Seam Lignite liquefaction preasphaltene.

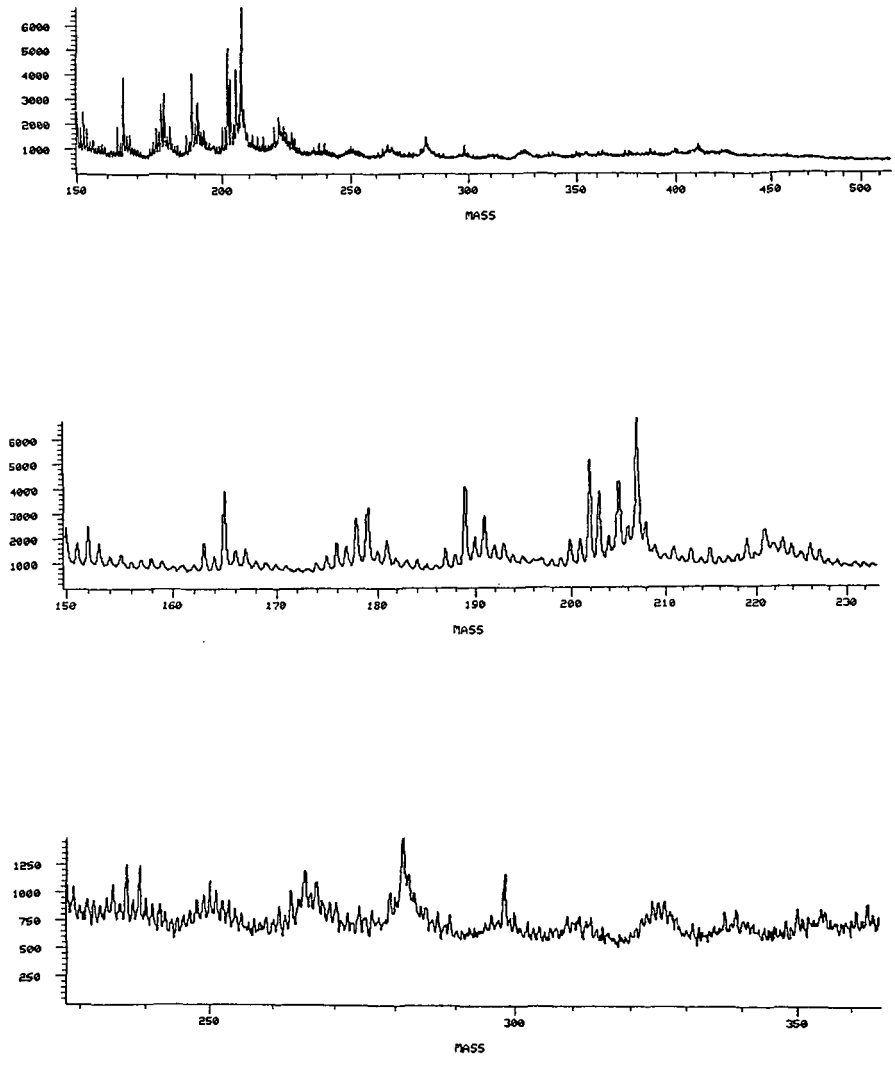

Figure 2: Positive ion CFPDMS spectrum of 1,2,3,6,7,8 Hexahydropyrene in the mass range 150 to 500 amu. Vignetts show detail of fragment ions (150 to 208 amu) and recombinant ions (220 to 340 amu).

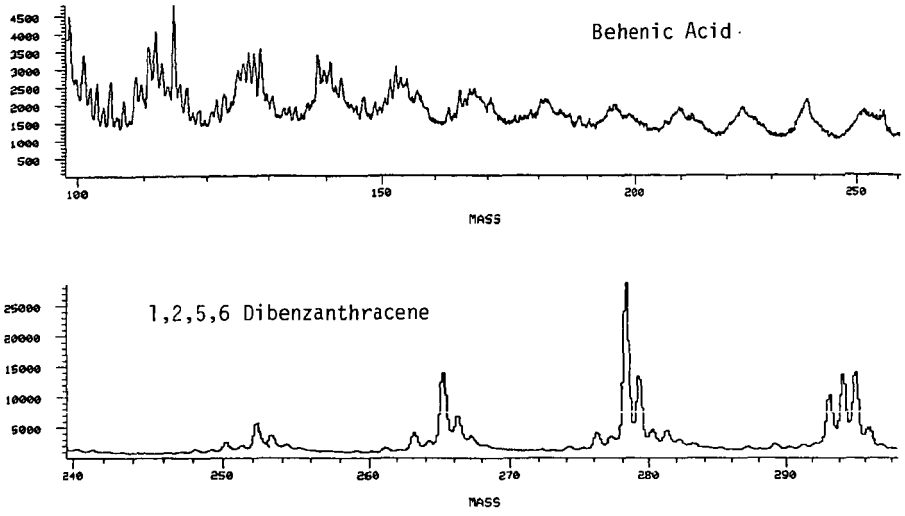

Figure 3: Periodic positive CFPDMS ion groups. Periodicity 14 amu fragments from cleavage of alkyl chain of Behenic acid (Top), and periodicity 13 amu methine extrusion fragments of Dibenzanthracene (Bottom). The Dibenzanthracene spectrum shows the parent ion at 278 amu and an oxygenated impurity at 294 amu.

CHANGES IN ASPHALTENES AND PREASPHALTENES WITH REACTION CONDITIONS AND EFFECTS ON COAL STRUCTURE

C.L. Knudson, R.J. Baltisberger, N.F. Woolsey, and W.G. Willson

University of North Dakota Energy Research Center
Box 8213, University Station
Grand Forks, North Dakota 58202

Asphaltenes (A) and preasphaltenes (PA) have broad chemical compositions because they are solubility fractions. Detailed separations by Baltisberger, et al. (1) of the A and PA fractions and detailed analyses (over 100) of samples produced at 12 different liquefaction conditions have provided a better definition of what chemical parameters most affect their solubility. Relating the A and PA changes to coal liquefaction operating conditions indicates that a key factor in upgrading these materials is to decrease their phenolic content. The changes in hydrogen content and distribution in asphaltenes observed when operating with H_2 or $CO-H_2$ (syngas) indicated CO was more effective in hydrogenating aliphatic positions in asphaltenes than H_2 gas. The change in hydrogen distribution has implications concerning coal structure (both lignites and bituminous coals) and initial coal decomposition mechanisms.

Experimental

The continuous process unit (CPU) used to produce the A and PA material has been described elsewhere (2). The A and PA fractions were separated from samples obtained from twelve different continuous process unit (CPU) tests performed at the University of North Dakota Energy Research Center (UNDERC). Nine tests were made with Beulah (B3) lignite, one with Big Brown (BB1) Gulf Coast lignite, and two with Powhattan (POW1) bituminous coal. Five tests were single-pass with coal and solvent; three of these five tests were at 400°, 440° and 460°C operating temperatures and a gas flow rate of 0.5 scfm of syngas using a continuous stirred tank reactor (CSTR) while two were at gas flow rates of 0.5 and 1.1 scfm at 460°C using an open tubular reactor. Seven tests were bottoms recycle tests at nominally 460°C and at operating pressures of 2000 to 4000 psi. Operating conditions have been previously reported (1). During CPU operation, a coal-solvent slurry (preheated to 200°C) and reducing gas (preheated to 300°C) was fed to a continuous stirred tank reactor (CSTR) or an up flow open tubular reactor (OTR). Thus, most of the heating to reaction temperatures occurred in the reactor. The redistribution of the feed to product streams is depicted in Figure 1. All streams were sampled after each bottoms recycle pass (4 h) or single pass test period (6 to 12 h) and extensively analyzed. In single pass operation a 40% coal and solvent slurry was passed once through the system. In bottoms recycle, the major portion of product slurry (PS) and usually the light oils (LO) were recycled as solvent for the next pass. Total insolubles including ash and insoluble organic matter (IOM) increase. These remain nearly constant after about ten passes due to the removal of PS not required for use as solvent. The amount of coal fed was 30 wt% of the feed slurry (FS). Only product slurry analyses will be considered in this paper.

Product Slurry Analysis. Product slurry was collected in a 1 gallon can during the last hour of a test period or pass. The contents of the can were shaken in a paint mixer (single pass) or transferred to a Waring blender and blended (bottoms recycle). After mixing, the material was rapidly split into small sample containers and the remainder returned to storage. Settling was not a problem except when distillate solvents were employed in a single pass run. The validity of analysis techniques using microgram quantities was verified by repeated analyses. Samples

were analyzed in duplicate or triplicate to define major product fractions. Water was usually 1% to 3% of the PS and was determined by Karl Fischer titration. Tetrahydrofuran (THF) insolubles were determined by dissolution of a sample in excess THF at ambient conditions and filtration through a 0.5 micron, Teflon, Millipore filter. Distillation residue (MDR) was determined by microdistillation of less than 0.5g at 250°C, 1 Torr for 0.5 h. Ash was determined by initially driving off volatile organics at about 200°C followed by ashing at over 800°C in a muffle furnace. The THF soluble portion of the MDR defined the soluble residue (SR) yield. The quality of the SR was routinely determined by high pressure liquid chromatography (HPLC) gel permeation chromatography (GPC) of the THF soluble fraction of the MDR (3). GPC provided the molecular weight (MW) distribution profile of the SR. Also, the GPC ratio of the absorbance at 254 nm of the exclusion peak or shoulder near 950 MW to the absorbance at 250 MW provided an index value to the amount of high MW material in the SR.

Asphaltenes. The product slurry stream samples were separated into A and PA fractions by exhaustive extraction using toluene and THF. Then each fraction was separated by molecular weight (MW) using Bio Beads -Sx-3 into narrower MW fractions (1). The MW fractions were each analyzed for carbon, hydrogen, nitrogen, sulfur, and phenolic hydroxyl (OH) content. The average MW was determined by vapor phase osmometry. Proton NMR analyses were performed to determine the hydrogen distribution as:

H_{ar} - hydrogens attached to aromatic carbon atoms,
H_a - hydrogens attached to carbons which are attached to an aromatic ring (benzylic hydrogen), and
H_o - hydrogen on carbon at least one carbon atom away from an aromatic ring or in an alphatic hydrocarbon (aliphatic hydrogen).

Single Pass Solvents. The CPU once through tests with the CSTR used an anthracene oil (AO1) purchased from Crowley Tar Products spiked with 10% tetralin while tests with the OTR used AOD1 solvent, which was a distillate fraction of AO1. The solvent analyses have been presented elsewhere (4, 5). Neither AO1 or AOD1 solvent contained any THF insolubles and would therefore not interfere with the preasphaltene analysis unless incorporated into that fraction during processing. The amount of hexane insolubles in the single pass solvents was only 1.28 wt%. In addition, this portion showed a uniform low absorbance value from 2000 to 100 g/mole as indicated in Figure 2. Assuming the low absorbance is consistent with a small concentration there should be no major contribution to the average molecular weight determined by VPO analysis of the asphaltene fractions of the SR samples.

The MDR of AO1 amounted to 8.05 wt% and was entirely soluble in THF. The GPC MW distribution of this material was bell shaped (Figure 2) with minimum values at 950 and 250 MW and therefore would have little influence on the GPC ratio determined for an SR.

Results

Coal Analysis and Reactions. Ultimate and Fischer-Schroeder Assay data (provided by the Alberta Research Council) for the coals are presented in Table I. The 18 to 21 maf wt% oxygen content of the lignites was considerably higher than the 8.6 value for the bituminoua coal. For the B3 lignite about 74% of the total sulfur was retained in the ash as sulfate due to its high molar Ca/S ratio. This increased the apparent ash resulting in the calculated maf oxygen value being low. POW1 and BB1 exhibited sulfur retention of 5% and 84%, respectively. Ignoring the effects of sulfur retention, most of the oxygen in the B3 lignite was observed during 500°C assay as CO_2 and chemical water (51% and 37% for B3, respectively). For the bituminous coal, 58% of the oxygen was observed in chemical water and only 22% in CO_2. Chemical water is water produced in excess of coal moisture (cf. Table I). Typical values depending on rank have been reported for many coals (6). For 200g of

Table I. Coal Analysis

A. Elemental

Rank	Coal[a]	Moisture %AR	Ash %MF	Ultimate, wt% maf C	H	N	O	S
Lig	B3	28.90	16.32	70.10	34.50	1.04	21.60	2 76
Lig	BB1	26.51	12.57	74.05	5.42	1.32	18.09	1.11
Bit	POW1	4.80	10.61	79.96	5.74	1.39	8.59	4.31

B. Fischer-Schroeder Assay Yields, wt% maf[b,c]

Coal	Char	Total Gas	Chemical Water[d]	Tar	Light Oil
B3	66.41	18.85	8.95	4.65	1.83
BB1	63.03	16.25	8.71	9.83	1.04
POW1	69.56	7.97	5.62	15.74	0.12

Coal	Gas	H_2	CO	CO_2	H_2S	C_1-C_6	CH_4	C_2H_6
B3	18.85	0.07	1.49	15.23	0.38	1.61	0.92	0.18
BB1	16.25	0.05	1.79	11.83	0.23	2.34	1.19	0.28
POW1	7.97	0.05	0.52	1.68	1.10	4.54	2.52	0.70

[a]Dry pyritic sulfur contents were 0.63, 0.16, and 0.91, respectively.
[b]Analyses provided by the Alberta Research Council Canada, M. Selucky and M.P. duPlessis.
[c]Dry ash values were 16.75, 11.35, and 10.00, respectively.
[d]Water produced in excess coal moisture under pyrolysis conditions.

B3 coal, CO_2 evolved rapidly prior to reaching 400°C in batch autoclave tests with coal only (7). Similar rates of chemical water and CO_2 production from this coal at various temperatures was observed by Solomon (7). In coal-CO-water-solvent autoclave tests rapid CO_2 production initiated at about 360°C coincident with CO consumption and some H_2 production (8, 9). However, in slurry dried coal CO tests CO_2 was observed with CO consumption but minimal H_2 gas was observed. In rapid heat up tests with about 150g of maf lignite (triple the normal amount) to 3 moles of CO, 98% of the CO was rapidly converted to CO_2. The amount of CO consumed was found to be proportional to the amount of coal charged.

In continuous process unit operation at the UNDERC with H_2 gas, the water and CO_2 yields are similar to the assay CO_2 and chemical water yields of the coal being processed. When CO gas was present the molar amount of CO consumed approximated the quantity of feed water (coal moisture plus chemical water) consumed. In summary, the chemical water was produced rapidly at temperatures above 360°C without consuming gaseous hydrogen but rather abstraction of coal hydrogen which reduces the net available hydrogen in the coal. Loss of this hydrogen in chemical water would increase aromatization during the initial coal reactions. This net available hydrogen has been found to correlate with liquefaction conversion and pyrolysis tar yields (10). The CO results indicated that CO reacted with the chemical water or

its functional group precursor to result in the net hydrogenation of the coal structure. This necessitates the presence in coal of functional groups that can thermally decompose to produce water at temperatures as low as 360°C.

Temperature Effects - Single Pass CPU Runs. The reaction temperature has a large effect on the characteristics of the SR, PA, and A fractions and on yield structures. Conversion values of coal increased with temperatures from 400° to 460°C but decreased at 480°C for these tests. The yield results at 480°C are solvent dependent. The SR fraction exhibited a rapid and then slower decrease in over 950 MW material with increasing temperature (Figure 3) as was observed in batch autoclave tests (3). The preasphaltene fraction indicated a similar decrease in the magnitude of the exclusion peak with temperature (Figure 4). The individual PA-MW fractions all exhibited uniformly decreased hydrogen content with increasing temperature as seen in Figure 5. The range of molecular weights for the PA-MW fractions compressed from 200-3000 to 400-2000 to 500-1000 with increasing temperature (see Figure 5). This indicated that the PA material became more refractory 500-1000 MW material through the loss of lower MW material. Solvent incorporation into the lower MW PA could also result in an upward shift in MW especially at 480°C since at this temperature coal conversion decreased relative to conversion at lower temperatures.

The A-MW fractions (not depicted) obtained at 480°C had higher hydrogen content than those obtained at 460°C indicating that hydrogen rich solvent had been incorporated. The phenolic contents of both A- and PA-MW fractions obtained at 400°C changed in a parallel manner but were higher than those obtained at 460°C and 480°C. The exception was the 460°C PA-MW fractions which were even higher then the values obtained at 400°C.

Pressure Effects During Bottoms Recycle. The relationship of A and PA material can be better understood by consideration of the effects of pressure on their hydrogen and phenolic OH content. Figure 6 presents the data for the hydrogen content changes with MW for the A- and PA-MW fractions of the bottoms recycle Runs 46 and 41 at 2000 and 4000 psi, respectively. The hydrogen content of both the A- and PA-MW fractions increased at any particular MW for the higher pressure indicating the greater hydrogenation which occurs at higher pressures was similar for both A and PA material. The OH content of the PA-MW fractions was higher and parallel to those of the A-MW fractions. However, as seen in Figure 7, the OH content for the PA-MW fractions of the same MW was higher when operating at 4000 psi than at 2000 psi (the A-MW fractions behaved similarly with pressure). The higher operating pressure increased the hydrogen content, as well as the phenolic content. At higher pressures the yield structure changed, as indicated in Figure 8. At 4000 psi operation, insoluble organic matter (IOM) was less (conversion was higher), and the amounts of A and PA produced were less than at 2000 psi operation. However, increased conversion due to increased operating pressure resulted in producing A and PA that had a higher OH content. The molecular weight distribution of the SR was also higher when operating at 4000 than at 2000 psi. The phenolic content of distillates also increased with conversion (12). The higher operating pressure increased 1) conversion, 2) the hydrogen content of the A and PA, 3) the phenolic content of the A and PA, and 4) the GPC molecular weight distribution of the SR fraction.

Effect of CO on Hydrogenation of Lignite and Bituminous Coal. The influence of CO on the hydrogenation of asphaltenes derived from lignite or bituminous coal indicated that CO preferentially hydrogenated the H_o position. Table II presents the operating conditions, conversions, and SR yields for four bottoms recycle tests with and without CO for two coals. $CO-H_2$ was somewhat more effective at converting lignite while H_2 was more effective for converting bituminous coal. SR yields also varied. The GPC-MW distributions were essentially identical for the two coals when

Table II. Effect of CO on the Hydrogenation of Asphaltenes

Coal	Lignite, B3		Bituminous, POW1	
CPU Run[a]	41	45A	69	53
Feed Gas	$CO-H_2$	H_2	$CO-H_2$	H_2
Total Pressure, psi	3841	1990	2633	2006
Partial Pressure, pH_2	1563	1707	1225	1907
pCO	1604	--	1291	--
pH_2O	600	270	71	98
pLO	58	13	47	0
Flow Rates:				
Feed Gas, scfh	44	55	38	32
Feed Slurry, kg/h	2.18	2.28	2.47	2.36
Ratio, PS/FS[b]	0.782	0.793	0.787	0.832
Yield, wt% maf coal:				
Conversion	92	88	87	92
SR	21	14	22	16
Asphaltene	12.0	10.5	15.6	--
Preasphaltene	6.0	5.5	6.3	--
Ratio PS/FS[c] H/C	0.996	1.022	0.981	1.028
Light Oil H/C	1.503	1.602	1.420	1.473
Asphaltenes:				
VPO MW, g/mol	372	384	347	336
H/C	0.911	0.865	0.809	0.765
% H_{ar}	37.4	43.8	48.9	54.5
% H_a	34.1	35.4	31.7	30.0
% H_o	26.1	18.3	17.8	13.7
% H_{OH}	2.4	2.5	1.6	1.8
Preasphaltenes:				
VPO MW, g/mol	671	676	702	701
H/C	0.727	0.740	0.636	0.676
% H_{ar}	43.5	43.3	52.1	53.9
% H_a	28.3	29.2	23.9	23.3
% H_o	24.7	23.4	21.6	19.6
% H_{OH}	3.5	3.4	2.4	3.2

[a]CPU bottoms recycle operation with light oil add back except in Run 52. The light oil partial pressure in the gas phase is expressed by pLO.

[b]The ratio of flow rate of the product slurry (PS) to the feed slurry (FS).

[c]The ratio of the H/C ratio of the product slurry to that of the feed slurry.

only H_2 gas was present. When the same start up solvent was used, the MW distribution of the SR was distinctly lower over the entire run when operating with CO than without CO and seen in the B3 runs.

The partial pressures of hydrogen were higher in the runs that used H_2 gas. This resulted in greater over all hydrogenation as indicated by somewhat higher H/C values for the light oil product and for the ratios of the (H/C ratio of the product slurry) to the (H/C ratio of the feed slurry). The A and PA data on Table II indicate great similarities when operating with and without CO except when comparing the H content and the hydrogen distribution of the asphaltenes. The asphaltene fraction from each coal showed a significant increase in the H content (also the H/C ratio) and in the H_o (aliphatic hydrogen) content when CO was used. The preasphaltenes had slightly lower H content but were slightly higher in H_o content. These results indicate a tangible benefit to the presence of CO on the hydrogenation of the asphaltene fraction.

Conclusions

Asphaltene and preasphaltene data have been presented to demonstrate the effect of temperature, pressure, and reducing gas composition on their hydrogen and phenolic content. The previous paper by Baltisberger (1) showed how the hydrogen and phenolic content of the A and PA defined whether or not a coal derived product will be classified as such. The influence of processing parameters as discussed in this paper indicates that reduction in the number of phenolic functional groups and cracking are required to further convert asphaltene and preasphaltene material to distillates.

The influence of CO on the H_o positions of asphaltene along with the previously discussed data on CO and water reactions has a significant effect on models postulated for the original coal structure and on possible initial steps in coal decomposition. Large numbers of hydroxyl functional groups must be present in the coal which will decompose to water as low as 360°C. However, the hydroxyl groups must be primarily in aliphatics or alkyl side chains on aromatics to satisfy the increase in H_o observed in reactions where CO was present. This suggests that a dewatering reaction occurs thermally (with or without H_2 gas) as indicated in Equation 1.

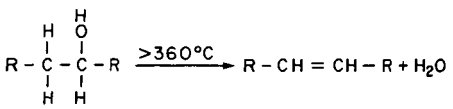

1)

Some phenolic functional groups may also decompose to water. However, hydrogenation at this position would not result in an increase in H_o content.

With carbon monoxide present, the overall reaction to hydrogenate the coal structure (without observing H_2 gas and less water products) would occur as in Equation 2.

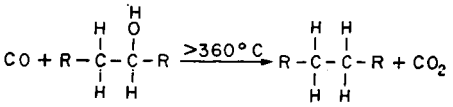

2)

The R-groups would need to activate dewatering since typical alcohols such as cyclohexanol do not decompose thermally to cyclohexene at 375°C (13). Glycols such as those found in cellulose, do decompose to water at about 360°C (14). Coal models

do not include water producing functional groups (15,16). However, these models were prepared to represent a coal model that would predict observed products (17) and are valid for reactions in H_2 gas. Also, cellulose is reported to decompose and therefore is considered to be absent. Indeed, only 0.01% cellulose was obtained by the direct extraction of a Beulah lignite (18). The presence of humic acids in coals is well documented (19). However, residual fragments of cellulose or humic acids incorporated into the coal structure may account for the presence of alcohol functional groups.

That alcohol groups are present in aromatic bridging structures was indicated in the data in this report by the decreased MW of SR when processed with CO present since after hydrogenation an aliphatic bridge would cleave easier. The rapid thermal cleavage of biphenylethane (bibenzyl) relative to the stability of biphenylethylene at liquefaction temperatures (20) is an analogous situation. The increased aliphatic hydrogen content in the asphaltene fraction when reacted with CO may also indicate that some alcohol groups were initially in the aromatic bridges. The presence of alcohol groups in long chain aliphatics has been indicated because increased yields of long chain alkanes were observed when CO was present (12).

In conclusion, the previous data has shown how operating conditions such as pressure and temperature affects the hydrogen content, phenolic content, and molecular weight range of asphaltene and preasphaltene fractions. The effects are reflected similarly in individual MW fractions of both A and PA material. The presence of alcohol groups in original coal (both lignites and bituminous coals) was strongly suggested. The preferential reaction of these alcohol groups with CO gas (but not H_2) to increase the hydrogen content of the asphaltenes, to reduce the overall MW distribution of coal, and to increase yields of alkanes indicates the beneficial effects of CO as a reductant of these functional groups which are present in both lignites and bituminous coals.

Acknowledgments

This work was performed at the University of North Dakota Energy Research Center, formerly the Grand Forks Energy Technology Center of DOE. This paper was prepared under Cooperative Agreement No. DE-FC21-83FE60181 for the U.S. Department of Energy, Office of Fossil Energy, Morgantown Energy Technology Center and the Grand Forks Project Office.

Literature Cited

1. Baltisberger, R.J.; Woolsey, N.F.; ACS Div. of Fuel Chem. Preprints, 1984, Aug. (submitted).
2. Willson, W.G.; Knudson, C.L.; Baker, G.G.; Farnum, S.; Severson, D.E.; Owens, T.C.; Souby, M. Proc. 1981 Lignite Symposium; San Antonio, June 1981.
3. Kundson, C.L.; Shiller, J.E.; Ruud, A.L. in "Organic Chemistry of Coal"; Larsen, J.W., Ed.; ACS SYMPOSIUM SERIES NO. 71, American Chemical Scoeity: Washington, D.C., August 1977, pp. 301-316.
4. Farnum, S.A.; Farnum, B.W.; Bitzan, E.F.; Willson, W.G.; Baker, G.G. Fuel 1983, 62, 799.
5. Knudson, C.L.; Farnum, B.W., in preparation.
6. Gomez, M.; Goodman, J.B., Bureau of Mines Report of Investigation 5009, 1953.
7. Solomon, P.R.; Hamblen, D.G.; Carangelo, R.M., Report by Advanced Fuel Research, April 22, 1981.
8. Sondreal, E.A.; Knudson, C.L.; Shiller,. J.E.; May, T.H. Proc. 1977 Lignite Symposium; DOE GFFETC/IC-77/1, pp. 129-158.
9. Knudson, C.L.; Willson, W.G.; Baker, G.G. ACS Div. of Fuel Chemistry Preprints, 26(1), 1981, p. 132.
10. Knudson, C.L.; duPlessis, M.P.; in preparation.

11. Willson, W.G.; Knudson, C.L.; Baker, G.G; Owens, T.C.; Severson, D.E., "Application of Liquefaction Process to Low-Rank Coals", Proc. 1979 Lignite Syumposium; Grand Forks, May 1979.
12. Farnum, S.A., private communication.
13. Reddy, P.A.; Stenberg, V.I., submitted.
14. Morita H.; Rice, H.M. Anal. Chem. 1955, 27, 336.
15. Whitehurst, D.D. in "Organic Chemistry of Coal"; Larsen, J.W., Ed.; ACS SYMPOSIUM SERIES NO. 71, American Chemical Society: Washington, D.C., August 1977,pp. 1-36.
16. Sondreal, E.A.; Willson, W.G.; Stenberg, V.I. Fuel 1982, 61, 925.
17. Wiser, W.; private communication, 1981.
18. Olsen, E.; private communication.
19. Fowkes, W.W. "Some Characteistics of Natural and Coal-Derived Humates: with Bibliography", DOE/GFERC/IC-75/1, NTIS, 67 pages.
20. Stenberg, V.I.; Van Buren, R.; Raman, K.; Knudson, C.L., "Process Chemistry of Direct Liquefaction of Lignite with Hydrogen and Carbon Monoxide", Penn State Short Course, June 1981.

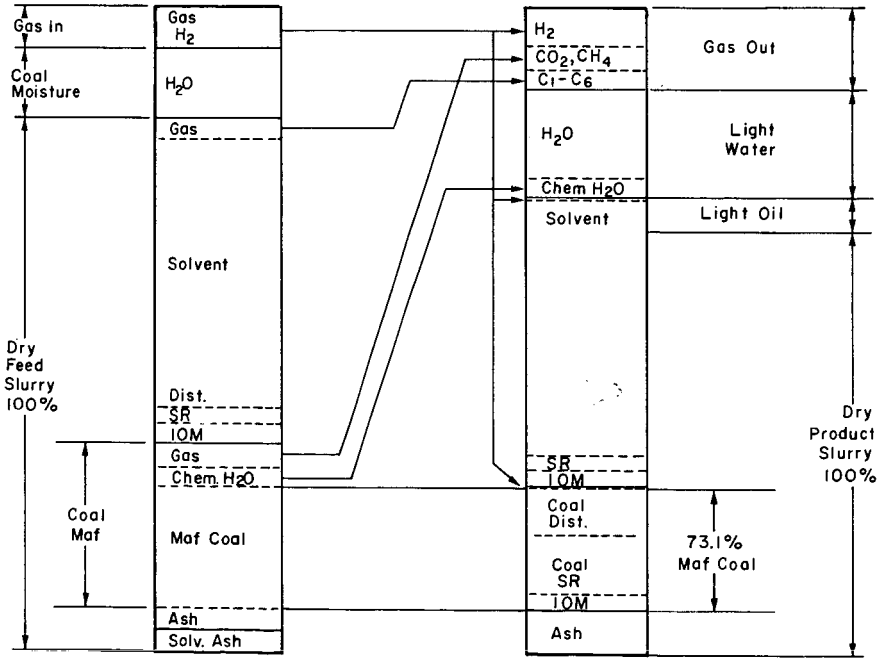

Figure 1. Redistribution of Continuous Process Unit feed streams to product streams.

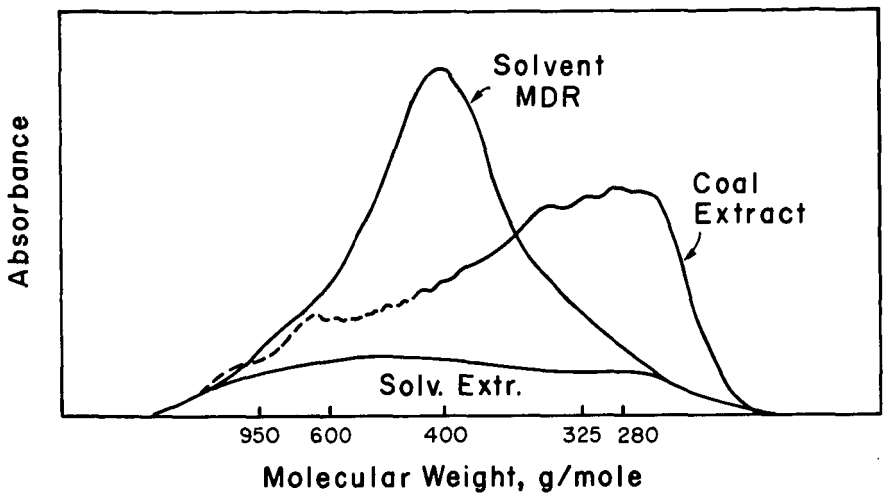

Figure 2. HPLC-GPLC molecular weight distribution of SR (Solvent MDR) and asphaltene fraction (solvent extract) of the solvent AO1. Asphaltene extracted from a coal-solvent slurry (coal extract) is also depicted.

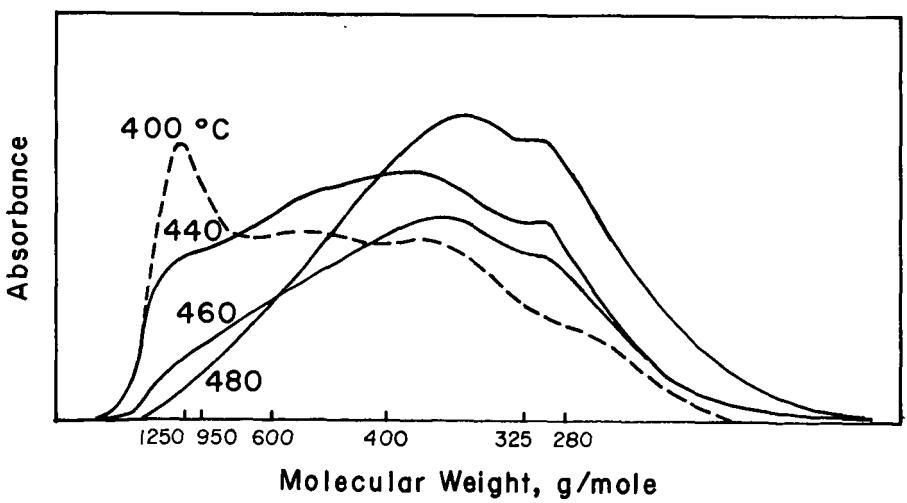

Figure 3. Changes in the MW distribution of SR with CPU operating temperature.

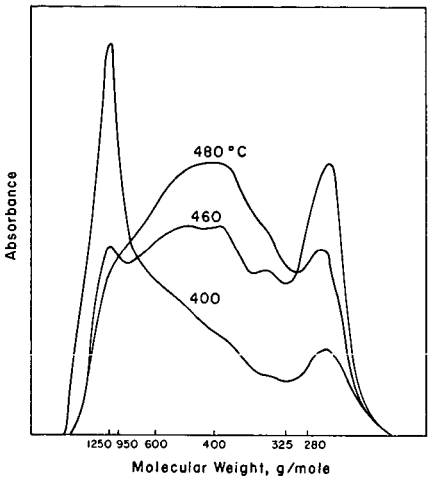

Figure 4. Changes in the MW distribution of the preasphaltenes with CPU operating temperature.

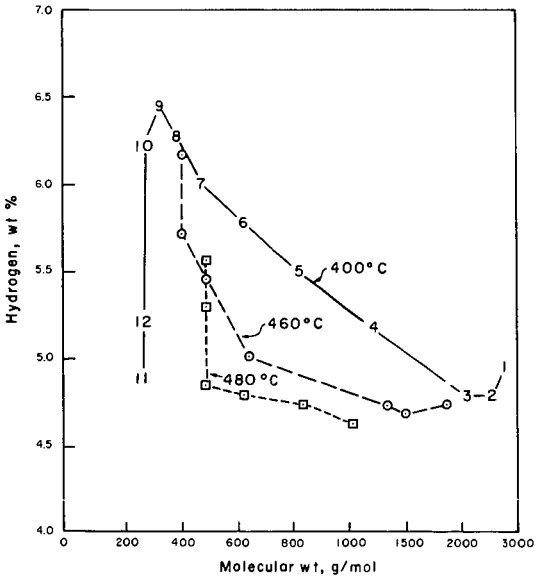

Figure 5. Changes in the hydrogen content of preaaphaltene MW-fractions with CPU operating temperature.

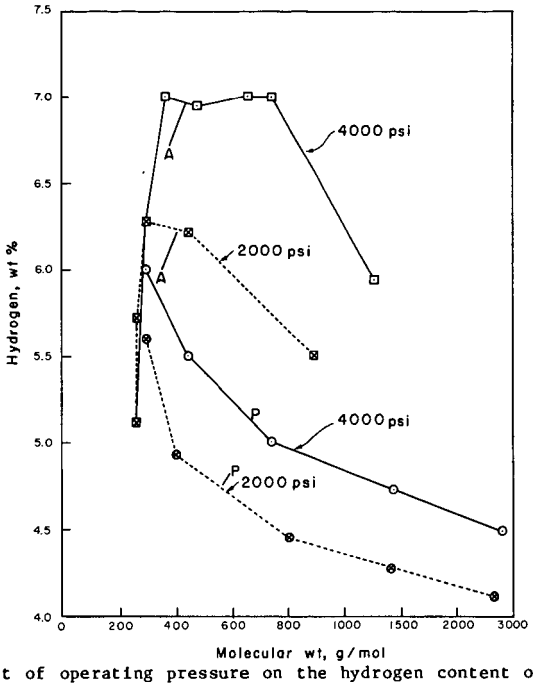

Figure 6. Effect of operating pressure on the hydrogen content of asphaltene and preasphaltene-MW fractions. Data for unseparated samples is indicated by A for asphaltenes (⊡,⊠) and P for preasphaltenes (⊙,⊗).

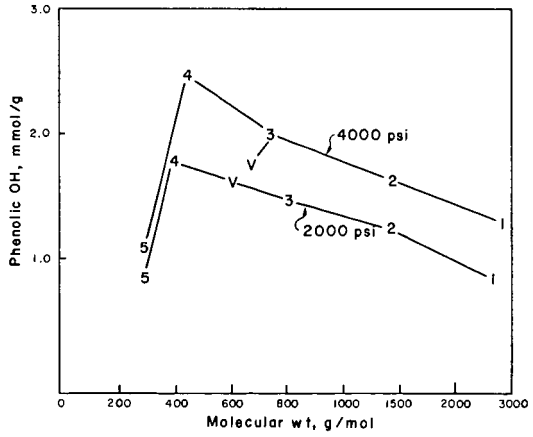

Figure 7. Effect of operating pressure on the OH content of preasphaltene-MW fractions. Unseparated sample data is represented as V.

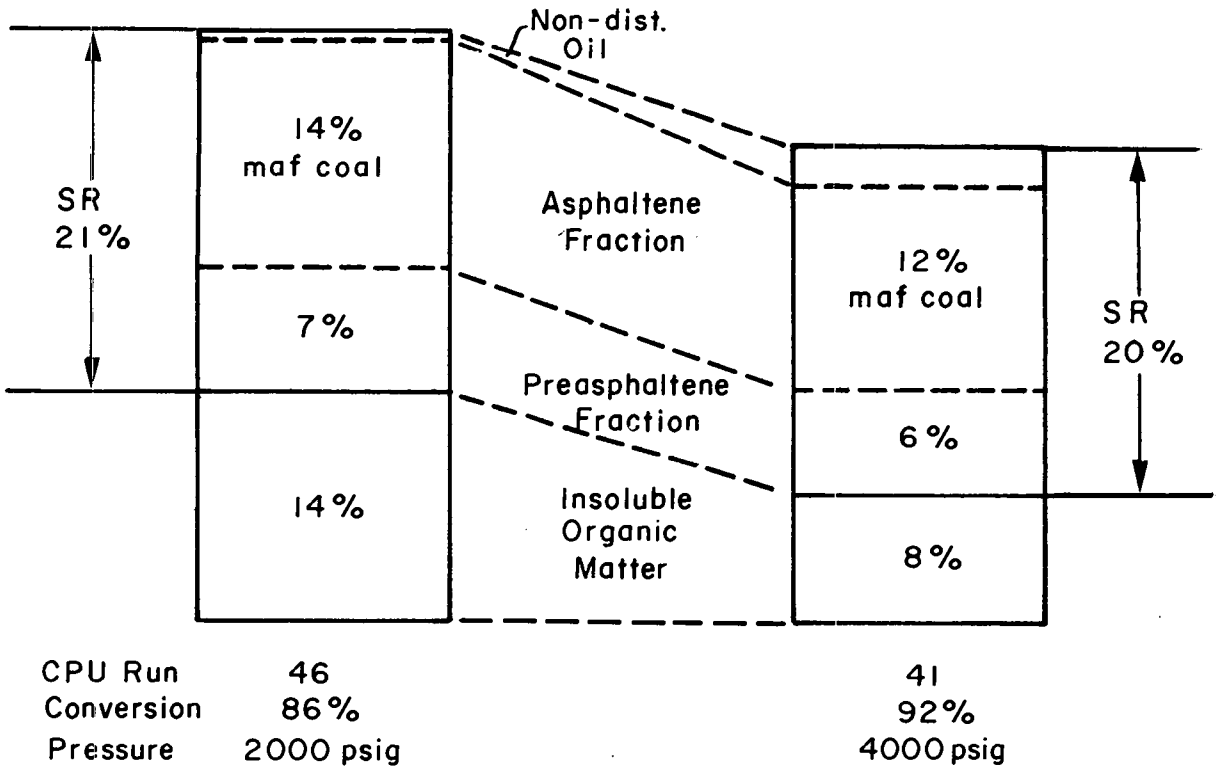

Figure 8. Effect of operating pressure on the yield structure.

SOLUBILITY PARAMETER RELATIONSHIPS BETWEEN LIGNITE DERIVED ASPHALTENES AND PREASPHALTENES

R.J. Baltisberger, N.F. Woolsey, J.F. Schwan, G. Bolton and C.L. Knudson

Department of Chemistry and University of North Dakota Energy Research Center, University of North Dakota, Grand Forks, North Dakota 58201

INTRODUCTION

In addition to the distillable products a sizeable portion of the low rank coal liquefaction products fall into asphaltene and preasphaltene categories. Asphaltenes are generally defined as those components in petroleum or coal liquids which under specific extraction conditions are soluble in benzene or toluene but insoluble in pentane or hexane (1,2). Preasphaltenes are those components that are soluble in pyridine or tetrahydrofuran but are insoluble in benzene or toluene. Farcasiu et al. (3) proposed the name, asphaltols, for this latter class of compounds because of the polyfunctional nature of these materials. In their work it was concluded asphaltenes are primarily monofunctional compounds while preasphaltenes are polyfunctional as determined by comparison of selective elution sequential chromatographic fractions and model compounds using thin layer chromatography (3,4). Preasphaltenes are formed in the initial stages of coal liquefaction where their formation may be responsible for the high viscosity of the products and for other processing difficulties (5). The preasphaltenes, on a weight basis, produce a viscosity about twice that for the asphaltene fraction (5).

Comparison of the structural features of asphaltenes and preasphaltenes show major differences between the two solubility categories occur with (1) their molecular weight distributions, (2) the fraction of total carbon present as aromatic carbons, (3) the fraction of total aromatic carbon present as edge aromatic carbons, (4) the fraction of oxygen present as phenolic and etheral oxygen atoms, and (5) the relative amount of hydrogen to phenolic content based on a per gram of total sample. Of all of these parameters a simple relationship of hydrogen and phenolic oxygen content has been found to establish the solubility of asphaltene and preasphaltene samples. The interrelationship between structural parameters will be discussed in this paper and in a subsequent paper (6) the relationship of these parameters to process conditions will be discussed.

EXPERIMENTAL

Liquefaction samples were obtained from the University of North Dakota Energy Research Center (formerly the Grand Forks Energy Technology Center). The reactor conditions are described in Table 1. The samples were isolated into asphaltene and preasphaltene fractions using exhaustive extraction techniques with toluene and tetrahydrofuran, respectively.

The asphaltene and preasphaltene samples were further separated using a preparative scale GPC column composed of 50 mm id x 120 cm glass column packed with Bio-Beads S-X3 (200-400 mesh) styrene-divinyl benzene copolymer. Prior to GPC separation all samples were acetylated with C-14 labeled acetic anhydride in order to convert all hydroxyl groups to acetate for minimization of hydrogen bonding during GPC fractionation. Elemental analyses were performed to determine elemental composition. Oxygen was determined by difference after

correction for labeled acetate present. The phenolic hydroxyl content was measured by combustion and C-14 counting content of resulting CO_2. Number average molecular weights of the samples were measured using a Model 117 Vapor Pressure Osmometer using pyridine as the solvent at 75°C. In normal runs, 2-3 concentrations over a range of 1 to 50 g/Kg of pyridine were employed for extrapolation to infinite dilution.

RESULTS AND DISCUSSION

The chemical composition and structural features of a number of over 100 different lignite and bituminous coal liquefaction asphaltene and preasphaltene samples were measured. The overall percentage by weight of the starting coal falling into either the asphaltene or preasphaltene class and conditions of preparation are given in Table 1. In the case of the 15 and 26 series samples insufficient data are available to correct the percentages to a maf basis. The basic analytical data for the asphaltenes and preasphaltenes studied by Baltisberger et. al. (7) are summarized in Table 2. The three most significant structural factors are the molecular weight, oxygen functionality and nature of the aromatic carbons.

A. Solubility Parameter Relationships

The lignite and coal derived products were obtained over a range of temperatures from 400° to 480°C, under hydrogen or hydrogen-carbon monoxide pressures from 1500 to 4000 psi and various donor solvent conditions. The samples were fractionated into asphaltenes and preasphaltenes by solvent extraction using toluene and tetrahydrofuran (THF). The extracts were further fractionated by preparative GPC techniques. The isolated fractions were then analyzed for elemental composition, number average molecular weight by VPO using pyridine as the solvent, hydroxyl oxygen content by acetylation procedures and carbon structure by NMR techniques.

Plots of mole fraction of hydrogen; mole ratio of H/C; mole ratio of H/(C+N+O+S); mole ratio edge aromatic carbons/aromatic carbons, H_{aru}/C_{ar}; or moles hydrogen per 100 g sample were constructed versus the phenolic oxygen content in OH moles/100 g sample or mole fraction of OH. All the plots show a similar differentiation between asphaltenes and preasphaltenes as illustrated in Figure 1 for the moles of hydrogen per 100 g sample. The separation of the asphaltene (87%) and preasphaltene (84%) samples fall into two distinct regions of the graph. The portion of samples that did not fit were primarily low molecular weight preasphaltene and high molecular weight asphaltene samples. This is probably due to imperfections in the solubility separation. For example, part of the asphaltene fractions may have become trapped by adsorption processes in the preasphaltene portions during the extraction process. Steffgen et al. (1) have shown that great care must be taken during the fractionation of oil from asphaltene samples. It would be expected that great care should be exercised during the separation of asphaltene and preasphaltene samples. Equation 1 gives the fit for the dividing line added to Figure 1.

$$Z = H\% - (0.486 \pm 0.008)\ OH\ mmole/g - (4.47 \pm .02) \quad (1)$$

Asphaltenes samples lie above the line giving positive Z values while preasphaltene samples give negative values. Samples which fit the wrong category are indicated by an X under the VTRA column of Table 2. The best differentiation occurred for the plot of molar density of moles H/100 g (wt % hydrogen) versus moles OH/100 g. Parameters which include parts of the total

data or terms calculated from parts of the data gave more mixing of the asphaltene and preasphaltene points. The most mixing occurred for H/C (Figure 2) or H_{aru}/C_{ar} (Figure 3) versus moles OH/100 g plots. Less mixing occurred for H/(C+N+O+S) while the best differentiation resulted when moles H/total sample wt were used. Correlation coefficient values (r values) computed using an IBM statistical analysis package are presented in Table 3. Overlap of the distinct regions shown in Figures 1 through 3 increased with the decreasing correlation of the parameter with mole fraction of hydrogen. Phenolic oxygen content have essentially with no linear correlation with hydrogen content for asphaltene samples while preasphaltene samples show some correlation (see Figure 4).

For the dissolution of a compound, A, into a solvent; the molar solubility

$$A(solid) \rightleftarrows A(liq) \qquad (2)$$

of A is a function of the activity coefficient, γ_A, where K° would be the

$$\text{Solubility} = S = \frac{K^\circ}{\gamma_A}$$

thermodynamic solubility constant for equation 1. From solubility parameter theory for regular solutions the activity coefficient, γ_i, for a solute i dissolving into solvent j is given by Equation 3 (8), where δ is the value of the Hildebrand solubility parameter of the solvent or solute and V_i is the

$$RT\ln\gamma_i = V_i(\delta_i-\delta_j)^2 \qquad (3)$$

molar volume of the solute. For maximum solubility the activity coefficient should approach unity and thus it is desirable to have $\delta_i = \delta_j$. The rule of thumb used in organic chemistry is that 'like dissolve like'. The solubility regions defined by Figure 1 suggest that the ordinate, hydrogen to other elements, is a function of the π and dispersive interactions of the coal matter while the abscissa, mmoles OH/g, is a function of the hydrogen bonding. Clearly the total hydrogen and hydroxyl contents are decisive parameters for establishing the benzene or THF solubility of the coal materials.

Equation 3 predicts an increase of the solubility activity coefficient with increasing molar volume of the solute. Several attempts were made to include V_i in the correlations by plotting log (H/C + MW) or log (H/C + MW/10) versus the acidity of the samples. This approach always mixed the asphaltene and preasphaltene regions. Asphaltenes and preasphaltenes have considerable overlapping of the molecular weights although on the average the total preasphaltene sample is several hundred grams/mole higher for the same process. We observed for all series of preasphaltene samples obtained from the same process conditions that the molecular weight increased as the H/C mole ratio decreased (see Figure 4). The molecular weights of each fraction of the preasphaltenes and asphaltenes from runs 46 and 32 are shown on Figure 4 so the overlap of the molecular weight ranges can be observed. Asphaltene samples show that molecular weights are virtually independent of the H/C ratio and that the acidity changes occur in no reproducible way. The major difference shown in Figure 4 is the removal of phenolic oxygen when going to recycle conditions (run 46) as opposed to those without bottoms recycle (run 32). Other oxygen is also lowered by the recycle conditions although this factor is not apparent in

the figure. The molecular weight data for Figure 4 is given in Table 4. This behavior is representative of all the samples when individual runs are compared. Because of the different molecular weight relationships for asphaltene and preasphaltene samples, it is not surprising that molecular weight terms can not correlate directly in the solubility plots such as Figure 1.

Plots of the mole fraction of hydrogen or H_{aru}/C_{ar} versus acidity are not as effective in defining the solubility regions as is the graph of mole fraction hydrogen. A major contributing factor in these correlations is due to the relationship between aromaticity and condensation and the carbon to hydrogen mole ratio. The fraction of aromatic carbons is defined by equation 4

$$f_a = \frac{C/H - (H^*_{al}/2)}{C/H} \tag{4}$$

where C/H is the carbon to hydrogen mole ratio and H^*_{al} is the mole fraction of aliphatic hydrogens in the sample as determined by NMR measurements (9). The condensation is represented by the number of hypothetical edge aromatic carbons (H_{aru}) per total aromatic carbons (C_{ar}) as defined by equation 5,

$$H_{aru}/C_{ar} = \frac{H^*_{ar} + H^*_{al}/2 + (OH + 2\ O)/H}{F_a(C/H)} \tag{5}$$

In equation 5, H^*_{ar} corresponds to the mole fraction of aromatic protons as determined by NMR and the oxygen terms are mole ratios to total hydrogen (9). The magnitude of both f_a and H_{aru}/C_{ar} are determined to a large extent by the C/H ratio. However, the solubility of a molecule must be determined by additional factors as well as the percentage and condensation of the aromatic carbons.

Oxygen comprises 4 to 8% of the sample by weight and is 40 to 70% phenolic depending on the solubility category. Table 5 shows the percentage of oxygen as phenolics and ethers. For most of the recycle samples preasphaltenes contain 40-50% of the oxygen as phenolics while asphaltenes are 60-75% phenolic. On the other hand, non-recycle conditions lead to nearly equal amounts of etheral and phenolic oxygen for both asphaltene and preasphaltene samples. Only the phenolic content of the samples is taken into account in the abscissa. The ether content undoubtedly has an influence on the size, shape and π-π interactions of the aromatic systems. Thus, the inclusion of oxygen content with the ordinate better correlates the dispersive, size, shape and π-π interactions of the molecules. Another factor influencing solubility would be the nature of the aliphatic carbons. Liquefaction under hydrogen alone tends to produce asphaltenes and preasphaltenes with (shorter average aliphatic chain length) than do hydrogen-carbon monoxide systems (10). Lacking inclusion of a specific term for the length of the aliphatic chains, the influence of aliphatic carbons is best taken into account using the total moles of hydrogen in the abscissa. Nitrogen contents are generally small and evenly distributed, except for a sizeable fraction of low MW preasphaltenes that had appreciably higher values. Sulfur contents are also small and both asphaltene and preasphaltene contents appear to respond similarly to processing condition.

CONCLUSIONS

Comparison of the total fractions of the preasphaltenes and asphaltenes of the same process show the following.

First, preasphaltene samples increase in the fraction of aromatic carbons and degree of condensation with increasing molecular weight. Asphaltenes samples, on the other hand, increase in the fraction of aromatic carbons with decreasing molecular weight. The degree of condensation maximizes at high and low molecules weight values.

Second, asphaltene samples have lower f_a and higher H_{aru}/C_{ar} values than the preasphaltenes. Asphaltenes contain fewer condensed aromatic molecules than do the preasphaltenes.

Third, the phenolic acid content is lower for the asphaltene samples in general. This acidic property works in combination with the total hydrogen content to ultimately determine into which solubility category a sample may fall.

Fourth, Table 3 shows that the recycle preasphaltene samples contain a higher percentage of oxygen and much of that is due to increased other (non phenolic) oxygen, possibly in ethers. Recycle asphaltene samples contain about 60-70% phenolic oxygen, while preasphaltenes contain 40-50% phenolic oxygen. Non-recycle conditions lead to higher total oxygen contents of both categories and to nearly the same distribution between asphaltene and preasphaltene samples. Recycling of the vacuum bottom leads to an etheral oxygen removal. This is probably one reason for the success of the plot of mole fraction of total hydrogen versus phenolic content rather than the plot of H_{aru}/C_{ar} versus phenolic content gives a better separation of asphaltene and preasphaltene samples. The mole fraction of the hydrogen term takes in account the oxygen content of the sample further separating the regions of Figure 1.

Fifth, molecular weight ranges of the two categories overlap. When a number of samples within a narrow range was examined, one observed that the majority of the preasphaltenes lie in a range from 600 to 2500 g/mol while the asphaltenes lie between 300 to 600 g/mol. Preasphaltene samples increased in phenolic content with decreasing molecular weight (see Figure 4). Asphaltene samples show random phenolic content with molecular weight. However, inclusion of the molecular weight directly in a solubility plot similar to Figure 1 was not successful.

For the lignite process samples studied, the differentiation of the asphaltene and preasphaltene samples follow equation 1 rather well for over 80% of the samples. Hydrogen and phenolic content seem to be the only parameters needed to specify into which solubility category the hexane insoluble portions (non distillable) of a lignite liquefaction process may lie. The implication is that it is desireable to lower the phenolic oxygen content while raising the H/C mole ratio during liquefaction.

ACKNOWLEDGEMENT

This research was supported by DOE through contract number DE-AB18-78FC02101.

REFERENCES

1. Steffgen, F.W.; Schroeder, K.T.; Bockrath, B.C. Anal. Chem. 1979, 51, 1164-1168. Steffgen, F.W.; Schroeder, K.T.; Bockrath, B.C. ibid, 1979, 51, 1168-1172.
2. Mima, M.J.; Schultz, H.; McKinstry, W.E., In "Analytical Methods for Coal and Coal Products", C. Karr, Ed.; Academic Press: New York, 1978; Vol I, Chapter 19, pp 557-568.
3. Farcasiu, M.; Mitchel, T.O.; Whitehurst, D.D. ACS Fuel Division Preprints 1976, 21 (7), 11-26.
4. Farcasiu, M. Fuel 1977, 56, 9-14.
5. Bockrath, B.C.; LaCount, R.B.; Noceti, R.P. Fuel 1980, 59, 621-626.
6. Knudson, C.L.; Willson, W.G.; Baltisberger, R.J.; Woolsey, N.F. ACS Fuel Division Preprints 1984, 29, following this article.
7. Baltisberger, R.J.; Stenberg, V.I.; Klabunde, K.J.; Woolsey, N.F. Final Report, The Chemistry of Lignite Liquefaction, DOE/FC/02101-23, July, 1983.
8. Karger, B.L.; Snyder, L.R.; Horvath, C. "An Introduction to Separation Science", Chapter Two, Wiley: New York, 1973.
9. Brown, J.K.; Ladner, W.R. Fuel 1960, 39, 87-96.
10. Farnum, S.A. Private communication.

Table 1. Asphaltene and Preasphaltene Yields and Continuous Process Operating Conditions

Sample	Yield, wt % maf Coal Asphaltenes[a]	Preasphaltenes[a]	Conversion	Gas	Gas Flow scfh	Press, Psig	Temp, °C	Coal[b]
Bottoms Recycle Operation[c]								
44-12[d]	9	5.0	92	$CO-H_2$	52	1978	458	B3
46-16[e]	14	7.0	52	$CO-H_2$	52	2013	458	B3
41-14	12	6.0	92	$CO-H_2$	44	3841	459	B3
45-15	10.5	5.5	88	H_2	55	3934	461	B3
58-15	11.3	5.7	95	H_2	41	2651	459	BB2
53-18	NA	NA	92	H_2	32	2006	469	POW1
69-12	15.6	6.3	87	$CO-H_2$	38	2633	458	POW1
103-17[f]	NA	NA	96	$H_2S-CO-H_2$	38	4050	438	ZAP2
Single Pass Operations[c]								
15-2[g]	(9)	(9.5)	NA	$CO-H_2$	27	4000	404	B3
26-7[g]	(7.8)	(6.4)	85	$CO-H_2$	28	3825	463	B3
26-11[g]	(8.3)	(5.3)	81	$CO-H_2$	29	3890	483	B3
32-3[h]	9.8	6.2	82	$CO-H_2$	32	3765	450	B3
34-4[h]	24	16	87	$CO-H_2$	70	4020	459	B3

[a]Yields in parenthesis are percentages of total SRL or SRC. Insufficient data is available to convert the number to a maf basis.

[b]Beulah and Indianhead are B3 and Zap2 Great Plains lignite samples; Big Brown is BB2 Gulf Coast lignite sample; and Powhattan is POW1 bituminous coal sample.

[c]Bottoms recycle utilized the product slurry containing ash, insolubles, and SRL as solvent for the subsequent pass in an open tubular reactor. Single pass utilized an anthracene oil and coal were passed through the reactor once (see DOE/GFETC/QTR-78/T4, NTIS).

[d]A heavy hydrogen donor (HAB1) was spiked each pass.

[e] Started up initially with a good H-donor solvent (HAB1).

[f]Feed gas ratio of CO to H_2 was 6:94. H_2S was nominally fed at 5 wt % of coal.

[g]CPU operation with a CSTR reactor and AO1-10% tetralin solvent.

[h]CPU operation with an open tubular reactor and AOD1 solvent (a distillate cut of AO1).

Table 2. Structural Features of Asphaltene Samples

RUN	PER	FRACT	WTPCT	VTRA[b]	Wt % C	H	N	O	S	MWVPO	NMR[c] OH	HTOC	HARUCAR	HAR	HAL	HOTH	Z[b]
15	2	0	100.00	.	83.75	6.09	0.81	8.15	1.21	500	1.853	0.872	0.852	36.3	48.3	12.4	0.7
15	2	1	5.33	.	81.73	6.30	0.91	9.85	1.21	2129	1.974	0.925	0.855	27.3	45.1	24.4	0.9
15	2	2	5.37	.	81.81	5.52	0.90	10.56	1.21	1510	1.986	0.809	0.671	22.3	40.3	33.8	0.1
15	2	3	8.52	.	81.61	5.86	0.77	10.54	1.22	1011	2.104	0.862	0.748	23.4	42.6	30.5	0.4
15	2	4	12.58	.	81.70	6.01	1.01	10.04	1.23	722	2.355	0.883	0.827	25.9	48.7	21.5	0.4
15	2	5	15.02	.	82.25	6.44	0.60	9.46	1.25	592	2.747	0.940	0.922	28.1	50.8	16.7	0.6
15	2	6	20.94	.	83.21	6.20	0.67	8.70	1.23	417	2.235	0.895	0.887	33.7	50.6	12.1	0.6
15	2	7	13.83	.	89.26	6.10	0.48	2.98	1.17	288	1.121	0.820	0.780	46.5	47.4	4.2	1.1
15	2	8	4.35	.	90.48	5.55	0.46	2.37	1.14	261	0.410	0.736	0.691	56.5	38.4	4.4	0.9
15	2	9	1.05	.	91.68	5.45	0.51	1.22	1.13	261	0.170	0.714	0.638	61.7	28.1	9.9	0.9
26	7	0	100.00	.	87.76	5.26	1.08	5.07	0.82	500	1.241	0.720	0.700	54.4	38.1	4.7	0.2
26	7	1	8.50	X	84.03	4.69	1.16	9.30	0.82	1663	1.231	0.669	0.640	50.1	30.6	16.6	-0.4
26	7	2	8.50	X	86.40	4.63	0.89	7.25	0.82	1104	1.241	0.644	0.608	50.8	34.2	12.3	-0.4
26	7	3	9.70	X	86.13	4.59	1.07	7.38	0.82	888	1.282	0.640	0.619	51.5	36.6	9.0	-0.5
26	7	4	9.70	.	86.25	4.95	0.87	7.10	0.83	595	1.412	0.689	0.664	50.5	37.5	9.2	-0.2
26	7	5	13.90	.	87.19	5.37	0.91	5.69	0.84	480	1.763	0.739	0.740	51.6	44.1	1.0	0.0
26	7	6	19.00	.	88.53	5.29	0.55	4.80	0.83	344	1.492	0.717	0.710	54.5	41.6	1.0	0.1
26	7	7	19.90	.	90.96	5.25	0.73	2.26	0.80	344	0.620	0.693	0.655	62.6	32.4	3.7	0.5
26	7	8	9.80	.	89.45	4.76	0.69	4.32	0.79	344	0.180	0.639	0.631	74.5	20.9	4.3	0.2
26	7	9	2.50	.	87.20	4.76	0.47	6.79	0.78	344	0.110	0.655	0.676	78.7	16.5	4.5	0.2
26	11	0	100.00	.	87.08	5.83	0.98	4.89	1.22	500	1.221	0.804	0.756	46.8	41.3	9.9	0.8
26	11	1	2.90	X	83.22	4.61	1.28	9.67	1.22	1556	1.282	0.665	0.592	37.4	36.2	23.6	-0.5
26	11	2	3.30	.	83.51	4.96	1.26	9.05	1.22	1205	1.282	0.713	0.628	37.9	35.0	24.5	-0.1
26	11	3	6.00	.	83.54	5.08	1.15	9.01	1.23	924	1.342	0.729	0.617	24.7	47.4	25.2	-0.0
26	11	4	11.00	.	84.61	5.58	1.02	7.57	1.23	690	1.442	0.791	0.694	37.1	37.6	22.8	0.4
26	11	5	15.00	.	84.74	5.61	0.88	7.51	1.25	517	1.833	0.794	0.734	38.0	42.3	16.4	0.2
26	11	6	30.00	.	86.63	5.82	0.64	5.68	1.24	353	1.602	0.806	0.804	46.4	48.4	2.5	0.6
26	11	7	14.80	.	90.70	5.65	0.17	2.30	1.18	267	0.380	0.748	0.704	56.0	39.5	3.9	1.0
26	11	8	22.30	X	91.89	5.32	0.33	1.29	1.16	261	9.000	0.695	0.662	69.9	27.4	2.6	-3.5
26	11	9	8.60	X	92.95	4.84	0.39	0.65	1.16	262	3.000	0.625	0.591	78.5	17.9	3.5	-1.1
32	3	0	97.00	.	84.35	5.95	1.22	7.93	0.55	390	2.571	0.846	0.808	40.9	39.7	15.2	0.2
32	3	1	3.10	.	83.16	5.43	2.06	8.82	0.54	1360	1.834	0.783	0.648	33.3	30.9	32.4	0.1
32	3	2	5.60	.	83.05	5.48	1.51	9.42	0.54	1540	2.043	0.791	0.697	35.3	34.2	26.8	0.0
32	3	3	6.90	.	84.04	5.77	1.48	8.16	0.55	1010	2.164	0.824	0.696	32.2	34.6	29.4	0.3
32	3	4	9.80	.	83.34	6.00	1.23	8.88	0.55	640	2.335	0.864	0.793	32.5	41.8	21.7	0.4
32	3	5	14.80	.	83.57	6.08	1.06	8.73	0.56	552	2.792	0.873	0.808	31.7	43.2	20.5	0.3
32	3	6	20.90	.	82.83	6.21	1.05	9.33	0.57	390	3.424	0.900	0.916	34.5	49.7	10.3	0.1
32	3	7	22.20	.	83.98	6.07	1.04	8.35	0.56	297	2.861	0.867	0.924	40.3	55.0	-0.0	0.2
32	3	8	12.10	.	88.94	5.72	0.91	3.91	0.52	242	0.970	0.771	0.767	56.8	41.6	-0.0	0.8
34	4	0	94.00	.	83.55	5.99	1.28	8.62	0.57	388	3.107	0.861	0.858	40.1	43.7	11.0	0.0
34	4	1	2.80	.	84.43	5.73	1.99	7.30	0.55	2330	2.221	0.815	0.614	27.8	29.6	38.7	0.2
34	4	2	5.30	.	84.58	5.68	2.06	7.13	0.55	1280	2.471	0.805	0.638	29.9	32.4	33.4	0.0
34	4	3	7.30	.	84.33	5.84	1.63	7.64	0.56	1050	2.663	0.831	0.691	31.1	34.2	30.2	0.1
34	4	4	10.80	.	84.31	6.00	1.56	7.56	0.56	765	2.969	0.854	0.736	30.5	38.5	26.1	0.1
34	4	5	16.40	.	83.93	6.18	1.38	7.93	0.57	550	3.502	0.884	0.815	31.5	42.9	20.0	0.0
34	4	6	21.70	X	83.02	6.16	1.36	8.87	0.59	374	4.377	0.890	0.909	33.7	50.9	8.3	-0.4
34	4	7	20.60	.	85.64	6.11	0.98	6.72	0.56	324	2.736	0.856	0.863	42.2	48.6	4.8	0.3
34	4	8	12.00	.	90.12	5.90	0.72	2.75	0.51	256	0.682	0.786	0.751	56.2	38.4	4.2	1.1
41	14	0	100.00	.	87.58	6.65	1.36	4.14	0.27	372	1.570	0.911	0.762	37.4	34.1	26.1	1.4
41	14	1	10.80	.	84.37	5.97	2.03	7.39	0.24	1250	1.493	0.849	0.661	29.1	31.7	36.7	0.8
41	14	2	5.40	.	85.51	7.03	1.52	5.69	0.24	740	1.532	0.986	0.691	23.2	27.8	46.9	1.8
41	14	3	7.30	.	86.09	6.98	1.43	5.28	0.21	645	1.593	0.973	0.713	23.8	32.2	41.7	1.7
41	14	4	11.40	.	85.84	6.95	1.22	5.78	0.22	470	1.842	0.971	0.784	27.5	36.0	33.9	1.6
41	14	5A	23.30	.	86.08	7.01	1.22	5.47	0.22	350	2.094	0.977	0.815	30.4	35.9	30.7	1.5
41	14	5B	28.50	.	88.37	6.30	1.25	3.87	0.21	280	0.985	0.856	0.740	42.7	35.6	20.2	1.4
41	14	5C	13.40	X	92.09	5.10	1.17	1.43	0.20	250	6.200	0.685	0.613	69.2	23.5	7.3	-2.4
44	12	0	100.00	.	88.52	5.57	0.87	4.71	0.32	378	0.962	0.755	0.694	54.2	31.0	13.1	0.6
45	15	0	100.00	.	88.68	6.39	1.17	3.48	0.27	384	1.599	0.865	0.759	43.8	35.4	18.3	1.1
46	16	0	100.00	.	90.10	5.93	1.09	2.55	0.32	333	1.136	0.790	0.704	54.5	29.2	14.4	0.9
46	16	1	9.20	.	86.34	5.51	1.53	6.39	0.23	876	1.247	0.765	0.607	40.5	24.0	33.3	0.4
46	16	2	22.90	.	87.16	6.22	1.09	5.33	0.19	431	1.464	0.857	0.727	38.9	33.6	25.1	1.0
46	16	3	25.90	.	88.69	6.27	1.17	3.66	0.21	290	1.124	0.848	0.771	47.1	37.3	13.8	1.3
46	16	4	25.60	.	91.65	5.74	0.68	1.73	0.20	250	0.399	0.751	0.697	62.5	29.8	7.0	1.1
46	16	5	16.20	X	93.37	5.06	0.64	0.73	0.20	260	5.300	0.650	0.621	81.1	15.1	3.7	-2.0
53	18	0	100.00	.	89.02	5.68	1.80	2.65	0.85	336	0.960	0.765	0.682	54.5	30.1	13.7	0.7
58	15	0	100.00	.	88.47	6.09	1.70	3.48	0.26	322	1.339	0.826	0.750	52.0	31.9	13.9	1.0
69	12	0	100.00	.	88.54	5.97	1.93	2.63	0.93	347	1.012	0.809	0.709	48.9	31.7	17.8	1.0

Table 2. Structural Features of Preasphaltene Samples

RUN	PER	FRACT	WTPCT	VTRA[b]	Wt % C	H	N	O	S	MWPO	OH	HTOC	HARUCAR	NMR[c] HAR	HAL	HOTH	Z[b]
15	2	1	15.40	.	80.47	4.95	1.59	12.42	0.56	2716	1.801	0.739	0.690	35.1	35.7	25.6	-0.4
15	2	10	1.92	X	88.58	6.21	0.53	3.77	0.90	272	0.569	0.842	0.729	42.5	37.6	19.0	1.5
15	2	11	1.25	.	75.01	4.88	0.24	18.98	0.88	272	4.400	0.781	0.913	51.7	37.7	10.5	-1.7
15	2	12	0.60	.	84.88	5.21	0.35	8.68	0.88	272	5.000	0.737	0.742	55.9	36.1	8.0	-1.7
15	2	2	26.44	.	80.50	4.78	1.40	12.70	0.61	2497	1.878	0.713	0.668	35.4	35.2	25.5	-0.6
15	2	3	17.32	.	80.36	4.79	1.31	13.54	0.00	2055	1.973	0.716	0.702	34.4	40.6	20.9	-0.6
15	2	4	7.36	.	80.04	5.14	0.98	13.31	0.53	1228	2.377	0.771	0.778	31.6	47.3	16.5	-0.5
15	2	5	7.11	.	78.48	5.52	0.95	14.53	0.52	823	2.736	0.844	0.895	31.0	50.0	14.0	-0.3
15	2	6	7.70	.	78.15	5.79	0.97	14.55	0.53	619	2.949	0.890	0.966	30.4	52.4	12.1	-0.1
15	2	7	4.27	.	78.03	6.01	1.00	14.38	0.58	459	2.944	0.924	1.023	30.9	54.4	9.9	0.1
15	2	8	6.78	X	79.57	6.26	1.12	12.06	0.99	382	2.896	0.944	0.992	31.9	49.9	13.5	0.4
15	2	9	3.85	X	82.17	6.42	0.84	9.62	0.95	314	1.919	0.938	0.905	34.9	42.3	19.9	1.0
26	7	1	8.49	.	83.86	4.74	2.01	8.85	0.54	1874	1.381	0.678	0.658	53.4	29.3	14.3	-0.4
26	7	10	2.40	.	91.68	5.69	0.31	1.69	0.63	404	2.800	0.745	0.708	65.6	30.8	3.6	-0.1
26	7	2	23.36	.	85.31	4.66	1.73	7.50	0.80	1496	1.479	0.656	0.616	50.7	31.6	14.5	-0.5
26	7	3	19.60	.	83.91	4.74	1.47	9.31	0.58	1314	1.694	0.678	0.677	55.5	29.5	11.5	-0.6
26	7	4	13.52	.	82.80	5.02	1.36	10.08	0.73	640	2.261	0.728	0.761	46.4	44.8	4.3	-0.5
26	7	5	8.40	.	82.69	5.46	1.29	10.01	0.55	488	3.037	0.792	0.831	38.9	51.9	3.6	-0.5
26	7	6	7.84	.	81.63	5.74	1.20	10.76	0.67	404	3.338	0.844	0.909	41.2	49.9	3.1	-0.4
26	7	7	6.08	.	83.98	6.03	1.09	8.18	0.72	404	3.227	0.862	0.886	41.1	48.4	5.2	-0.0
26	7	8	4.96	X	88.06	6.16	0.49	4.62	0.66	404	1.255	0.839	0.810	46.4	44.4	7.2	1.1
26	7	9	4.96	X	90.61	6.05	0.32	2.38	0.64	404	0.205	0.801	0.746	55.3	37.4	7.0	1.5
26	11	1	21.68	.	85.79	4.61	1.49	7.63	0.48	1039	1.021	0.645	0.623	56.8	28.9	12.1	-0.4
26	11	2	31.24	.	86.03	4.73	1.34	7.41	0.50	829	1.426	0.659	0.645	54.2	33.9	8.9	-0.4
26	11	3	22.22	.	85.67	4.79	1.35	7.70	0.49	621	1.501	0.671	0.671	54.7	35.8	6.3	-0.4
26	11	4	9.17	.	84.88	4.82	1.32	8.29	0.69	480	1.882	0.682	0.695	53.0	38.6	4.5	-0.6
26	11	5	3.03	X	84.81	5.54	0.93	8.06	0.67	480	0.985	0.784	0.799	55.5	37.0	5.7	0.6
26	11	6	1.86	X	90.56	5.56	0.36	2.87	0.65	480	0.212	0.736	0.696	62.2	31.5	5.9	1.0
26	11	7	0.78	.	91.23	5.28	0.23	2.61	0.64	480	3.900	0.695	0.666	71.1	24.0	4.8	-1.1
26	11	8	0.15	.	91.32	5.27	0.61	2.15	0.64	480	3.200	0.693	0.645	74.0	16.2	9.7	-0.8
32	3	0	97.00	.	83.22	5.06	2.16	8.99	0.57	588	3.115	0.730	0.721	40.8	43.2	9.9	-0.9
32	3	1	16.20	.	83.78	4.53	2.30	8.85	0.54	1320	1.912	0.649	0.564	39.8	29.7	26.3	-0.9
32	3	2	19.90	.	83.38	4.70	2.40	8.97	0.55	1800	2.376	0.677	0.647	42.2	38.8	14.0	-0.9
32	3	3	13.30	.	82.37	4.95	2.15	9.97	0.56	837	2.935	0.721	0.696	41.8	35.8	16.5	-0.9
32	3	4	12.40	.	83.01	5.07	2.39	8.93	0.59	648	4.374	0.732	0.747	42.7	43.0	5.7	-1.5
32	3	5	13.00	.	81.25	5.36	1.94	10.86	0.58	570	3.714	0.792	0.839	45.3	42.0	5.7	-0.9
32	3	6	11.30	.	80.25	5.56	1.88	11.72	0.59	397	4.179	0.831	0.888	40.2	45.2	7.1	-0.9
32	3	7	8.80	.	76.52	6.04	1.95	14.91	0.59	290	4.053	0.946	1.046	33.6	47.1	12.6	-0.4
32	3	8	2.70	X	83.95	6.25	2.53	6.72	0.55	241	2.291	0.893	0.804	34.6	40.4	21.4	0.7
34	4	0	97.00	.	83.49	5.07	2.15	8.73	0.56	612	2.824	0.729	0.715	41.2	43.0	10.2	-0.8
34	4	1	13.60	.	83.58	4.55	2.73	8.61	0.53	2020	1.616	0.653	0.550	37.4	30.5	28.5	-0.7
34	4	2	24.30	.	83.58	4.72	2.44	8.72	0.54	1780	1.925	0.677	0.600	39.5	33.1	23.3	-0.7
34	4	3	13.90	.	82.98	5.03	2.57	8.88	0.55	940	2.525	0.727	0.694	39.8	40.9	14.2	-0.7
34	4	4	12.20	.	82.50	5.18	2.26	9.50	0.56	690	2.957	0.753	0.738	38.7	43.4	12.2	-0.7
34	4	5	12.60	.	81.24	5.30	1.96	10.92	0.57	470	3.187	0.783	0.804	39.6	44.7	9.7	-0.7
34	4	6	9.80	.	80.53	5.40	2.00	11.49	0.57	390	3.545	0.805	0.848	37.8	48.2	7.5	-0.8
41	14	0	100.00	.	85.27	5.17	1.98	7.35	0.24	671	1.790	0.727	0.631	43.5	28.3	24.7	-0.2
41	14	1	21.40	.	86.72	4.47	1.56	7.03	0.21	2850	1.321	0.619	0.530	47.8	24.0	25.2	-0.6
41	14	2	16.60	.	85.00	4.73	2.01	8.05	0.21	1420	1.603	0.667	0.590	45.2	28.0	23.5	-0.5
41	14	3	26.10	.	84.48	5.02	1.91	8.44	0.15	740	2.010	0.713	0.661	44.5	33.4	18.1	-0.4
41	14	4	24.10	.	83.96	5.51	1.81	8.50	0.22	430	2.492	0.788	0.744	41.5	37.3	16.6	-0.2
41	14	5	11.80	X	86.90	6.02	1.65	5.23	0.21	290	1.102	0.831	0.679	42.2	26.6	29.3	1.0
44	12	0	100.00	.	87.76	4.90	1.44	5.69	0.21	600	1.540	0.670	0.621	58.8	23.5	14.6	-0.3
45	15	0	100.00	.	85.58	5.28	1.57	7.42	0.15	676	1.783	0.740	0.649	43.3	29.9	23.4	-0.1
46	16	0	100.00	.	88.48	4.85	1.44	4.80	0.44	608	1.604	0.657	0.609	59.0	25.5	12.2	-0.4
46	16	1	15.50	.	87.64	4.12	2.03	6.07	0.14	2650	0.808	0.564	0.531	69.5	12.0	16.6	-0.7
46	16	2	14.40	.	87.16	4.28	1.90	6.48	0.18	1420	1.232	0.589	0.551	61.7	19.6	15.9	-0.8
46	16	3	23.10	.	86.52	4.46	1.81	6.99	0.21	806	1.426	0.619	0.584	57.7	24.6	14.6	-0.7
46	16	4	25.60	.	86.64	4.93	1.58	6.69	0.16	390	1.777	0.683	0.650	54.7	29.7	12.0	-0.4
46	16	5	21.30	X	87.29	5.60	1.41	5.49	0.21	290	0.861	0.770	0.695	54.2	25.9	18.4	0.7
53	18	0	100.00	.	85.80	4.55	2.28	6.51	0.87	701	1.433	0.636	0.568	53.9	23.3	19.6	-0.6
58	15	0	100.00	.	86.68	5.05	2.50	5.62	0.15	620	1.804	0.699	0.631	53.8	25.0	17.6	-0.3
69	12	0	100.00	.	86.56	4.88	2.47	5.16	0.93	702	1.177	0.676	0.584	52.1	23.9	21.6	-0.2

Table 2. Structural Features of 103[a]

					Wt %									NMR[c]				
RUN	PER	FRACT	WTPCT	VTRA[b]	C	H	N	O	S	MWVPO	OH	HTOC	HARUCAR	HAR	HAL	HOTH	Z[b]
103	17	0	100.00	.	87.77	5.62	1.70	4.67	0.24	560	2.120	0.768	d	-	-	-	0.1
103	17	1	16.60	.	87.51	4.57	1.90	5.67	0.34	1600	0.690	0.627	-	-	-	-	-0.2
103	17	2	11.40	.	84.67	5.36	2.46	6.77	0.73	930	1.470	0.760	-	-	-	-	0.2
103	17	3	14.30	.	86.10	5.76	2.12	5.65	0.37	510	1.920	0.803	-	-	-	-	0.4
103	17	4	19.80	.	85.51	6.06	1.82	6.04	0.57	330	2.460	0.851	-	-	-	-	0.4
103	17	5	21.70	.	85.59	6.39	1.47	6.26	0.29	140	2.050	0.896	-	-	-	-	0.9
103	17	6	14.10	.	87.07	6.11	1.21	5.17	0.45	140	0.940	0.842	-	-	-	-	1.2

a. 103 is a total SRL containing both asphaltenes and preasphaltenes.
b. X in VTRA indicates Z = H% - 0.486(OH) - 4.67 mismatch. If Z = negative sample is a preasphaltene. If Z = positive sample is an asphaltene.
c. $H_{ar} + H_{al} + H_{OH} = 100$, sum of mole fractionof aromatic, aliphatic and phenolic protons equals 100. To obtain H_{OH} subtract $H_{ar} + H_{al}$ from 100. H_{α} equals mole percent of protons on aliphatic carbons more than one carbon unit from an aromatic ring, alpha + other protons equals total aliphatic protons.
d. Data not measured.

Table 3. Correlation Coefficients (r) Between Various Asphaltene and Preasphaltene Parameters

Asphaltenes	r value			
Parameter	H[a]	H/M[b]	H/C[c]	H_{aru}/C_{ar}[d]
H	1.0	0.996	0.943	0.56
H/M	---	1.0	0.970	0.60
H/C	---	---	1.0	0.64
H_{aru}/C_{ar}	---	---	---	1.00
OH	-0.14	-0.13	-0.100	0.03

Preasphaltenes				
Parameter	H	H/M	H/C	H_{aru}/C_{ar}
H	1.0	0.998	0.97	0.91
H/M	---	1.0	0.98	0.93
H/C	---	---	1.0	0.96
H_{aru}/C_{ar}	---	---	---	1.0
OH	0.78	0.793	0.82	0.83

a. Mole fraction of hydrogen (wt %).
b. Mole ratio of H/(C+N+O+S).
c. Molar H/C ratio.
d. Mole ratio of edge aromatic to aromatic carbon.

Table 4. Molecular Weight Values for Runs 46 and 32

Sample	Molecular Weight[a] Asphaltene	Preasphaltene
46-1	875	2650
46-2	430	1420
46-3	290	810
46-4	250	390
46-5	260	290
32-1	1360	1320
32-2	1540	1800
32-3	1010	840
32-4	640	650
32-5	550	570
32-6	390	400
32-7	300	---

[a]determined by VPO, solvent pyridine

Table 5. Comparison of Oxygen Functionality for Various Asphaltene (A) and Preasphaltene (PA) Samples

Sample	Recycle[a]	Oxygen Content mmoles/g Total O_2	Phenol	% O_2 as phenol
41 PA	yes	4.39	1.79	41
41 A	yes	2.48	1.57	63
45 PA	yes	4.42	1.78	40
45 A	yes	2.09	1.60	77
53 PA	yes	3.92	1.43	37
53 A	yes	1.61	0.96	60
69 PA	yes	3.13	1.12	36
69 A	yes	1.60	1.01	63
103 Total[b]	yes	2.91	2.12	73
32 PA	no	5.61	3.12	55
32 A	no	5.51	2.57	52
15 PA	no	7.89	2.11	17
15 A	no	5.09	1.85	36
26 PA	no	5.16	1.89	37
26 A	no	3.16	1.24	40

[a]No indicates petroleum derived solvent passed once through. Yes indicates bottom recycle solvent used.

[b]In this case asphaltene and preasphaltene sample not separated. H_2S run.

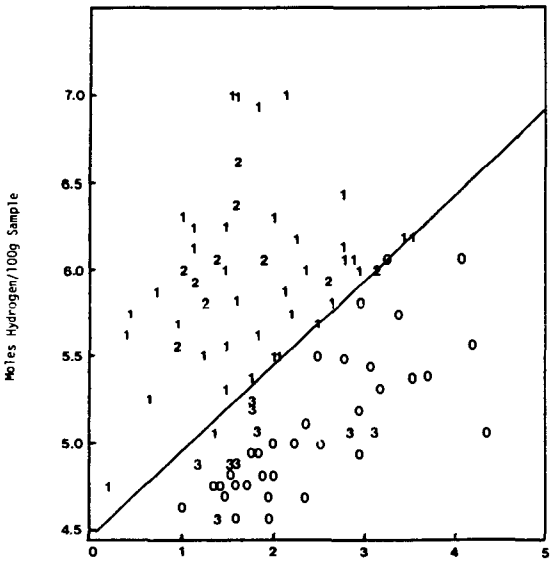

Figure 1 The hydrogen and acid content of asphaltene (1) and preasphaltene (0) fractions. Total preasphaltene (3) and asphaltene (2). Samples (unfractionated) are also plotted.

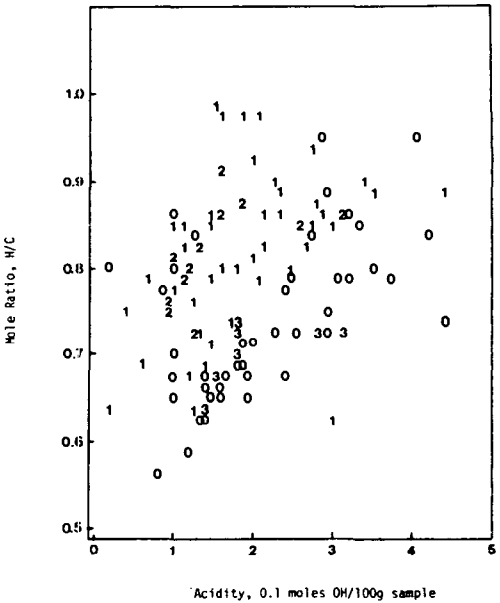

Figure 2 The relationship of H/C mole ratio to acidity of asphaltene (1), and preasphaltene (0) fractions. Total preasphaltenes (3) and total asphaltenes (2) are also plotted (unfractionated).

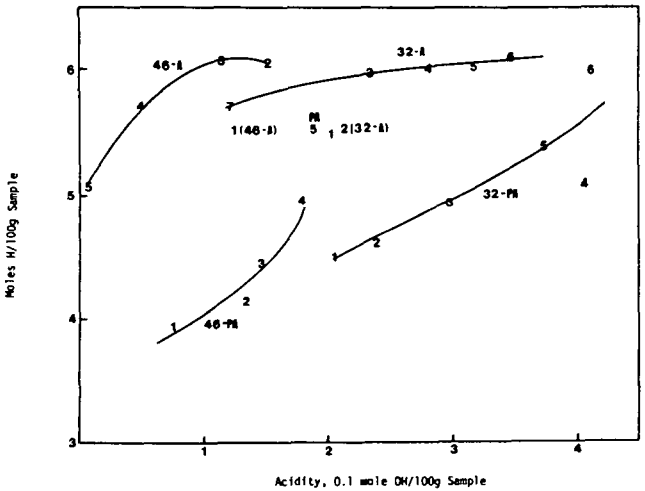

Figure 4 Hydrogen and phenolic hydroxyl dependence of Runs 32 and 46. A=Asphaltene, PA=Preasaphaltene; Molecular wt decreases with fraction number 1-7.

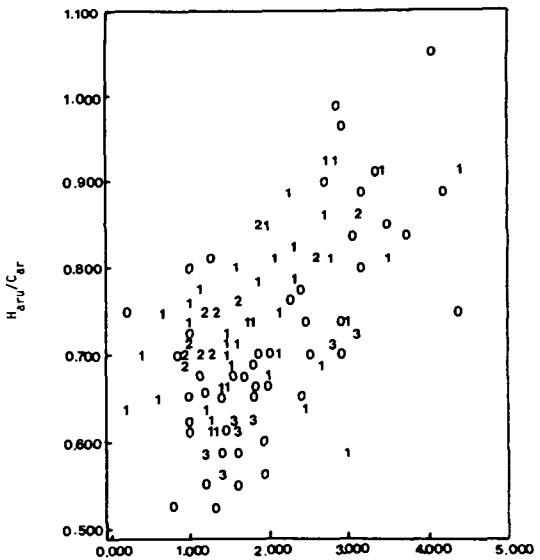

Figure 3 The degree of condensation and acidity of asphaltene (1) and preasphaltene (0) fractions. Total preasphaltene (3) and asphaltene (2) samples (unfractionated) are also plotted.

REACTIVITY OF SOME NITROGEN-CONTAINING COMPOUNDS AT SUPERCRITICAL WATER CONDITIONS

David M. Tiffany, Thomas J. Houser, Michael E. McCarville and Michael E. Houghton

Department of Chemistry, Western Michigan University
Kalamazoo, MI 49008

INTRODUCTION

The possible use of supercritical fluid extraction (SFE) of coal to produce liquids has been attracting significant interest recently. The temperatures at which SFE is generally carried out, about 400°C and above, will cause bond ruptures to occur in the coal structure. Thus, the extracting capability of the fluid is important in terms of both the intermediate products, usually involatile at these temperatures, as well as the original coal components. In addition, the fluid has the opportunity to participate as a reactant at process conditions, which may yield extracts of different compositions that will be dependent on the fluid used.

Thermodynamic consideration of SFE leads to the prediction that the enhanced solubility (volatility) of the solute has a very strong dependence on pressure (1). The enhancement may be as large as a factor of 10^4 under very favorable conditions (2). Thus, this method combines many of the advantages of distillation with those of extraction. The general advantages of SFE as applied to coal processing have been previously enumerated (1). Many of the reported studies in this area, using toluene as the fluid, have originated in Great Britain. The influence of residence time, temperature, and pressure on yield from the SFE of coal, using bench-scale and small pilot plant units has been reported (3). Economic (4) and energy efficiency (5) evaluations have indicated that SFE is competitive with most other coal conversion processes. However, despite the strong interest in SFE there has been very little reported on the basic chemistry that takes place during coal extraction by this technique.

One important function which coal processing can perform is the removal of heteroatoms to yield a cleaner product. In particular, the current program is concerned with nitrogen removal from model compounds thought to be representative structures found in coal. Studies have shown that quinoline type structures in coal liquefaction are among the most difficult to remove (6); more recent studies on catalytic hydrodenitrogenation of quinoline (7-9) have supported this assessment. Thus, experiments have concentrated on examining the reactivities of quinoline and isoquinoline; the reactivities of other compounds were studied briefly also. The selection of water as the fluid was based on several properties, in addition to solvent expense, which makes it suitable for the application of interest. Briefly, these properties are: (a) Critical temperature, 374.2°C. Theoretical considerations have shown that extract volatility enhancement is greatest when extraction is carried out near the fluid critical temperature (10). (b) Temperature and pressure dependence of the dielectric constant which will allow control of solvent properties (11). (c) High reactivity with cyanide wastes to form ammonia (12). (d) Molecular polarity since polar solvents exert a stronger depolymerizing action on coal than nonpolar ones and also increase extraction rate (1). Experimental verification of the effectiveness of water as an extracting fluid was indicated by the results reported in a study of solvent effects in supercritical extraction of coal (13); water was more effective than predicted from the theoretical calculations. The present paper discusses the results obtained to date of the treatment of several nitrogen-containing compounds and alkylbenzenes with supercritical water, including some treatments using acid catalysts to enhance reactivity. The expectation is to determine the least severe conditions at which nitrogen can be removed from several types of molecular structures.

EXPERIMENTAL

The experiments were carried out in a small (47 cc) stainless steel, batch reactor which is not equipped with a pressure gauge or gas vent. The procedure was essentially the same for all experiments. The reactor was loaded with organic compounds (usually 2.00 mL for liquids, or 2.00 grams for solids, although a few quinoline experiments had different amounts), sufficient water was added to produce the desired pressure at reaction temperature as calculated from PVT data (14), catalyst was added as needed, the reactor purged with argon and bolted closed. The reactor was placed in the preheated furnace for the required reaction time. Initial experiments used an electric furnace but times to reach reaction temperature were found to be too long, which prompted a switch to a fluidized sand bath furnace, thus reducing heating times to reach critical temperature to about 15 minutes. Following reaction, the vessel was air cooled, opened, the reaction mixture removed and the water and organic layers filtered and separated. The reactor was washed with a portion of methylene chloride solvent and a second portion of solvent was used to extract the water layer. The organic layer was combined with the solvent portions and diluted to a standard volume of 25 mL with additional solvent.

The various phases were then measured quantitatively. The remaining volume of water and the mass of the char (defined as filterable solids) were determined. A few elemental analyses of the char were obtained. The ammonia produced and dissolved in the water layer was determined for some of the experiments with an ion specific electrode. The methylene chloride solution was examined gas chromatographically for products and extents of reaction. When a component was identified, standard solutions were prepared for quantitative determinations. Some components were confirmed using GC/MS analyses. There still was a significant fraction of product that remained dissolved and/or suspended in the solvent that did not show up on the chromatograms. This was termed the tar portion. Currently, this tar is being examined more closely.

RESULTS AND DISCUSSION

Isoquinoline

The results of the reaction of isoquinoline at supercritical water conditions and with water at these conditions are summarized in Table 1. The extents of reaction are significant but their dependence on time and pressure are not entirely unequivocal. The extents appear to level off at longer times and two increases in water pressure increased reaction extents while a third gave a small decrease. However, as with quinoline, the extents of reaction and the products found are different than those from the inert pyrolysis (15). The addition of zinc chloride appears to increase extents somewhat, as does the addition of tetralin or dihydroanthracene. The hydrogen transfer agents were consumed to a large extent also, but DA did not yield products that interfered with the reactant product chromatogram and estimates from a tetralin experiment run later allowed adjustments in the product peaks to produce the yields reported.

The results which are encouraging in terms of nitrogen removal are: (a) about 35 to 55 molar % of the converted reactant is in the form of desirable aromatics, benzene and alkyl benzenes, (b) most of the converted nitrogen appears as ammonia in the water phase and (c) the char is significantly reduced in nitrogen content as compared to the reactant. Other results to note are: (a) a rise in temperature appears to produce a relative increase in lighter molecular weight products as well as increasing extents of reaction, (b) the identifiable products are formed from heterocyclic ring rupture exclusively, thus leaving the homocyclic ring primarily intact, (this may not be true for the reactions leading to the tar/char formation) and (c) the effect of the hydrogen transfer agents indicate that prereduction, followed by water treatment may improve conversions.

It should also be noted that one experiment run at 450°C and for 48 hrs. without water showed less than 10% reaction (as compared to about 50% with water) and no mea-

surable product or char was found.

Quinoline

The results of the reaction of quinoline at supercritical water conditions are summarized in Table 2. The following observations can be made when comparing these with those from isoquinoline: quinoline is significantly less reactive, thus would require a catalytic agent, except at 500°C., and the product distribution is very different yielding a smaller fraction of identifiable products which also are primarily aromatic amines, aniline, toluidine and a small amount of quinaldine. The elemental analysis of one char sample did show a reduction in nitrogen content, but it was not as large as that found for the isoquinoline sample. One interesting observation is that two catalytic experiments at 400°C. gave essentially quantitative yields of ammonia. This will be investigated further including elemental analyses of tar and char. It is evident that there is a very large fraction of product in the form of unidentified tar.

Miscellaneous Compounds

The reactivities of several other compounds with supercritical water were examined and the results are summarized in Table 3. Benzonitrile and carbazole represent nitrogen-containing compounds with different functionalities than the quinolines and these exhibited the extremes in reactivity. Carbazole appears essentially unreacted at our conditions. Benzonitrile evidently hydrolyzed, followed by decarboxylation, very quickly and cleanly, no discoloration of the reaction mixture was observed.

Ethylbenzene and aniline were included because they were observed as products which may have further degradation. Ethylbenzene did react to a small extent, again very cleanly to predictable products, benzene and toluene. Aniline reacts to a larger extent yielding only two organic products in the chromatograms. The aniline results can be considered only qualitative at this point.

Because tetralin and dihydroanthracene were consumed in the reaction with isoquinoline, they were also examined. The tetralin was completely consumed, about half of which formed naphthalene; the other half undergoes ring rupture to produce benzene and at least four alkylbenzenes. Calibrations have not been determined as yet for the two products with the longer retention times than o-xylene, but mass spectra of these are consistent with a C_3-benzene and a C_4-benzene. A tetralin experiment run for 48 hours at 450°C. without water gave only 26% reaction, 58% of which formed naphthalene. The next larger product peak had a retention time consistent with those of n-butyl- or o-diethylbenzenes (which were not present in the water reaction product). The dihydroanthracene results are only qualitative but it appears that about half is converted to anthracene. In addition, at least five other products are formed in small amounts and these have retention times between those of naphthalene and anthracene.

CONCLUSIONS

It is evident from the results that supercritical water can be effective as an active reactant in the removal of nitrogen from several organic compounds as well as influencing the mechanism of hydrocarbon degradation. The effectiveness varies with molecular structure and there are indications that acidic catalysts, e.g., zinc chloride, can improve this effectiveness. Consideration of the extents of reaction shows that isoquinoline is much more susceptible to bond rupture than is quinoline. For isoquinoline, the product distribution shows a distinct preference to rupture the heterocyclic ring, but that rupture may occur with about equal probability between the 1-2 or 2-3 positions, followed by hydrolysis and decarboxylation. The 1-2 break would lead to o-xylene, the 2-3 to ethylbenzene, which are formed in about equal amounts. These products can then undergo further sidechain shortening or elimination.

Quinoline, on the other hand, does not react as readily and although the heterocyclic ring appears to be the preferential point of attack, the rupture is more probably between the 1-2 position than the 1-9 position. This fragment would not hydrolyze, but would produce alkyl anilines which could then further react. It was found that tar formation is far more probable with this reactant. It is interesting to note that supercritical water has a profound effect on both the extent of reaction (100 vs. 26%) and reaction mechanism of even the hydrocarbon, tetralin. Further mechanistic speculation will be deferred until additional data is obtained.

REFERENCES

1. N. Gangoli and G. Thodos, Ind. Eng. Chem., Prod. Res. Dev., 16, 208 (1977).

2. J.C. Whitehead and D.F. Williams, J. Inst. Fuel (London), 182 (1975).

3. J.C. Whitehead, "Development of a Process for the Supercritical Gas Extraction of Coal," 88th AIChE National Meeting, Philadelphia, June 1980.

4. R.R. Maddocks, J. Gibson and D.G. Williams, Chem. Eng. Prog., 75, 49 (1979).

5. F.R. Benn, "Production and Utilization of Synthetic Fuels - an Energy Economics Study," Halsted Press, New York, N.Y. 1981, pp. 19-36 and 175-201.

6. H.F. Silver, "Effects of Solvent Characteristics on Wyodak Coal Liquefaction," (FE-2367-5), April 1977.

7. J.F. Cocchetto and C.N. Satterfield, Ind. Eng. Chem. Process. Des. Dev., 20, 49 (1981).

8. C.N. Satterfield and J.F. Cocchetto, Ind. Eng. Chem. Process. Des. Dev., 20, 53 (1981).

9. L.J. Boucher, N.L. Holy and B.H. Davis, "New Approaches in Coal Chemistry," Am. Chem. Soc., 1981, p. 319.

10. P.F.M. Paul and W.S. Wise, "The Principles of Gas Extraction," M & B Monographs CE/5, Mills & Boon (London) 1971.

11. E.U. Frank, Endeavour, 27 (101), 55 (1968).

12. Chementator, Dec. 25, 1972/Chem. Eng.; 20.

13. N.P. Vasilakos, J.M. Dobbs and A.S. Parisi, Preprint, Div. Fuel Chem., Am. Chem. Soc., 28 (4), 212 (1983).

14. J.H. Keenan, F.G. Keyes, P.G. Hill and J.G. Moore, "Thermodynamic Properties of Water Including Steam Tables," J. Wiley & Sons, New York, N.Y. (1969).

15. J.J. Madison and R.M. Roberts, Ind. Eng. Chem., 50, 237 (1958).

Table 1. Reaction of Water with Isoquinoline[a]

Temperature (C)	350	400						450						500
Pressure (psi)	2400	3640	3640	3870	3870	3870	3870	3580	4680	4680[c]	4680[c]	4680	5200	4700
Density (g/cc)	0.255	0.170	0.170	0.213	0.213	0.213	0.213	0.106	0.170	0.170	0.170	0.170	0.213	0.128
Time (hour)	72	48	48	48	96	144	96	48	48	48	48	120	48	48
Catalyst	$ZnCl_2$	-	$ZnCl_2$	-	-	-	$ZnCl_2$	-	-	Tet	DA	-	-	-
(g)	(.08)	-	(.05)	-	-	-	(.05)	-	-	(1.22)	(.50)	-	-	-
% Converted	34	18	54	30	50	50	57	50	42	93	58	85	81	70
Products (% of Converted Reactant)[b]														
Benzene	0	0	0	0	0	0	0.4	1.0	0.7	3.9	0	3.9	3.0	4.3
Toluene	0	5.0	6.3	10.7	8.8	14.2	10.5	17.0	24.0	16.7	9.0	21.3	21.1	16.6
Ethylbenzene	0.6	6.7	7.4	13.3	15.2	16.6	13.2	10.5	16.9	20.2	13.6	11.4	9.9	6.4
o-xylene	2.1	6.1	7.2	13.0	14.0	13.8	16.0	6.2	13.8	6.3	8.4	7.2	7.4	6.7
Ammonia	-	-	-	-	-	-	-	-	-	-	63	-	-	74
Water Recovered	-	99	92	98	98	98	-	90	99	99	90	84	90	87
Char	0	0	10.5	6.2	12.6	12.7	13.2	30.6	12.6	10.7	18.8	15.7	10.0	15.1[d]

a. An experiment run at 450C for 48 hours with no water gave greater than 90% reactant recovered and no products by GC or char.

b. Compounds are given as mole %, char as weight %. The remainder of the sample is tar and a few minor products - small peaks which appear to be aniline and toluidine were found but not measured.

c. These experiments were with added tetralin and dihydroanthracene. The extents of reaction are believed reliable but product distribution more uncertain because of consumption of hydrogen transfer agents.

d. Elemental analysis of this char gave the atom ratio $C_{21.7}\ H_{9.3}\ N_{1.0}\ O_{0.6}$.

Table 2. Reaction of Water with Quinoline

Temperature (C)	400				450						500
Pressure (psi)	3870	4020	4020	4660	4680	4680	5200	5200	5200	5200	5650
Density (g/cc)	0.213	0.255	0.255	0.426	0.170	0.170	0.213	0.213	0.213	0.213	0.170
Time (hour)	48	48	48	48	48	48	48	48	48	48	48
Catalyst	$ZnCl_2$	$AlCl_3$	$ZnCl_2$	-	-	$ZnCl_2$	-	$ZnCl_2$	$ZnCl_2$	$ZnCl_2$	-
(g)	(.05)	(.05)	(.05)	-	-	(.10)	-	(.01)	(.05)	(.08)	-
% Converted	22	60	53	27	28	81	7	15	67	54	62
Products (% of Converted Reactant)[a]											
Benzene	0	0	0	0.7	0	0.7	0	0	0.6	0.2	3.9
Toluene	0.9	0	0	0	3.6	2.6	8.6	2.7	2.5	1.5	5.3
Ethylbenzene	2.7	0	0	0	1.8	1.0	8.6	4.0	1.2	1.5	1.9
o-xylene	2.7	0	0	0	0.4	0.5	4.3	4.7	0.9	0.9	0.2
Aniline	2.3	1.2	1.7	0	4.3	6.0	14.3	4.7	7.0	9.3	8.2
Toluidene	3.2	1.2	1.5	0	5.4	3.3	8.6	4.7	3.0	4.8	3.2
Ammonia	-	96	115.	-	-	-	-	-	-	-	-
Char	7.2	13.3	5.9	0	0	6.1	0	0	13.7	-	27[b]

(a) Compounds are given as mole %, char as weight %. The remainder of the sample is unidentified minor products or tar. Quinaldine was found but not measured.

(b) Elemental analysis of this char gave the atom ratio of $C_{13.9}H_{6.9}N_{1.0}O_{0.6}$.

Table 3. Reaction of Water with Other Compounds

Compound	Benzonitrile	Ethylbenzene	Tetralin[b]		DA[c]	Carbazole[d]	Aniline[e]	
Temperature (C)	400	450	450	450	450	450	450	450
Pressure (psi)	3640	5200	5200	5200	5200	5200	5200	5200
Density (g/cc)	0.170	0.213	0.213	0.213	0.213	0.213	0.213	0.213
Time (hour)	24	48	48	48	48	48	48	48
Catalyst	-	-	$ZnCl_2$	-	-	$ZnCl_2$	-	$ZnCl_2$
(g)	-	-	(.05)	-	-	(.05)	-	(.05)
% Reacted	100	10	100	100	>50	<15	21	74
Products[a]								
Benzene	95	22	1.5	1.5	0	0	s	s
Toluene	-	78	10	7.0	0	0	0	0
Ethylbenzene	-	-	13	8.9	0	0	0	0
Naphthalene	-	-	52	45	0	0	0	0
Anthracene	-	-	-	-	ℓ	0	0	0
Diphenylamine	-	-	-	-	-	-	ℓ	ℓ
Ammonia	-	-	-	-	-	-	66	59

a. Mole % of consumed reactant. No char found for any reactant.

b. Two other chromatographic peaks with retention times consistent with indan and methylindan were found but calibrations have not been made for these yet. The largest after that of naphthalene was the indan peak.

c. The dihydroanthracene chromatogram showed about six products, all having longer retention times than naphthalene but shorter than anthracene which was by far the largest, another was benzophenone but the others have not been identified as yet.

d. Carbazole appeared close to zero % reacted.

e. Due to chromatogram anomalies, the extents of these reactions are more uncertain. The only significant organic products in the chromatograms are the two reported in relatively small and large amounts. The s and ℓ indicate small and large product peaks respectively.

NOVEL LIQUEFACTION SOLVENT: H_2O-H_2S

Virgil I. Stenberg, Robert D. Hei, Philip G. Sweeny, Jan Nowok

Department of Chemistry, University of North Dakota
Box 7185 University Station, Grand Forks, ND 58202

Warrack G. Willson

University of North Dakota Energy Research Center
University of North Dakota, Grand Forks, ND 58202

INTRODUCTION

The liquefaction solvent has two roles to fulfill: (1) a slurrying liquid for the coal which enables slurry compression into a continuous flow reactor, and (2) a hydrogen shuttler which enables the transfer of hydrogen atoms from H_2 or synthesis gas to the coal molecules. Additionally, the solvent serves as a medium for reducing gas and coal product dissolution.

We now wish to describe the use of H_2O-H_2S as a substitute for organic slurrying solvents. The philosophy for doing so is that the water fulfills the role of the slurrying liquid and H_2S is the hydrogen atom donor. Since the first bond dissociation energy of water is 118 kcal/mole, rarely, if at all, would it be expected to react with carbon radicals. On the other hand, H_2S has the first bond dissociation energy of 93 kcal/mole and the second of 83 kcal/mole making it a good but not excellent hydrogen atom donor to carbon radicals (reaction 1). At the higher temperatures of conventional coal liquefaction reactors the thermodynamics would probably be more favorable. Reaction 2 has proven to be rapid at coal liquefaction temperatures and is

$$2R^{\cdot} + H_2S \rightarrow 2RH + S \qquad (1)$$

$$S + H_2 \rightarrow H_2S \qquad (2)$$

perhaps the principal advantage of H_2S over an organic solvent. The corresponding reaction for the organic solvent is usually slow. In organic liquefaction solvents, H_2S is known to enhance liquefaction yields,[1] and it has been used for both coal and organic model compound reactions.[2]

Water becomes supercritical at 374°C and its supercritical state has the potential of influencing the liquefaction processes in several ways: it (1) becomes a fine solvent for hydrocarbons[3] (Fig. 1), (2) loses much of its ability to dissolve inorganic material (Fig. 2)[3], (3) adds to the reaction pressure, and (4) becomes more ionic (acidic and basic)[4] since the ionization constant increases by ca. 3 powers of ten (Fig. 3).[4] If water is to be substituted for an organic slurrying liquid, the increase in reaction pressure

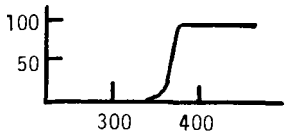

Fig. 1. Hydrocarbon solubility (wt %) in water

Fig. 2. Inorganic solubility (wt %) in water

(to ca. 5,000 psi) must be tolerated. Therefore, one must insist there be compensating factors for this pressure increase which more than make up for the cost of increased operating pressures. Batch autoclave data now indicate this is so. Indeed, water appears to have a positive effect on liquefaction yields in addition to its role as a slurrying liquid.

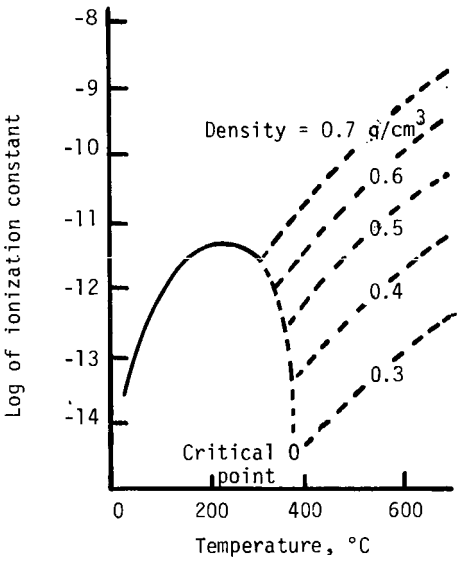

Fig. 3. Ionization constant of water in high-temperature fluids of various densities. The solid line is the experimentally determined curve for liquid water under its own vapor pressure. The estimated extrapolation of the curve to the critical point is shown as a dashed line. The other dashed lines shown calculated values of the constant for single-phase fluid water under sufficient pressure to maintain the indicated densities.

RESULTS AND DISCUSSION

The data of Table 1 compare the H_2O-H_2S results along with those using (1) a petroleum-coal based organic solvent, anthracene oil (A04) together with a solvent refined coal middle distillate from the demonstration plant at Tacoma, Washington (SRCMD) and (2) dihydropyrene (DHP), a reputedly excellent hydrogen donor solvent. Three ranks of coals are represented in the data.

Water with synthesis gas outperform A04-SRCMD with synthesis gas for the conversion of two coal samples into volatile materials at the conditions used, cf. runs 5 vs. 7 and 14 vs. 16. The presence of a small amount of H_2S enhances the as-defined yields whether in water, cf. runs 1 vs. 2, 7 vs. 8, 16 vs. 17, 21 vs. 22, 26 vs. 27 and 31 vs. 32 or in an organic solvent, cf. 5 vs. 6, 12

vs. 13, 14 vs. 15, 19 vs. 20, 24 vs. 25 and 34 vs. 35. The reactions which had the temperature programmed from 300°C to 500°C using H_2O-H_2S and synthesis gas gave the best of the aqueous-H_2S conversion yields, cf. runs 8 vs. 9, 17 vs. 18, 22 vs. 23, 27 vs. 28 and 32 vs. 33. Synthesis gas is superior to pure H_2 (980 psig), cf. runs 3 vs. 5 and 12 vs. 14.

The philosophy behind the temperature programmed reactions was the belief that the thermally produced, coal-derived radicals would be formed in a more controllable fashion, i.e., in a more steady, slower rate, within the coal-water slurry than with a sudden thermal jump to a preselected reaction temperature. The latter is assumed to momentarily deplete the hydrogen donor capacity of the solvent system at least in the vacinity of the thermal reaction events. In the case where water is the principal solvent, the hydrogen donor capacity is the H_2S concentration. The consequence of this depletion is the occurrence of retrograde reactions which result in lower conversions.

The dihydrophenanthrene (DHP) runs gave better conversions than either water or A04-SRCMD given otherwise the same experimental conditions. However, DHP decomposes to the extent of 11% at 420°C at 30 minutes, and the non gaseous products are solids rather than liquids as they are with the water runs. The water runs were the easiest to separate from the product slurry. The distillation was complete in ca. 3 hours with the water runs whereas it took from 5-7 hours to get to constant weight with the organic solvent-based runs. The oil separated by gravity from the water in the water based run distillates.

In summary, the H_2O-H_2S solvent runs with various ranks of coals give respectable yields of total volatile materials at 420°C and with temperature programming the reactor from 300° to 500°C, the yields were as good if not better than using one of the best of hydrogen donor model compound solvents. The H_2S concentration the programing rates or ranges have not been optimized.

ACKNOWLEDGMENT

We are grateful to the U.S. Department of Energy for the financial support of this study.

REFERENCES

1. (a) Stenberg, V.I.; Baltisberger, R.J.; Ogawa, T.; Raman, K., and Woolsey, N.F., Hydrogen Sulfide Catalysis of Low Rank Coal Liquefaction, ACS Fuel Division Preprints, 1982, 27(3-4), 22. (b) Stenberg, V.I.; Raman, K.; Srinivas, V.R.; Baltisberger, R.J., and Woolsey, N.F., H_2S as a Promotor for the Water Gas Shift Reaction, Angew. Chemie, Int. Ed., Engl., 1982, 21(8), 619. (c) Sondreal, E.A.; Wilson, W.G., and Stenberg, V.I., Mechanisms Leading to Process Improvements in Lignite Liquefaction Using CO and H_2S, Fuel, 1982, 61, 926.
2. (a) Gatsis, J.G., U.S. Patent No. 3 503 863 (1970). (b) Bearden, R., Jr. and Albridge, C.L., U.S. Patents Nos. 4 077 867 (1978), 4 094 765 (1978) and 4 149 959 (1979). (c) Lambert, J.M., Jr., Fuel, 1982, 61, 777. (d) Abdel-Baset, M.B. and Ratcliffe, C.T., Preprints. Div. of Fuel Chemistry, Amer. Chem. Soc., 1979, 25(1), 1. (e) Baldwin, R.M. and Viciguerra, S., Fuel, 1983, 62, 498. (f) Okutani, T., Yokoyama, S. and Maekawa, Y., Ind. Eng. Chem. Process Des. Dev., 1983, 22, 306.
3. (a) Josephson, J., Environ. Sci. Technol., 1982, 16(10), 548A. (b) Mackay, M.E., and Paulaitis, Ind. Eng. Chem. Fundam., 1979, 182), 149. (c) Johnston, K.P., Ziger, D.H., and Eckert, C.A., ibid, 1982, 21, 191. (d) Procaccia, I., and Gitterman, M., AIChE Journal, 1983, 29(4), 686. (e) Johnston, K.P., and Eckert, C.A., ibid., 1981, 27(5), 774.
4. Krauskopf, K.B., "Introduction to Geochemistry", McGraw-Hill Book Company, New York, NY, p. 496.

Table 1. The Conversion of Coals in H_2O-H_2S and A04-SRCMD

	Lignites	Reducing gases	Temperature, °C	Sovent	Conversion, %
1	Indianhead (Zap I)	CO-H_2	420	H_2O	37.4
2	Indianhead	H_2S-CO-H_2	420	H_2O	42.8
3	Big Brown (BB1)	H_2	420	A04-SRCMD	35.2
4	Big Brown	H_2S-H_2	420	A04-SRCMD	35.3
5	Big Brown	CO-H_2	420	A04-SRCMD	42.5
6	Big Brown	H_2S-CO-H_2	420	A04-SRCMD	48.1
7	Big Brown	CO-H_2	420	H_2O	43.7 ± 2.0
8	Big Brown	H_2S-CO-H_2	420	H_2O	48.9 ± 1.2
9	Big Brown	H_2S-CO-H_2	300-500	H_2O	71.0
10	Big Brown	CO-H_2	420	DHP	50.7 ± 4.4
11	Big Brown	H_2S-CO-H_2	420	DHP	65.3 ± 3.5
12	Beulah (B3)	H_2	420	A04-SRCMD	22.2
13	Beulah	H_2S-H_2	420	A04-SRCMD	29.3
14	Beulah	CO-H_2	420	A04-SRCMD	30.1
15	Beulah	H_2S-CO-H_2	420	A04-SRCMD	40.5
16	Beulah	CO-H_2	420	H_2O	33.8 ± 1.0
17	Beulah	H_2S-CO-H_2	420	H_2O	36.8 ± 0.3
18	Beulah	H_2S-CO-H_2	300-500	H_2O	51.6 ± 1.1
19	Beulah	CO-H_2	420	DHP	46.6
20	Beulah	H_2S-CO-H_2	420	DHP	53.3 ± 3.0
	Subbituminous coals				
21	Decker (DEC 1)	CO-H_2	420	H_2O	38.6 ± 0.4
22	Decker	H_2S-CO-H_2	420	H_2O	40.6 ± 1.5
23	Decker	H_2S-CO-H_2	300-500	H_2O	52.3 ± 0.7
24	Decker	CO-H_2	420	DHP	48.4
25	Decker	H_2S-CO-H_2	420	DHP	60.2 ± 8.0
26	Absaloka (ABS 1)	CO-H_2	420	H_2O	29.6 ± 0.3
27	Absaloka	H_2S-CO-H_2	420	H_2O	34.1 ± 1.1
28	Absaloka	H_2S-CO-H_2	300-500	H_2O	51.0 ± 0.7
29	Absaloka	CO-H_2	420	DHP	N.A.
30	Absaloka	H_2S-CO-H_2	420	DHP	49.6 ± 3.5
	Bituminous coals				
31	Powhattan (POW 1)	CO-H_2	420	H_2O	24.7 ± 0.4
32	Powhattan	H_2S-CO-H_2	420	H_2O	30.5 ± 0.8
33	Powhattan	H_2S-CO-H_2	300-500	H_2O	41.9 ± 0.7
34	Powhattan	CO-H_2	420	DHP	43.5
35	Powhattan	H_2S-CO-H_2	420	DHP	51.6 ± 3.5

The experimental conditions are: reaction time, 1 hour; H_2S, 250 psig; CO, 490 psig; H_2, 490 psig; coal, 1 gram; and water, 1 gram. When H_2 alone was used, its pressure was 980 psig. The conversion yields were determined by distilling the volatile material (gases and liquids) from the reactor contents at 250°C at 1 Torr for 5 hours (H_2O) and 7 hours (A04-SRCMD). The coal samples are cited from the mine site: Indianhead from the Indianhead Mine at Zap, North Dakota; Big Brown from the Big Brown Mine at Fairfield, Texas; Beulah from the South Beulah Mine, Beulah, North Dakota; Decker from the Decker Mine at Big Horn, Montana; Absaloka from the Absaloka Mine at Sarpy Creek, Montana; and Powhattan from the Powhattan Mine at Belmont, Ohio.

LOW SEVERITY CATALYTIC HYDROGENATION OF COALS IN THE ABSENCE OF SOLVENT

P. Stansberry, M-T. Terrer, F. J. Derbyshire, and D. H. Finseth*

Department of Materials Science and Engineering
The Pennsylvania State University
University Park, PA 16802

*U.S. Department of Energy
Pittsburgh Energy Technology Center
P. O. Box 10940
Pittsburgh, PA 15236

Introduction

Historically, models of coal structure have been developed on the premise that its principal characteristics can be attributed to those of a complex solid phase. Attempts to describe and portray this phase have focused on embodying measured compositional parameters into an 'average' molecule which presents a statistical representation of the whole molecular assembly. The value of such an approach is very limited particularly in its ability to describe behavioral characteristics. Furthermore, it does not take account of the existence of comparatively low molecular weight extractable liquids which are present in all except anthracitic coals (1).

In bituminous coals, the chloroform soluble materials have been shown to directly influence coal fluid properties (2-4). The role of the 'bitumens' has been suggested to be that of solvating and hydrogen-donating agents for the remainder of the coal substance (2). By analogy, it has been proposed that extractable coal liquids can provide a similar function during coal liquefaction (5). Experiments have shown that the extraction of bituminous and subbituminous coals in chloroform prior to liquefaction adversely influences the net liquefaction yield (6).

At moderate temperatures only a small proportion of coal may be extractable in solvents such as chloroform. However, it has long been recognized that by preheating the coal up to temperatures of 400°C and above, the yield can be increased several fold (2,7-8). Brown and Waters (2) concluded that the normal yield of extract is related to the accessibility of the pores to solvent, which is enhanced by preheating (swelling). Similarly, it has been found that the yields of alkanes present in benzene/ethanol solvent extracts was higher by 8-10 times in the liquefaction products of the same coals, although the distribution of the various species was very similar in both cases. It was concluded that the increased yield of alkanes on liquefaction was due to their liberation from regions of the structure hitherto inaccessible to solvent (9).

The work of Vahrman (10) has shown that in the Soxhlet extraction of coals extended for several hundred hours, the quantity of extract progressively increases, albeit at very low rates, and ultimately approaches that of the tar produced in low temperature (450°) pyrolysis. These findings are consistent with more recent suggestions to the effect that proportion of coal which is potentially extractable is much larger than is generally assumed but that it is not readily available due its being contained in closed or restricted porosity (11).

There are at least two possible sources of extractable or trapped liquids; by reactions during coalification leading to the formation and accumulation of lower molecular weight material (2); by physical entrapment of relatively unmodified components of plant origin (9,12-14). The presence of these materials in the

coal mass and their influence on its properties have promoted a number of suggestions concerning coal structure (1,2) which have been revitalized in recent years (15-17). Essentially coal is considered to comprise a relatively rigidly bonded three dimensional network which acts as a host for lower molecular weight species contained in both open and closed or partially closed pores. In effect, the structural model is that of a multicomponent system which, in the light of present knowledge, appears to be a more consistent and realistic basis for coal research than the earlier single phase concepts.

With this background, research investigations have been initiated to examine the low temperature ($\leq 400^{\circ}C$) catalytic hydrogenation of coals. The general objectives are to determine if it is possible to increase the yield of extractable liquids through the breakdown or modification of the network under mild hydrogenative conditions. Through, so doing, it is hoped i) to derive information about the structures and interactions of the 'network' and 'mobile' phases and ii) to ascertain the influence of such a pretreatment upon the behavior of coal in subsequent reactions. Earlier research has shown that low temperature chemical reduction of coals (treatment with a solution of lithium in ethylamine) can increase the H/C ratio and solubility in pyridine (18).

The approach which has been adopted follows the work of Hawk and Hitsehue (19) and Weller (20) who investigated catalytic coal hydrogenation in the absence of solvent in order to reduce the number of variables in the system and the problems of interpretation. The principal difference in the studies reported here, compared to the earlier work, is that reactions have been conducted at substantially lower temperatures and pressures.

Experimental

Coal Preparation

Samples of a bituminous coal were obtained in undried 1/2" lump form from The Pennsylvania State University Coal Sample Bank. The coals were ground, without drying to minus 800×10^{-6} m in a glove box which was first purged and maintained under pressure using a flow of oxygen-free nitrogen. The total ground product was riffled and then divided into approximately 20 gram lots which were sealed into vials while still in the glove box. The origin and analysis of the ground coals are summarized in Table 1.

The molybdenum catalyst used in these experiments was impregnated onto the coals using an aqueous solution of ammonium hepta molybdate $(NH_4)_6Mo_7O_{24}\cdot 4H_2O$ (supplied by courtesy of Climax Molybdenum, Co.). The procedure was to mix the prerequisite quantity of the molybdenum salt with the coal following which sufficient distilled water was added to form a thick slurry which was stirred for 30 minutes at room temperature. The excess water was removed by vacuum at room temperature overnight. (It was estimated that by this technique more than 98% wt of catalyst was retained on the coal.)

Reaction and Product Workings

Reactions were carried out using standard tubing bombs (20 cc capacity) constructed out of 316 stainless steel which were loaded with approximately 5 g of sample. The bombs were first purged of air several times with nitrogen and, if required, purged of nitrogen and sealed with the reactant gas to a cold pressure of 1000 psig. The bombs were heated by immersion in a preheated fluidized sandbath heater which rapidly raised the contents of the bomb to reaction temperature. Agitation was provided by oscillating the bomb through a vertical displacement of 5 cm at a frequency of 50 sec^{-1}. At the end of the reaction period, the bomb was

removed from the sandbath and quenched by immersion in water.

The excess pressure in the bomb was released by venting at room temperature during which time gas samples were collected for analysis. The reactor contents were completely removed to a predried ceramic Soxhlet thimble using chloroform as wash solvent. Soxhlet extractions were then carried out for 12 hours in boiling chloroform under a protective blanket of nitrogen. The resulting residue was dried in vacuo at 110°C for 12 hours to remove remaining solvent.

The chloroform extracts were filtered (Whatman 42 filter paper) under a nitrogen blanket and the excess chloroform removed on a rotary evaporator at 40°C. The resulting product was then further dried in vacuo for 1 hour at 110°C. The residual and extract products were sealed under nitrogen and stored under refrigerated conditions.

The total yields of chloroform soluble extract and gases were calculated from the mass of dried chloroform insoluble residue and reported as a percentage of dmmf coal. In those cases where catalyst had been added, the assumption was made that the molybdenum in the residue had been converted to a 50-50 mixture of MoO_3 and MoS_2. This assumption requires verification but any resulting inaccuracy does not affect the general trend shown in the data. The reproducibility of the total yields was found to be within 2%.

Analytical

The chloroform soluble extracts, the insoluble residues and nonextracted coals were analyzed for elemental composition. The extracts were also analyzed by ^1H n.m.r. spectroscopy (using pyridine as solvent) and by high resolution mass spectrometry (KRATOS M-50 spectrometer, resolution 1:30,000). The mass spectrometric method employed direct probe sample introduction which allows analysis of materials which are volatilized at 350°C and a pressure of 10^{-6} mm of mercury.

The parent coals and nonextracted, reacted samples were analyzed by ^{13}C n.m.r. using two independent methods to detemine differences in aromaticity; cross-polar magic angle spinning and the Bloch decay technique.(21)

Results and Discussion

Extract Yields

The total yields of chloroform extracted liquids and gases obtained under different reaction conditions are shown in Table 2 and are presented in Figure 1. It can be seen that the extract yield obtained in nitrogen increases with temperature from 0.9% at 61°C to a value of 9.2% at 400°C. The effects of heating on extract yield are consistent with those reported previously (1,2,7,8) and the value at 400°C is of the same order as has been measured for coals of similar rank (2).

More notably, at temperatures above about 325°C, the total yield is increased to some degree by the presence of hydrogen gas and more appreciably by the combination of hydrogen and impregnated catalyst. In the latter case, the yield at 400°C amounted to 43.1% of dmmf coal which is more than a factor of two higher than obtained in hydrogen alone and over four times that in nitrogen. Accurate figures for the gas make are not yet available although from preliminary estimates the quantity does not appear to be higher than about 5% dmmf coal at the maximum total yield measured. Consequently, it can be seen that by catalytic hydrogenation a substantial proportion of the coal substance has been rendered soluble and

TABLE 1

COAL ANALYSIS

Coal Identification	
Rank	Bituminous HVA
Sample Band I.D.	PSOC 1266
Seam	Ohio #5 (Lower Kittanning)
Mine	East Fairfield C
Analysis	
Moisture % a.r.	3.36
Mineral Matter % m.f.*	6.09
Elemental Analysis (dmmf)	
C	83.20
H	4.97
O (by diff)	8.64
N	2.06
S	1.35
H/C atomic ratio	0.76

*by low temperature ashing

TABLE 2

TOTAL YIELDS (CHLOROFORM SOLUBLES AND GASES) FROM BITUMINOUS COAL REACTED FOR 1 h, 1000 psig GAS (COLD)

Reaction Temperature, °C	Yield % dmmf+ Noncatalyzed	Catalyzed*
250	0.9	0.3
300	1.2	1.3
350	6.3	9.2
400	19.3	43.1

+Yields are the average of at least two results. Estimated error ±1%.

*5% Mo on a.r. coal added as ammonium hepta molybdate.

extractable in chloroform. The lesser improvement in yield found in hydrogen alone may be attributable to catalysis by dispersed mineral matter.

From these data it is not possible to ascertain whether the chloroform soluble materials realized under hydrogenative conditions are derived solely from the more efficient liberation of trapped species or whether there is some accompanying decomposition of the 'network.' Nevertheless, the high yields obtained with impregnated catalyst suggest that a proportion of the extractable products may be produced through reactions which involve breaking relatively strong chemical bonds.

Coal and Extract Composition

The coal aromaticities measured by ^{13}C n.m.r. are shown in Table 3. The results obtained by the two methods differ significantly in absolute terms, reasons for which are currently being investigated. The differences are, however, systematic and depict the same relative changes in f_a, which show that under both sets of reaction conditions the aromaticity increases. In the presence of catalyst the extent of aromatization is reduced but the net chemical reactions evidently involve dehydrogenation rather than hydrogenation.

The hydrogen contents and the H/C ratios of the coals and residues, Table 4, are consistent with the ^{13}C n.m.r. analyses. The results for the chloroform soluble extracts do not reflect the same trend, the hydrogen content of the extracts derived following reaction being similar to or higher than that from the parent coal. In the absence of gas analyses, it is difficult to draw any inference from these data, although it is noteworthy that the hydrogen content of the extracts is little influenced hy the substantial changes in yield.

The role of the added catalyst is not at all clear. Its addition results in a two-fold increase in an extractable material while apparently there is only a small effect on net hydrogenation.

Further compositional analyses of the extracts were undertaken to attempt to elucidate the function of the catalyst and the origins of the additional chloroform soluble liquids. The hydrogen type distributions by ^{1}H n.m.r. of extracts, derived from hydrogenative reactions in the presence and absence of added catalyst, were found to be virtually indistinguishable, Table 5.

A comparison of the distribution of hydrocarhon fractions of these same samples obtained by high resolution mass spectrometry (HRMS) and subsequent data reduction is shown in Figure 2. The format for this figure is simply a plot of ion intensity vs Z number class (C_xH_{2x-z}) with each Z number class ordered by carbón number. (Thus, benzenes contribute to Z=6 napthalenes to Z=12 phenanthrenes to Z=18 and pyrenes to Z=22.) The yield of hydrocarbons (as a fraction of total extract) was approximately the same for the two extracts (32% for catalyzed, 35% noncatalyzed) and the similarity of the HRMS profiles indicates that the distribution and composition of the bydocarbons is also very similar. This close correspondence of HRMS profiles was also observed for other compound classes in the extracts ($C_xH_yO_2$, C_xH_yO, C_xH_yN).

A number of minor differences were detected in all of the profiles but it is not yet known if they are reproducible or significant. A further and possibly important distinction was that in the monoxygenate profile (C_xH_yO) the extract from the catalyzed reaction showed a higher concentration of monoaromatic phenols. Examination by dispersive infrared spectrometry confirmed that this extract contained a measurably higher concentration of phenolic -OH groups. This particular phenomenon which has been noted in earlier studies of low temperature coal reduction (18) is the subject of continuing investigation.

TABLE 3

AROMATICITIES OF NONEXTRACTED COALS BY ^{13}C n.m.r.

		Reaction at 400°C, 1 h, 1000 psig H_2 (cold)	
	Parent Coal	No Added Catalyst	Mo Impregnated
f_a (CP-MAS)	0.71	0.78	0.74
f_a (Block Decay)	0.75	0.84	0.79

TABLE 4

HYDROGEN CONTENT AND H/C ATOMIC RATIO OF COALS, EXTRACTS AND RESIDUES

			Reaction 400°C, 1 h, 1000 psig H_2 (cold)	
Sample		Parent Coal	No Added Catalyst	Mo Impregnated
Coal	H wt% dmmf	4.97	4.51	5.06
	H/C Atomic ratio	0.72	0.65	0.71
Residue	H % dmmf	4.86	4.00	4.61
	H/C atomic ratio	0.71	0.58	0.63
Extract	H % dmmf	6.52	7.25	6.95
	H/C atomic ratio	1.01	1.05	1.00

TABLE 5

HYDROGEN TYPE DISTRIBUTION OF CHLOROFORM SOLUBLE EXTRACTS BY ^1H n.m.r.
(coal reacted at 400°C, 1000 psig H_2)

Sample	H_α	H_β	H_γ	H_{Ar}
No added catalyst	0.36	0.25	0.06	0.32
Mo impregnated	0.34	0.24	0.07	0.30

Overall (and excepting the possible production of phenols) although the catalyst has been found to have a major influence upon the release and/or production of chloroform soluble material, the available compositional information indicates that its mechanism is unusually subtle. The additionally extractable liquids, whether originally trapped or derived from the 'network' are very similar in structure to those generated in the absence of catalyst.

Acknowledgements

These research investigations have been conducted as a cooperative effort between the Pittsburgh Energy Technology Center and the Department of Materials Science and Engineering at The Pennsylvania State University. The authors particularly wish to express their gratitude to Charles Schmidt (HRMS) and Rich Sprecher (^{13}C n.m.r.) for their efforts in obtaining and interpreting analytical data.

References

1. van Krevelen, D. W., Fuel 1976, 44, 229.

2. Brown, H. R. and Waters, P. L., Fuel 1966, 45, 17-39.

3. van Krevelen, D. W., "Coal," Elsevier Publishing Co., New York, 1961.

4. Walters, J. G., Shultz, J. L., and Glaenzer, J. A., U.S. Bureau of Mines Report of Investigations G973, 1967.

5. Neavel, R. C., "Coal Science," Volume 1, Academic Press, New York, 1982.

6. Larsen, J. W., Sams, T. L., and Rodgers, B. R., Fuel 1980, 59, 667-668.

7. Illingworth, S. R., J. Soc. Chem. Ind. 1920, 39, 111-118.

8. Dryden, I. G. C. and Pankhurst, K. S., Fuel 1955, 34, 363-366.

9. Youtcheff, J. S., Jr., Ph.D. Thesis, The Pennsylvania State University, 1983.

10. Vahrman, M., "Chemistry in Britain," 1972, 8, 16-24.

11. Jurkiewicz, A., Marzec, A., and Pislewski, N., Fuel 1982, 61, 647-650.

12. Baset, Z. H., Pancirov, R. J., and Ashe, T. R. "Advances in Organic Geochemistry," Ed. A. G. Douglas and J. R. Maxwell, Pergaman, Oxford, 619-630.

13. Snape, C. E., Stokes, B. J., and Bartle, K. D., Fuel 1981, 60, 903-908.

14. Calkins, W. H., ACS Division of Fuel Chemistry, Preprints, Vol. 28, No. 5, 85-105.

15. Larsen, J. W., "Chemistry and Physics of Coal Utilization" (Ed. B. R. Cooper and L. Petrakis) American Institute of Physics, New York, 1980, pp. 1-27.

16. Lucht, L. M. and Peppas, N. A., "Chemistry and Physics of Coal Utilization" (Ed. B. R. Cooper and L. Petrakis) American Institute of Physics, New York, 1980, pp. 28-48.

17. Lucht, L. M. and Peppas, N. A., "New Approaches in Coal Chemistry," Amer. Chem.

Soc. Symp. Series 169, 1981, 43-59.

18. Given, P. H., Lupton, V., and Peover, M. E., Proceedings of the Conference on Science in the Use of Coal, Institute of Fuel, Sheffield, U.K., 1958.

19. Hawk, C. O. and Hiteshue, R. W., U. S. Bureau of Mines Bulletin 622, 1965.

20. Weller, S. W. (1982), Coal Liquefaction with Molybdenum Catalysts, IV Internat. Conf. on Chem. and Uses of Molybdenum, Golden, Colorado.

21. Reinhold, Michael Bruker Instruments, Inc. Personal communication.

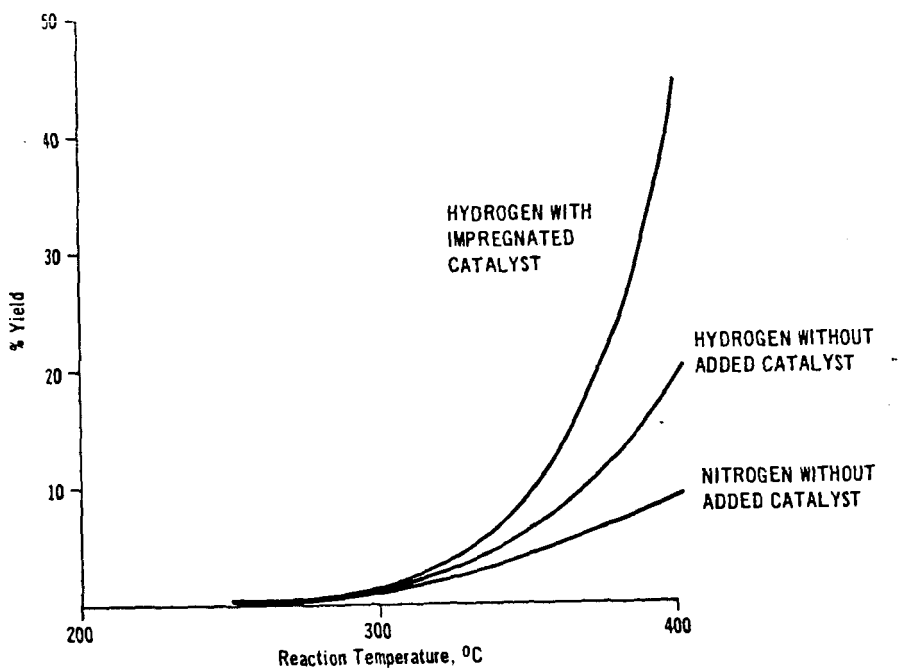

Figure 1. YIELD OF CHLOROFORM SOLUBLE LIQUIDS AND GASES AS A FUNCTION OF REACTION TEMPERATURE
(Bituminous coal, 5% M_0 *loading on* as-received coal, reaction 1h, 1000 psig cold pressure)

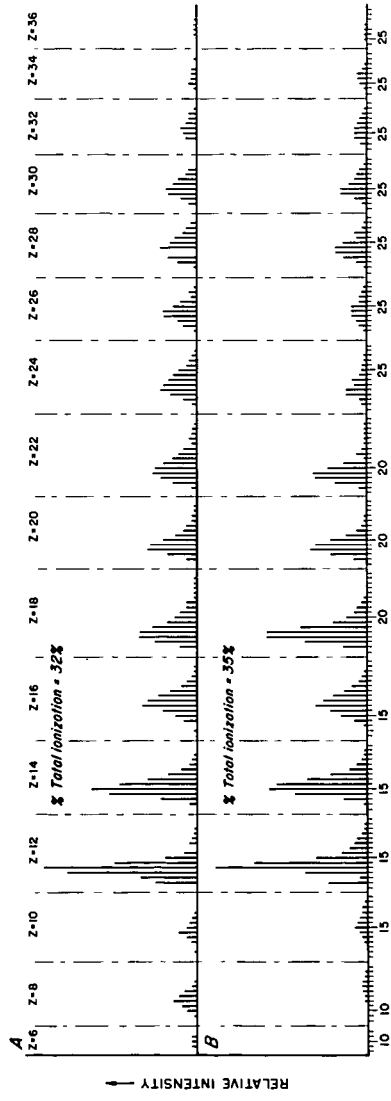

Figure 2. HRMS Comparison of CH Formulas Identified in Coal Extracts (A) Catalyzed (B) Uncatalyzed

COAL LIQUEFACTION AND HYDROGEN UTILIZATION AT LOW TEMPERATURES

B.C. Bockrath, E.G. Illig,
D.H. Finseth, and R.F. Sprecher

U.S. Department of Energy
Pittsburgh Energy Technology Center
P.O. Box 10940
Pittsburgh, PA 15236

The initial conversion of coal to material that may be extracted by polar solvents such as tetrahydrofuran or pyridine requires only relatively mild liquefaction conditions. The chemistry of the initial dissolution steps is very likely to be of great importance to the overall liquefaction process in that the yield and character of the initially formed products may greatly influence the success of subsequent liquefaction steps. Although conversion to the initial products seems to require a minimum of bond breaking, hydrogen-deuterium exchange reactions indicate that a rich chemistry transpires at the same time (1-4).

In the following experiments, the conversion of coal was examined as a function of several variables over the range of temperatures from 300°C to 450°C. The net change in both the content and the distribution of hydrogen among the products was followed using an analytical scheme based on elemental and NMR analyses. This method has been used to determine the net hydrogen utilization divided among categories for hydrogenation, hydrocarbon gas formation, heteroatom removal, and matrix bond breaking (5).

Experimental

Coal liquefaction was conducted in a 0.5-L stirred autoclave. In a typical experiment, 30 g (maf) of coal ground to pass 60 mesh was charged to the autoclave along with 70 g of coal-derived solvent. The solvent was a distillate cut (240°C-450°C) obtained from operations at the SRC-II pilot plant at Ft. Lewis, Wash. The autoclave was pressurized with the appropriate amount of hydrogen or nitrogen to obtain the desired operating pressure at temperature. Heat-up time to liquefaction temperatures was about 45 minutes. The autoclave was held at temperature for the specified time and then rapidly cooled by means of internal water-cooling coils. Grab samples of the off-gas were taken for analysis by gas chromatography as the autoclave was depressurized.

Conversion data in Figures 1 and 2 were obtained by first filtering the autoclave contents through a Whatman #541 filter on a Buchner funnel maintained at 60°C. The residue was then washed with tetrahydrofuran (THF) until the washings were nearly colorless. Data in Figure 3 were obtained by first digesting the liquid product from the autoclave with THF. The digest was vacuum-filtered through Whatman #2 filter paper, and the residue was washed with THF until the extract was nearly colorless. All residues were dried at 110°C and weighed. Conversion values were based on the weight of dried residue.

The methods used to determine hydrogen utilization data have been described (5). Data from the elemental analysis of the feed coal and liquefaction solvent, including the direct oxygen analysis, were used in these calculations (see Table 1). The liquid products were separated by Soxhlet extraction with methylene chloride. The carbon aromaticities were determined by ^{13}C NMR using CP/MAS techniques on the insoluble fraction and high resolution ^{13}C NMR in CD_2Cl_2 for the extract.

Results and Discussion

Liquefaction. The reactivities of the two bituminous coals are compared in Figure 1 as a function of temperature. The pronounced difference in reactivity at 325°C decreases rapidly with increasing liquefaction temperature. Although a difference in reactivity of these coals was expected, it is nonetheless remarkable that the conversion of the Illinois coal remains high even at a temperature as low as 325°C. The differences in patterns of hydrogen utilization discussed below are not striking for these two coals. The structural differences between the coals that are responsible for their individual responses to reaction temperature is a matter still open to question. At least, these data indicate that the choice of feedstock coal is even more critical for liquefaction at lower temperatures than at conventionally used temperatures.

The conversion of the Illinois coal is shown in Figure 2 as a function of reaction time after reaching temperature for three temperatures. It is evident that most conversion is complete within a short initial period of reaction even for the lowest of liquefaction temperatures. Undoubtly, some of this conversion occurs during heat-up. Although conversion to low molecular weight products may require more severe conditions, the breakdown of the matrix structure of coal requires little time at modest temperatures. This same pattern of reactivity was noted earlier for liquefaction of coal in tetralin at 400°C (6). The present experiments show that the "prompt" yield of extract increases somewhat with temperature.

The effect of hydrogen pressure on conversion is quite significant. Figure 3 contains conversion data obtained at various temperatures and pressures of hydrogen or nitrogen. As expected, conversions increase with hydrogen pressure but hardly change with increasing nitrogen pressure. The sensitivity of conversion to hydrogen pressure is a function of liquefaction temperature. For example, increasing hydrogen pressure from zero to 2000 psi produces a larger increase in conversion at 400°C than at 350°C. It is not known whether this difference is related to the thermochemistry of bond scission reactions or to the state of reduction of pyrite in the mineral matter to pyrrhotite, which may act as a modest catalyst for coal liquefaction. Under these reaction conditions, analysis of the off-gases for H_2S and of the recovered mineral residues for pyrrhotite content shows that the reduction of pyrite is incomplete at 350°C. It is somewhat greater at 400°C, but probably not yet complete.

The character of the liquefaction solvent is well-known to have a major influence on conversion under conventional conditions. A number of experiments were made to determine whether conversions obtained at the relatively low temperatures employed here would be sensitive to modifications in the coal-derived liquefaction solvent. In one case, 10% of the weight of the coal-derived solvent was replaced by tetralin, a well-known hydrogen donor. Many studies have shown that coal conversion increases with minor addition of tetralin to a liquefaction solvent that is poor in donable hydrogen (7). Conversions were not changed within experimental error for reaction temperatures of 325°C, 350°C, and 400°C under hydrogen pressures of either 1000 or 2000 psig. Thus the amount of conversion under these conditions is not limited by lack of hydrogen donor compounds in the coal-derived solvent.

In a similar way, 10% of the weight of the coal-derived solvent was replaced by pyrene, a compound reported to be especially effective as both a hydrogen transfer agent (8) and a physical solvent for promoting liquefaction (9). Addition of this compound also had no effect within experimental error on conversion obtained at 350°C or 400°C under 1000 psig hydrogen. Taken together, these experiments indicate that for liquefaction at relatively low temperatures, the coal-derived solvent employed is not lacking in components suited for hydrogen donation, hydrogen shuttling, or physical solvation.

Hydrogen Utilization. A second set of autoclave experiments was performed to determine if changes in hydrogen distribution during liquefaction were different for coals of different reactivity. For initial experiments, the reaction conditions selected were 2000 psi hydrogen and 15 min. at various temperatures. In order to improve the reliability of the hydrogen distribution data, the work-up procedure was modified to use only solvents compatible with the NMR measurements needed to monitor hydrogenation. The entire contents of the autoclave were Soxhlet-extracted with methylene chloride to yield soluble and insoluble fractions. The yield of soluble material is less using methylene chloride, but residual solvent does not interfere with subsequent NMR aromaticity measurements. Both the soluble and insoluble fractions undergo elemental and NMR analysis. Thus, the relative amount of each fraction does not affect the values determined for the net amount of hydrogen used. For both coals, the gas yield was negligible at 300°C and 350°C, but increased to 1.2%-1.5% at 400°C and 8.2%-8.4% at 450°C on an maf basis.

The total hydrogen utilization is divided into four categories in Table 2. These results are arrived at using an analytical approach described previously (5). Entries in Table 2 give the net number of hydrogens incorporated (positive sign) or produced (negative sign) per 100 carbons of feed slurry. It must be emphasized that these numbers indicate only net changes in hydrogen involved in a particular mode of utilization and they include all the carbon in the whole feed slurry not just that in the coal. Negative numbers appearing in Table 2 for hydrogenation and matrix bond cleavage indicate that hydrogen (not necessarily in the form of H_2 gas) is being generated within the slurry by dehydrogenation (aromatization) or condensation reactions, respectively.

The data in Table 2 indicate that cracking reactions producing C_1-C_4 hydrocarbon gases are not significant hydrogen consumers up to at least 400°C. Heteroatom removal increases with reaction temperature and is primarily oxygen removal under these conditions. (The maximum consumption by removal of N + S in these runs was 0.5 H/100 C for Illinois #6 at 450°C.) The higher content of labile oxygen of the Illinois #6 coal is reflected in Table 1.

The effect of temperature on the aromaticity of the total product (sols + insols + gases) is indicated in Figure 4. The trend to increasing product aromaticity with increasing temperature is the same for both coals. The data indicate that at low temperatures the net chemistry is hydrogenation, but above about 400° the total product aromaticity exceeds that of the feed slurry. This indicates that the net reaction above 400°C, even under 2000 psi hydrogen gas, is aromatization of the feed slurry (coal + solvent).

A similar pattern was observed in an earlier study of hydrogen utilization in a small continuous reactor, although in that case the magnitude of the variation of net hydrogenation with temperature was larger (5). This dominance of aromatization over hydrogenation at high temperatures is expected on thermodynamic grounds.

During liquefaction, bonds are being both broken (thermolysis) and formed (condensation). The category "matrix cleavage" in Table 2 attempts to quantitate the amount of hydrogen involved in bond-making/bond-breaking chemistry of the feed slurry. This value for the hydrogen involved in bond cleavage is necessarily determined by difference and thus should be interpreted with caution. With this warning it can be noted that for the Blacksville liquefaction experiments at 400°C and 450°C, the net hydrogen utilized in matrix cleavage is nil, indicating that any bond cleavage that occurs consuming hydrogen is balanced by condensation reactions producing hydrogen. At 325°C for the Blacksville coal, the data indicate net production of 2 hydrogens per 100 slurry carbons or a slight dominance of condensation reactions over thermolysis reactions. It is not unreasonable to expect condensation to predominate at low temperatures. The 325°C

experiments with Illinois #6 coal also indicate a predominance of condensation reactions, but the scatter of the data for the Illinois #6 coal liquefaction experiments is too high to comment on with confidence.

The net amount of hydrogen consumed in matrix cleavage is a measurement of the resultant of two opposing reaction routes and is thus expected to be a function of solvent type, reaction time, catalyst, coal, and temperature. The response of hydrogen utilization to these variables is now under investigation. The present data form a baseline for future comparisons. Improvements in the analytical method will make it easier to form firm conclusions on the relative importance of condensation versus thermolysis as a function of reaction conditions.

It is interesting to note, however, that both in this work (325°C data) and in the previous study of continuous unit operation, there is evidence for the dominance of condensation reactions under mild conditions. The analytical approach used to generate the data in Table 2 is still undergoing refinement, but it appears that it may be quite useful for characterizing differences in liquefaction chemistry and their dependence on reaction conditions.

REFERENCES

1. J.A. Franz, Fuel, 58, 405 (1979).

2. I.B. Goldberg, H.R. Crowe, J.J. Ratto, R.P. Skowronski, and L.A. Heredy, Fuel, 59, 133 (1980).

3. M.A. Wilson, P.J. Collin, P.F. Barron, and A.M. Vassallo, Fuel Processing Technology, 5, 281 (1982).

4. F.K. Schweighardt, B.C. Bockrath, R.A. Friedel, and H.L. Retcofsky, Anal. Chem., 48, 1254 (1976).

5. D.H. Finseth, B.C. Bockrath, D.L. Cillo, E.G. Illig, R.F. Sprecher, H.L. Retcofsky, and R.G. Lett, Am. Chem. Soc. Div. Fuel Chem. Preprints, 28(5), 17 (1983).

6. R.C. Neavel, Fuel, 55, 237 (1976).

7. B.C. Bockrath, in "Coal Science," (M.L. Gorbaty, J.W. Larsen, and I. Wender, Eds.) Vol. 2, pp. 65-124, Academic Press, NY (1983).

8. F.J. Derbyshire and D.D. Whitehurst, Fuel, 60, 655 (1981).

9. I. Mochida, A. Takerabe, and K. Takeshita, Fuel, 58, 17 (1979).

TABLE 1. ELEMENTAL ANALYSES, MAF

	C	H	N	O	S
BLACKSVILLE COAL	80.6	5.6	1.4	9.4	3.1
ILLINOIS #6 COAL	73.7	5.6	1.5	14.8	4.5
SOLVENT	87.1	8.0	1.4	3.0	0.4

MOISTURE FREE ASH CONTENTS WERE BLACKSVILLE = 11.9%, ILLINOIS #6 = 13.6%, SOLVENT < 0.1%.

TABLE 2.
HYDROGEN UTILIZATION VS. COAL REACTIVITY AND TEMPERATURE: HYDROGENS INCORPORATED PER 100 CARBONS OF FEED SLURRY

	BLACKSVILLE #2			ILLINOIS #6					
FATE OF HYDROGEN	325°	400°	450°	300°	300° Dup.	325°	400°	450°	450° Dup.
Gas Make	0	0	3	0	0	0	0	3	3
Heteroatom Removal	0	1	1	1	0	1	2	3	3
Hydrogenation	1	-2	-3	1	1	2	0	-3	-3
Matrix Cleavage	-2	0	0	0	+2	-2	+2	-1	0
TOTAL	-1	-1	+1	+2	+3	+1	+4	+2	+3

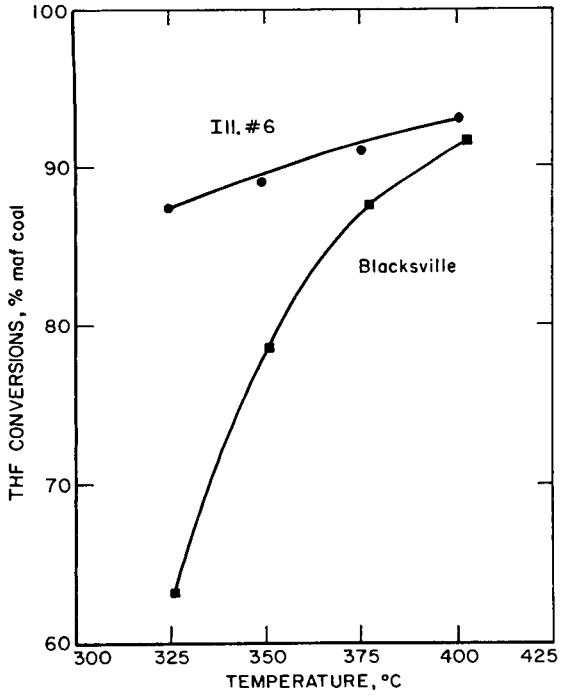

Figure 1 - Conversion of two coals versus temperature at 2000 psi hydrogen for 60 minutes.

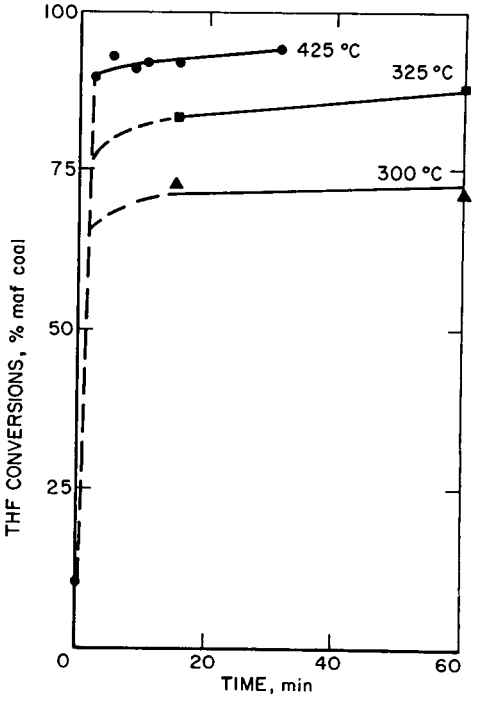

Figure 2 - Conversion of Illinois #6 (River King) Coal at 2000 psi hydrogen.

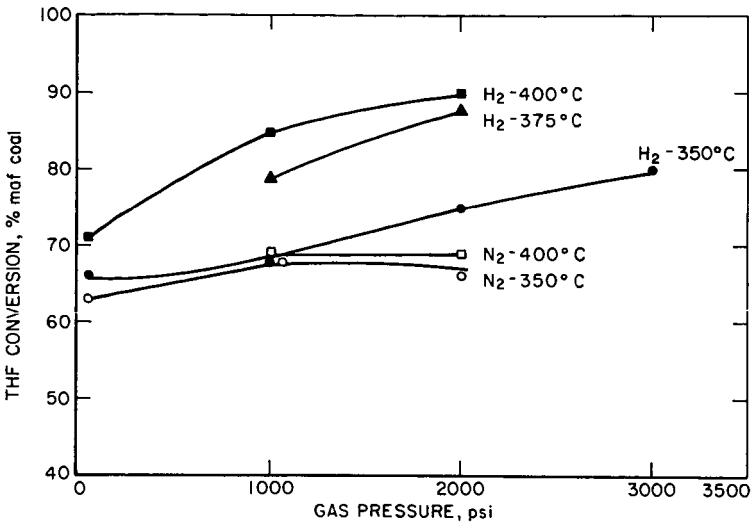

Figure 3 - Pressure effect at various temperatures on Illinois #6 coal, 15 min at temperature.

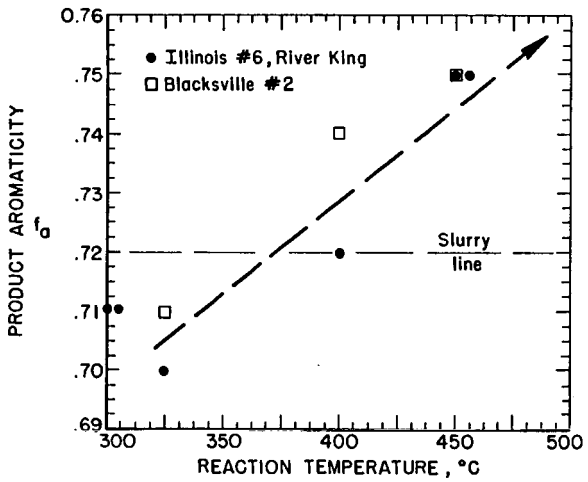

Figure 4. Product Aromaticity Versus Reaction Temperature for Blacksville #2 and Illinois #6

The Response of High Temperature Catalytic Tetralin-Hydrogen Reaction to Free Radical Addition

W. M. Reed
A. R. Tarrer
J. A. Guin
C. W. Curtis
D. Gary

Auburn University
Department of Chemical Engineering
230 Ross Hall
Auburn University, AL 36849

I. INTRODUCTION

The literature is ambiguous regarding the reaction products obtained when tetralin and hydrogen are reacted above 425°C in the presence of a catalyst. Yen et al. (1) reported that tetralin disproportionation occurs, at 455°C, and naphthalene and only one of the decalin isomers are formed. They also reported the presence of an unidentified product. Hooper et al. (2), with the aid of recent advances in chromatographic analysis, suggested that the compound identified as a decalin isomer could be methyl indan and attempted to show that tetralin disproportionation did not occur. However, they did not analyze any actual products from catalytic hydrotreatment of tetralin.

In this report, gas chromatographic analyses of the products from catalytic dehydrogenation of tetralin at 450°C are presented. These analyses served as the baseline for comparison of reactions in which dibenzyl was added to provide a source of free radicals similar to those produced during the initial stages of coal liquefaction.

II. EXPERIMENTAL

The experiments were carried out in a tubing bomb microreactor constructed from a six inch length of 316 seamless stainless steel, 1/2-inch O.D. tubing. One end of the microreactor was sealed with a 1/2-inch Gyrolok cap. The other end was connected to a 3 and 1/4-inch length of 316 seamless stainless steel, 1/4-inch O.D., tubing with a Gyrolok reducing union. A Nupro fine metering valve was connected to the other end of the 1/4-inch O.D. tubing.

The reaction temperature was maintained by immersing the microreactor in a fluidized sand bath which was equipped with a temperature controller and a thermocouple for monitoring the temperature. The microreactor was agitated in a vertical plane with a 1 and 1/2-inch stroke. An agitation rate of 860 rpm has been shown (3) to reduce mass transfer effects in the microreactor. Two steel ball agitators of 1/8-inch diameter were also added to the microreactor to ensure good end-to-end mixing during reaction.

At the end of the desired reaction time, the microreactor was quenched in water (20-25°C) to stop the reaction. The microreactor was then vented and its contents collected in a vial.

The reaction products were analyzed using a Varian 3700 gas chromatograph equipped with a CDS-111 integrator. Separation was accomplished with a 60-meter, 0.314 mm I.D., fused silica capillary column with a DB-5 bonded phase (0.25 μm). To assist in the identification of the reaction products, some of the samples were analyzed with a gas chromatography-mass spectroscopy (GCMS) unit. A capillary column

was used for separation of the products. The composition of the other reaction experiments were then identified by comparison of the chromatograms with the chromatograms of the samples analyzed with GCMS.

III. RESULTS AND DISCUSSION

Three reaction parameters were chosen for manipulation to investigate the tetralin-hydrogen reaction at a relatively high temperature (450°C). These parameters were:

(1) addition of dibenzyl as a free radical precursor
(2) catalyst addition
(3) addition of gaseous hydrogen

Dibenzyl was selected as the free radical precursor. Dibenzyl cleaves at coal liquefaction conditions, producing benzyl free radicals. The primary reaction of dibenzyl is assumed to be thermal cracking followed by stabilization of the benzyl free radicals. Cronauer et al. (4) observed no increase in the rate of dibenzyl conversion with the addition of catalysts.

Table 1 presents the response of the product distribution to the addition of dibenzyl, and hence, the presence of free radicals. The principal products of the dibenzyl-tetralin-hydrogen reaction were benzene, toluene, methyl indan, and naphthalene. Very small amounts of ethyl benzene, butyl benzene, and trans-decalin were found in some experiments. Traces of cis-decalin and stilbene were also detected.

With the addition of dibenzyl, the most significant result was an increase in the formation of methyl indan, the isomer of tetralin. Approximately twenty percent of the tetralin was isomerized with the addition of dibenzyl, both with and without catalyst. Cronauer et al. (5) and McNeil et al. (6) have also reported an increase in the isomerization of tetralin with the addition of dibenzyl.

Even when there was no dibenzyl present, some isomerization of tetralin was observed (i.e., 5.7 wt% and 7.9 wt% methyl indan was formed with and without catalyst present, respectively). Isomerization of tetralin has been reported at temperatures as low as 350°C in a nitrogen atmosphere (2). Penninger and Slotboom (7,8) heated tetralin with hydrogen in the absence of catalyst at pressures of 10 to 100 atm and temperatures of 460 to 560°C. Methyl indan was reported among the principal products. They proposed that the dehydrogenation of tetralin to naphthalene provided the hydrogen atoms (i.e. free radicals) to initiate the isomerization reaction.

The formation of benzyl free radicals from dibenzyl is a thermal process. Thus, the use of catalysts was not intended to change the amount of dibenzyl converted; instead it was felt that its addition would alter the product distribution, i.e., mainly the relative amounts of tetralin isomerization and dehydrogenation products. The rate of formation of the tetralin isomer, methyl indan, changed slightly with the addition of presulfided $CoMo/Al_2O_3$ catalyst. However, the rate of tetralin dehydrogenation to from naphthalene increased significantly with the addition of catalyst. This increase was even more pronounced when no dibenzyl was added; the amount of naphthalene formation increased from 1.3 wt% to 13.0 wt% with the addition of catalyst. When dibenzyl was present, the amount of naphthalene formation increased only from 6.6 wt% to 9.8 wt% with the addition of catalyst.

For the product analyses given in Table 1, only a small amount of trans-decalin was observed, and that was when catalyst was present. No significant amount of cis-decalin was observed in any of the products analyzed. For the reaction

conditions used here then (450°C, etc.), catalyst addition caused an increase in the rate of dehydrogenation of the tetralin rather than an increase in that of hydrogenation.

The third reaction parameter which was studied was the addition of gaseous hydrogen. Vernon (9) has shown that molecular hydrogen can react directly with the benzyl free radical to yield toluene. Shah and Cronauer (10), however, have demonstrated that the benzyl free radicals have a distinct preference for combined hydrogen over molecular hydrogen under reaction conditions similar to those used in this work. They reported that this preference is enhanced if the concentration of hydroaromatics is high. The molecular hydrogen was believed to provide hydrogen for "rehydrogenation" of depleted hydrogen donor solvent. In this work, tetralin serves as the hydrogen donor, and a primary objective of the study was to evaluate the response of the rehydrogenation rate of the tetralin versus that of isomerization to the addition of gaseous hydrogen.

Two extremes of reactor atmosphere were used: a hydrogen atmosphere (800 psig at room temperature) and an inert nitrogen atmosphere (300 psig at room temperature). The product distributions for each case are presented in Table 2. The conversion of dibenzyl was approximately the same in each case. The rate of isomerization of tetralin to form methyl indan was lower in the nitrogen atmosphere. This result suggests that molecular hydrogen can participate in the reaction mechanism for tetralin isomerization. However, this participation may be indirect. In a hydrogen atmosphere the dehydrogenation rate for tetralin should be lower than that in a nitrogen atmosphere. As a result, more tetralin should be available for isomerization. A more direct role of the hydrogen could be that the benzyl radicals react with the molecular hydrogen to produce hydrogen atoms, then these atoms could participate directly in the tetralin isomerization reactions (8,9).

The rate of tetralin dehydrogenation was higher than that of isomerization with an inert nitrogen reaction atmosphere (Table 2). The opposite was true with a hydrogen atmosphere.

The reaction of tetralin in the presence of both dibenzyl and hydrogen was used as a baseline system for comparison. The increase in the amount of tetralin dehydrogenation that occurred, when no hydrogen was initially present, relative to that obtained with this baseline system was determined. The increase observed when no dibenzyl was present was also determined. These responses are compared in Table 3. Apparently the increase in the rate of tetralin dehydrogenation, in response to the absence of hydrogen, was much higher than it was in response to the absence of dibenzyl.

When no hydrogen was present there was about an 8.4 wt.% decrease from the baseline value (19.9 wt.%) in the amount of tetralin that isomerized to form methyl indan (Table 4). Similarly, when no dibenzyl was present, the amount of tetralin converted to methyl indan decreased by about 12.0 wt.% below the baseline value.

A number of compounds such as tetrahydroquinoline (THQ) have been shown to have a higher hydrogen donor reactivity than that of tetralin (12). A crude measure of the relative reactivity of the tetralin for donating hydrogen to the benzyl radicals was made by determining the decrease in the extent of tetralin dehydrogenation that occurred in response to the addition of either quinoline or phenanthridine. Quinoline and phenanthridine are basic nitrogen-containing aromatic compounds similar to those found in coal-derived liquids. These compounds have a relatively high adsorptivity. As a result, these compounds adsorb preferentially onto the catalyst surface and are hydrogenated in preference to compounds like naphthalene (i.e., the dehydrogenated tetralin product) which have a lower relative adsorptivity (13). The hydrogenated products of these compounds (eg. THQ) are excellent hydrogen donors.

McNeil et al. (6) measured the response of tetralin dehydrogenation and isomerization in the presence of dibenzyl to the addition of different polynuclear aromatic compounds (e.g. phenanthrene, pyrene). They observed an insignificant response to occur in the tetralin isomerization. However, a significant decrease in the tetralin dehydrogenation occurred in response to the addition of certain aromatics. In an earlier work (11), this decrease in tetralin dehydrogenation was observed to vary directly with the number of condensed rings in the aromatic compound added.

The response of tetralin isomerization to the addition of either quinoline or phenanthridine is shown in Figure 1. The presence of quinoline or phenanthridine had a significant influence on the extent of tetralin isomerization that occurred. However, as shown in Figure 2, the addition of either quinoline or phenanthridine caused only a slight decrease in the amount of tetralin dehydrogenation (14.2 wt.% versus 6.6 and 10.4 wt%). The relative insensitivity of the tetralin dehydrogenation to the addition of these basic nitrogen-containing compounds is somewhat surprising. Earlier it was shown that the presence of a catalyst caused a significant increase in tetralin dehydrogenation (Table 1). Preferential adsorption of the quinoline or phenanthridine on the catalyst should inhibit dehydrogenation. It appears, however, that these compounds act more to quench the benzyl radicals and thereby inhibit tetralin isomerization without significantly inhibiting dehydrogenation of the tetralin.

IV. SUMMARY OF RESULTS

The principal products of the high temperature, catalytic reaction of tetralin in the presence of dibenzyl and gaseous hydrogen were found to be naphthalene and methyl indan. A small amount of trans-decalin was observed to be formed. The isomerization of tetralin increased with the addition of dibenzyl, a free radical precursor. The addition of a presulfided $CoMo/Al_2O_3$ catalyst had a small effect on tetralin isomerization and dehydrogenation in the presence of dibenzyl. However, in the absence of dibenzyl, catalyst addition had a significant effect on tetralin dehydrogenation.

Tetralin dehydrogenation increased significantly when an inert nitrogen atmosphere rather than a hydrogen atmosphere was used.

Tetralin isomerization decreased significantly with the addition of either quinoline or phenanthridine; whereas tetralin dehydrogenation decreased only slightly with the addition of either of these compounds.

References

1. Yen, Y. K., Furlani, D. E., and Weller, S. W., Ind. Eng. Prod. Res. Dev., 15, 24 (1976).
2. Hooper, R. J., Battaerd, H. A., and Evans, D. G., Fuel, 58, 132 (1979).
3. Gallokato, S. V., "Analysis of Mass Transfer in Coal Liquefaction reactors," Ph.D. Dissertation, Auburn University, AL (March 1984).
4. Cronauer, D. C., Jewell, D. M., Shah, Y. T., and Modi, R. J., Ind. Eng. Chem. Fund., 18, 153 (1979).
5. Cronauer, D. C., Jewell, D. M., Shah, Y. T., and Kueser, K. A., Ind. Eng. Chem. Fund., 17, 291 (1978).
6. McNeil, R. I., Cronauer, D. C., and Young, D. C., Fuel, 62, 401 (1983).
7. Penninger, J. M. and Slotboom, H. W., Rec. Trav. Chim. Pays-Bas, 92, 513 (1973).
8. Penninger, J. M. and Slotboom, H. W., Rec. Trav. Chim. Pays-Bas., 92, 1089 (1973).
9. Vernon, L. W., Fuel, 59, 102 (1980).
10. Shah, Y. T. and Cronauer, D. C., Catal. Rev. - Sci. Eng., 20, 209 (1979).
11. Cronauer, D. C., McNeil, R. I., Young, D. C., and Ruberto, R. G., Fuel, 61, 610 (1982).
12. Curtis, C. W., Guin, J. A., and Kwon, K. C., "Coal Solvolysis in a Series of Model Compound Systems," Fuel, (in press).
13. Shridharani, K. G., "Mineral Catalysis of Oil-Producing Reactions in Coal Liquefaction," Ph.D. Dissertation, Auburn University, Auburn, Al., March 17, 1983.

Table 1

Response in Product Distribution to Addition of Dibenzyl, with and without Catalyst Present

Initial Dibenzyl (wt%)	Catalyst (ppm)	Product Distribution, wt%					
		Tetralin	Naphthalene	Methyl Indan	Benzene	Toluene	Dibenzyl
0	0	92.9	1.3	5.7	--	--	--
20	0	56.9	6.6	16.4	0.6	11.4	8.0
0	1000	71.2	13.0	7.9	--	--	--
20	1000	54.3	9.8	15.9	0.6	10.4	8.8

Reaction Mixture: 5.0g dibenzyl and tetralin
Catalyst Loading: 1000 g of total metal in presulfided $CoMo/Al_2O_3$ per 10^6 g of tetralin.
Reaction Conditions:
- Temperature = 450°C
- Initial H_2 Pressure = 800 psig at 25°C
- Time = 60 minutes
- Agitation Rate = 860 rpm
- Reactor = Tubing Bomb Microreactor

Table 2

Comparison Between Product Distribution in a Hydrogen Atmosphere with That in a Nitrogen Atmosphere

Atmosphere	Product Distribution, Weight %					
	Tetralin	Naphthalene	Methyl Indan	Benzene	Toluene	Dibenzyl
H_2	54.3	9.8	15.9	0.6	10.4	8.8
N_2	47.0	23.6	9.2	0.3	9.8	9.8

Reaction Mixture: 5.0 g 20 wt% dibenzyl in tetralin
1000 g metal in presulfided $CoMo/Al_2O_3$ ctalyst per 10^6 of tetralin
Reaction Conditions:
- Temperature = 450°C
- Initial Pressure = 800 psig H_2, or 300 psig N_2, at 25°C
- Time = 60 minutes
- Agitation Rate = 860 rpm
- Reactor = Tubing Bomb Microreactor

Table 3

Comparison Between the Change in the Weight Percent of the Tetralin Dehydrogenated with No Dibenzyl Present and That with No Hydrogen Gas Present

Change from Baseline Conditions*	Increase in Amount of Tetralin Dehydrogenated (ΔWt.%)
No Dibenzyl Present	0.7
No Hydrogen Present	17.5

*Baseline Reaction Conditions:

Reaction Mixture:	5.0g of 20 wt.% dibenzyl in tetralin	
Catalyst Loading:	1000 g of total metal in presulfided $CoMo/Al_2O_3$ per 10^6 g of tetralin	
Reaction Conditions:	Temperature	= 450°C
	Initial H_2 Pressure	= 800 psig at 25°C
	Time	= 60 minutes
	Agitation Rate	= 860 rpm
	Reactor	= Tubing Bomb Microreactor

Table 4

Comparison Between the Change in the Weight Percent of the Tetralin Isomerized with No Dibenzyl Present and That with No Hydrogen Gas Present

Change from Baseline Conditions*	Decrease in Amount of Tetralin Isomerized (ΔWt.%)
No Dibenzyl Present	12.0
No Hydrogen Present	8.4

*Baseline Reaction Conditions:

Reaction Mixture:	5.0g of 20 wt.% dibenzyl in tetralin	
Catalyst Loading:	1000 g of total metal in presulfided $CoMo/Al_2O_3$ per 10^6 g of tetralin	
Reaction Conditions:	Temperature	= 450°C
	Initial H_2 Pressure	= 800 psig at 25°C
	Time	= 60 minutes
	Agitation Rate	= 860 rpm
	Reactor	= Tubing Bomb Microreactor

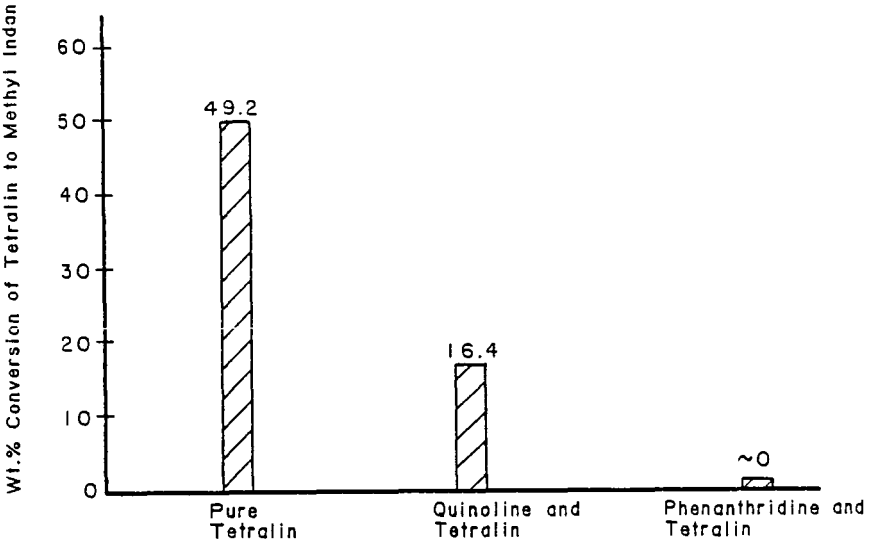

Reaction Mixture:	2.0 g 50 wt% dibenzyl in tetralin or 1:1 wt. ratio of tetralin to quinoline or phenanthridine 1000 g of Mo per 10^6 g of tetralin and quinoline or phenanthridine mixture	
Reaction Conditions:	Temperature	= 450°C
	Initial H_2 Pressure	= 800 psig at 25°C
	Time	= 60 minutes
	Agitation Rate	= 860 rpm
	Reactor	= Tubing Bomb Micro-reactor

Figure 1. Response of Tetralin Isomerization to the addition of either Quinoline or Phenanthridine

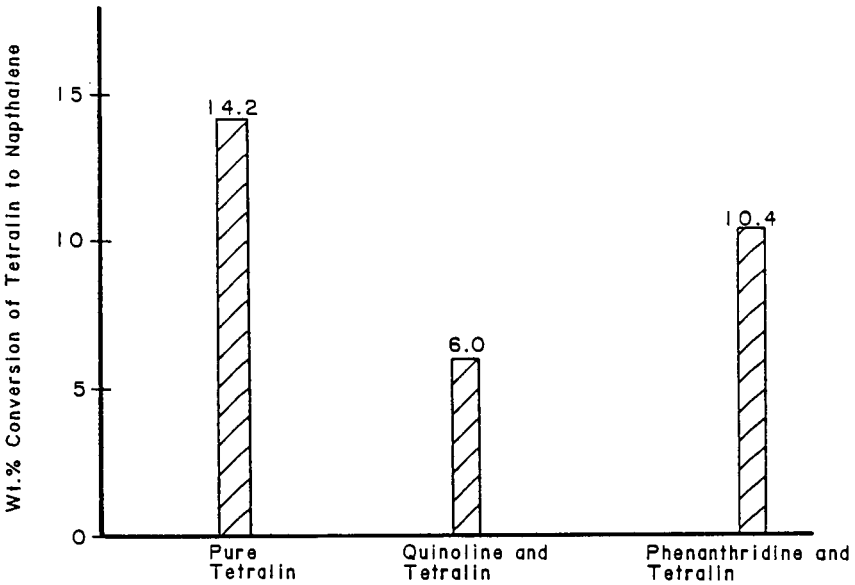

Reaction Mixture: 2.0 g 50 wt% dibenzyl in tetralin or 1:1 wt. ratio of tetralin to quinoline or phenanthridine 1000 g Mo per 10^6 g of tetralin and quinoline or phenanthridine mixture

Reaction Conditions:

Temperature	=	450°C
Initial H_2 Pressure	=	800 psig at 25°C
Time	=	60 minutes
Agitation Rate	=	860 rpm
Reactor	=	Tubing Bomb Micro-reactor

Figure 2. Response of Tetralin Dehydrogenation to the addition of either Quinoline or Phenanthridine

LIQUEFACTION OF WYODAK COAL IN INDOLINE*

Thomas D. Padrick and Steven J. Lockwood

Sandia National Laboratories, Albuquerque, NM 87185

INTRODUCTION

Several investigators have observed an enhancement of Wyodak coal liquefaction when 1,2,3,4-tetrahydroquinoline (THQ) is used as the solvent (1,2). A difficulty in evaluating the cause of this observed enhancement was that THQ possesses both hydrogen-donor and polar (basic nitrogen) characteristics. We examined the liquefaction behavior of Wyodak coal in a variety of heterocyclic solvents to learn the role of the nitrogen functionality in coal liquefaction (3). We observed high conversion for Wyodak coal in indole, a non-hydrogen-donor, nitrogen-heterocyclic solvent. We found that a large fraction of the Wyodak coal was held together by hydrogen bonds which were disrupted by interaction with the N-H functionality of indole to form associatively bound coal-indole complexes. These coal-indole complexes were THF soluble and accounted for the high conversion observed for Wyodak liquefaction in indole under mild liquefaction conditions. We feel this mechanism would also explain the role of the basic nitrogen functionality in other solvents with the N-H structure, such as THQ.

Having an understanding of the role of the basic nitrogen characteristic of the solvent, we began a study of a solvent possessing both basic-nitrogen and hydrogen-donor characteristics. We chose to investigate indoline (2,3-dihydroindole) because it has both solvent characteristics, has a single dehydrogenated species (indole), which along with the hydrogenated form is readily monitored, and knowledge of the liquefaction behavior of its dehydrogenated form had already been obtained. We have now conducted experiments in indoline to learn if there is a possible further enhancement of the liquefaction reaction in this type of solvent due to an actual complexing of the hydrogen donor molecule to the coal molecule. We have determined that liquefaction in indoline, which can first complex to the coal and then donate its hydrogen, is much more effective than liquefaction in either a pure hydrogen donor (tetralin) or a combination of hydrogen donor + nitrogen heterocyclic (tetralin + indole).

EXPERIMENTAL

The data reported below were obtained from batch microreactor runs using Wyodak coal (South Pit Mine) and selected model solvents. The 25 cm microreactors were loaded with an 8 gram sample of a 2/1 solvent to coal mixture. They were then pressurized to 1000 psig with nitrogen. The microreactors were heated (~3 minutes to reach reaction temperature) in a fluidized sand bath and held at temperature for the specified time. The microreactors were then cooled (~30 seconds for a 200°C quench) in a second fluidized sand bath held at room temperature. Conversion to THF soluble products was obtained by subsampling the whole liquid product from the microreactor, sonicating the sample in THF and then pressure filtering through a 0.2 micron Millipore filter. The filter was then analyzed by gel permeation high performance liquid

* This work supported by the U. S. Department of Energy at Sandia National Laboratories under contract DE-AC04-76DP00789.

chromatography (HPLC) to observe differences in product distribution (4). This technique separates the filtrate into high, intermediate and low molecular weight fractions. These fractions are comparable to the classical preasphaltene (mw ∿ 1000), asphaltene (mw ∿ 450) and oil (mw ∿ 250) fractions obtained by Soxhlet analysis.

RESULTS AND DISCUSSION

We began our study of the effects of indoline on Wyodak coal conversion by liquefying Wyodak coal at various times and temperatures in indoline, indole and tetralin and measuring the conversion to THF soluble products. Figures 1 and 2 show these results.

We can see from Figure 1 that at 375°C the conversion of Wyodak coal to THF solubles is very high for liquefaction in indoline, even at short reaction times. Comparison of the conversions in tetralin and indoline at 20 minutes shows that in indoline the conversion is more than double that obtained with tetralin (82% to 40%). The conversion in both of these solvents continues to increase with time, suggesting continued reaction between the coal and these hydrogen donors. We also observe in Figure 1 that as a function of time at 375°C, conversion of Wycdak coal in indole levels off. This is attributed to the fact that at a fixed temperature a certain level of coal hydrogen bond disruption will take place after the time necessary for ccmplete interaction of the solvent with the coal structure. Beyond this time, no additicnal indole-coal reactions can occur in this system.

Figure 2 likewise shows that for all temperatures and a 20-minute reaction time, conversion in indoline is greater than conversion in tetralin. However, we do observe that at high temperatures the two hydrogen donor solvents appear to be approaching the same conversion level. This suggests that at high temperature the hydrogen transfer reactions begin to dominate the reaction mechanism and therefore indoline and tetralin begin to behave similarly.

Further evidence that at high temperatures a hydrogen transfer mechanism begins to dominate the liquefaction chemistry can be seen in Figure 3. In Figure 3, we have plotted the ratio of the indole to indoline concentrations measured in the product material formed in an experiment with Wyodak coal and indoline. These concentrations were measured by HPLC analysis. This ratio is a measure of the degree of indoline dehydrogenation. We can see from Figure 3 that between 375°C and 400°C, a significant increase in the hydrogen transfer rate occurs.

The data in both Figure 1 and Figure 2 confirm that when indoline is used as the solvent for Wyodak liquefaction, there is enhancement of the conversion above that obtained in a good hydrogen donor. We believe that this is due to the interaction of the N-H functionality of indoline with the coal structure. This results in coal-indoline complexes, similar to those observed in our study of Wyodak liquefaction in indole. Figure 4a is the HPLC spectrum that we obtained for products of Wyodak liquefaction in indole. Here we see a large peak in the molecular weight distribution due to the indole-coal complex. Figure 4b is the HPLC spectrum for products obtained from liquefaction of Wyodak coal with indoline as the solvent. We see a peak for indoline and indole (dehydrogenated indoline) and a peak for the coal-indole complex and the coal-indoline complex. The peak for the coal-indoline complex never becomes as large as the complex peak in Figure 4a because the complex undergoes hydrogen transfer resulting in an indole molecule and a non-associative coal molecule. Thus in the indoline system, the complex is an intermediate species as compared to the indole system where the complex is a stable product.

The mechanism discussed above is illustrated in Figure 5. In this proposed liquefaction mechanism, the structure for the hydrogen bonded

coal fragment has not been determined in our work but is merely intended to be representative of possible structures. The heat is apparently needed to fluidize the coal sufficiently for solvent access. This fluidization is actually a weakening of the coal-coal hydrogen bonds.

We have proposed that the hydrogen transfer occurs from the indoline molecule involved in the associatively bound complex rather than from neighboring molecules. Thus, the hydrogen transfer and the disruption of the coal hydrogen-bonded structure do not occur independently. To test our hypothesis, we have performed experiments with Wyodak coal in a mixture of indole and tetralin to simulate the total solvent characteristics of indoline, but with separation of these characteristics into individual molecules. Figure 6 is a comparison of the THF conversions for Wyodak coal in these solvents. The conversion using indole + tetralin is much lower than the conversion in indoline (45% vs 82%). This is consistent with our hypothesis, i.e., that liquefaction of Wyodak coal in indoline, where the solvent first complexes to coal molecule and then transfers its hydrogen, is much more effective than hydrogen transfer from a non-interactive solvent.

The results in Figure 6 were somewhat surprising in that we expected the conversion level in the mixture of indole plus tetralin to be at least as high as the conversion found in indole. In order for the conversion in the mixed solvent system to be lower than the indole conversion, we must have interaction between the solvents or one solvent must interface with the mechanism of the other solvent. If we had had interaction between the tetralin and the indole, we would observe a difference in conversion if we increased the overall solvent to coal ratio. We doubled the solvent to coal ratio, but only increased the conversion by a few percent. Tetralin must interfere with the indole liquefaction mechanism to result in the observed conversion level.

We collected the THF solubles from a liquefaction run of Wyodak coal and indole (mostly coal-indole complex). We then reacted this material with tetralin at 375°C for 20 minutes to determine if there was any degradation of the complex and/or production of insoluble material (insols). There was no production of insols or change in the complex concentration. As far as we were able to determine, the tetralin did nothing to the soluble products from the liquefaction of Wyodak in indole. Therefore, tetralin is unable to interfere in the indole liquefaction mechanism after the coal and indole have reacted.

Although the measured conversion for Wyodak coal in tetralin is only 40% at 375°C, the tetralin may interact with a significantly larger fraction of the coal; just not producing THF soluble products. In addition, the coal itself could undergo condensation reactions at sites which are otherwise stabilized through associative bonding with indole, i.e., two hydrogen bonded hydroxyls may eliminate H_2O and form an ether linkage. To determine if either of these situations might be occurring, we reacted the THF insols from the liquefaction of Wyodak in tetralin with indole at 375°C for 20 minutes. If these insols were unaltered coal, then we might expect ~33% conversion of the insols during reaction with indole to bring the overall coal conversion to 60%. However, we measured ~10% conversion. This indicates that either condensation reactions are occurring in the coal or that a step in the tetralin liquefaction mechanism results in retrogressive reactions at 375°C. The former seems more probable and would have occurred in our mixed solvent experiment if tetralin blocked indole access to a portion of the coal hydrogen-bonding sites. Additional experiments are being performed to determine if condensation reactions at coal hydrogen bonding sites are the cause of the low conversion observed during liquefaction of Wyodak in indole + tetralin.

CONCLUSIONS

We have found that indoline is an excellent liquefaction solvent for Wyodak coal, liquefying over 80% of the coal in 20 minutes at 375°C. The indoline system is a good solvent medium for kinetic studies of hydrogen transfer because it has only one, easily monitored, dehydrogenated form. Liquefaction with indoline is much more effective than liquefaction in either a pure hydrogen donor (tetralin) or a combination of hydrogen donor plus nitrogen heterocyclic (tetralin plus indole).

We believe that the effectiveness of indoline is the result of a liquefaction mechanism in which the indoline first functions as a basic nitrogen solvent to disrupt the coal-coal hydrogen bonds and form coal-indoline complexes. The indoline then functions as a hydrogen donor solvent and transfers its hydrogen within the complex to the coal molecule. This mechanism would apply to other similar solvents such as THQ and is much more effective than hydrogen transfer from non-interactive solvents.

We have also determined that if the coal structure is not first interacted with an associative solvent (N-H functionality) to disrupt coal-coal hydrogen bonds, condensation reactions or other retrogressive reactions which make the coal less reactive may occur.

REFERENCES

1. Dwain Spencer, EPRI Journal, May, p. 31 (1982).

2. Thomas D. Padrick, Arthur W. Lynch, and Howard P. Stephens, Integrated Two-Stage Liquefaction Meeting, Albuquerque, NM, October 6-7, 1982.

3. Thomas D. Padrick and Steven J. Lockwood, Preprins, Amer. Chem. Soc., Div. of Fuel Chem. 29, No. 1, p. 153 (1984).

4. Arthur W. Lynch and Michael G. Thomas, Fuel Processing Technology 8, p. 13 (1983).

FIGURE 1. WYODAK LIQUEFACTION AT 375 C AS A FUNCTION OF TIME

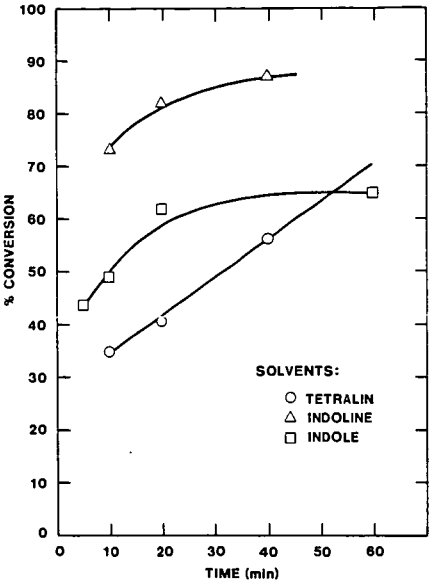

FIGURE 2. WYODAK LIQUEFACTION AS A FUNCTION OF TEMPERATURE

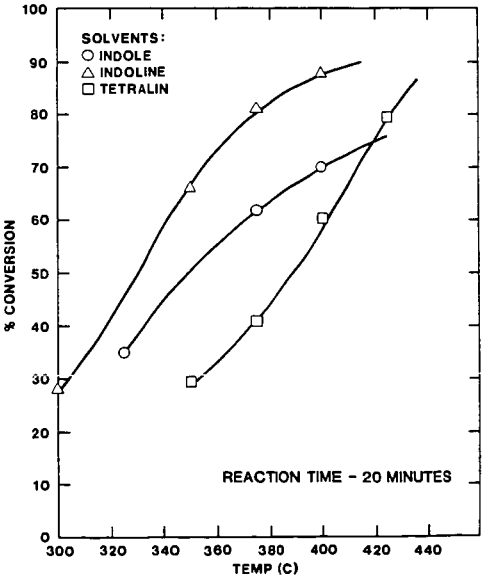

FIGURE 3. PLOT OF INDOLE/INDOLINE RATIO vs TIME FOR WYODAK LIQUEFACTION AT 375 C

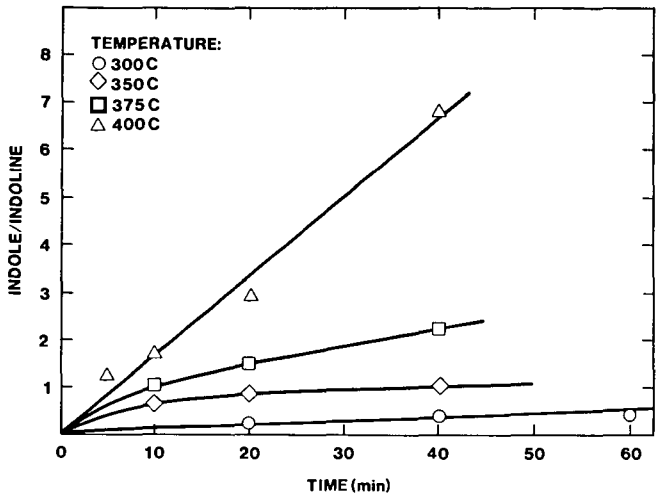

FIGURE 4. HPLC SPECTRA OF WYODAK LIQUEFACTION PRODUCTS

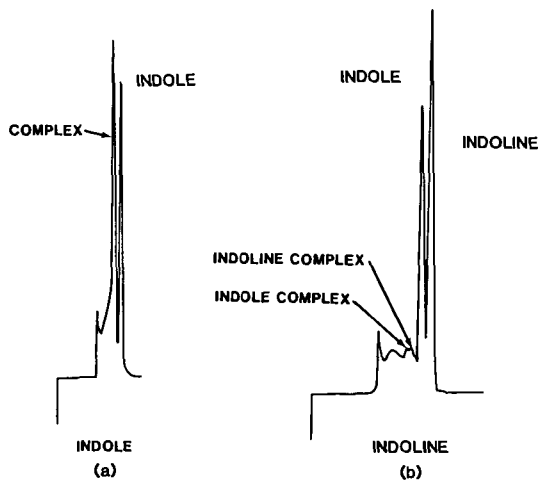

LIQUEFACTION CONDITION: 375C, 20min

FIGURE 5. PROPOSED MODEL FOR THE INDOLINE LIQUEFACTION MECHANISM OF WYODAK COAL

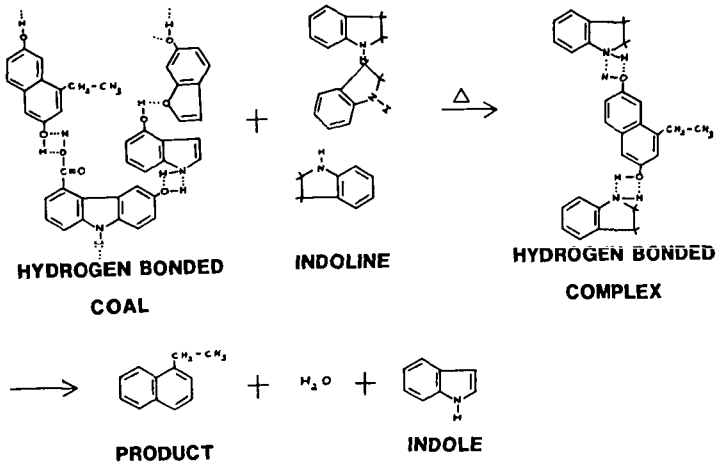

FIGURE 6. THF CONVERSIONS FOR WYODAK COAL IN MODEL SOLVENTS

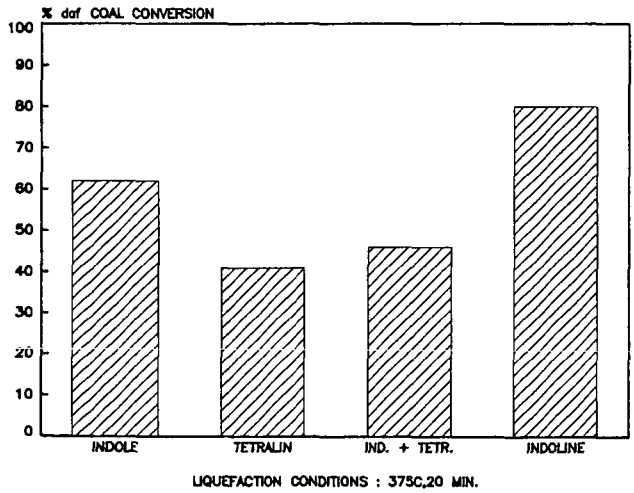

THE FATE OF NITROGENOUS MODEL PROCESS SOLVENTS IN COAL LIQUEFACTION

J. W. Hellgeth, P. G. Amateis and L. T. Taylor
Department of Chemistry

Virginia Polytechnic Institute and State University
Blacksburg, VA 24061

INTRODUCTION

The nature and role of the liquefaction solvent are the keys to understanding liquefaction chemistry. Solvent apparently serves many purposes during the dissolution of coal but two of the most significant roles have been suggested to be as a hydrogen transfer mechanism and as a catalyst (1). In this regard recent work with 1,2,3,4-tetrahydroquinoline (THQ) as a model liquefaction solvent has demonstrated its ability to convert a variety of coals, both bituminous and subbituminous, to pyridine and toluene solubles in a rapid and nearly complete fashion (2-4). While high conversions to soluble products have been realized, the ultimate goal of conversion to distillate materials in high yields remains to be attained. It is now apparent that during liquefaction, significant portions of THQ are adducted to the dissolving coal to give a non-distillable yet toluene/pyridine soluble material. The purpose of the present work is to quantify this adduction with respect to product distribution and to discern the possible modes of solvent nitrogen loss either through adduction into the coal-derived product or through thermal cracking of the solvent. Products from an in-house tubing bomb reactor and from Kerr McGee Corp. are examined. In addition a series of THQ-related model solvents will be examined in order to ascertain the effect of slight changes in solvent basicity, nitrogen atom substituent and nitrogen atom ring position upon the extent of coal conversion to soluble and distillable material.

EXPERIMENTAL

Liquefaction experiments on a Wyodak #3 western subbituminous coal were performed both in-house and at Kerr McGee Corp. (Cresent, OK). The in-house experiments involved preparation of the feed coal by drying at 293°K, 12 hours under a stream of dry nitrogen and then grinding to less than 60 mesh particle size. The Kerr McGee sample was prepared in a different manner which involved drying under vacuum at room temperature for 24 hours followed by grinding to 60 mesh particle size. The proximate and ultimate analysis (MF basis) for both samples are presented in Table I.

TABLE I

	Proximate Analyses			Ultimate Analyses	
	% Wt.[a]	% Wt.[b]		% Wt.[a]	% Wt.[b]
			Carbon	56.1	57.2
			Hydrogen	3.2	4.6
Ash	17.5	18.7	Nitrogen	0.8	0.8
Volatiles	58.4	47.9	Oxygen	11.8	15.6
Fixed Carbon	24.1	33.4	Sulfur	7.6	3.02

[a]In-house Sample (19.2% H_2O); [b]Kerr McGee Sample (24.1% H_2O)

Liquefaction of the feed coal proceeded under the general conditions of 2:1 solvent:coal, 691°K reaction temperature, 30 minutes reaction time and 7.5 MPa hydrogen atmosphere (cold charge). Experiments performed in-house were conducted in 40 mL microautoclave vessels with 4 grams of coal. The Kerr McGee experiment involved a 1 liter autoclave vessel and 100 grams of coal. Sample workup for the in-house samples involved extraction with toluene and pyridine to obtain a conversion based on solubility and through distillation to a 1050°F endpoint (300°C, 1.3 Pa). The Kerr McGee product work-up involved distillation of the products to a 850°F endpoint at atmospheric pressure (400°F, 13.3 Pa). Nitrogen determinations of these products were obtained from Galbraith Laboratories (Knoxville, TN).

RESULTS AND DISCUSSION

The model compounds used as process solvents in the liquefaction runs were 1-methylnapthalene (MN), tetralin (TET), 1,2,3,4-THQ, 2,3-cyclohexenopyridine (CHP), 1,2,3,4-tetrahydroisoquinoline (THIQ), 1-methyl-2,3,4-trihydroquinoline (MTHQ) and quinoline (QU). We determined (1) the extent of conversion to both solvent soluble and distillate material and (2) the level of solvent incorporation into the residuum in terms of solvent basicity, position and presence of donatable hydrogen, substituent interference (MTHQ) and presence of nitrogen in the ring (THQ vs. CHP).

A comparison of the toluene and pyridine conversions obtained for these runs is described in Figure 1. With respect to these conversions, the solubilities reported were obtained in the presence of the process solvent. Therefore, co-solvency effects may be involved. For example, as expected percent pyridine conversions are consistently higher than percent toluene conversions regardless of the model process solvent. For MN, TET and QU, the differences average more than 25%; whereas, with THQ, THIQ, MTHQ and CHP the differences are 6% or less. Co-solvency rather than depolymerization to smaller fragments may account for the relatively high toluene solubilities observed with most of the nitrogen-containing solvents. From these data conversion to pyridine solubles appears to be solely dependent upon the presence of readily donatable hydrogen as evidenced by comparing MN/TET (69.9% vs 96.8%) and QU/THQ (76.8% vs 95.5%). A dependence of toluene soluble conversion on the presence of nitrogen in the ring system is not very striking, MN/QU (51.1% vs 54.2%); whereas, if the nitrogen is accompanied by donatable hydrogen the dependence is great, TET/QU (71.4% vs 89.5%). Dependence of conversion to toluene or pyridine soluble products on the position of nitrogen in the ring, the basicity of the model solvent and the positional relationship of nitrogen to the donatable hydrogen in the ring structure was not found.

The product mass balances for the samples obtained through distillation are shown in Figure 2. Inspection of the figure demonstrates several points. First, the only run to demonstrate a net increase in distillate recovery was that of MN. In the TET case there was a net conversion of the insoluble MF coal. However, a recovery of volatile products demonstrated a conversion to light ends and gases rather tahn to slightly less volatile material. In all of the nitrogen heterocyclic cases, a net gain in residuum mass was found. In general, the distillate recoveries were greater than that in the tetralin case but they were still less than that predicted by the starting solvent mass. The reduction in distillate recovery correlates with incorporation of solvent into the residuum or a cracking of distillate to light ends of approximately 10-15% of the starting solvent mass. The exception found here was THIQ where even a larger amount of process solvent was lost to the light ends material.

The nitrogen content distributions for the products recovered in these runs are displayed in Figure 3. The nitrogen analyses were obtained from Galbraith Laboratories with use of the Kjeldahl method. In the cases of MN and tetralin, the sole source of nitrogen within the run was the coal itself. In both these products a shift of nitrogen content to the distillate mass was found. Under these conditions, approximately 20% of the nitrogen content in the coal is dynamic. When nitrogen heterocyclic compounds were employed a considerable amount of the nitrogen base was found to have adducted into the residuum or lost to the light ends. The percent nitrogen increase in the residuum reflects an incorporation of between 8 and 15% of the starting solvent mass. Steric interference was not found for MTHQ since the expected reduction in adduction did not occur. Distillate analysis via GC-FTIR demonstrated that a rapid dissociation of MTHQ to THQ had occurred resulting in a similar quantity of adduction.

To further delineate and quantify the coal-solvent interaction, nitrogen and mass balance data have been obtained on the products produced from a liquefaction run performed by Kerr McGee. The results of this investigation are presented in Table II. Upon inspection of these data, it is apparent that the nitrogen content of the initial solvent (THQ) is highly mobile. Approximately 8.0% of the original THQ material is lost to light ends, gas product and residuum material. The major portion of this loss was to the residuum (67.5% of N loss from solvent). This adduction was further found to be restricted to the solvent (THF) soluble material. The remaineder of the loss was to ammonia and small chain alkyl amines located in the gas product and light end. See Figure 4.

It is apparent from these data that adduction of process solvent to non-distillate and high boiling distillate materials is significant. Though some breakdown of process solvent was found, its contribution to the loss of the dynamic nitrogen component is minimal in comparison to the problem of adduction.

REFERENCES

1. Atherton, L., EPRI Journal, Jan.-Feb., 1984, 37.

2. Atherton, L. and Kulik, C., Advanced Coal Liquefaction, AICHE Meeting Los Angeles, March, 1982.

3. Whitehurst, D. D.; Mitchell, T. D.; Farcasiu, M. and Dichert, J. J., "The Nature and Origin of Asphaltenes in Processed Coal", EPRI Report AF-1298, Final Report under Project RP-410, December, 1979.

4. "Fundamental Studies in the Conversion of Coals to Fuels of Increased Hydrogen Content", Derbyshire, F. J.; Odoefer, G. A.; Rudnick, L. R.; Varghese, P. and Whitehurst, D. D., EPRI Report AP-2117, Volume 1, November, 1981.

Acknowledgments to EPRI for funding of this project and to Kerr McGee Corp. for sample preparation are gratefully extended.

TABLE II

MASS BALANCE AND NITROGEN CONTENT DATA

Starting Material

Mass		Total Wt. Nitrogen	21.66 g
THQ	200 g	% contribution	
Tetralin	--	by solvent	97.14%
Solvent	200 g		(21.06 g)
Coal	100 g	by coal	2.86%
MF Coal	75.9 g		(0.62 g)

Recovered Products

Distillate Wt.	203.19 g	Residuum Wt.	
%N	9.55%	%N	55.23 g
Wt. N	19.40 g	Wt. N	3.18%
% Total N Retained	89.48%	% Total N Retained	1.74 g 8.03%
Net Gain or Loss From solvent (initial weight)		Net Gain or Loss from Moisture free Coal (initial weight)	
Mass	+3.19 g (1.6%	Mass	-20.67 g (-27.2%)
Nitrogen	-1.66 g (-7.88%)	Nitrogen	+1.12 g (181%)

Product Distributions

% Total Mass Recovered as Distillate and Residuum	86.14%	% Total Mass as Light Ends and Gas Product (by difference)	13.86%
% Total Nitrogen Retained in Residuum and Distillate	97.51%	% Total Nitrogen in Gas Product and Light Ends (by difference)	2.49%

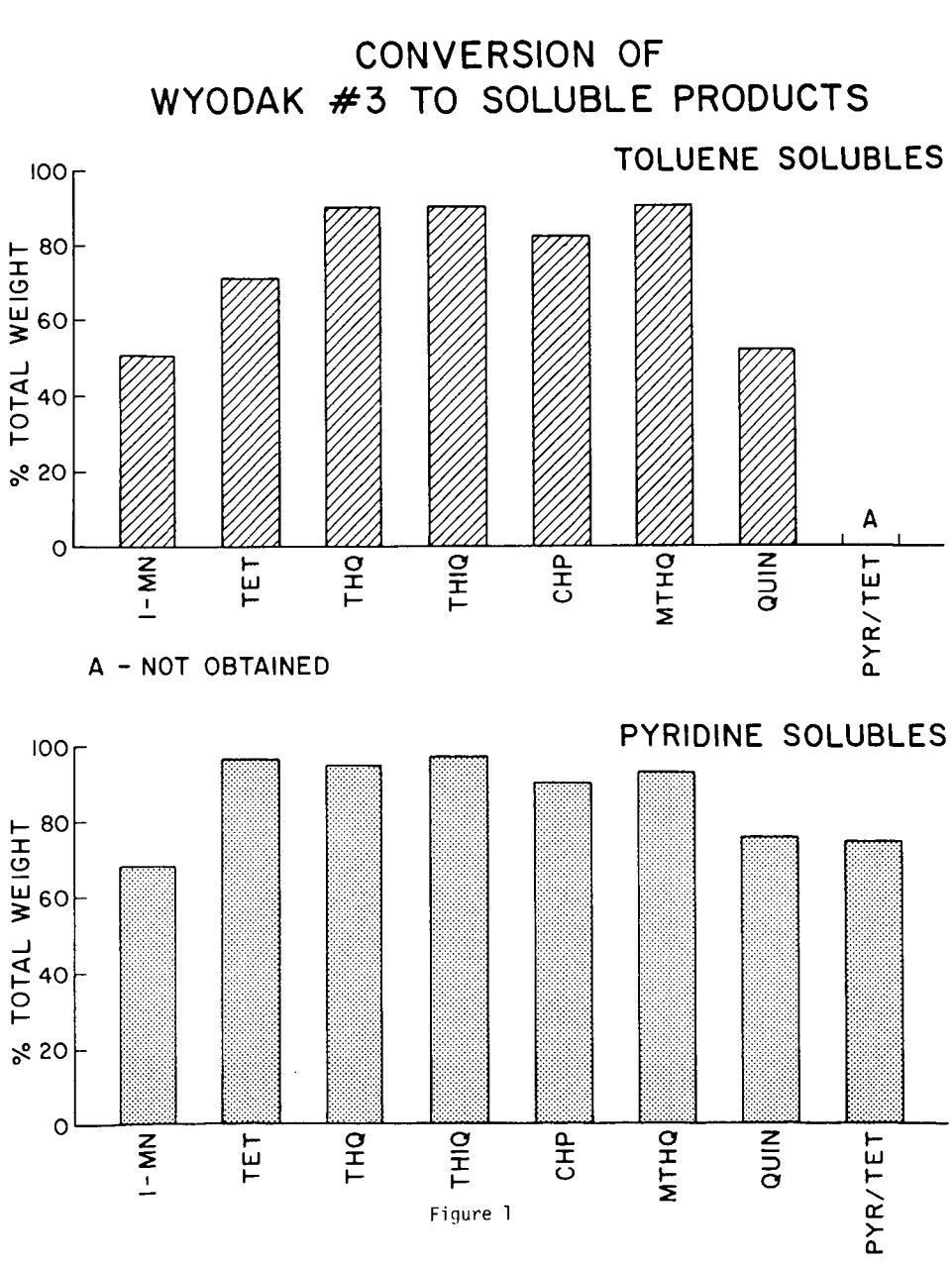
CONVERSION OF
WYODAK #3 TO SOLUBLE PRODUCTS
TOLUENE SOLUBLES
% TOTAL WEIGHT
100
80
60
40
20
0
A
1-MN
TET
THQ
THIQ
CHP
MTHQ
QUIN
PYR/TET
A - NOT OBTAINED
PYRIDINE SOLUBLES
% TOTAL WEIGHT
100
80
60
40
20
0
1-MN
TET
THQ
THIQ
CHP
MTHQ
QUIN
PYR/TET

Figure 1

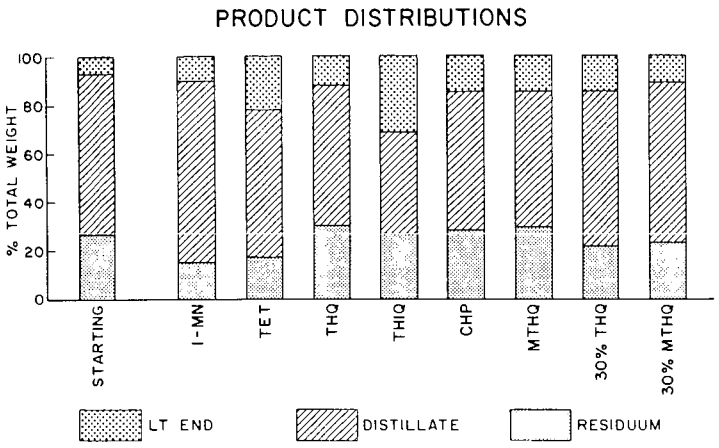

Figure 2

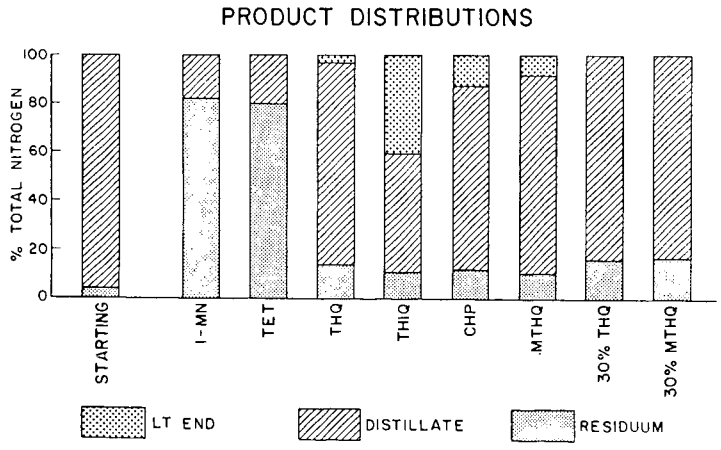

Figure 3

KERR MCGEE RUN P-24
MASS AND NITROGEN DISTRIBUTIONS

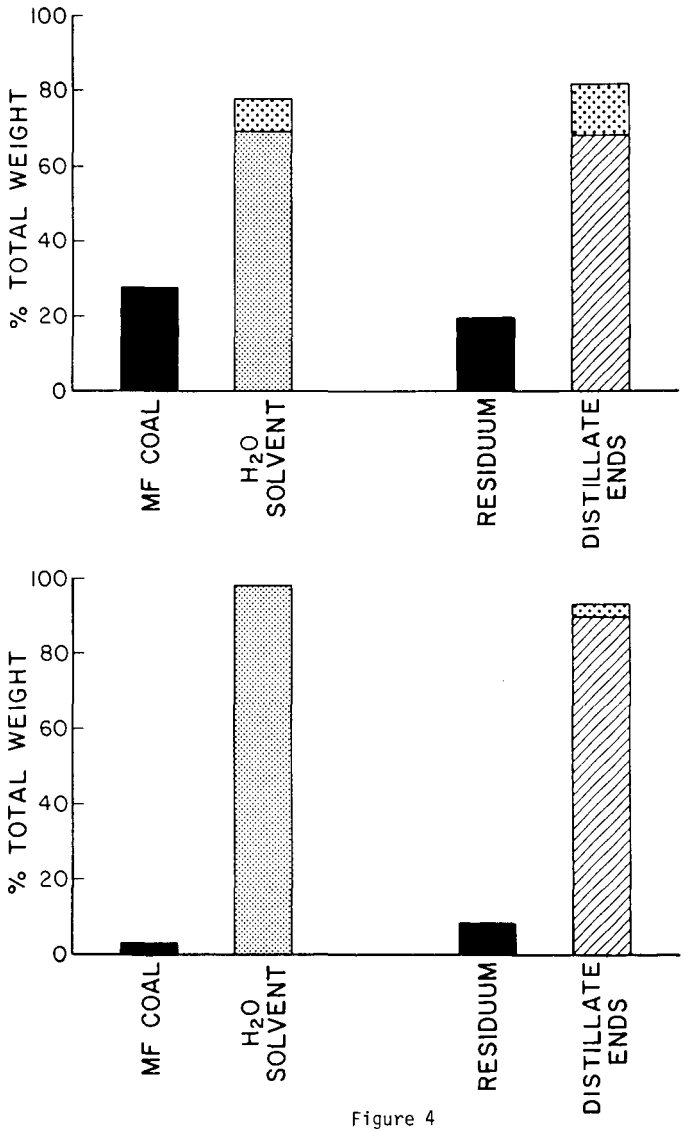

Figure 4

EFFECTS OF START-UP SOLVENT ON COMPOSITION OF RECYCLE LIQUEFACTION PRODUCT SLURRY FROM LOW-RANK COALS

R.C. Timpe, S.A. Farnum, D.J. Miller,
A.C. Wolfson, J.R. Rindt, and Y.R. Potts

University of North Dakota Energy Research Center
Box 8213, University Station
Grand Forks, North Dakota 58202

Introduction

As part of the on-going research in the liquefaction of low-rank coal, the University of North Dakota Energy Research Center (UNDERC) carried out two bottoms recycle runs. The purpose of these 40 pass runs was to investigate the effect of two different start-up solvents on the composition of the product from pass to pass, especially the bottoms portion used as recycle solvent, and the final lined-out composition of the product.

Runs 101 and 103 were carried out in the bottoms recycle mode in the Continuous Processing Unit (CPU) (1). Zap, North Dakota lignite from the Indian Head mine was introduced at 5 lbs/hr as a 30% slurry (wt % as-received coal) in recycle feed with H_2S addition in both runs. The nominal temperature was 440°C and the nominal pressure was 4000 psig H_2/CO (95/5). The startup solvent for Run 101 was a typical anthracene oil, A04, purchased from Crowley Tar Products, NY, previously described (2,3). Run 103 was started up with a Process Development Unit (PDU) recycle solvent obtained from the University of North Dakota Chemical Engineering Department's Project Lignite (4). The PDU solvent was derived from Zap, North Dakota Indian Head lignite. It has been characterized in detail (3). A short summary of the relevant properties of the two startup solvents appears in Table I. Both solvents provided adequate operability of the CPU and were greater than 95% distillable. These two startup solvents were chosen because they differ in several important ways. The PDU solvent contained about seven times more total alkanes and ten times more n-alkanes than the A04 solvent (Table I). The PDU solvent also contained a higher concentration of methylated and other alkylated aromatic hydrocarbons than A04. For example, 2- and 3-methylphenanthrene are present in the PDU solvent at 4.6 and 3.0 times their concentrations in A04. The PDU solvent also contains hydroaromatics (such as dihydro-, tetrahydro- and octahydro-phenanthrene, dihydropyrene, and tetrahydrofluoranthene) and phenols (6.2%). A04, deficient in both hydroaromatics and phenols, is composed mainly of unsubstituted aromatic hydrocarbons including larger amounts of aromatic compounds with more than three fused rings (i.e., chrysene and benz(a)anthracene) than the PDU solvent. These differences in composition are expected to affect the solvating power of the solvent toward coal and coal-derived products. The difference in reactive nature of the solvents at high temperature and pressure is expected to lead to different initial products.

The liquefaction products were examined from pass to pass in order to follow the compositional changes as the reaction proceeded toward steady-state composition (lineout) and to determine whether the products were chemically the same for both runs after 40 reactor passes.

Table I. Properties of Startup Solvents A04 and UND PDU Solvent Used In CPU Runs 101 and 103

	A04	PDU
Elemental Analysis:		
% C	90.33	82.36
H	6.54	7.89
N	0.83	0.21
S	0.57	1.19
O (by difference)	1.73	2.49
Ash, %	0.03	1.43
Water, %	0.20	4.43
Selected Organic Component Analysis, wt %:		
n-alkanes	0.6	6.8
total alkanes	2.2	13.9
Selected Hydrocarbons and Ethers:		
naphthalene	0.75	0
2-methylnaphthalene	1.44	0.14
acenaphthene	9.54	0.08
phenanthrene	16.6	6.99
dibenzofuran	6.67	0.39
3-methylphenanthrene	0.66	3.06
2-methylphenanthrene	0.84	2.55
fluoranthene	0.52	0.82
pyrene	6.87	0.46
fluorene	6.67	0.36
benzo(a)anthracene	0.26	0.06
chrysene	0.27	0.16
9,10-dihydrophenanthrene	0	0.23
octahydrophenanthrene	0	0.02
1,2,3,4-tetrahydrophenathrene	0	0.18
4,5-dihydropyrene	0	0.44
1,2,3,4-tetrahydrofluoranthene	0.01	0.06
polars (phenols, base and polar aromatics)	18.4	21.4
phenols	0	6.2

Our previous efforts were concentrated on analysis of distillable portions of the products from earlier runs which averaged approximately 13 passes (5). When we investigated these runs we noticed that some irreversible changes caused by heating had occurred to the vacuum bottoms during the ASTM D-1160 distillation. We carried out several preliminary separations using Soxhlet extraction, sonication and sonication with heat, none of which proved satisfactory for this study. A method was then selected for separation of the slurry that excluded all severe handling of the product to avoid changes in the heavy product composition during separation.

The preliminary characterization of the separated heavy products and their composition as compared with the composition of the oils are the focus of this report. Changes in the startup solvent as it reacts with coal and is diluted by coal-derived products are discussed with emphasis on the heavy components. Differences between the two runs started up with different solvents are described.

Experimental

The method chosen to separate the product slurry is based on solubilities at room temperature (Figure 1). This separation yielded a pentane soluble, volatile oil fraction (oil), a pentane insoluble, methylene chloride soluble heavy fraction (soluble heavy ends), and a methylene chloride insoluble fraction (insoluble heavy ends), Table II. Further fractionation of the oils and soluble heavy ends from pass 40 was carried out by silica gel open column chromatography. Three fractions were collected: alkanes (eluted with pentane, isooctane, pentane), aromatics (eluted with methylene chloride), and polars (eluted with methanol) (Table III). The chromatographic method involved 100 g Aldrich Grade 12 28-200 mesh silica gel activated at 250°C for 24 hours packed dry between two glass wool plugs in a Pyrex column that had a 75-100 μ fritted glass plate. The silica gel was wetted with HPLC grade pentane and then loaded with ~1 gram of sample. Elution was in the following sequence with HPLC grade solvents: 150 ml pentane, 100 ml isooctane, 50 ml pentane, 250 ml methylene chloride, and 100 ml methanol. The first three listed elute alkanes, the fourth elutes aromatics and the polar compounds are eluted with the fifth.

Characterization studies were carried out on the fractions using elemental analysis, tetrahydrofuran (THF) solubility, thermogravimetric analysis (TGA), size exclusion high performance liquid chromatography (mobile phase THF, UV and refractive index detection), IR spectrometry, 200 MHz ^{1}H NMR and 50 MHz ^{13}C NMR spectrometry, capillary GC/MS and direct probe MS.

Results and Discussion

The variation in composition of the product slurries from Runs 101 and 103 during 40 recycle passes is shown in Figure 2 and Table II.

Insoluble Heavy Ends. The insoluble heavy ends increased during both runs. A steadier, earlier increase was seen during Run 101 (Figure 2), coinciding with the increasing viscosity. During Run 101 the reactor was "blown down" only once (pass 25) to remove accumulated reactor solids resulting in a rapid drop in viscosity. The viscosity then rose slowly until pass 40 where a rapid increase was seen (3). The insoluble heavy ends increased more slowly during Run 103. This slower increase may be related to the much lower viscosity observed

Table II. Composition of Recycle Slurries (Wt %) During CPU Runs 101 and 103

Fractions	Pass No. 0	7	19	30 (31)	40
Oil:					
101	94.5	70.9	50.2	54.7	48.4
103	88.3	67.0	59.0	46.3	46.1
Soluble Heavy Ends:					
101	4.1	14.3	19.9	16.4	16.1
103	2.7	18.9	19.6	16.2	19.7
Insoluble Heavy Ends:*					
101	0.04	8.6	19.1	27.6	29.8
103	3.1	9.9	12.7	24.4	25.6
Total % Recovery:					
101	98.6	93.8	89.2	98.7	94.3
103	94.1	95.8	91.3	86.9	91.4
Ash:					
101	0.03	6.6	10.8	11.2	11.4
103	4.4	6.9	9.8	13.0	11.5

*Includes mineral matter.

Table III. Silica Gel Column Fractionation of CPU Runs 101 and 103 Pass 40 Oils and Soluble Heavy Ends (Wt %)

	101 Pass 40		103 Pass 40	
	Soluble Heavy Ends	Oil	Soluble Heavy Ends	Oil
Alkanes	0.1	5.6	0.6	8.0
Aromatics	56.2	59.1	45.0	58.6
Polars	35.3	28.1	36.6	31.2
% Recovery	92.6	92.8	82.2	97.8

during Run 103. The viscosity was controlled during Run 103 by scheduling reactor blowdown every twelfth pass. Direct insertion probe MS heating profiles of the insoluble heavy ends from Runs 101 and 103 gave non-quantitative profiles of the small percentage of the material that could be analyzed by this method. The insoluble heavy ends sample from Run 101 gave a prominent peak that volatilized early in the run. This peak gave a mass spectrum that appeared to be identical with that of 1,2'-binaphthyl. This component was not present in the insoluble heavy ends from Run 103. It was not a prominent component of the soluble heavy ends from either run. After subtracting the ash content and the THF soluble portion of the heavy ends, 7.5% of Run 101 and 6.7% of Run 103 is intractable THF insoluble organic matter (Table IV).

Soluble Heavy Ends. The soluble heavy ends also increased gradually from pass to pass during both Runs 101 and 103 as the coal-derived materials began to replace the >91% soluble startup solvents (Figure 2 and Table II) until pass 40 where the sum of the insoluble and soluble heavy ends reached about 45% to 46%. This leaves 48.4% (Run 101) and 46.1% (Run 103) oils as products at pass 40 (Figure 2 and Table II).

Characterization of the soluble heavy ends is much more difficult than the characterization of distillable oils which can be easily separated by capillary GC and identified by GC, GC/MS and NMR comparisons with known standard compounds. However the soluble heavy ends resemble the oils in some very important ways. They can be separated by simple column chromatography on silica gel into fractions easily identified as alkanes (δ0.5-1.4), aromatics (δ7.2-8.7), and polars (δ6.2-7.2) by 200 MHz ^{1}H NMR (Figure 3) and 50 MHz ^{13}C NMR spectrometry. The soluble heavy ends from Runs 101 and 103 partitioned differently with our separation (Table III). Run 103 produced more C-9 and larger alkanes in the heavy and oil fractions than Run 101. Small contamination of both alkane fractions by phthalates occurred (note extraneous peaks on Figure 3, top right). Small amounts of phthalate contaminants were accidentally introduced into the slurry. They appear in all three column fractions, but mainly in the heavy ends polar fraction of Run 101. Run 103 also produced more polars in the oil and heavy fractions than Run 101 (Table III). Run 101 produced slightly more aromatic hydrocarbons than Run 103.

Soluble Heavy Ends-Aromatic Fractions. Differences between aromatic fractions of the soluble heavy ends of Runs 101 and 103 may be seen by inspection of the elemental analyses (Table V), the ^{1}H NMR spectra (Figure 3, middle), the IR spectra (not shown), TGA volatiles, and the average molecular weight maxima (Table IV). Direct insertion probe MS heating profiles from 30° to 350°C at 5°/min obtained at 10 ev and 70 ev were compared for samples of aromatic fractions of the soluble heavy ends Run 101 and 103. During the first part of the heating profiles small amounts of materials with masses recognizable as common hydrocarbons were noted. These included such masses as 128,142 (probable naphthalenes), 178,192 (phenanthrenes) and 202,216 (pyrenes) which were seen in the heavy aromatic fractions of both Runs 101 and 103. Masses 168,182 and 196 (probable dibenzofurans) were much more prominent in the heavy aromatics from Run 103 than Run 101. These parent ions, present in both high- and low-voltage mass spectra, are probably small hydrocarbons and ethers partitioned into the heavy fraction during our initial solubility separation. As the heating progressed a large number of masses giving the maximum ion current

Table IV. Properties of Oils, Soluble Heavy Ends, and Insoluble Heavy End Fractions of CPU Runs 101 and 103, Pass 40

Sample	THF Insoluble (wt %)	Nonvolatiles (TGA) (wt %) (T_{max})	Average MW Maxima (Size Exlusions HPLC)
Total Samples:			
101 Sol. Heavy Ends	0.00	32.52 (800C)	10,000, 1200, 475
103 Sol. Heavy Ends	0.00	31.62 (800C)	10,000, 1200, 475, 280, 240
101 Oil	0.00		1200, 540, 420, 360
103 Oil	0.00		620, 505, 360, 210, 340, 290, 260
Silica Gel Column Fractions 3 (aromatics):			
101 Sol. Heavy Ends	0.00	42.69 (500C)	1200, 1000, 550
103 Sol. Heavy Ends	0.00	36.25 (500C)	10,000, 1200, 600, 450, 320
101 Oil	0.00	2.83 (500C)	610, 385, 345, 320, 220, 160
103 Oil	0.00	1.75 (500C)	330, 310, 220, 210, 170, 150
Silica Gel Column Fractions 4 (polars):			
101 Sol. Heavy Ends	1.97	31.98 (500C)	13,000, 1350, 520, 450
103 Sol. Heavy Ends	4.61	17.75 (500C)	1200, 480, 430, 380
101 Oil	0.00	11.31 (500C)	15,000, 1100, 680, 540, 450, 360, 330, 150
103 Oil	4.46	13.53 (500C)	16,000, 1000, 520, 380, 360, 250, 200
Insoluble Heavy Ends:			
101	63.5 (18.9% of slurry)		
103	71.0 (18.2% of slurry)		

Table V. Elemental Analyses of Products from CPU Runs 101 and 103, Pass 40

Sample	Column Fraction	Elemental Analysis C	H	N	O	C-100 Formula
101 Oils	Aromatics	85.06	7.34	0.28	7.32	$C_{100}H_{102.82}N_{0.28}O_{6.46}$
101 Sol. Heavy Ends	Aromatics	88.89	5.77	1.43	3.91	$C_{100}H_{77.30}N_{1.38}O_{3.30}$
103 Oils	Aromatics	88.56	7.66	1.67	2.11	$C_{100}H_{103.11}N_{1.61}O_{1.79}$
103 Sol. Heavy Ends	Aromatics	90.44	5.81	1.21	2.54	$C_{100}H_{103.11}N_{1.61}O_{1.79}$
101 Oils	Polar	77.96	7.66	1.33	13.05	$C_{100}H_{117.09}N_{1.46}O_{12.57}$
101 Sol. Heavy Ends	Polar	70.63	4.94	2.36	22.07*	$C_{100}H_{83.33}N_{2.86}O_{23.46}$*
103 Oils	Polar	77.12	7.88	1.06	13.94	$C_{100}H_{121.74}N_{1.18}O_{13.57}$
103 Sol. Heavy Ends	Polar	80.76	6.61	1.86	10.77	$C_{100}H_{97.62}N_{1.98}O_{10.02}$
101 Oils	Total	85.31	8.31	0.58	5.80	$C_{100}H_{116.06}N_{0.58}O_{5.10}$
101 Sol. Heavy Ends	Total	85.87	5.88	1.65	6.60	$C_{100}H_{81.54}N_{1.65}O_{5.77}$
103 Oils	Total	82.23	7.98	0.78	8.01	$C_{100}H_{114.29}N_{0.81}O_{7.22}$
103 Sol. Heavy Ends	Total	85.98	6.05	1.75	6.22	$C_{100}H_{83.80}N_{1.75}O_{5.44}$

*Contaminated by phthalate plasticizer.

around mass 500 were observed. This result agrees with the maxima of mass 550 and 450 in the size exclusion chromatographic HPLC average molecular weight profiles from both Runs 101 and 103 (Table IV). There were a large number of both even and odd masses represented in profiles from both runs. Run 103 had a particularly prominent odd mass homologous series of 381, 395, 409, 423, 439, 453, and 467. The unit resolution of our quadrupole MS did not permit confirmation of these masses as aromatic nitrogen compounds, however they were tentatively assigned to neutral aromatic nitrogen compounds after considering the N/C ratios (Table V) and the separations used to obtain the fractions.

Soluble Heavy Ends-Polar Fractions. ^{13}C NMR and ^{1}H NMR spectroscopy (Figure 3, bottom) show a predominance of phenolic oxygen functionality in the soluble heavy ends polar fractions from both Runs 101 and 103. Although the total polar nitrogen content in the two runs was almost the same, the distribution of nitrogen compounds differed. The polar compounds from Runs 101 have a higher N/C ratio than those from Run 103 (Table V). Direct insertion probe MS heating profiles comparing the polar fractions from Runs 101 and 103 indicated a lower molecular weight range than that of the aromatic fractions, thus supporting the size exclusion chromatographic HPLC distribution (Table IV). Even and odd masses were plentiful within the molecular weight range found for heavy samples from Runs 101 and 103. A strong correlation between oxygen content (mostly phenolic) and viscosity for solvent-refined coals was noted in our laboratory but the same study failed to find a correlation between total nitrogen content and viscosity (6). At the present time it is not clear whether the differences found in nitrogen compound type distribution in the present study have any effect on viscosity.

Oils. Analysis of the oils from pass 40 of Runs 101 and 103 were carried out in order to provide comparison with the soluble heavy ends and to supply mass balance for the slurry separation analysis. A much more detailed characterization of the oils throughout the entire run is being prepared. The percentage of oils decreases from >85% in the solvents at the beginning of the runs to 45%-58% at the last pass. Differences in composition of the oils from Runs 101 and 103, pass 40, were assessed using the analytical procedures already described and solvent extraction (7). Base extraction of the phenols gave the same percent phenols for both Runs 101 and 103. The amounts of methylated phenanthrenes in the aromatic fraction of Run 103 were larger than in Run 101. The difference in the phenanthrene composition between Runs 101 and 103 pass 40 oils may be seen by observing the region between the resonances for unsubstituted phenanthrene hydrogens at 8.71 and 8.68 δ and the pyrene peak at 8.20δ in the 200 MHz ^{1}H NMR spectra at the bottom of Figure 4. The peaks between these values are characteristic of substituted phenanthrenes. The unsubstituted aromatic hydrocarbons, phenanthrene (8.71, 8.68 δ), fluorene (3.98δ), and acenaphthene (3.39δ) are more plentiful in Run 101 pass 40 oils than in Run 103 oils.

Pass to pass composition changes during the two recycle runs were observed (Table II, Figure 4). These changes are graphically displayed in Figure 4 which shows 200 MHz ^{1}H NMR spectra of some of the product oils as they change in composition from pass to pass. These changes are more evident during the initial dilution of startup solvent with product and become more subtle between the 30th and 40th

pass. The composition of product oil from both Runs 101 and 103 still appear to be changing slowly at pass 40.

Summary

A room temperature solubility separation method was used to separate the products of two 40 pass CPU runs that used different startup solvents. Although the composition was not investigated in detail, the insoluble heavy ends fraction from Run 101 appeared to contain binaphthyl while Run 103 did not. The oils and soluble heavy ends portions from the 40th pass were fractionated by silica gel column chromatography. The separation into alkanes, aromatics, and polars gave clean fractions based on NMR spectral data. The ^{1}H and ^{13}C NMR spectra of the corresponding oil and heavy fractions within a slurry sample resembled each other with oil polars (known to be mainly phenolic) resembling heavy polars and oil aromatics resembling heavy aromatics. The difference between oil and heavy polar fractions that causes them to be separated by solubility appears to be polarity rather than molecular weight differences. However, the major difference between oil and heavy aromatic fractions causing solubility separation is apparently due to molecular weight differences.

The success of these separations with materials of moderately high molecular weight makes possible a survey of a larger percentage of the liquefaction product slurry. The characterization of the fractions by a combination of techniques is now possible. A lack of high molecular weight model compounds to serve as knowns for further analysis presents a problem; however, additional work is in progress.

The products from Runs 101 and 103 after 40 passes were chemically dissimilar. Both the oils and the heavy ends showed a number of differences. It was of interest to note that the run started up with the PDU recycle solvent that contained more alkanes (13.9%) still yielded a product with more alkanes after 40 passes but the total amount was only 8% of the oil, 3.8% of the product slurry. The percent phenols in the oil (by extraction) was very close to equal for pass 40 from Runs 101 and 103 but the aromatic hydrocarbon character of the startup solvent appeared to be recognizable after 40 passes in both Runs 101 and 103. Run 103 still contains more alkylated and methylated aromatic hydrocarbons like the PDU solvent while Run 101 contained more unsubstituted aromatic hydrocarbons such as phenanthrene, acenaphthene, and fluorene like A04. There was an unequal distribution of nitrogen within the products from the two runs.

Various composition data were examined in an attempt to find a correlation with the much higher viscosity of Run 101. There did not seem to be much difference in the size of any heavy fraction when Runs 101 and 103 were compared, although the insoluble heavy ends were somewhat larger in Run 101 (29.8% of the slurry compared with Run 103 25.6%). The portion of the slurry that represents THF insoluble very heavy intractable organic matter was 7.5% for Run 101 and 6.7% for Run 103. The composition of the soluble heavy ends with respect to amounts of phenols and aromatics did not appear to be the cause of the viscosity. Only one difference was noted and that was Run 101 heavy ends polar fraction showed a higher N/C ratio indicating a different compound type distribution than Run 103. The viscosity difference could not be explained based on the oil composition. The percent phenols in the oil was the same in both Runs 101 and 103 although the polar (mainly phenolic) fraction of Run 101 also showed the higher N/C ratio indicating different compound types are present than in Run 103.

Acknowledgments

UNDERC carried out this work for the U.S. Department of Energy under Cooperative Agreement No. DE-FC21-83FE60181. The authors wish to thank Art Ruud for the elemental analyses and Ed Bitzan for size exclusion chromatography data.

Literature Cited

1. Rindt, J.R.; Willson, W.G.; and Stenberg, V.I. "Recent Advances in Catalysis of Lignite Liquefaction," 1983 Lignite Symposium, Grand Forks, North Dakota (in press).
2. Farnum, S.A.; Farnum, B.W.; Bitzan, E.F.; Willson, W.G.; and Baker, G.G. Fuel, 1983, 62, 799.
3. Quarterly Technical Progress Report, January-March 1982, DOE/FC/QTR-82/2 (DE83013383), pp. 2-5.
4. Severson, D.E.; Souby, A.M.; and Owens, T.C. 1982, Energy Sources, 6 (3), 173-192.
5. Farnum, S.A.; Farnum, B.W.; Baker, G.G.; and Lechner, T.J. Amer. Chem. Soc. Div. Fuel Chem., Preprints 1982, 27 (3,4) 6.
6. Schiller, J.E.; Farnum, B.W.; and Sondreal, E.A. 1977, Amer. Chem. Soc. Div. Fuel Chem., Preprints, 22 (6), 33.
7. Farnum, S.A.; and Farnum, B.W. 1979, Anal. Chem. 1982, 54, 979.

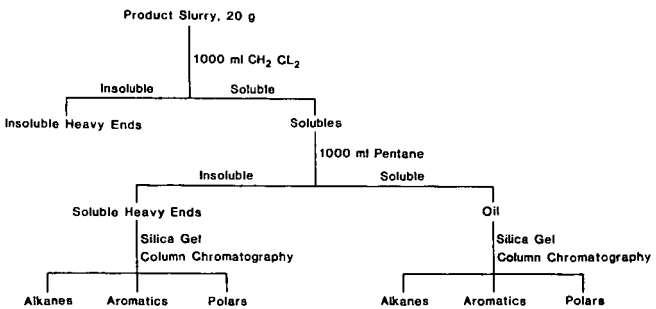

Figure 1. Separation of CPU product slurry by solubility and silica gel column chromatography.

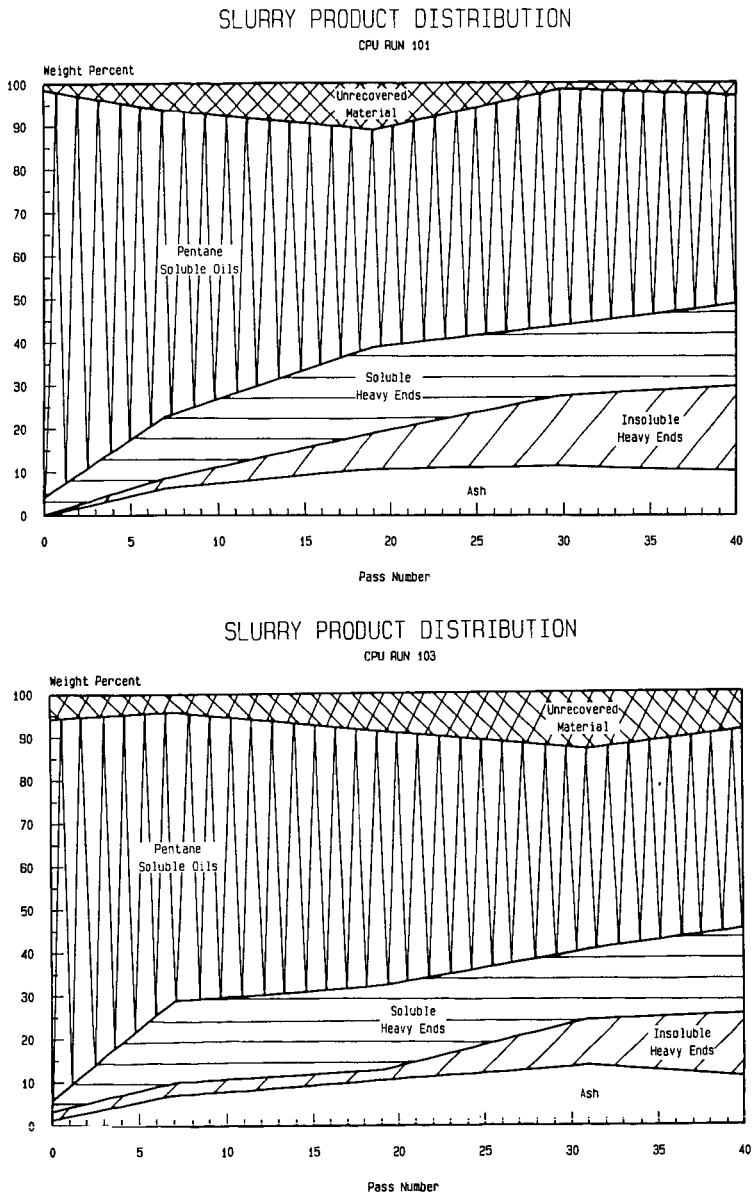

Figure 2. Product distribution as determined by solubility separation and ash analysis for CPU product slurries from Runs 101 and 103.

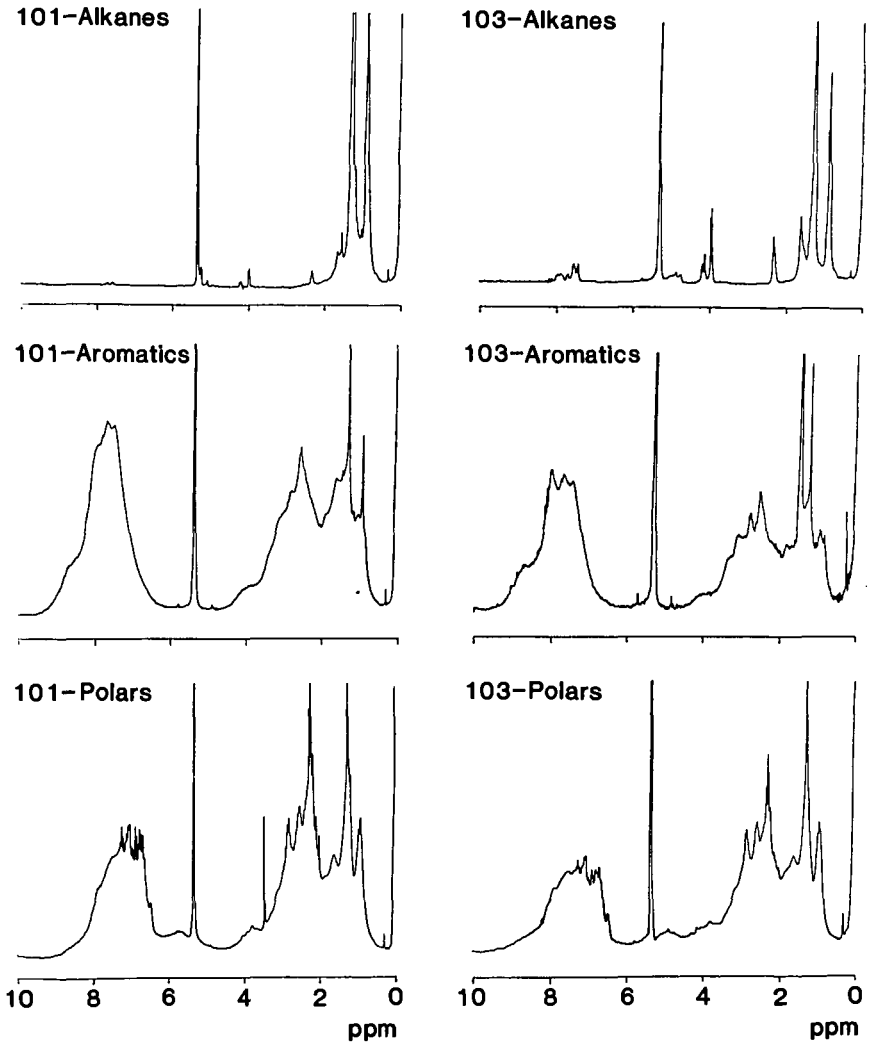

Figure 3. 200 MHz ^{1}H NMR spectra of silica gel column chromatographic fractions from soluble heavy ends, CPU Runs 101 and 103.

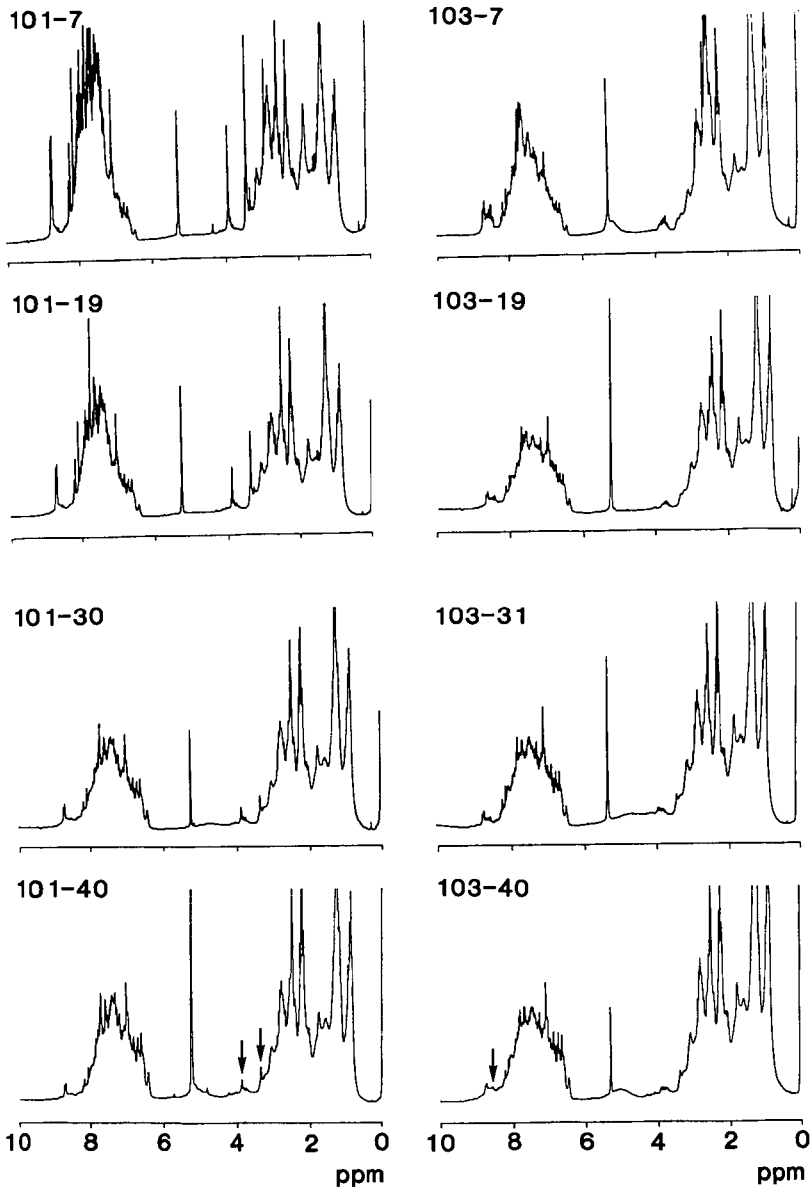

Figure 4. Changes in the oils during CPU Runs 101 and 103 as shown by 200 MHz ^{1}H NMR spectroscopy.

Chemical Interactions Between Heavy Solvent Components and Coal During Coal Liquefaction

James R. Longanbach

Battelle Columbus Laboratories
505 King Avenue
Columbus, Ohio 43201

Introduction

Interest in the heavy components in recycle solvents from direct coal liquefaction processes was generated when Kerr-McGee and Conoco reported that the addition of light SRC, a fraction from the critical solvent deashing step in the SRC Process, to the recycle solvent greatly improved overall solvent quality.[1] However, some heavy components are not beneficial and can lead to coke formation. Clearly, recycling some high molecular weight solvent components is beneficial to direct coal liquefaction processes while recycling others is not. The objective of this study has been to look at the chemical reactions of the heavier materials from an actual recycle solvent during the dissolving step of two-stage coal liquefaction.

Experimental Approach

The experimental approach has been to (1) obtain a recycle solvent from the Lummus integrated two-stage liquefaction (ITSL) process pilot plant, (2) distill the solvent to 454°C, (3) separate each distillation cut into fractions of chemically similar compounds, (4) characterize the separated fractions in detail, and (5) study the effects on liquefaction when each solvent fraction is used as a heavy recycle solvent additive in a microautoclave liquefaction experiment.

Coal and Solvent

Illinois #6 bituminous coal (Burning Star) which had been ground to 80 percent -200 mesh and dried to 4 percent moisture for use in the Lummus ITSL pilot plant was used for this work. An analysis is shown in Table 1. This coal was ground in Alabama and shipped to New Jersey so it may have experienced some oxidation, but it is probably typical of the coals which would actually be used in direct liquefaction processes. The coal was stored under nitrogen in glass jars after it was received in an attempt to minimize additional oxidation during storage.

Recycle solvent from the Lummus ITSL pilot plant was used as the solvent. This solvent is a +343°C distillation residue which had been partially hydrogenated in the process. The recycle solvent was distilled under vacuum to 427°C and a -427°C distillate and a +427°C residue were obtained and analyzed. Analysis of the starting recycle solvent and the two distillation fractions are listed in Table 2. Of the total solvent, 36 percent boiled below 427°C and 64 percent boiled above 427°C. The residue contained most of the heteroatoms; 80 percent of the nitrogen, 84 percent of the sulfur and 76 percent of the oxygen.

Solvent Separation

Separations of the solvent fractions obtained by distillation to 454°C were carried out as shown in Figure 1 using a column chromatography method developed by Later and Lee[2]. The sample (10 g) was coated on Brockman Activity 1 neutral alumina (200 g) and eluted with hexane, benzene, chloroform, and tetrahydrofuran. The chemical types eluted were non-aromatic hydrocarbons, aromatic hydrocarbons, N-aromatics, and O-aromatics, respectively. Some polar material was retained on the column.

TABLE 1. ANALYSES OF ILLINOIS #6 COAL FROM THE LUMMUS ITSL PROCESS PILOT PLANT

Proximate Analyses, Wt %	As-Received	Dry
Moisture	3.99	-
Ash	9.72	10.12
Elemental Analyses, Wt %		
Carbon	69.73	72.63
Hydrogen	4.93	4.67
Nitrogen	1.18	1.23
Sulfur	2.88	3.00
Oxygen (by difference)		8.35
H/C		0.77
Particle Size Distribution, Wt %		
+70 mesh	0.07	
-70 +120	3.64	
-120 +200	18.90	
-200 +325	14.84	
-325	62.55	

TABLE 2. ANALYSES OF RECYCLE SOLVENT FROM THE LUMMUS ITSL PROCESS PILOT PLANT

Sample	SCT Recycle Solvent (2SCT16-1122)		-427°C	+427°C	
Elemental Analyses, Wt %		MAF			MAF
Ash	1.30	-	<0.01	2.00	-
Carbon	86.77	87.91	90.96	87.88	89.67
Hydrogen	6.88	6.97	7.12	6.18	6.31
Nitrogen	0.94	0.95	0.57	1.30	1.33
Sulfur	0.53	0.54	0.23	0.69	0.70
Oxygen (by difference)	3.6	3.63	1.12	1.95	1.99
H/C	0.95		0.94	0.84	
Distillation Data, Wt %					
-427°C	35.6				
+427°C	64.4				
Molecular Weight, g/mole	477		257	456	

A second separation was carried out on partially deactivated silicic acid (3 g water/100 g silicic acid) by coating it with the N-aromatic fraction (3.35 g) and eluting with carbon tetrachloride, benzene and tetrahydrofuran. These single solvents were used instead of the two-component solvents described by Later and Lee[2] so that they could be recycled in the large scale column chromatography equipment. Only the +454 C N-aromatic fraction was separated on silicic acid.

The results of the first column chromatography separation are shown in Figure 2. Of the -454 C fraction, 9.6 percent is non-aromatic hydrocarbons, 72.9 percent is aromatic hydrocarbons, 5.6 percent is N-aromatics and 0.4 percent is O-aromatics. Only 3.8 percent is polar material which did not elute from the column. Overall, 82.5 percent of the -454°C solvent fraction are heteroatom-free hydrocarbons.

The +454°C fraction consists of only 1.3 percent non-aromatic hydrocarbons, 27.0 percent aromatic hydrocarbons, 4.8 percent N-aromatics and 33.3 percent O-aromatics. A large amount of polar material, 29.1 percent, is also present and does not elute from the column. The heteroatom-free hydrocarbons total only 28.3 percent of the +454°C recycle solvent fraction.

Several separations of the +454°C N-aromatic fraction on silicic acid gave yields of 13-26 percent primary nitrogen compound (aromatic amines), probably contaminated with tertiary nitrogen compounds in which the basic nitrogen is sterically "protected". The yield of acidic secondary nitrogen compounds (pyrroles, etc.) was 20-30 percent and the yield of basic tertiary nitrogen compound (pyridine derivatives) was 30-45 percent. Total recoveries ranged from 75-85 percent.

Results and Discussion

The separated fractions were characterized by measuring molecular weight (by Vapor Phase Osmometry using THF as the solvent), elemental analyses and H^1-NMR. This data was used to obtain average structural parameters by application of the Brown-Ladner equations.[3] Titrations of basic nitrogen were done using perchloric acid in acetic acid.[4] Titrations of acidic hydrogen were done by refluxing with metallic sodium in tetrahydrofuran, adding water after removing excess sodium, and back titrating the sodium hydroxide formed with standard HCl.[5] The analytical results are summarized in Table 3.

All of the coal liquefaction experiments were done in a microautoclave liquefaction apparatus using 5 minutes reaction time at 427°C under 1000 psi hydrogen (room temperature) with a solvent/coal/additive ratio of 2:1:0.5.

A diagram of the microautoclave reactor is shown in Figure 3. It consists of a 3/4-inch union-tee microreactor which has a volume of 22.4 cc, a valve to add and release gases, a thermocouple which extends into the microautoclave to monitor temperature, and a pressure transducer to monitor pressure during each experiment. The microautoclave is heated in a sand bath and shaken horizontally. A 3/8-inch ball bearing is added to facilitate mixing.

The product gases were analyzed by GC and the liquids and solids were fractionated by their solubilities in THF, toluene and heptane into insoluble organic material (IOM) plus ash, preasphaltenes, asphaltenes and oils. Yields were calculated and a complete mass balance was done for each experiment. Mass balances averaged 99.2 percent, excluding water and gases.

Non-Aromatic Hydrocarbons

The non-aromatic hydrocarbon fractions are complex mixtures of paraffins, olefins and naphthenes. The -454°C fraction has an average molecular formula of $C_{21}H_{32}$ (5 unsaturations or rings) and the +454°C fraction has an average molecular formula of $C_{26}H_{45}$ (3.5 unsaturations or rings). Comparison of the conversions to THF solubles (Table 4) shows that the heavier fraction is a better solvent. The non-aromatic hydrocarbons are expected to act only as a physical solvent since they contain few or no hydroaromatics which can lose hydrogen readily. The heavier material therefore appears to be better able to dissolve the products of liquefaction, possibly because more of the heavier fraction is in the liquid state and less in the vapor phase due to the higher boiling point range.

TABLE 3. ANALYSES OF -454 C AND +454 C RECYCLE SOLVENT FRACTIONS SEPARATED BY COLUMN CHROMATOGRAPHY

Fraction	Non-aromatic Hydrocarbons		Aromatic Hydrocarbons		N-Aromatics		+454 C N-Aromatic Fractions			OH-Aromatics	
Temp	-454 C	+454 C	-454 C	+454 C	-454 C	+454 C	Secondary-N	Primary-N	Tertiary-N	-454 C	+454
Solvent	Hexane		Benzene		Chloroform		Carbon Tetrachloride	Benzene	Chloroform	THF/Ethanol	
Elemental Analyses, wt % MAF											
Carbon	89.03	87.26	92.40	93.18	86.30	87.14	88.83	88.12	86.89	76.50	73.02
Hydrogen	10.97	12.70	7.59	6.58	6.82	6.51	7.05	6.33	7.05	7.20	7.21
Nitrogen	0.00	0.00	0.00	0.00	4.41	2.47	1.64	2.53	2.03	1.86	1.37
Sulfur	0.00	0.00	0.00	0.00	0.58	0.57	0.29	0.44	1.07	1.02	0.58
Oxygen (diff.)	0.00	0.00	0.00	0.00	1.89	3.31	2.19	2.58	2.96	13.42	17.82
H/C	1.48	1.75	0.99	0.84	0.95	0.90	0.95	0.86	0.97	1.13	1.18
Molecular Weight, g/mole	289	352	247	300	230	347	398	381	396	217	325
Hydrogen Distribution, % of Total Hydrogen											
Aliphatic	74.2	100.0	31.0	25.9	20.4	23.3	34.8	31.1	26.9	28.2	24.1
Aliphatic α to aromatic	22.0	0.0	41.0	35.4	42.5	30.8	28.2	29.8	35.0	45.5	54.4
Aromatic (1)	3.8	0.0	28.0	38.7	37.0	44.7	36.8	38.3	35.3	25.9	20.0
Phenolic (2)	0.0	0.0	0.0	0.0	0	1.3	0.21	.76	2.9	1.8	1.5
Donatable H, Wt % of Sample	-	-	1.52	1.42	1.43	0.88	1.31	0.93	1.17	1.53	1.77
Structural Parameters (4)											
f_a - aromaticity	0.29[5]	-	0.65	0.74	0.70	0.76	0.70	0.77	0.70	0.58	0.54
R_A - number of aromatic rings	-	-	2.6	4.1	2.1	3.6	3.8	4.7	3.7	0.48	0.84
H_{aro}/C_{aro} - substitutable aromatic edge atoms/total aromatic atoms	-	-	0.74	0.65	0.1	0.73	0.72	0.64	0.73	1.	1.
σ - fraction aromatic edge atoms substituted	-	-	0.42	0.31	0.38	0.30	0.30	0.32	0.38	0.59	0.70
C_A - total no. aromatic C atoms	-	-	12.3	17.2	11.6	19.0	20.6	20.7	20.1	8.0	10.5
R_S - substituted aromatic ring carbons	-	-	3.9	3.5	3.6	4.2	4.4	4.2	5.6	4.7	7.3
n - carbon atoms/saturated substituent	-	-	1.8	1.7	1.5	1.8	2.2	2.0	1.8	1.6	1.5
Molecular Formula											
C	21	26	19	23	17	25	29.	28.	29.	14	20
H	32	45	19	20	16	23	28.	24.	28.	16.	23.
N					0.7	0.6	0.5	0.7	0.6	0.3	0.3
S					0.04	0.06	0.04	0.05	0.13	0.07	0.06
O					0.3	0.7	0.2	0.6	0.7	1.8	3.6
Nitrogen types, wt % MAF											
Basic nitrogen					2.08	0.84	0.09	0.52	1.58	0.69	0.54
Non-basic nitrogen (diff.)					2.33	1.63	1.55	2.01	0.45	1.17	0.83
Oxygen types, wt % MAF											
Acidic oxygen	-	-	-	-	-	1.35	0.24	0.77	3.27	2.07	1.73
Non-acidic oxygen (diff.)	-	-	-	-	1.89	1.96	1.95	1.81	0.31	11.35	16.09

(1) Corrected for phenolic hydrogen

(2) Assumes all acidic hydrogen is phenolic

(3) Measured by titration of NaOH from refluxing in Na/THF followed by addition of H_2O

(4) From application of Brown-Ladner parameters to NMR data

(5) Aliphatics contaminated with some aromatics

Aromatic Hydrocarbons

The molecular formulas are $C_{19}H_{19}$ for the -454°C material and $C_{23}H_{20}$ for the +454°C fraction. The aromaticities (f_a) are 0.65 and 0.74 for the two fractions. These are hydrogenated materials and there are significant amounts of aliphatic rings (hydroaromatics) present. The molecular weights of the two fractions differ by only 53 g/mole.

Comparison of the liquefaction results (Table 4) shows that the lower boiling range fraction is the better solvent. The major reaction of these fractions is expected to be hydrogen transfer. The -454°C fraction has a higher H/C ratio (0.99 vs 0.84), is less aromatic (f_a 0.65 vs 0.74) and contains more hydroaromatic hydrogens (1.52 vs 1.42 wt %), as measured by assigning portions of the H^1-NMR spectrum to hydrogens in cyclic structures α and β to an aromatic ring. Another factor, which has not been measured, is molecular size, which may also have an impact on the relative ability of the smaller and larger molecules to get close enough to the dissolving coal to transfer hydrogen. Only the larger size and boiling point of the +454°C molecules, which should make those molecules more able to physically support the dissolving coal, favor the heavier material.

N-Containing Aromatics

The difference in molecular weight between the N-aromatic fractions is large, 117 g/mole. The molecular formula of the +454°C fraction indicates that there is also one atom of oxygen present in each molecule. These fractions are polar but are also made up of condensed hydroaromatic structures, so they should be able to act both as hydrogen donors and as physical solvents. The H/C ratios are similar for the -454°C and +454 °C fractions, 0.95 and 0.90 respectively, but estimation of donatable hydrogen by H^1-NMR[6] indicates that the lighter fraction should be a much better hydrogen donor, 1.43 weight percent donatable hydrogen vs 0.88 for the +454°C fraction.

The differences in hetero atoms types between the -454°C and +454°C fractions are significant. All of the oxygen in the -454°C fraction is non-acidic while only about 60 percent of the oxygen in the +454°C fraction is non-acidic. Of the nitrogen in the -454°C fraction 47 percent is basic (tertiary) but only 34 percent is basic in the +454°C fraction. The N/C mole ratio is also twice as large (.041 vs .024) in the lighter fraction.

The liquefaction results are compared in Table 4. Both N-aromatic solvent additives result in lower conversions, although the -454°C material is by far the more effective solvent. The hydrogen donation potential of the lighter N-aromatic fraction may be able to overcome most of the negative reactions which occur as a result of the increased polarity of the N-aromatics, compared to the aromatic hydrocarbons. A major reaction of these fractions is adduction of solvent to the dissolving coal to produce large yields of asphaltenes. This is also more pronounced in the +454°C fraction and may be due to the higher amount of acidic (phenolic) oxygen.

Primary, Secondary and Tertiary +454°C N-Aromatics

The +454°C aromatic fraction was split into three fractions by nitrogen type, as shown below:

N-Type	Primary	Secondary	Tertiary
Compound Type			
% of Total N			
Basic	24	5	78
Non-basic (diff.)	76	95	22
% of Total O			
Acidic	30	11	100
Non-acidic (diff.)	70	89	0

TABLE 4. COMPARISON OF EFFECTS OF -454 C AND +454 C SOLVENT FRACTIONS ON COAL LIQUEFACTION (427 C, 5 min, 1000 psi (cold) hydrogen, 3 g Illinois #6 coal, 6.0 g -454 C recycle solvent, 1.5 g solvent fraction)

Added Solvent Fraction	Temp. °C	Net Change (MAF basis) % of MAF Coal				Hydrogen Balance
		THF Insolubles	Preasphaltenes	Asphaltenes	Oils	
None	-	-80.4	34.3	13.7	20.5	-.12
Aliphatic	-454	-81.2	33.3	33.7	5.4	-.15
Hydrocarbons	+454	-84.1	27.9	35.0	-2.8	.48
Aromatic	-454	-87.6	33.1	27.2	15.5	.090
Hydrocarbons	+454	-83.4	33.8	28.9	9.4	-.14
N-Containing	-454	-79.5	25.6	40.6	7.3	-.065
Aromatics	+454	-67.1	30.3	47.6	-6.4	-.060
Primary Nitrogen Aromatic	+454	-79.5[1]	29.4	42.0	- 8.2	+0.05
Secondary Nitrogen Aromatic	+454	-81.0[1]	29.8	28.8	-15.2	-0.06
Tertiary Nitrogen Aromatic	+454	-71.7[1]	19.7	48.6	-14.0	0.00
O-Containing	-454	(-58.3)[2]	24.6	38.9	-18.1	-.030
Aromatics	+454	-71.1	30.8	26.9	0.6	-.050

(1) All N-aromatic fraction data are based on single liquefaction experiments

(2) Incomplete THF insolubles recovery

The purity of nitrogen types in each fraction can be estimated from the ratios of basic to nonbasic nitrogen present. The primary nitrogen fraction is expected to be contaminated with significant amounts of tertiary nitrogen compounds in which the nitrogen is sterically protected[2]. About 24 percent of the nitrogen in this fraction is basic (tertiary) and the other 76 percent is assumed to be the desired primary nitrogen compounds. The secondary (acidic) nitrogen fraction is expected to be the most pure and it is 95 percent nonbasic nitrogen. The tertiary (basic) nitrogen fraction is 78 percent basic nitrogen.

Acidic (phenolic) oxygen is associated primarily with the basic nitrogen, probably in hydrogen bonds. The oxygen associated with secondary (acidic) nitrogen is primarily non-acidic, possibly substituted furans, also in hydrogen bonds. The same oxygen-nitrogen pairs also appear to be present in the contaminated primary nitrogen fraction. Although the primary nitrogen is neutral it should also be able to form hydrogen bonds with non-acidic oxygen.

All of the individual N-aromatic fractions are better solvents than the combined N-aromatics fraction as shown in Table 4. The tertiary nitrogen N-aromatics give the lowest conversions of the three fractions and the most asphaltenes. Based on net hydrogen used, the tertiary nitrogen compounds do not shuttle hydrogen. They may strongly bond with solvent and dissolving coal.

The secondary N-aromatics give the highest conversions and significantly lower asphaltene yields. They result in the largest net loss of oil which indicates that they are also adducted to the dissolving coal and solvent. They show some indication of shuttling hydrogen.

Although the nitrogen compounds have been reported to be good solvents for coal liquefaction, particularly if they are present when the coal moisture is released during drying and can replace the moisture in the coal pores before liquefaction temperatures are reached[7], under the conditions used in these experiments they are relatively poor liquefaction solvents, particularly the tertiary-N fraction.

O-Containing Aromatics

The final fraction studied is an oxygen-containing aromatic fraction which eluted from the column chromatography separation. Although much of the oxygen in the coal liquefaction solvents is probably phenolic, titration of acidic hydrogen showed that 90-96 percent of the oxygen on the molecules that eluted was non-acidic, probably in functional groups such as substituted benzofurans. These materials have lower aromaticities than the other fractions and are highly substituted. The -454°C fraction contains an average of 2 oxygens per molecule and the +454°C fraction contains an average of 4 oxygens per molecule. The H/C ratios are high, 1.13 and 1.18, respectively, as are the weight percentages of donatable hydrogen, 1.53 and 1.77, respectively, however, as shown in Table 4, these fractions are very poor solvents. Apparently, the major reaction of this class of compounds is not hydrogen transfer. This may be because the "donatable" hydrogens are not really hydroaromatic but are α to oxygen atoms. They seem to adduct in large amounts to solvent, as shown by the negative oil yields. They apparently are also poor physical solvents, possibly due to their low aromaticities and relatively large steric size, caused by the large number of substituents.

Conclusions

The hydrocarbon fractions in the recycle solvent have a positive effect on liquefaction while the heteroatom containing fractions have a negative effect. Since the combined amount of non-aromatic and aromatic hydrocarbons is about 82.5 weight percent of the -454°C recycle solvent and only 28.3 weight percent of the +454°C recycle solvent, it is not surprising that the overall effect of adding more -454°C solvent is positive and the overall effect of adding more +454°C solvent is negative (Table 5).

Among the opposing properties of higher molecules weight solvent components which can affect their efficiency as liquefaction solvents are improved

TABLE 5. COMPARISON OF EFFECTS OF +454°C AND -454°C RECYCLE SOLVENTS ON COAL LIQUEFACTION (427°C 5 min, 1000 psi (room temperature) hydrogen, 3 g Illinois #6 coal, 6 g -454°C recycle solvent)

Added Solvent Fraction	Total Solvent/ Coal	Net Change (MAF basis), % of MAF Coal[1]				
		THF Insolubles	Preasphaltenes[2]	Asphaltenes[3]	Oils[4]	Hydrogen Balance
None	2.0:1	-80.4	34.3	13.7	20.5	-.12
-454°C/1.5	2.5:1	-86.1	42.9	25.3	19.5	-.063
+454°C/1.5	2.5:1	-77.2	29.2	34.6	12.4	-.36

(1) Net change = $\frac{\text{Final weight (MAF)-Initial weight coal + solvent (MAF)}}{\text{WT MAF coal}} \times 100$

Initial weights measured by extraction

(2) Preasphaltenes = THF soluble-toluene insolubles

(3) Asphaltenes = Toluene soluble-heptane insolubles

(4) Oils = Heptane solubles

facility for hydrogenation reactions, but lower amount of donatable hydrogen present, lower vapor pressure at elevated temperature but the possibility that their increased size has a negative steric effect on their ability to transfer hydrogen. Comparisons of solvent fractions of differing molecular weights gives mixed results. Of the solvent components which are expected to react primarily by H-transfer (N-aromatics and aromatic hydrocarbons) the heavier fractions are less effective, possibly because of steric hindrance to hydrogen transfer and less available hydrogen to transfer, but of the solvent components expected to act only as physical solvents (non-aromatic hydrocarbons and O-containing aromatics) the heavier components are more effective than the corresponding lower molecular weight fractions.

There appears to be a relationship between the type of heteroatoms present in the recycle solvent fraction which is based on hydrogen bonding. These relationships appear to be an area where additional research may increase understanding of the weak bonds which are made and broken during liquefaction which result in net solvent loss and improved coal solubility. Another area where further research is needed is on the effect of steric size of the solvent components on coal liquefaction.

The overall effect of recycling heavy ends in the ITSL process is positive because it results in the production of a single, higher-value liquid product with low carcinogenicity, in higher yields than would otherwise be possible. The hydrocarbons, about 25 percent of the heavy ends, are productive liquefaction solvent components as well.

Acknowledgements

Many people assisted in the completion of this work. In particular, Mr. E. Lawson did much of the laboratory work. This work was prepared with the support of the U.S. Department of Energy, Grant No. DE-FG22-82PC50783.

References

(1) Process Development for Improved SRC Options; Kerr-McGee Critical Solvent Deashing and Fractionation Studies, EPRI Project 1134-2 Final Report by Kerr-McGee Corporation, July, 1981.

(2) Later, D.W., Lee, M.L., Bartle, K.D., Kong, R.C., and Vassilaros, D.L., Chemical Class Separation and Characterization of Organic Compounds in Synthetic Fuels, Anal. Chem., 1981, 53, pp. 1612-1620.

(3) Brown, J.K. and Ladner, W.R., Fuel, 39, 87 (1960).

(4) Moore, R.T., McCutchan, P. and Young, D.A., Anal. Chem., 23 (11), 1639-41 (1951)

(5) Sternberg, H.W., Raymond, R. and Schweighardt, F.K., Science, 188 (4), 49-51 (1975)

(6) Burke, F.P. and Winschel, R.A., Recycle Slurry Oil Characterization, Conoco Quarterly Report #1, Prepared for U.S. DOE, June, 1981, p. 9

(7) Advanced Coal Liquefaction, EPRI Journal, May, 1982, p. 31-34

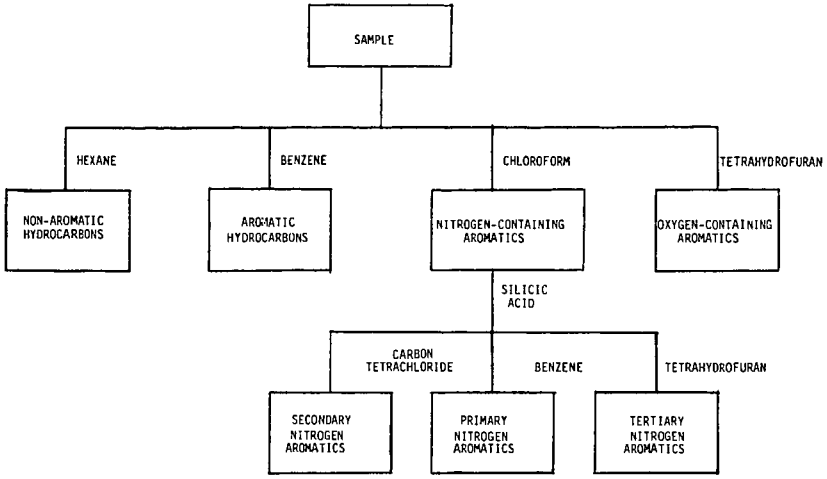

FIGURE 1. METHOD FOR SEPARATION OF FRACTIONS INTO CHEMICAL CLASSES BY COLUMN CHROMATOGRAPHY

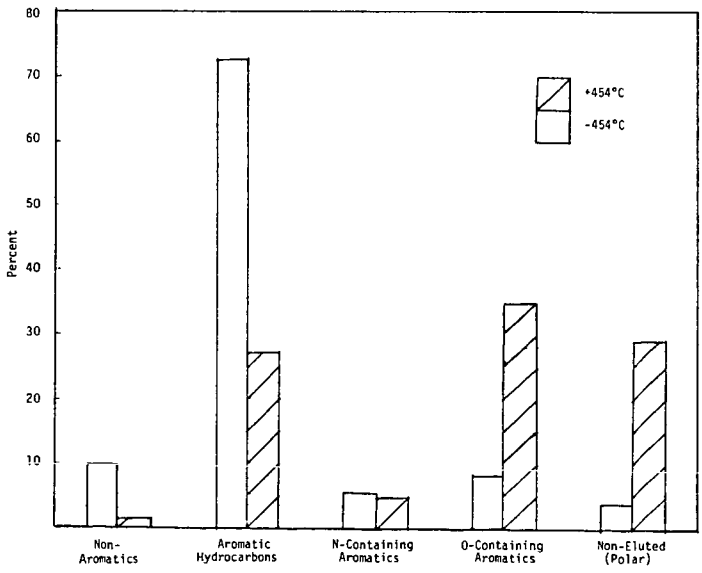

FIGURE 2. DISTRIBUTION OF CHEMICAL TYPES IN -454°C AND +454°C RECYCLE SOLVENT

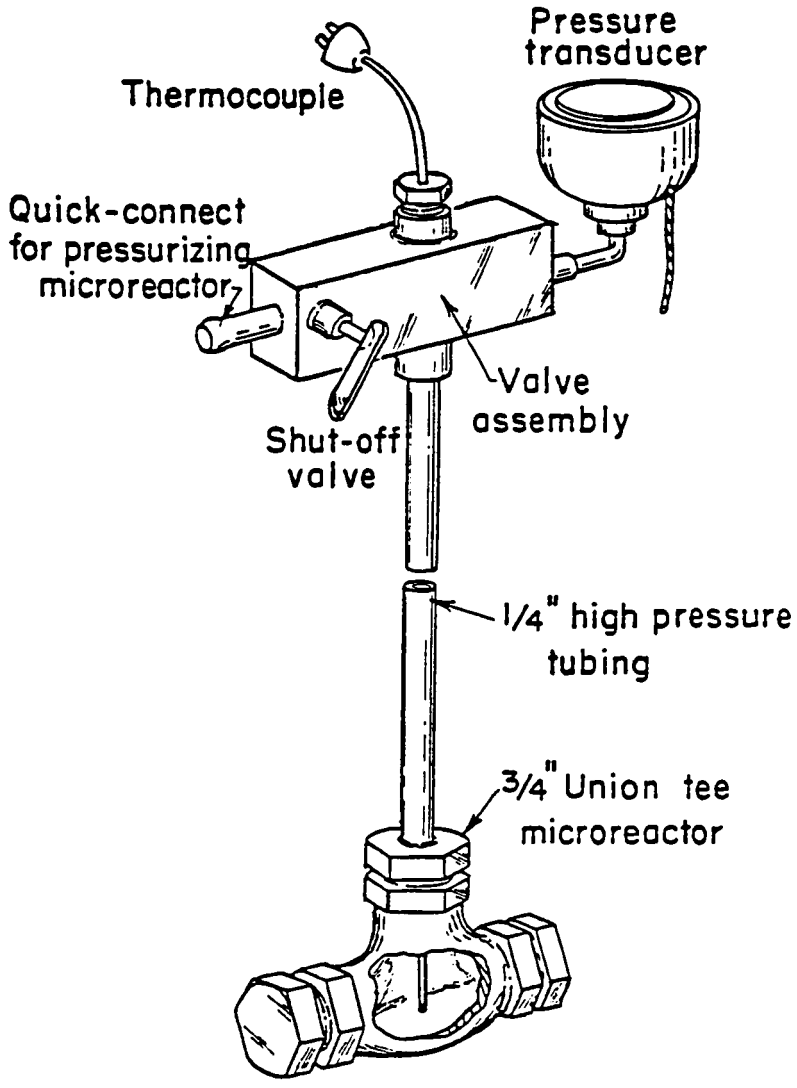

FIGURE 3. MICROAUTOCLAVE REACTOR

BEHAVIOR OF PHENOLICS IN COAL LIQUEFACTION: SAMPLE CHARACTERIZATION AND EFFECT ON COAL CONVERSION IN A CSTR UNIT

by

D. C. Cronauer
R. I. McNeil
L. G. Galya
D. A. Danner

Gulf Research & Development Company
P.O. Drawer 2038
Pittsburgh, PA 15230

INTRODUCTION

Phenolic components of coal liquefaction solvents have been considered to be beneficial for conversion of coal (1,2). Orchin and Storch (2), for example, reported that the addition of small amounts of cresol to tetralin increased the conversion of coal compared with the yield observed with tetralin alone. Kamiya and co-workers (3) observed a similar effect with phenol or cresol added to a solvent composed of tetralin and 1-methylnaphthalene; the magnitude of the increase was dependent upon the coal used. The reported effect has been ascribed to a variety of factors, one of which is a hydrogen-bonding interaction between the phenolic species and ethers in the coal (2,3), leading to increased cleavage of various ethers.

Awadalla and Smith (4) observed an increase in conversion with p-cresol but suggested that the effect was an artifact of the extraction process, a co-solvent effect arising from lack of prior removal of the phenolic material. Larsen et al. (5), investigating the use of phenol as a solvent for liquefaction of Bruceton Pittsburgh Seam coal, found that a solvent/coal ratio of 1.5 and reaction temperature of 460°C led to a weight increase of the coal of 9% after a 15-min reaction. This large amount of adduction with only a 10% conversion to pyridine-soluble material indicates that phenol is a very poor solvent under these conditions. Runs made at 482°C resulted in an increase in conversion, up to 82% for a 10/1 phenol/coal feed. However, the liquid product contained 14% by weight phenol of which 6% was attached to the coal by other than hydrogen-bonding interactions. An additional 8% was exchangeable with unlabeled material.

Our (6) past work with naphthols, phenol, and cresols using a micro-autoclave unit indicated that phenol and naphthols were poor solvents for coal liquefaction due to high levels of adduction. However, less adduction was observed with the addition of cresols to the solvents. Therefore, a series of runs were made in a CSTR unit to evaluate the effect of adding phenol and cresols to anthracene oil (AO) and SRC-II derived solvents. In addition, an "OH-reduced" solvent and a solvent mixture of AO plus OH-concentrate were tested.

EXPERIMENTAL

The coal was Powhatan No. 5 Mine (Pittsburgh No. 8 Seam) ground to pass at least 98% through 100 mesh screen. Analyses of the coal and solvents are given in Table 1.

The bench-scale liquefaction runs were made in a continuous feed stirred-tank reactor (CSTR) system. A flow diagram of the coal liquefaction unit is shown in Figure 1; its operation has been previously described (7). Samples of the reactor slurry were first stripped with nitrogen, and they were then subjected to sequential Soxhlet extraction using pentane, toluene, and tetrahydrofuran (THF), respectively. Fractions were defined as follows, using as a basis MAF coal feed:

wt% oils = {(MAF coal-pentane insolubles)/MAF coal} x 100
wt% asphaltenes = {pentane insoluble, toluene soluble/MAF coal} x 100
wt% preasphaltenes (PA) = {toluene insoluble, THF soluble/MAF coal} x 100
wt% THF insolubles = {THF insoluble material/MAF coal} x 100

RESULTS AND DISCUSSION

Characterization of the OH-Concentrate: The OH-concentrate (OH-CONC) was isolated by contacting SRC-II solvent with activated Rohm and Haas Co. IRA-904 resin. The OH-CONC was then freed by washes of CO_2/methanol acid and HCO_2H/methanol followed by solvent stripping.

The hydroxyl concentrate of SRC-II solvent was added to a small amount of methylene chloride and analyzed by capillary GC/MS. The greatest portion (56%) of the chromatographic peaks other than solvent was phenol (10%) or alkyl-substituted phenols (46%). Methyl phenols (23%) account for approximately half of the alkyl-substituted phenols with the remainder (23%) being C_2 to C_5 phenols. Other peaks include $C_9H_{10}O$ isomers (10%) and $C_{10}H_{12}O$ isomers (9%) which are probably indanols and methylindanols. Hydroxybiphenyl (1%) and carbazole (3%) were identified. Polynuclear aromatic hydrocarbons accounted for 16% of the peaks. The largest of these was methylphenanthrene (4%). The remainder of the peaks (5%) were small and unidentified.

The ^1H spectrum of the OH-CONC fraction is shown in Figure 2, and the results are summarized in Table 2. This fraction has aromatic, hydroxyl, hydroaromatic, and alkyl substituent functionality. The aromatic region spans from 6 ppm to 8.6 ppm. These aromatic hydrogens represent 39.7% of the total hydrogen. Even though the nitrogen content is relatively low (1.1%), the small amount of intensity between 8.4 ppm and 8.6 ppm in the aromatic region can be assigned to protons ortho to the nitrogen in pyridine-type structures. These protons represent less than 0.3% of the hydrogen. There is a broad resonance at 5.4 ppm which can be assigned to hydroxyl hydrogen. This accounts for 11.3% of the hydrogen in the spectrum. In the region around 3.4 ppm are several smaller signals which can be assigned to methylene bridges between aromatic rings. These methylene bridge hydrogens represent 0.9% of the hydrogen present.

The main type of aliphatic substituent is methyl groups on aromatic rings as evidenced by the sharp signals at 2.2, 2.5, and 2.8 ppm. These signals account for 25.7% of the hydrogen present. There are also some (16.7% of hydrogen) long-chain aliphatic substituents with an average chain length of five carbons. Combining a broad signal at 1.7 ppm, together with an equivalent amount of intensity from the signal at 2.8 ppm, about 5.6% of the hydrogen is hydroaromatic.

The ^{13}C NMR spectrum, given in Figure 3, shows the OH-CONC to have an aromaticity of 77.4%. The ratio of aromatic carbons to hydroxyl-bearing carbons is 8.5:1. The ratio of total carbon to oxygen is 10.9:1, which is reasonably consistent with that of the elemental carbon-to-oxygen analysis of 12.3:1.

The amount of ortho substitution is determined as the difference between the area of the region from 152 ppm to 156 ppm and one-half of the area between 110 ppm and 117 ppm. The amount of meta substitution is determined from the signals at 154-155 ppm, and the difference between the amount of hydroxyl-bearing carbon and the amounts of ortho and meta substitution is para substitution. The results are given in Table 3.

Since the observed ratio of aromatic carbons to hydroxyl-bearing carbons is 8.5:1 and every molecule theoretically has an acidic hydroxyl group, the OH-CONC consists of a mixture of one- and two-ring systems. Because only a small amount of the concentrate has been identified as naphthols, the remainder of two-ring systems should be comprised of single rings joined by short alkyl bridges. There is evidence for both methylene and ethyl bridges in the carbon spectrum. The distribution is shown in Table 3.

The total alkyl-substituted aromatic carbon is 12.8%. This was determined by summing the methylene bridge area times 2, the ethyl bridge area, one half the hydroaromatic area, and the methyl groups on aromatic rings area. The total nonprotonated aromatic carbon is difficult to determine from the normal spectral regions due to the presence of hydroxyl groups which induce an upfield shift to the carbons ortho and para to it. To study this, a NORD-CDRE (noise off-resonance decoupled convolution difference resolution enhancement) experiment was run. The signals upfield of 129.5 ppm are due to bridge carbons in 1- and 2-naphthols. The total bridge carbon is 15.5% as determined from the difference between the total nonprotonated carbon and the alkyl-substituted carbon plus hydroxyl-bearing carbon (11.8%). Therefore, the level of protonated aromatic carbon is 58.5% of the aromatic carbon.

CSTR Experiments: The results of the CSTR runs are summarized in Table 4. As anticipated, SRC-II distillate is a better solvent than AO at short reaction times (4 min) as indicated by higher overall coal conversion, a lower level of preasphaltenes, and lower hydrogen consumption. With both solvents the yields of oils were negative. With an increase in space time to 15-19 minutes, overall conversions increased to about the same level (72-75%). The recoveries of preasphaltenes were essentially the same at about 5%, and the hydrogen consumptions were equal at 3.5 g/100 g MAF coal. However, a

sizable negative yield of oils was observed in the AO run at 15 minutes. This was apparently due to a high yield of asphaltenes. While this observation appears to be anomalous, the product slurry was extracted a total of five times with essentially the same results.

The direct addition of phenol to AO (4-min space time) was detrimental. While % solvation increased marginally, the yield of asphaltenes increased greatly over that of the run with AO alone. The product slurry was also very sticky and difficult to handle; therefore, pentane may have had some difficulty penetrating into the slurry sample and then extracting the oils. The yields of preasphaltenes were essentially the same for the runs with AO and AO plus phenol.

The addition of OH-concentrate, recovered from an ion exchange resin treatment (Rohm and Haas IRA-904) of SRC-II solvent, to AO had little effect on the distribution of products. Considering the OH-concentrate had a moderate level of hydroaromaticity while that of AO was low, and that the OH-concentrate had already effectively passed through a liquefaction reactor, the OH-concentrate may not react sufficiently with coal radicals to form additional asphaltenes.

The addition of m-cresol appeared to be of particular benefit to the AO runs. This addition resulted in an increase in the yield of oils along with a marginal increase in % solvation. In the case of m-cresol addition to SRC-II solvent at a 15-minute reaction time, there was a small increase in % solvation with nominal increases in each of the product fractions.

Due to a limited amount of available feed sample, only a single CSTR run was made with the solvent recovered after treatment with IRA-904 resin. This solvent contained 1.9% oxygen, while the as-received SRC-II solvent contained 2.8% oxygen. Even this partial removal of hydroxyls appears to be of benefit, as observed by an increase in oil yield, a decrease in asphaltenes yield, and a marginal increase in % solvation (THF solubles).

SUMMARY

Coal liquefaction experiments were carried out at 450°C in a continuous feed stirred-tank reactor (CSTR) to observe the effect of adding phenolics to anthracene oil (AO) and SRC-II recycle solvents. At nominal space times of 4 and 15 minutes, the levels of conversion (THF solubles) were significantly higher with SRC-II recycle solvent than with anthracene oil. The addition of phenol to AO at a ratio of 5/65 resulted in a nominal increase in coal conversion to THF solubles, but the amount of asphaltenes more than doubled resulting in a sizable net loss of solvent. The addition of m-cresol to both AO and SRC-II solvents had a positive effect on coal conversion to both THF and pentane solubles (oils). The partial removal of an OH-concentrate from SRC-II solvent was carried out using Amberlyst IRA-904 ion exchange resin. The "OH-reduced" oil was only marginally better than raw SRC-II recycle solvent for coal liquefaction. A characterization of the OH-concentrate by ^{13}C and ^{1}H NMR and FTIR indicated a moderate level of aromaticity (77%), a

sizable amount of short-chain aliphatic substitution, and also a sizable amount of hydroaromaticity. GC/MS characterization pointed out a high concentration of one- and two-ring substituted phenolics.

LIST OF REFERENCES

1. A. Pott and H. Broche, U.S. Patent 1,881,927.

2. M. Orchin and H. H. Storch, 1948. Solvation and Hydrogenation of Coal. Ind. Eng. Chem., 40:1385.

3. Y. Kamiya, H. Sato, and T. Yao, 1978. Effect of Phenolic Compounds on Liquefaction of Coal in the Presence of Hydrogen-Donor Solvent. Fuel, 57:681.

4. A. A. Awadalla and B. E. Smith, 1982. Apparent Enhancement of Coal Conversions Using Cresol-Tetralin Solvents. Fuel, 61:631.

5. J. W. Larsen, T. L. Sams, and B. R. Rodgers, 1981. Internal Rearrangement of Hydrogen During Heating of Coals with Phenol. Fuel, 60:335.

6. R. I. McNeil and D. C. Cronauer. Behavior of Phenolics in Coal Liquefaction: Adduction Tendency and Coal Conversion Capability. Fuel Proc. Tech. in press.

7. J. S. Abichandani, Y. T. Shah, D. C. Cronauer, and R. G. Ruberto, 1982. Fuel, 61:276.

WPC#4087A

Table 1

Analyses of Solvents and Coal

Chemical Analysis (wt%)	Raw AO	Raw SRC-II	OH-CONC	OH Reduced	Coal*
Carbon	91.2	87.2	82.0	88.4	72.3
Hydrogen	5.9	8.7	7.8	8.5	5.1
Nitrogen	1.0	0.9	1.1	0.9	1.5
Oxygen	1.3	2.8	8.9	1.9	7.9
Sulfur	0.6	0.4	0.2	0.3	0.6
Ash	-	-	-	-	9.7
	100.0	100.0	100.0	100.0	100.0

*Powhatan No. 5 Mine (Pittsburgh Seam) coal.

Table 2

^{1}H NMR Analysis of SRC-II Hydroxyl Concentrate

Aliphatic Hydrogens		
Methylene bridge	0.9%	
Methyl	25.6	
Hydroaromatic	5.6	
Long alkyl chain (i.e., C_5)	16.7	
Total aliphatic		48.7
Hydroxyl Hydrogens		11.3
Aromatic Hydrogens		
Aromatic hydrogen ortho to N	0.3	
Others	39.7	
Total aromatic		40.0
Total		100.0%

Table 3

^{13}C NMR Analysis of SRC-II Hydroxyl Concentrate

Aliphatic Carbons			
Methylene bridges between rings		1.4%	
Other carbons α to aromatic rings		2.0	
Methyl groups attached to rings		5.7	
Hydroaromatic carbons		7.3	
Long-chain alkyls (from ^{1}H) (est.)		6.2	
Total aliphatic carbons			22.6%
Aromatic Carbons (Ar-C)			
Ortho methyl groups (to OH)	3.0		
Naphthols	1.0		
Unknown ortho substituents	0.9		
Total substituted Ar-C's ortho to OH groups		4.9	
Substituted Ar-C's meta to OH groups		9.9	
Substituted Ar-C's para to OH groups		7.4	
			22.2*
Hydroxyl substituted Ar-C			9.3
Protonated Ar-C			45.9
Total			100.0

*This is also subdivided as follows:

Alkyl-substituted Ar-C	10.0
Aromatic bridge carbons	12.2
Total	22.2

Table 4

Summary of CSTR Runs with Phenolic Additives

Solvent/Additive	Space Time (min)	% Solvation[1] (g/100 g)	Hydrogen Consumption[2] (g/100 g)	Yields[2] (g/100 g) Oils	Asphaltenes	Preasphaltenes
Anthracene Oil	4.2	55.4	3.0	-7.0	29.9	19.9
+m-Cresol	4.3	58.3	2.4	9.6	30.2	27.0
+Phenol	4.4	58.5	2.1	-46.5	71.3	22.1
+OH-CONC	4.1	56.7	2.5	-9.9	33.5	23.6
Anthracene Oil	15.2	74.7	3.4	-35.5	82.9	6.7
+m-Cresol	19.1	80.2	4.3	-2.1	55.3	3.7
SRC-II Solvent	4.7	61.3	1.8	-5.3	41.8	14.0
OH-Reduced SRC-II	4.6	63.9	2.7	2.1	34.5	17.8
SRC-II Solvent	19.0	71.7	3.6	12.3	33.2	4.7
+m-Cresol	15.0	76.6	3.6	14.5	34.9	7.5

Notes: [1] Solvation is given as grams of tetrahydrofuran solubles/100 grams MAF coal.
[2] Yields are given as grams/100 grams MAF coal.

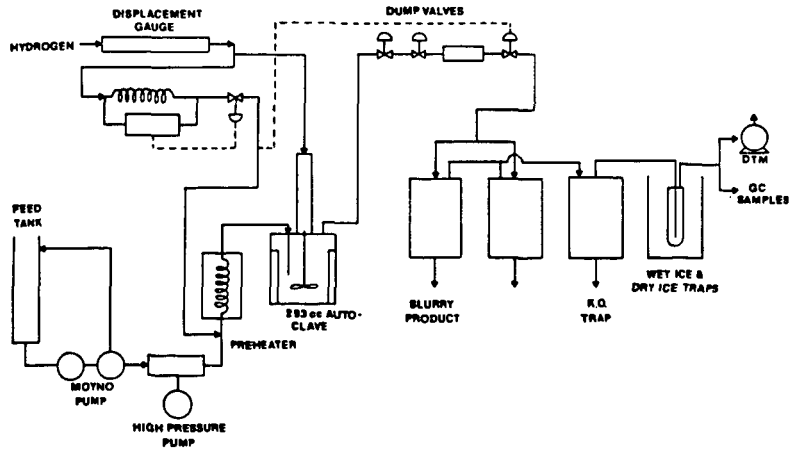

FIGURE 1 SCHEMATIC OF THE BENCH-SCALE CSTR UNIT

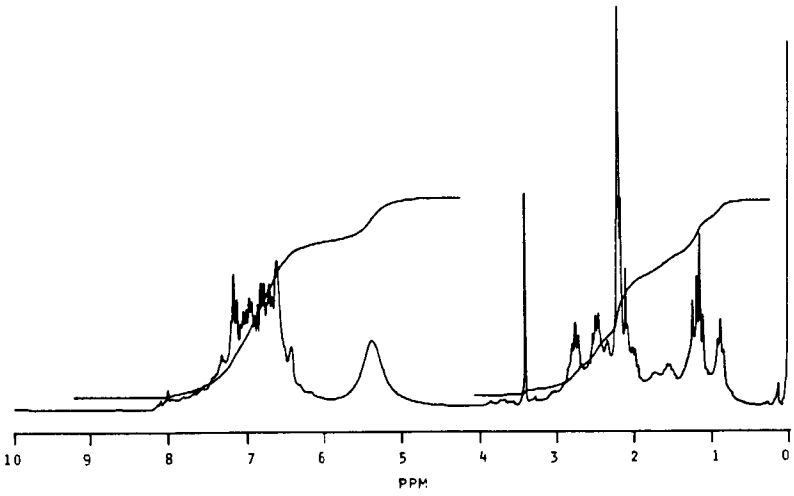

FIGURE 2 ^{1}H-NMR SPECTRUM OF SRC-II DERIVED HYDROXYL-CONCENTRATE

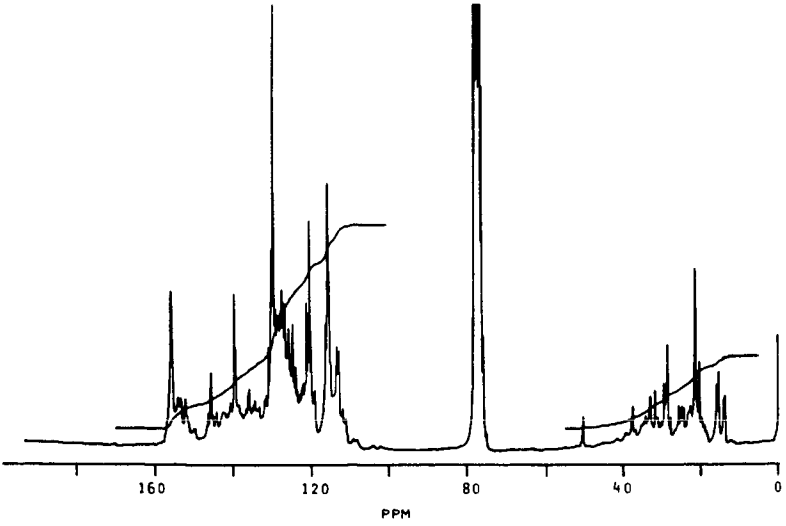

FIGURE 3 ^{13}C-NMR SPECTRUM OF SRC-II DERIVED HYDROXYL-CONCENTRATE

A Comparison of Anthracene and Phenanthrene in Coal Liquefaction

K. C. Kwon

Chemical Engineering Department
School of Engineering and Architecture
Tuskegee Institute, Alabama 36088

INTRODUCTION

A comparison of anthracene and phenanthrene was made by liquefying either Wyodak coal or Kentucky 9/14 coal in the presence of either hydrogen or nitrogen. 1-methylnaphthalene (1-MN) was employed as a physical solvent. Reaction products are separated into a tetrahydrofuran (THF)-soluble fraction, a preasphaltene fraction, an asphaltene fraction and an oil-plus-gas-plus water fraction.

EXPERIMENTS

A series of reactions were conducted in a 25 cc, 316 stainless steel microreactor to liquefy either Wyodak coal or Kentucky 9/14 coal under the various operation conditions. Another series of reactions were performed in a 50 cc flask to dissolve either Wyodak coal or Kentucky 9/14 coal with either neat aromatic compounds such as anthracene and phenanthrene, or mixtures of neat aromatics and their dihydroaromatics under the atmospheric pressure. The reaction product is separated by using a pressure filtration procedure. Conversions of aromatics into hydroaromatics are analyzed by using a gas chromatograph. Coal conversions are calculated on a moisture-and-ash-free-coal basis.

DISCUSSION

Both anthracene and phenanthrene are converted more into their hydroderivatives in the presence of Kentucky 9/14 coal than in the presence of Wyodak coal. This fact may suggest that minerals in Kentucky 9/14 coal act as more active catalysts than minerals in Wyodak coal in hydrogenating aromatics such as anthracene and phenanthrene in the presence of molecular hydrogen (Table 1).

Wyodak coal is converted more into an oil-water-gas fraction in the presence of anthracene than in the presence of phenanthrene, while producing the same amount of preasphaltene plus asphaltene in the presence of either anthracene or phenanthrene. Therefore, anthracene and its derivatives are to some degree better solvents than phenanthrene and its derivatives in liquefying Wyodak coal (Table 1).

The conversion of Kentucky 9/14 coal is influenced more by hydrogen pressure than the conversion of Wyodak coal in the presence of either anthracene or phenanthrene (Table 1). This fact suggests that molecular hydrogen may play a more dominant role than hydroaromatics in liquefying Kentucky 9/14 coal or that the minerals in Kentucky 9/14 coal are actively hydrogenating the aromatic solvent. The analysis of the oil fraction suggests the latter.

The conversion of both anthracene and phenanthrene to dihydroderatives increases as the initial hydrogen pressure increases. The conversion of Wyodak coal increases from 44 % to 58 % and the hydrogenation of anthracene increases from 6 % to 17 % in the presence of anthracene, whereas the conversion of Wyodak coal increases from 40 % to 48 % and the hydrogenation of phenanthrene does not increase by increasing the initial hydrogen pressure from 500 psig to 1100 psig (Table 1). These facts show that anthracene is readily hydrogenated and its derivatives are better hydrogen donors or shuttlers than phenanthrene and its derivatives in liquefying Wyodak coal.

The conversion of Ky 9/14 coal is 42.4 % and the hydrogenation of anthracene is 4.4 % in the presence of nitrogen (Table 1). The conversion of Ky 9/14 coal is 38 % and no hydrogenation of phenanthrene is observed in the presence of nitrogen. This fact demonstrates that anthracene is more active than phenanthrene

in liquefying Ky 9/14 coal in the absence of hydrogen, by extracting hydrogen from coal to be converted into dihydroanthracene and then breaking down coal structure.

Conversions of Ky 9/14 coal and anthracene to hydroanthracenes are 72.4 % and 17.6 % respectively in the presence of 500 psig hydrogen, while conversions of Ky 9/14 coal and phenanthrene are 75.3 % and 0 % respectively in the presence of 500 psig hydrogen, in spite of the fact that more hydrogen donor is available in the former case (Table 1). Preasphaltene-plus-asphaltene fraction is 53 % in the presence of anthracene and 500 psig hydrogen, whereas preasphaltene-plus-asphaltene fraction is 46 % in the presence of phenanthrene and 500 psig hydrogen. This fact may indicate that either solubility of Ky 9/14 coal in phenanthrene and its derivatives is inherently better than in anthracene and its derivatives, or that dihydroanthracene may be undergoing extensive retrogressive reaction with coal or itself, producing more preasphaltene-plus-asphaltene fraction. This evidence may also suggest that the transfer rate of labile hydrogen from coal to anthracene is much faster than that of molecular hydrogen from the gaseous phase to liquid anthracene during the very early reaction stage due to low hydrogen pressure.

A series of runs were carried out to understand solvent quality on conversion of Wyodak coal in the presence of hydrogen, as shown in Run 3, Run 4 and Run 44 in Table 2. Conversions of coal in the presence of anthracene and its derivative is considerably higher than in the presence of either phenanthrene or 1-MN, where conversion of anthracene is 22.2 % as shown in Run 3. This indicates that a good hydrogen donor solvent may play a more dominant role than molecular hydrogen in liquefying Wyodak coal and that the solvent power of 1-MN is better than that of phenanthrene in the presence of hydrogen for the liquefaction of Wyodak coal.

Another series of runs were conducted to determine solvent quality on the liquefaction of Wyodak coal in the presence of nitrogen as shown in Run 45, Run 48 and Run 49 in Table 2. Conversion of Wyodak coal is higher in the presence of phenanthrene than in the presence of anthracene in the absence of hydrogen. This fact may demonstrate that phenanthrene is a better physical solvent than anthracene in the absence of hydrogen in the liquefaction of Wyodak coal, suggesting that it is the ease of hydrogenation of anthracene and the excellent H-donor behavior of its hydroderivatives that makes anthracene a good solvent in the presence of hydrogen.

Conversion of coal in the presence of anthracene is higher than that of phenanthrene at the reaction temperature of both 350 °C and 425 °C. Phenanthrene is not hydrogenated at 350 °C or 425 °C, but hydrogenations of anthracene are 2.6 % at 350 °C and 4.4 % at 425 °C (Table 2). The difference in coal conversion between anthracene and phenanthrene is less significant at lower reaction temperature. This fact suggests that less labile hydrogen from coal to anthracene is transferred at the lower temperature and the inherent solvent power of the vehicle used is important.

A series of experiments were carried out by liquefying coal with neat aromatic compounds or mixtures of neat aromatic compounds and their hydroderivatives at their boiling temperature under the atmospheric environment (Table 3). Conversion of Wyodak coal in the presence of phenanthrene is higher than in the presence of anthracene, where no hydrogenation of both anthracene and phenanthrene was observed. This fact shows that the solubility of Wyodak coal in phenanthrene is higher than in anthracene under the atmospheric environment and in the absence of other solvents.

Conversion of Ky 9/14 in the presence of phenanthrene is higher than in the presence of anthracene, where hydrogenation of both phenanthrene and anthracene was not observed as shown in Run 19 and Run 22 in Table 3. On the other hand, the conversion of Ky 9/14 coal in the presence of phenanthrene is lower than in the presence of anthrance at 350 °C under 2000 psig nitrogen pressure, as shown in Run 40 and Run 41 in Table 2. This fact suggests that either labile hydrogen does not react with anthracene or escapes into the atmosphere before reacting with anthracene due to the low pressure, whereas labile hydrogen reacts with

anthracene at high pressure. The conversion of Ky 9/14 coal in the presence of a mixture of phenanthrene and dihydrophenanthrene is higher than in the presence of a mixture of anthracene and dihydroanthracene, and the conversion of dihydrophenanthrene is higher than that of dihydroanthracene, as shown in Run 23 and Run 24 in Table 3. On the other hand, the effect of dihydroanthracene on the increment of coal conversion, as shown in Run 19 and Run 23 in Table 3 is higher than the effect of dihydrophenanthrene on the increment of coal conversion, as shown in Run 22 and Run 24 in Table 3. This fact again suggests that dihydroanthracene is a better hydrogen donor solvent than dihydrophenanthrene. Neat anthracene is a poorer solvent than neat phenanthrene (about 1/3) for both Wyodak coal and Ky 9/14 coal at 330 °C. But when 20 % of the dihydrocompound is present, the anthracene compound mixture is a better solvent than the phenanthrene mixture. With Ky 9/14 coal, the phenanthrene is the best solvent, neat and in the presence of the dihydrocompound.

The disappearance of the dihydrocompounds is in agreement with the liquefaction of coal. In the presence of Ky 9/14 coal, dihydrophenanthrene is lost most rapidly, whereas in the presence of Wyodak coal, dihydroanthracene is lost most rapidly (Table 3).

A series of reactions were performed in the presence of neat aromatic compounds and 1100 psig nitrogen (initial) as shown in Table 4. The conversions of Ky 9/14 coal are 32 % in the presence of anthracene and 51 % in the presence of phenanthrene whereas the conversions of Wyodak coal are 33 % in the presence of anthracene and 43 % in the presence of phenanthrene. These data also show that neat phenanthrene is a better physical solvent than neat anthracene in liquefying both Wyodak coal and Ky 9/14 coal in the absence of hydrogen.

Another series of runs with Ky 9/14 coal were compared in the absence of hydrogen in terms of initial nitrogen pressure, as shown in Table 1. The conversions of Ky 9/14 coal are 42 % in terms of the THF soluble fraction and 29 % in terms of the preasphaltene-plus-asphaltene fraction at the 1100 psig initial nitrogen pressure, whereas the conversions of Ky 9/14 coal are 39 % and 24 % respectively at the zero psig initial nitrogen. The closeness of the values for dihydroanthracene formed suggests that the conversion and product distribution would also be similar. The only firm conclusion is that pressure helps total liquefaction and seems to hint oil-water-gas formation. Anthracene is a better solvent than phenanthrene under these conditions.

CONCLUSIONS

The relative behavior of phenanthrene and anthracene depends on whether the solvents are compared neat or in the presence of other solvents, upon the gaseous environment, and upon the coal. When anthracene is the better solvent, conditions appear to favor the formation of dihydroanthracene which is an excellent hydrogen donor. When phenanthrene is the better solvent, the inherently better solvent power of phenanthrene itself for that coal appears to be the dominant factor. The minerals in the coal, and possibly the coal itself, are also important in determining the preferred solvent.

REFERENCES

1. Appell, H. R. "The Effect of Solvent Composition on Product Distribution." Unpublished, Pittsburgh Energy Technology Center.

2. Curtis, C. W., J. A. Guin, and K. C. Kwon. "Coal and Solvolysis in a Series of Model Compound System." Presented to the AICHE Annual Meeting, November, 1982, Los Angeles.

3. Curtis, C. W., J. A. Givin, K. C. Kwon, and N. L. Smith. "Selectivity of Coal Minerals Using Cyclohexane as a Probe Reactant." Fuel (In Press), London, England.

4. Derhyshire, F. J. and D. D. Whitehurst. "The Influence of Polyaromatic Solvent Components on Coal Liquefaction." Proceedings on the Fifth Annual EPRI Contractor's Conference on Coal Liquefaction", p. 9-1, 1980.

5. Gangwar, T. E. and H. Prasad. "HYdrogen-Trasfer Catalytic Activity of Minerals Common to Coal." Fuel, 58, p. 577, London, England, 1979.

6. Garg, D. and E. N. Givens. "Pyrite Catalysis in Coal Liquefaction." Ind. Eng. Chem. Process Design and Development, 21, p. 113, 1982.

7. Guin, J. A., C. W. Curtis, and K. C. Kwon. "Pyrite Catalyzed Coal Liquefaction Using Quinoline/Tetrahydroquinoline as a H-Donor System." Fuel, In Press, London, England, 1983.

8. Jackson, W. R., F. P. Larkins, M. Marshall, D. Rash, and N. White. "Hydrogenation of Brown Coal. 1. The Effects of Additional Quantities of the Inorganic Constituents." Fuel, 58, p. 281, London, England, 1979.

9. Lytle, J. M., R. E. Wood, and W. H. Wiser. "Kinetics of Coal Liquefaction: Effect of Catalyst, H_2 Concentration and Coal Type." Fuel, 59, p. 471, London, England, 1980.

10. Mochida, I., A. TaKarabe, and K. Takeshita. "Solvolytic Liquefaction of Coals with a Series of Solvents." Fuel, 58, p. 17, London, England, 1979.

11. Neavel, R. C. "Exxon Donor Solvent Liquefaction Process." Phil. Trans. Royal Society, London, A 300, p. 141, London, England, 1981.

12. Padrick, T. D., A. W. Lynch and H. P. Stephens. "Effect of Solvent on the Dissolution of Wyodak Coal." Proceedings of the Department of Energy Integrated Two-Stage Liquefaction Meetings, p. 6-2, Alberque, New Mexico, October, 1982.

13. Rottendorf, H. and M. A. Wilson. "Effects of In-Situ Mineral Matter and a Nicket-Molybdenum Catalyst on Hydrogenation of Lidell Coal." Fuel, 59, p. 175, London, England, 1980.

14. Utz, B. R., H. R. Appell and B. D. Blaustein. "Vehicle Studies in Short Contact Time Liquefaction." Proceedings of the Department of Energy Integrated Two-Stage Liquefaction Meetings. p. 7-1, Alberquerque, New Mexico, October, 1982.

15. Utz, B. R., Narain, N. K., Appell, H. R. and Blaustein, B. D. "Solvent Analysis of Coal Derived Products, Using Pressure Filtration," Am. Chem. Soc. Symp. Ser., edited by Fuller, American Chemical Society, Washington, D. C., 1982.

Table 1 - Effects of Hydrogen Pressure on Coal Conversions for 15 min. at 425 °C

RUN NO.	45	1	3	2	4	37*	9	6	38*	10	7	47**
Hydrogen Charge at the Room Temperature (psig)	0	500	1100	500	1100	0	500	1100	0	500	1100	0
1 gm Aromatics plus 4 g 1-MN												
Anthracene	-	+	+	-	-	+	+	+	-	-	-	+
Phenanthrene	-	-	-	+	+	-	-	-	+	+	+	-
Type of Coal												
Wyodak	+	+	+	+	+	-	-	-	-	-	-	-
Ky 9/14	-	-	-	-	-	+	+	+	+	+	+	+
Coal Conversion (wt %)												
THF Soluble	36.1	44.3	57.7	40.3	47.9	42.4	72.4	83.8	37.7	75.3	84.7	39.5
Preasphaltene	-	-	-	-	-	11.0	26.3	26.9	13.4	21.0	27.6	10.0
Asphaltene	-	-	-	-	-	18.1	26.5	33.6	14.9	25.1	30.0	13.9
Preasphaltene plus Asphaltene	8.0	14.0	12.6	11.6	10.6	29.1	52.7	60.5	28.3	46.2	57.6	23.9
Oil, Water and Gas	28.2	30.3	45.1	28.7	37.3	13.2	19.7	23.2	9.5	29.1	27.0	15.6
Conversion of Aromatics (wt %)												
Conversion to Dihydroaromatics	NA	6.4	16.9	0	0	4.4	17.6	28.4	0	0	3.8	4.5
Unconverted Aromatic	NA	93.6	77.2	100	100	95.6	71.7	50.7	100	100	95.3	95.5

*1100 psig initial nitrogen pressure at the room temperature

**14.7 psig initial nitrogen pressure at the room temperature

Table 2 - Conversions of Coals under the Various Reaction Conditions and for 15 min. at 425 °C

RUN NO.	3	4	6	7	37	38	40**	41**	42*	44*	45*	46*	48	49
Type of Coal (1 g)														
Wyodak	+	+	-	-	-	-	-	-	-	+	+	-	+	+
Ky 9/14	-	-	+	+	+	+	+	+	+	-	-	+	-	-
1 g Aromatic Plus 4 g 1-MN														
Anthracene	-	+	+	-	+	-	+	-	-	-	-	-	+	-
Phenanthrene	+	-	-	+	-	+	-	+	-	-	-	-	-	+
Gas Charge at the Room Temperature (1100 psig)														
Hydrogen	+	+	+	+	-	-	-	-	+	+	-	-	-	-
Nitrogen	-	-	-	-	+	+	+	+	-	-	+	+	+	+
Coal Conversion (wt %)														
THF Soluble	57.7	47.9	83.8	84.7	42.4	37.7	30.1	27.9	84.5	51.2	36.1	39.8	37.1	39.5
Preasphaltene	-	-	26.9	27.6	11.0	13.4	11.6	15.7	21.3	-	-	7.6	-	-
Asphaltene	-	-	33.6	30.0	18.1	14.9	13.7	12.6	31.2	-	-	16.4	-	-
Preasphaltene plus Asphaltene	12.6	10.6	60.5	57.6	29.1	28.3	25.3	27.9	52.4	14.1	8.0	23.9	8.6	9.1
Oil, Water and Gas	45.1	37.3	23.2	27.0	13.2	9.5	4.9	0	32.1	37.1	28.2	15.9	28.5	30.4
Conversion of Aromatics (wt %)														
Conversion to Dihdro-aromatics	16.9	0	28.4	3.8	4.4	0	2.6	0	NA	NA	NA	NA	3.3	0
Unconverted aromatic	77.8	100	50.7	95.3	95.7	100	97.4	100	NA	NA	NA	NA	96.8	100

*5 g 1-Methylnaphthalene introduced in the absence of aromatics

**350 °C of reaction temperature

Table 3 - Effects of Aromatic Compounds and Dihydroaromatic Compounds on Coal Conversion at the Atmospheric Pressure and in the Absence of 1-Methylnapthalene

RUN NO.	5	8	11	12	19	22	23	24
Type of Coal								
Wyodak	+	+	+	+	-	-	-	-
Ky 9/14	-	-	-	-	+	+	+	+
Aromatics								
10 g Anthracene	+	-	-	-	+	-	-	-
10 g Phenanthrene	-	+	-	-	-	+	-	-
8 g Anthracene plus 2 g Dihydroanthracene	-	-	+	-	-	-	+	-
8 g Phenanthrene plus 2 g Dihydrophenanthrene	-	-	-	+	-	-	-	+
Temperature (°C)	339	335	340	330	336	334	333	329
Coal Conversion (wt %)								
THF Soluble	6.5	18.3	51.8	21.6	9.8	32.6	37.3	45.8
Preasphaltene	2.2	1.0	2.3	1.4	6.2	7.2	19.4	15.8
Oil, Water, Gas and Asphaltene	4.3	17.3	49.5	20.2	3.6	25.4	17.9	30.0
Conversion of Dihydro-aromatic (wt %)	0	0	36.3	18.9	0	0	14.8	26.0

Table 4 - Effects of Neat Aromatic Compounds at 425 °C and 15 min. on Coal Conversion in the Presence of 1100 psig Nitrogen at the Room Temperature and in the Absence of 1-Methylnaphthalene

RUN NO.	50	51	52	53
Type of Coal (1 g)				
Wyodak	-	-	+	+
Ky 9/14	+	+	-	-
5 g Aromatics				
Anthracene	+	-	+	-
Phenanthrene	-	+	-	+
Coal Conversion (wt %)				
THF Soluble	32.4	51.3	33.1	42.6
Preasphaltene	10.8	11.1	10.8	0.5
Asphaltene	8.8	14.0	6.7	14.1
Preasphaltene plus asphaltene	19.6	25.1	17.5	14.5
Oil, Water and Gas	12.8	26.1	15.7	28.1
Conversion of Aromatic (wt %)				
Conversion to Dihydroaromatic	0	0	2.7	0
Unconverted Aromatic	100	100	97.3	100

THE EFFECT OF SHORT REACTION TIME ON THE LIQUEFACTION OF AN AUSTRALIAN BROWN COAL

M.G. Strachan[A], N.R. Foster[B], R.B. Johns[A] and R.S. Yost[A]

A. Departments of Organic Chemistry and Chemical Engineering, University of Melbourne, Parkville, Victoria, Australia 3052.
B. C.S.I.R.O. Division of Fossil Fuels, North Ryde, N.S.W., Australia 2113.

INTRODUCTION

Short Reaction Time (SRT) liquefaction has attracted much research in recent years (1-11). The process, which involves dissolution of coal in a donor solvent during a short time domain, has many advantages over conventional longer reaction time systems. These include the consumption of negligible gaseous hydrogen, utilizing instead the inherent hydrogen in the coal via shuttling and aromatic transfer mechanisms (1,2). The design and mathematical modelling of continuous reactors is also facilitated by the knowledge of the behaviour of the coal at short residence times. The rapidity of the process has led to the development of two-stage liquefaction systems based on this new technology, thus enabling the decoupling of thermal from catalytic processes. Preliminary research on SRT systems has shown their potential to give significantly lower gas and higher liquid yields, hence enabling more efficient utilization of hydrogen in the liquefaction process.

The majority of the research has involved US bituminous coals, with Whitehurst (3) reporting that optimum oil yields are achieved with coals in the 77-87% C_{MAF} range. He postulated the observed lower yields for the lower rank coals were a consequence of the insolubility of the initially formed fragments in the donor solvent due to their more polar nature. Other workers (12) have suggested the lack of rapid dissolution is a function of these coals having more alicyclic, rather than hydroaromatic and aromatic systems, and hence are less capable of internal hydrogen donation.

The liquefaction of an Australian bituminous coal, Liddell, at SRT conditions has recently been reported (9,10,11). The authors observed trends similar to those found for US bituminous coals, with significant conversion occurring within the first few minutes of reaction. To determine whether Australian low rank coals display similar SRT behaviour to their US counterparts a Victorian brown coal has been investigated. This paper reports the results of the study; emphasizing conversion, oil yields and product analyses.

The coal used for this study was a medium-light lithotype Victorian brown coal from the Loy Yang Field (bore 1277, depth 67-68 m). The dried coal (particle size range: 90-150 μm) was injected into the donor solvent, tetralin, at temperature. The SRT reactor and details of its operation are described elsewhere (10,11). The reaction temperature was 380°C, the solvent to coal ratio 6:1, and the hydrogen pressure after injection typically 2100-2350 psig. The reaction times investigated were: 0,2,3,4,10,20,45 and 120 minutes.

The Total Oils (defined as CH_2Cl_2 solubles) and residues have been investigated and characterized by a variety of analytical and spectroscopic methods. This has enabled both physical and chemical insights into the reactions occurring during the initial and subsequent dissolution of the brown coal.

RESULTS AND DISCUSSION

The product distribution data (Table 1) shows both the conversion and oil yields to increase with reaction time. Surprisingly, there is conversion at zero time, which is associated mainly with gas production as reflected in the very high gas/oil yield ratio. Gas analyses however show its composition to be overwhelmingly carbon oxides with only a minor portion of hydrocarbon gases. Similar gas compositions are observed at the other reaction times with only the absolute amounts of the gases varying. The general trend is to increasing gas yields with reaction time. Although CO_2 and CO dominate the gas production at all reaction times, the hydrocarbon gases do not become significant until 20 minutes of reaction time. Prior to this they are only in trace amounts. The zero time conversion suggests that contact of the dried coal with the hot solvent for only a few seconds is sufficient to promote decarboxylation,

decarbonylation and to a much lesser extent dealkylation reactions. The oil yield at zero time may possibly arise from the easily extractable, non-covalently bonded material in the coal matrix as 3.47% of the coal is solvent extractable (14). Decomposition and dissolution of the coal structure is significant even at 3 minutes with conversions of greater than 20%.

The data indicate the existence of two distinct reaction time zones; the first being prior to 10 minutes and the second from this time. In the first few minutes of reaction there is much gasification as defunctionalization reactions of the coal matrix occur. This is markedly illustrated by both the gas yields and gas/oil yield ratios. The amount of water production is relatively constant indicating the major reaction processes are rupture of the weaker bonds in the coal structure rather than dehydroxylation and upgrading of solubilized species. However, in the second time zone gas production remains constant, with the gas/oil yield ratio actually decreasing, suggesting that gasification is now mainly dependent on the removal of alkyl substituents rather than carboxyl and carbonyl functional groups. These have been predominantly removed within the first few minutes of reaction. The water yield increases significantly as does the H_2O/oil yield ratio indicating the removal of hydroxyl moieties. These may arise either from dehydroxylation of the coal matrix to aid its dissolution or from the upgrading of the already solubilized fragments.

Donor solvent hydrogen consumption data also supports the concept of two separate reaction periods. As expected, little hydrogen is consumed during the initial stages of dissolution, where the removal of carboxyl and carbonyl groups, via gasification, is dominant. This low hydrogen consumption may be a direct result of the coal utilizing its inherent hydrogen by shuttling type mechanisms. Although consumption does increase with time, it is much greater during the latter reaction period. The hydrogen is required to stabilize radical species produced by both cleavage and more vigorous defunctionalization of the coal matrix.

The conversion value for 120 minutes is very similar to that reported (15) for the same coal hydrogenated under conventional batch autoclave conditions (56% cf. 60%), although the oil yields differ markedly (25% cf. 46%). This difference is difficult to rationalize and results from the much higher water and gas yields for the SRT experiment. The Loy Yang conversions and oil yields are lower than those reported for Liddell coal under similar conditions. The parallel between increasing water production and oil yield tends to give credence to Whitehurst's hypothesis that the lower oil yields at short times for low rank coals are due to the insolubility of the very polar initially formed fragments.

The elemental analyses of the residues (Table 2) shows increasing carbon and decreasing oxygen contents with increasing reaction time. The removal of heteroatom moieties is further evidenced by the O/C ratios which similarly decrease. The H/C ratios however decrease only slightly with time suggesting the difficulty of dealkylation reactions and hence the relative preservation of hydrogen in the residues. The similar H/C values for the various reaction times indicate the residues are mainly the result of loss of peripheral heteroatom functionalities and not subject to gross structural alteration such as forming polycondensed aromatic systems. If this were the case it would be reflected in a significant lowering of H/C values with time. The H/C ratio for the zero time residue is lower than for the parent coal confirming the instantaneous gasification and extraction of non-bound material. The general trends in the Total Oils are also decreasing oxygen and increasing carbon contents with time. This correlates with increasing H/C and decreasing O/C ratios, showing a loss of heteroatom functionality and a lowering of the condensed nature (16) of the oils with time. Again the data can be divided into two regions centered on 10 minutes, as demonstrated by the much lower H/C and O/C ratios after this time compared to those prior. This further implies the time dependency of different liquefaction processes.

The IR Spectra (Fig. 1) of the residues both qualitatively and semiquantitatively support the forementioned data. The hydroxyl absorption decreases only marginally in the first few minutes of reaction but more markedly at longer times. This corresponds with the observed water yields. Similarly the carbonyl

absorption decreases rapidly with time and correlates with the production of carbon oxides. Whitehurst (3) has observed for low rank coals a good correlation between the loss of oxygen and the formation of carbon dioxide and carbon monoxide. There is also proportionate increases in aromatic C=C stretching and C-H bending with time, suggesting the residues are acquiring greater aromatic character. The proportion of aliphatic C-H stretching and bending vibrations slightly increase with time paralleling the loss of heteroatom functionality. This further illustrates the relative inertness of alkyl compared to heteroatom functionalities, and supports the forementioned gas composition data.

The trends are not as well defined for the Total Oil (TO) (Fig. 2), with the hydroxyl absorptions although being proportionately larger (approx. 16%) varying little with time. This implies that the forementioned increased water production is more likely a result of cleavage and dissolution of the matrix rather than upgrading of the already solubilized species. There is a general decrease in the carbonyl absorptions with time, while the converse is observed for the aliphatic C-H stretchings. The aromatic C-H bending, although a large percentage at 2 minutes (approx. 15%) decreases rapidly to a constant value (approx. 8%) from 4 minutes onwards. This is generally at the expense of increasing aromatic C=C and aliphatic C-H stretchings.

CP-MAS ^{13}C nmr of the residues (Fig. 3) further illustrates the significant reactivity of the coal at SRT. The aromaticity, f(a), increases dramatically after only 2 minutes reaction from 0.61 in the parent coal to 0.78 in the residue. Even at zero time f(a) is 0.63, reflecting the loss of carboxyl and carbonyl groups as gases. The f(a) values increase only marginally from 0.78 to 0.83 with time, supporting earlier conclusions from elemental analyses that all the residues have similar aromatic structure, differing mainly in degree of functionality.

^{1}H nmr and structural parameters derived from Brown-Ladner equations (Table 3) give additional information on the nature of the TO. The percentage of exchangeable protons [H(exch)] increases with time, showing an increasing proportion of phenolic groups in the oils. This trend was not as evident from IR data. The values for H(exch) further suggest two reaction time zones as they cluster into two discrete groups. Although there are no discernable trends with the percentage of aromatic protons (H_{ar}), the percentage of protons on carbons β and further from aromatic rings (H_o) tend to increase with time. This is also shown in the values for the average chain length (n). The oil produced at zero time has both the greatest proportion of H_o and the largest value of n, suggesting it is only the solvent extractable material from the coal. Solvent extracts of a Victorian brown coal of the same lithotype have been observed to contain a significant amount of straight chain material, either as alkanes, alcohols or fatty acids (17). The value of n then decreases to a minimum at 10 minutes and increases to 120 minutes; indicating more complete decomposition of the coal in this longer time domain. The increased chain lengths could result from cleavage of alicyclic systems. The aromaticity, f(a), and degree of aromatic substitution, σ, generally decrease with increasing reaction time. The trends for the parameter $\frac{H_{aru}}{C_{ar}}$, i.e., the degree of condensation, are not as clearly defined, but it appears to increase with time implying smaller size aromatic systems. The decrease in aromaticity and substitution of the oil implies that either some upgrading of the initially solubilized material has occurred or the later dissolved material was more defunctionalized prior to dissolution. More likely it is a combination of both processes.

The Molecular Weights (MW) of the Total Oil (Table 3) are all similar with the number average MW ($\bar{Mn}$) varying from 210-320 with no readily identifiable trend with time. The values of $\bar{Mn}$ are low compared to that reported for an oil produced from the same coal under normal batch autoclave conditions ($\bar{Mn}$ = 487). The weight average MW ($\bar{Mw}$) and MW distribution (MWD) also show no apparent trends. These observations are most likely a direct consequence of the insolubility of a large portion of the oils in the solvent, THF, used for MW determination. Hence only smaller MW species from the very heterogeneous Total Oil have been selectively dissolved. This insolubility may be itself indicative of the high MW of these Total Oils.

Pyrolysis-Gas Chromatography of the residues (Fig. 4) reveals a major

reduction of aliphatic components within the first 4 minutes of reaction, and with only alkyl phenols and catechols remaining after 45 minutes. This indicates that the more easily accessible and removable aliphatic material is extracted preferentially from the coal matrix in the initial stages of dissolution, while at longer times the coal structure itself must be more severely decomposed to increase the oil yield. This is also revealed by the decrease in the percentage of residue pyrolysed. The presence of phenolic species is directly relatable to the lignin input to the brown coal. Their existence in the pyrograms of the residues from 20 and 45 minutes supports the hypothesis that further oil production results from cracking of the lignin-type components of the coal macromolecules. Pyrolysis-Gas Chromatograms of the TOs, which are in effect simulated distillation profiles, all appear very similar. They differ quantitatively rather than qualitatively in composition.

The residues were degradatively oxidized by peroxytrifluoroacetic acid, a technique known as Deno Oxidation (18). It selectively oxidizes aromatic rings and leaves the aliphatic portion essentially intact. The data (Table 4) reveals that even at 0 minutes there is a marked reduction in the total yield of aliphatic hydrogen (65.6% cf 54.3%) compared to the parent coal from both assignable and unassignable material. Overall there is a reduction with time for both the total aliphatic and total spectrum hydrogen yields, suggesting the residues are becoming more aromatic in nature. Acetic acid (derived from aryl methyl grou \) varies little with time suggesting little increase in dealkylation reactions. Succinic acid (derived from hydroaromatic structures) well illustrates the existence of two reaction zones. It is much reduced in the second due to both a possible internal hydrogen donation and a more severe rupture of the coal structure. Similarly, malonic acid (derived from bridging methylene groups) is also reduced in the second period as a result of bond cleavages and probably accompanying fragmentation of aromatic clusters. The 1° and 2° protons decrease in accord with the total aliphatic hydrogen, whereas the 3° protons vary little with time. However, the protons on carbons α to carbonyl containing functional groups decrease significantly with time, parallelling the loss of the functional groups as carbon oxides. The data support earlier conclusions from other techniques.

This paper has reported the results of a donor solvent SRT study of a Victorian brown coal. Although oil yields and conversion are lower than for bituminous coals they show trends similar to those reported for USA low rank coals. The dissolution process appears to occur in two chemically and physically distinct phases. One primarily involves extraction of the coal and removal of carboxyl and carbonyl groups while the other involves a more severe disruption and decomposition of the coal matrix and removal of hydroxyl moieties. In both phases dealkylation is not a dominant reaction.

ACKNOWLEDGEMENT

M.G. Strachan acknowledges the award of a University of Melbourne Research Scholarship.

REFERENCES

1. Han, K.W. and Yen, C.Y., Fuel, 1979, 58, 779
2. Whitehurst, D.D. and Mitchell, T.O., in Liquid Fuels from Coal, Ed. Ellington, R.T., p. 153, Academic Press, N.Y., 1977.
3. Whitehurst, D.D., A.C.S. Symp. Ser., 1980, 139, 133
4. Farcasiu, M., A.C.S. Symp. Ser., 1981, 192, 151.
5. Longanbach, J.R., Droege, J.W. and Chauhan, S.P., A.C.S. Symp. Ser., 1980, 139, 165.
6. Kulik, C.J., Lebowitz, H.E. and Rovesti, W.C., A.C.S. Symp. Ser., 1980, 139, 193.
7. Heck, R.H., Mitchell, T.O., Stein, T.R. and Dabbkowski, M.J., A.C.S. Symp. Ser., 1981, 139, 199.
8. Winnans, R.E., King, H.H., McBeth, R.L. and Botto, R.B., A.C.S. Div. Fuel Chem. Prepr., 1983, 28(5), 8.
9. Foster, N.R., Clark, K.N., Wilson, M.A. and Weiss, R.G., Proc. of the Symp. on the characterisation of Aust. Coal and their Consequences for Utilization p. 30-1, Sydney, May 1982.

10. Foster, N.R., Wilson, M.A., Weiss, R.G. and Clark, K.N., Ind. Eng. Chem. Prod. Res. Dev., 1983, in press
11. Foster, N.R., Weiss, R.G., Clark, K.N. and Young, M.M., Proc. Int. Conf. Coal Sci., p. 129, Pittsburgh, August 1983.
12. Reggel, L., Wender, I. and Raymond, R., Fuel, 1973, 52, 163.
13. Strachan, M.G., Johns, R.B. and Yost, R.S., J. Chromatog. Submitted for publication.
14. Strachan, M.G., McGavan, D.G. and Johns, R.B., Unpublished results.
15. Strachan, M.G., Vassallo, A.M. and Johns, R.B., A.C.S. Div. Fuel Chem. Prepr., 1983, 28(5), 226.
16. Curtis, C.S., Fuel, 1980, 59, 579.
17. Chaffee, A.L., Ph.D. Thesis, University of Melbourne, 1981.
18. Deno, N.C., Greigger, B.A. and Stroud, S.G., Fuel, 1978, 57, 455.

TABLE 1: PRODUCT DISTRIBUTION

Reaction Time (min)	Conversion %	Oil[A] yield	H_2O[A] yield	Residue[A]	Gas[A,B]	H_2O/oil yield	Gas/oil yield
0	9.0	0.90	2.59	91.00	5.50	2.88	6.12
2	12.61	5.12	2.04	87.39	5.45	0.40	1.06
3	21.02	6.08	2.43	78.98	12.51	0.40	2.06
4	27.53	7.63	2.89	72.47	17.01	0.38	2.23
10	32.39	10.65	4.77	67.61	16.91	0.45	1.59
20	39.91	18.08	7.17	60.09	14.66	0.40	0.81
45	48.95	19.55	15.32	51.05	14.08	0.78	0.72
120	56.28	25.92	15.96	43.72	14.40	0.62	0.56

A - g/100 g DAF Coal B - By difference

TABLE 2: ELEMENTAL ANALYSES

Time (min)	C	H	O[A]	N	H/C	O/C[A]	N/C	Ash
LY 1277	62.35	5.20	31.89	0.59	1.00	0.38	0.01	0.71
Total Oils								
0	74.69	2.48	22.30	0.53	0.40	0.22	0.01	6.00
2	76.43	3.50	19.74	0.33	0.55	0.19	0.00	0.90
3	76.87	4.18	24.50	0.49	0.65	0.24	0.01	2.0
4	68.30	3.77	27.50	0.40	0.66	0.30	0.01	1.0
10	73.84	4.17	21.81	0.16	0.68	0.22	0.00	0.70
20	84.55	5.96	9.14	0.35	0.85	0.08	0.00	0.40
45	82.93	5.87	10.72	0.41	0.85	0.09	0.00	2.40
120	86.98	6.23	6.20	0.50	0.86	0.05	0.00	0.40
Residues								
0	65.24	4.68	29.44	0.65	0.86	0.34	0.01	0.79
2	67.28	4.62	27.39	0.71	0.82	0.31	0.01	0.12
3	68.86	4.62	25.78	0.73	0.81	0.28	0.01	1.13
4	69.35	4.62	25.29	0.74	0.80	0.27	0.01	1.06
10	70.51	4.70	24.06	0.79	0.80	0.26	0.01	1.06
20	72.16	4.70	22.37	0.83	0.78	0.23	0.01	1.06
45	74.40	4.87	19.79	0.95	0.79	0.20	0.01	1.97
120	75.71	5.03	18.23	1.01	0.79	0.18	0.01	2.29

A - Oxygen by difference

TABLE 3: ^{1}H NMR AND MW DATA ON TOTAL OILS

	^{1}H NMR DATA									MW DATA[C]		
Time (min)	Ho	Hα	Har	H(exch)	$\frac{Hali}{Har}$	$n=\frac{Ho}{H\alpha}+1$	f(a)[A]	$\frac{Haru}{Car}$[A]	σ[A]	$\bar{Mn}$	$\bar{Mw}$	MWD
0	61.9	15.7	22.4	N.D.	3.47	4.96	0.84	0.41	0.74	210	411	1.96
2	28.8	20.1	48.6	1.4	0.95	2.29	0.87	0.59	0.48	260	210	0.81
3	58.3	19.8	24.7	1.8	3.22	3.56	0.67	0.83[B]	0.61	295	432	1.46
4	31.8	26.6	38.8	1.9	1.51	2.20	0.79	0.88[B]	0.63	279	331	1.19
10	35.5	29.9	32.1	3.1	2.02	2.18	0.78	0.69	0.59	282	442	1.57
20	47.3	25.4	24.0	3.3	3.03	2.86	0.69	0.57	0.48	319	754	2.36
45	35.7	27.6	32.5	3.7	1.95	2.30	0.73	0.67	0.44	298	304	1.02
120	45.7	20.0	30.5	3.8	2.15	3.28	0.72	0.66	0.35	249	393	1.58

N.D. - Not Determined. A - Brown-Ladner Method. B - High oxygen content in sample.
C - GPC-HPLC method for molecular weight determination

TABLE 4: ^{1}H NMR SPECTRAL DATA OF (WT %) YIELD OF HYDROGEN APPEARING IN TFA[A] OXIDATION PRODUCTS

Time (min)	1° & 2° Protons (0.3-1.45 ppm)	3° Protons (1.45-2.20 ppm)	Protons α to acids and esters (2.20-3.45 ppm)	Total Aliphatic	Acetic Acid	Succinic Acid	Malonic Acid	Methanol	Total Spectrum	% Oxidized
LY 1277	18.2	17.0	18.4	53.6	6.5	3.8	1.3	0.4	65.6	98
0	11.9	13.1	10.2	35.2	11.0	4.7	2.4	1.0	54.3	93
2	10.1	9.1	9.5	28.7	10.8	3.2	2.0	2.7	47.4	98
3	13.1	11.6	10.0	34.7	14.4	4.5	2.2	2.2	58.0	99
4	13.2	11.0	8.7	32.9	14.0	4.0	2.0	2.2	55.1	98
10	10.1	10.9	9.8	30.8	13.0	4.3	2.3	3.2	53.6	99
20	11.2	11.3	7.1	29.6	12.0	2.7	0.7	3.2	48.2	97
45	9.6	10.5	6.8	26.9	11.7	3.5	1.0	2.9	46.0	98
120	6.5	9.5	5.2	21.2	11.7	3.0	0.8	0.7	37.4	95

A - Peroxytrifluoroacetic acid

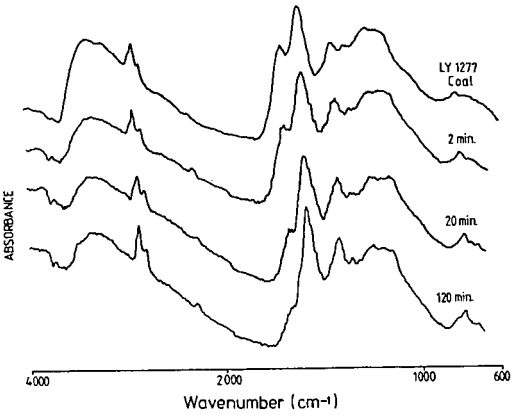

FIG. 1. IR SPECTRA OF LIQUEFACTION RESIDUES

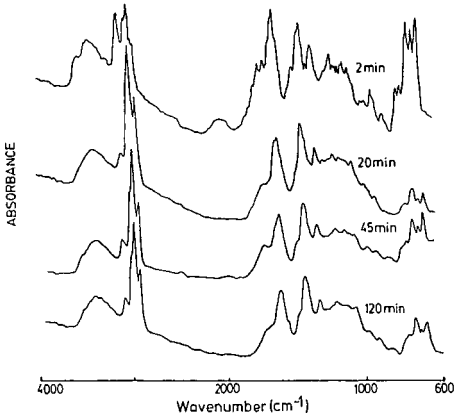

FIG 2. IR SPECTRA OF TOTAL OILS

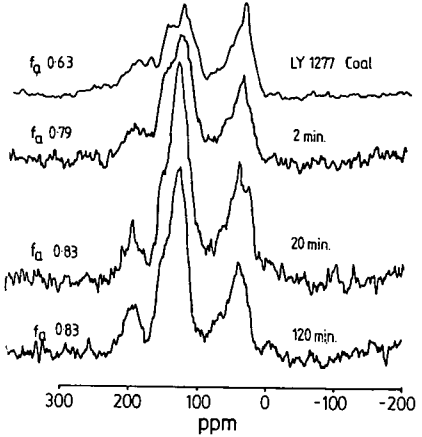

FIG. 3. CP-MAS ^{13}C NMR SPECTRA OF LIQUEFACTION RESIDUES

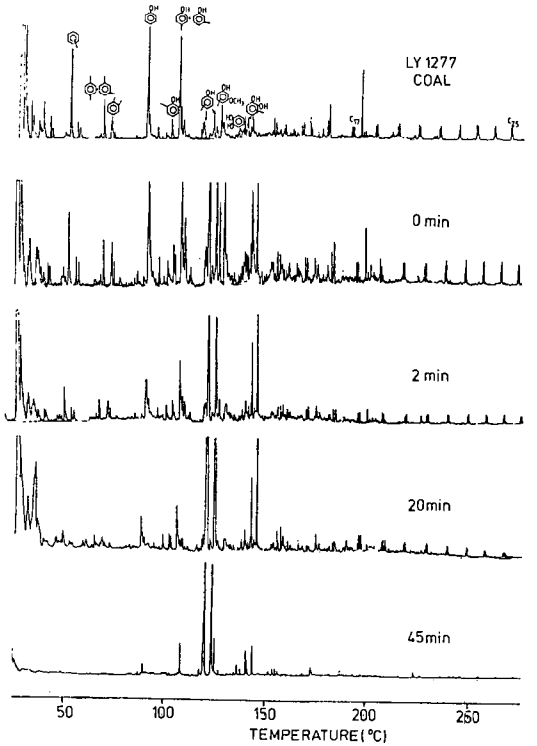

FIG. 4. PYROGRAMS OF LIQUEFACTION RESIDUES AND COAL

Combined Upgrading of Coal and Petroleum Residua

Christine W. Curtis, James A. Guin, Milo Pass, and Kan Joe Tsai

Chemical Engineering, Auburn University, Alabama 36849-3501

This investigation examines the feasibility of using heavy petroleum crudes and residua as solvents in coal liquefaction. The concept being explored is to determine if coal and heavy petroleum crudes and residua can be simultaneously processed with mutual upgrading of both materials. Previous work by Moschopedis and coworkers[1-4] has examined the liquefaction of coal using Athabasca oil sands bitumen, Lloydminster heavy oil, Coker gas oil and Cold Lake bitumen. The effectiveness of these materials as hydrogen donor solvents and their thermal stability under liquefaction conditions was also examined. The effects of process parameters on the production of reaction products was also investigated. Other investigations have been performed by Mochida and coworkers[5] in which several coals were liquefied in the presence of a Khafji vacuum residue. Other studies by Mochida[6,7] have included the liquefaction of an Australian brown coal in a prehydrogenated petroleum pitch and the liquefaction of subbituminous coals using pyrene and various Ashland pitches.

This study examines the conversion of a bituminous coal to soluble products through coprocessing with six heavy petroleum crudes and residua. These reactions were performed thermally, in an inert and in a hydrogen atmosphere, and catalytically in a hydrogen atmosphere. The petroleum materials used range from a whole crude to a variety of residua. Chemical and physical characterizations have been performed to determine what factors are most influential in producing the end product. To determine the sensitivity of coprocessing to reaction conditions and to determine the most optimal parameters, an evaluation of key reaction parameters has been performed.

Experimental

Feedstock. Six petroleum crudes and residua, supplied by Cities Service Research and Development Company, have been examined for potential use as solvents for coal liquefaction processing. Analysis of the petroleum feedstocks are given in Table 1. The coals used in this study are a high volatile bituminous Illinois #6 coal, a Blacksville mine coal and a subbituminous coal, Clovis Point from Wyoming.

Screening Experiment. Screening experiments were performed at 400°C using a nitrogen atmosphere and a hydrogen atmosphere. Catalytic screening experiments with a hydrogen atmosphere were performed at 400° and 425°C. The equipment and reaction conditions used in these experiments were: a 50 cc stainless steel tubing bomb reactor, reaction time of 30 minutes, agitation at 860 cpm, and a solvent to coal ratio of 2:1. The reaction products were analyzed by a solvent separation scheme in which the product is successively extracted by pentane, benzene and methylene chloride/ methanol. The liquid fractions obtained are oil (pentane solubles), asphaltenes (benzene soluble, pentane insolubles), and preasphaltenes (benzene insoluble, methylene chloride/methanol solubles), and insoluble organic matter. The weight of gases produced was also determined.

Parametric Evaluation. The reaction parameters evaluated as to their effect on coal conversion and product distributions from combined processing were reaction temperature, initial hydrogen reaction pressure, reaction time and diffusional pathlength of the catalyst. The reaction conditions for these evaluations are summarized below:

Reaction Conditions	Parameter		
	Temperature	Pressure	Time
Time	30 minutes	30 minutes	---
Temperature	----	425°C	425°C
Pressure	1250 psig H_2	----	1250 psig
Agitation Speed	860 cpm	860 cpm	860 cpm
Coal	3 g, Illinois #6 or 3 g, Blacksville	3 g, Illinois #6	3 g, Illinois #6
Solvent	6 g, Maya Crude	6 g, Maya Crude	6 g, Maya Crude
Catalyst	None	1 g, Presulfided Shell 324 $NiMo/Al_2O_3$ powdered (from 1/32" extrudates)	3 conditions were used: a. None Presulfided b. Shell 324 $NiMo/Al_2O_3$ 1/16" extrudates c. Presulfided Shell 324 $NiMo/Al_2O_3$ (from 1/16" extrudates)

The effect of thermal and catalytic combined processing on the reaction products from Clovis Point coal was also evaluated.

Characterization of the Petroleum Crudes and Residua. The petroleum crudes and residua were characterized by elemental analysis, molecular weight by vapor phase osmometry in pyridine, viscosity, Conradson Carbon, proton distribution, and specific gravity. Table 1 presents a composite of the physical and chemical characteristics of the petroleum crudes and residua.

Results and Discussion

Six heavy petroleum crudes and residua have been used as solvents in a series of coal liquefaction experiments to determine their ability to liquefy coal. The experiments were performed at 400° and 425°C using Illinois #6 coal and in three different environments: (1) a N_2 atmosphere, (2) a H_2 atmosphere and (3) and H_2 atmosphere using a pelletized presulfided $NiMo/Al_2O_3$ catalyst.

Analyses of the solvents using a solubility extraction procedure developed for coal materials showed that the petroleum crudes were between ~80% to 90% soluble in pentane and the pentane insoluble materials were mostly benzene solubles, asphaltenes. The coal derived solvent CPDU-200A was ~85% pentane soluble with the remainder being asphaltenes. The petroleum solvents have hydrogen to carbon ratios of ~1.45 to 1.65 and sulfur contents between 2.8% and 4.6%.

Liquefaction in a Nitrogen Atmosphere. Liquefaction experiments were performed in a hydrogen deficient, nitrogen atmosphere to determine how readily the hydrogen-rich petroleum solvents could transfer hydrogen directly to coal, thereby converting coal to a soluble product. The ability of tetralin and coal-derived CPDU-200A to convert coal was also determined.

Coal conversion obtained using tetralin was 57.5%, by CPDU-200A was 51.5%, and the most converted by a petroleum crude was 36.0%. At 400°C, the coal conversion in the petroleum materials range from 28% to 36%. These data indicate and the proton distribution as determined proton nuclear magnetic resonance (^{1}HNMR) substantiate that the petroleum crudes and residua do not contain hydrogen which can be easily

donated to coal. In fact, the majority of the protons in the petroleum materials lie in the alkyl β and γ regions. In these experiments, tetralin, a known hydrogen donor, was the only solvent that produced an increase in oils above that present in the original 2:1 solvent/coal mixture. In the hydrogen deficient atmosphere, donor hydrogen as present in hydroaromatic compounds, appears to be necessary for both coal conversion and the production and maintenance of the oil fraction. Similar results using model hydroaromatic and aliphatic solvents are present in the literature.[8-9]

Compared to the original product distribution, the reaction products from the combined processing lost pentane solubles. A general increase in the asphaltene content of the product liquids was observed as compared with the original charge. In the hydrogen deficient environment, both the coal and the heavy petroleum materials may undergo polymerization forming coke-like material which appears as IOM. In addition, the reacting coal may incorporate a significant portion of the petroleum soluble material into the coal matrix.

Noncatalytic Experiments with a Hydrogen Atmosphere. To eliminate some of the possible retrogressive reactions of the petroleum materials and the coal associated with the inert atmosphere, a hydrogen atmosphere was used. As with the nitrogen atmosphere, tetralin converted the most coal, yielding 71.2%, while the coal-derived material CPDU-200A converted 56.8%. Compared to the nitrogen atmosphere, substantially more coal was converted in the hydrogen atmosphere with the petroleum solvents. The coal conversion ranged from ~43% to 54% depending upon the petroleum material used. The hydrogen atmosphere also either maintained or increased the oil yield as compared to the original charge. Three of the less viscous lighter petroleum materials, Maya Crude, West Texas TLR and Mayan TLR showed a positive increase in oil; whereas, in nitrogen, each of these crudes showed a reduction in oil content when compared to the original solvent. Kuwait resid, West Texas vacuum short and West Texas TLR showed the greatest oil production improvement (> 7%) when a hydrogen rather than a nitrogen atmosphere was used.

Catalytic Liquefaction Using a Hydrogen Atmosphere. The effect of adding a presulfided $NiMo/Al_2O_3$ extrudate catalyst on the conversion of coal and on reaction products has also been investigated. The reactions were performed at 400°C and 425°C. For all the solvents used, the addition of presulfided $NiMo/Al_2O_3$ increased both oil production and coal conversion. In the compilation of data presented in Table 2, it is apparent that at 400°C and 425°C the presence of the $NiMo/Al_2O_3$ hydrogenation catalyst caused a significant improvement in the oil yield. The same improvement is observed in coal conversion. In those cases where the catalytic reactions were performed at both 400°C and 425°C, the twenty-five (25) degree rise in temperature seemed to be a secondary effect on both coal conversion and oil yield with the possible exception of the West Texas vacuum short resid. For West Texas vacuum short resid, coal conversion seemed to be affected by temperature both in catalytic and noncatalytic reactions with hydrogen atmospheres. The addition of a hydrogenation catalyst can significantly improve the oil production and coal conversion in combined processing.

Chemical and Physical Properties of the Petroleum Crudes and Residua. Among the six petroleum materials individual differences are apparent in their ability to convert coal and produce pentane soluble materials. A number of chemical and physical properties of the petroleum materials have been evaluated and are given in Table 1. A typical coal liquid, CPDU-200A, is also shown in Table 1 and has been used as a point of comparison between the coal-derived and petroleum solvents.

From these analyses, general comments can be made concerning the properties of the petroleum solvents. Each petroleum crude and residuum contains large asphaltenic compounds as evidenced by a lack of solubility of ~6 to ~20% of the petroleum material in pentane and that much solubility in benzene. All of the petroleum solvents are hydrogen-rich and high in sulfur as compared to coal-derived liquids.

The typical hydrogen to carbon ratio for coal-derived liquids is 1.0 or less; all of the petroleum crudes and residua used in this study have H/C ratios in the range of 1.45 to 1.65. The ash levels in the petroleum crudes range from 0.012 wt % for West Texas vacuum short resid to 0.082 wt% for Mayan topper long resid. This low ash content is insignificant in this work in terms of the product distribution obtained after coprocessing with coal. All of the petroleum solvents are highly aliphatic, having f_a values between 0.32 and 0.37. Proton distributions of the petroleum solvents show the protons to be primarily alkyl β and γ protons. Few hydroaromatic protons are present. CPDU-200A, by contrast, is quite aromatic, having a f_a value of 0.71. A higher percentage of cyclic alpha protons are present in the CPDU-200A than in any of the petroleum materials. The aromatic nature and the presence of some hydroaromatics may account for the CPDU-200A's ability to convert more coal than do the petroleum solvents.

Coal conversion in the petroleum solvents using a hydrogen atmosphere at 400°C can be correlated with the viscosity of the petroleum material and with the Conradson Carbon number. The highly viscous solvents, Kuwait resid and West Texas vacuum short resid, give less coal conversion than do the less viscous petroleum solvents. The petroleum solvents with lower Conradson Carbon numbers promote higher coal conversion. A similar trend is observed with molecular weight. The petroleum solvents with lower molecular weights, Lloydminster reduced crude, West Texas TLR, Maya Crude and Mayan TLR, correlate with increased coal conversion. West Texas TLR which has the lowest Conradson Carbon and the second lowest molecular weight and viscosity gives the highest coal conversion of any of the petroleum solvents during coprocessing. The addition of a catalyst changes the order of the coal conversion among the six petroleum solvents and apparently the relative importance of the solvent's properties. No obvious correlations exist between the abovementioned solvent properties and coal conversion when a catalyst is used.

Parametric Evaluation. The effect of reaction conditions on combined coal and heavy residua processing has been evaluated using the parameters of reaction temperature, initial hydrogen pressure, reaction time and diffusional pathlength of the catalyst. For these studies, Maya Crude was used as the solvent. Three coals were used, Illinois #6, Blacksville, and Clovis Point, with Illinois #6 coal being used for the majority of the experiments. Solvent extraction of Illinois #6 at room temperature showed the coal to be ~90% insoluble at room temperature. When reacted at 425°C in hydrogen in the absence of a solvent, ~35% of Illinois #6 coal was converted, primarily to preasphaltenes. Under the same conditions, ~46% of the Clovis Point was converted with all solubility fractions being present. The upgradability of the Maya Crude was also examined to determine if the asphaltenes present could be upgraded to oil. After thermal reaction the Maya Crude did not change substantively although 2.7% of the product was gas. A 4% increase in oil was observed on catalytic hydrogenation with a further increase in gas production.

Effect of Temperature on the Product Distribution from Illinois #6 and Blacksville Coals. To determine the effect of reaction temperature on the product distributions from coprocessing, the reactions were performed at 375°, 400°, 425°, 450° and 475°C. With increasing temperatures, oil production and higher coal conversion were observed for both coals up to a temperature of 425°C where a maximum in oil yield and a minimum of IOM occurred. For both coals, the greatest coal conversion was observed at 425°C. At higher temperatures, 450° - 475°C, higher gas yields and IUM yields (lower coal conversion) are observed for both coals. Based on these data, a temperature of 425°C was selected for combined processing.

Effect of Initial Hydrogen Pressure on Coprocessing. To determine the sensitivity of combined processing to initial hydrogen pressure, the initial hydrogen pressure was increased from 0 psig to 1500 psig. A powdered Shell 324 $NiMo/Al_2O_3$ was added to the reaction mixture. The products distributions shown in Figure I demonstrate the need for a hydrogen environment to convert coal and simultaneously to upgrade the petroleum crudes. When no hydrogen is present, only 8.6% coal conversion is

observed. Comparing this conversion to that of thermally reacted coal with no solvent in a hydrogen atmosphere, the hydrogen atmosphere increases coal conversion by more than 20%. In a hydrogen deficient atmosphere, the petroleum solvent may also be undergoing retrogressive reactions forming coke-like materials adding to the IOM. At an initial hydrogen pressure of 250 psig, the pentane solubles produced were higher than that in the original mixture; coal conversion was 52.5%, suggesting that even low levels of hydrogen can be effective in reducing the number of retrogressive reactions when solvent and catalyst are present to aid in the transfer of hydrogen to coal. At 500 psig, the coal conversion again increased significantly to 78.7% while the pentane soluble yields increased to 70.4%. As the hydrogen pressure was increased even further, coal conversion continued to climb yielding 86.9% at 1500 psig. The oil produced also increased at 1500 psig to 78.5%. Above 500 psig, the rate of increase for both coal conversion and pentane soluble yields was lower than between 0 and 500 psig.

Effect of Time and Catalyst Diffusion Pathlength on Product Distributions from the Liquefaction of Illinois #6 Coal. To determine the effect of time on combined processing, three sets of experiments were performed: (1) thermal reaction with no catalyst present, (2) $NiMo/Al_2O_3$ pelletized catalysts, and (3) $NiMo/Al_2O_3$ powdered catalysts.

A comparison of the ability of Maya Crude to convert coal under these three conditions is given in Figure 2. For all three cases, long reaction time, 90 minutes, increased coal conversion when compared to the shorter time experiments. The use of powdered catalyst increased the amount of coal conversion substantially compared to the thermal and catalyst pellet experiments. This increase occurred for all reaction times. The coal conversion in the thermal and extrudate experiments are very similar and are about 20% less than the powdered catalyst.

From these experiments, it is apparent that the longer residence time the coal has in a hydrogen atmosphere the more coal will be converted. The use of a catalyst increases the availability of the hydrogen to the coal and increases the rate of coal dissolution. The use of a powdered catalyst makes hydrogen more available to the coal by providing contact between the catalyst particles and the dissolving coal matrix. This increased availability is caused by decreasing the diffusional pathlength required for the coal to traverse before coming into contact with an active hydrogenation site.

Hydrogen consumption in the thermal and in both catalytic experiments increased with increasing time. The coprocessing experiments using the powdered catalyst consumed more hydrogen than did either the experiments using pellets or no catalyst. The hydrogen consumption data correlate with the yields of pentane solubles produced under the three conditions. More pentane solubles were produced in the powdered catalyst experiments than in the extrudate experiments which was more than the thermal. The data is presented in Figure 3 which shows the oil production from the three cases as a percentage of the upgradable material present in the reaction, the upgradable material being defined as the maf coal and petroleum asphaltenes present at the beginning of the reaction. The catalyst obviously aids in oil production, with the powdered form yielding significantly greater oil production than the extrudate pellets. These data are a clear indication of the influence of pore diffusional restrictions in limiting the oil yield with extrudate pellets.

Illinois #6 coal was also liquefied in tetralin with a powdered catalyst for 30 minutes. The coal conversion obtained was 92.4% and the oil production was 86.7%. Both the coal conversion and oil production are higher in tetralin than in Maya Crude under equivalent reaction conditions. The values obtained from the combined processing are 81.6% and 76.7%, respectively. Longer reaction times of 90 minutes with Maya Crude produce higher yields of coal conversion and oil, 83.4% and 82.7%, respectively.

The effect of thermal and catalytic combined processing from Clovis Point coal was also evaluated. The product distributions obtained from 30 minutes of reaction are given in Table 4. The product distributions from Clovis Point coal from the three reaction conditions show similar trends to those obtained from Illinois #6 coal. Oil production and coal conversion increased with catalytic treatment, the highest yields being produced from the powdered catalyst. For comparable reaction times, coal conversion from Clovis Point was slightly higher than Illinois #6 for the thermal and pelletized catalyst case. Oil production from Clovis Point coal was consistently 5 to 6% higher than Illinois #6 coal.

Summary and Conclusions

Petroleum crudes and residua and coal have been coprocessed at typical liquefaction conditions in atmospheres of nitrogen and hydrogen and in the presence of hydrogen and a catalyst. At 400°C coal conversion in a nitrogen atmosphere was low and at the same level as the thermal coal reaction with no solvent, indicating that no transfer of hydrogen from the petroleum solvents to the coal occurred. Coal conversion increased in the presence of hydrogen; further increases in coal conversion were observed in the presence of catalyst at 400°C and 425°C. The dominant factor of the increased conversion in the majority of the heavy petroleum materials was the presence of the catalyst with the 25° temperature rise being a secondary effect. Oil production from combined processing showed negative or level yields in the N_2 atmosphere, level or slightly positive yields in the H_2 atmosphere and for most petroleum solvents significant increases when a catalyst and hydrogen were both present. As in the case of coal conversion, the catalyst appears to be the dominant factor in the increase with temperature having a secondary effect.

Individual differences among the petroleum solvents are observed in the product distributions obtained from combined processing. Coal conversion in the H_2 atmosphere appears to be correlated with viscosity, molecular weight and Conradson Carbon number of the petroleum crude. These particular solvent characteristics do not seem as important in coal conversion when a catalyst is present.

The parametric evaluation has shown that optimal conditions for combined processing are:

- Reaction Temperature: 425°C
- Hydrogen Pressure: above 500 psig initial hydrogen pressure
- Time: 90 minutes
- Catalyst: powdered hydrogenation catalyst

Coal conversion and oil production from combined catalytic (powdered) processing compare favorably with that from tetralin with a powdered catalyst. Comparison of the final oil yields to the initial charge shows that combined processing yields a net oil increase of 23.3% for 90 minute reaction while tetralin provides a net oil increase of 17.7% for 30 minutes of reaction.

Table 1. Analysis of Liquefaction Solvents

Solvents	Product Distribution (wt%) Oil	Asphaltenes	Preasphaltenes	IOM	Ash, wt%	Elemental Analysis C	H	N	S	H/C
Maya Crude	84.4	15.6			0.058	84.6	11.5	1.21	3.09	1.63
West Texas TLR	93.6	6.4			0.033	86.4	11.0	0.34	2.80	1.51
Mayan TLR	79.5	20.5			0.082	85.3	10.8	0.51	4.19	1.51
Lloydminster Reduced Crude	84.0	16.0			0.039	85.0	10.7	0.34	4.35	1.49
Kuwait Resid	88.96	10.99	0.05		0.031	79.5	10.3	0.19	4.63	1.55
West Texas Vacuum Short Resid	88.7	11.3			0.012	86.1	10.4	0.44	3.33	1.47
CPDU-200A	85.48	12.47	1.16	0.89		89.3	7.3	1.20	0.56	0.97

Solvents	Molecular Weight	f_a	n_D	Viscosity (poise)	Specific Gravity	°API	Conradson Carbon
Maya Crude	577	0.32	1.52		0.920	22.3	10.41
West Texas TLR	545	0.35	1.55	28.2	0.979	13.0	10.34
Mayan TLR	668	0.37	1.56	317	1.000	10.0	15.87
Lloydminster Reduced Crude	481	0.36	1.57	389	1.004	9.44	14.23
Kuwait Resid	961	0.34	1.58	3470	1.014	8.05	17.00
West Texas Vacuum Short Resid	922	0.35	1.58	7075	1.014	8.05	17.33
CPDU-200A		0.71					

Table 2. Effect of Atmosphere and Catalyst on Oil Production and Coal Conversion

Oil, Wt %	Tetralin	Maya Crude	West Texas TLR	Mayan TLR	Lloydminster Reduced Crude	Kuwait Resid	West Texas Vacuum Short	CPDU 200A
Original	67.5	56.9	63.2	53.7	56.7	60.0	59.8	57.7
N_2, 400°C	70.6	58.7	60.4	53.2	55.7	56.0	54.0	53.4
H_2, 400°C	71.2	59.9	65.8	56.4	58.8	60.4	58.4	56.3
H_2 + cat, 400°C		69.2			68.1		64.0	
N_2, 425°C		58.2			51.5			
H_2, 425°C		62.0	65.1		62.2		58.1	
H_2 + cat, 425°C	83.1	72.3	73.7	66.3	71.5	68.2	66.9	73.8
Average Conversion, %								
N_2, 400°C	57.2	28.4	30.2	34.9	28.4	30.2	26.7	50.3
H_2, 400°C	70.6	49.8	53.5	49.3	48.9	45.2	44.5	56.6
H_2 + cat, 400°C		67.3			72.1		52.9	
N_2, 425°C		28.9			13.2			
H_2, 425°C		62.5			64.7		58.5	
H_2 + cat, 425°C	81.0	66.2	68.9	62.3	75.2	69.2	65.4	81.6

Table 3. Hydrogen Distributions in Petroleum and Coal-Derived Solvents

Solvents	% Condensed Aromatics	% Uncondensed Aromatics Plus Hydroxyl	% Cyclic α	% Alkyl α	% Cyclic β	% Alkyl β	% γ
Maya Crude	1.7	2.2	7.2	5.5	16	44	23
West Texas TLR	3.1	1.2	6.1	4.9	17	46	21
Mayan TLR	3.6	3.0	7.1	5.9	15	43	22
Lloydminster Reduced Crude	5.9	2.6	8.5	6.5	18	38	20
Kuwait	4.6	2.0	7.3	6.6	17	45	18
West Texas Vacuum Short Resid	7.0	0.0	14	7.0	29	33	9.9
CPDU-200A	35	13	17	12	8.8	9.7	5.3

Table 4. Product Distribution of Clovis Point Coal Reacted in Maya Crude Under Thermal and Catalytic Conditions

Product Distribution, wt%	Thermal	Catalyst	
		Pellets	Powder
Gas	5.7	5.7	4.9
Oil	68.4	75.0	81.1
Asphaltenes	9.0	5.5	5.1
Preasphaltenes	5.2	4.9	2.9
IOM	11.7	8.9	6.0
% Coal Conversion	62.3	71.6	80.8

Reaction Conditions: 30 minutes, 1250 psig initial H_2 pressure, agitation 860 cpm, 425°C.

References

1. Moschopedis, S. E., Fuel, 590, 1980, 67.
2. Moschopedis, S. E., Hawkins, R. W., Fryer, J. F. and Speight, J. G., Fuel, 59, 1980, 647.
3. Moschopedis, S. E., Hawkins, R. W. and Speight, J. G., ACS Fuel Preprints, 26, (3), 1981, 131.
4. Moschopedis, S. E., Hawkins, R. W. and Speight, J. G., Fuel Processing Technology, Vol. 5, 1982, 213.
5. Mochida, I., Takanabe, A. and Takeshita, K., Fuel, 58, 1979, 17.
6. Mochida, I., Moriguchi, Y., Korai, Y., Fujitsu, H., and Takeshita, K., Fuel, 60, 1981, 746.
7. Mochida, I., Iwamoto, K., Tahara, T., Korai, Y., Fujitsu, A. and Takeshita, K., Fuel, 61, 1982, 603.
8. Neavel, R., Fuel, 1976, 55, 237.
9. Curtis, C. W., Guin, J. A., and Kwon, K. C., AIChE National Meeting, paper 62b, November, 1982.

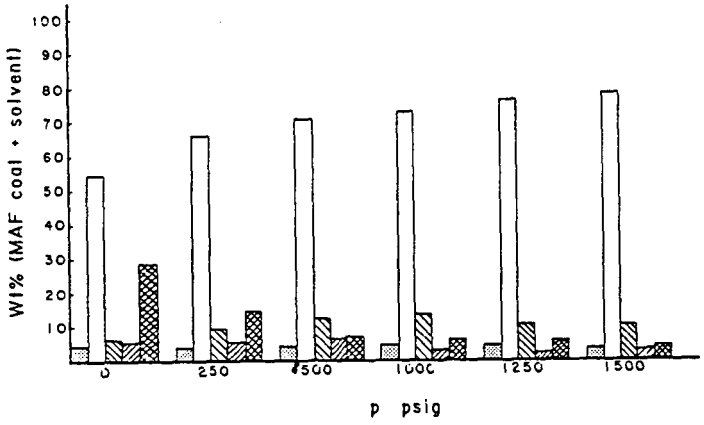

Figure 1. Effect of Initial Hydrogen Pressure on Product Distributions from Combined Processing of Illinois #6 and Maya Crude.

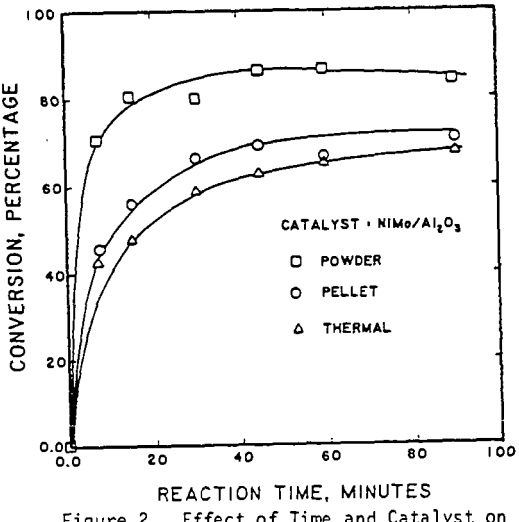

Figure 2. Effect of Time and Catalyst on Coal Conversion from Combined Processing of Illinois #6 Coal and Maya Crude.

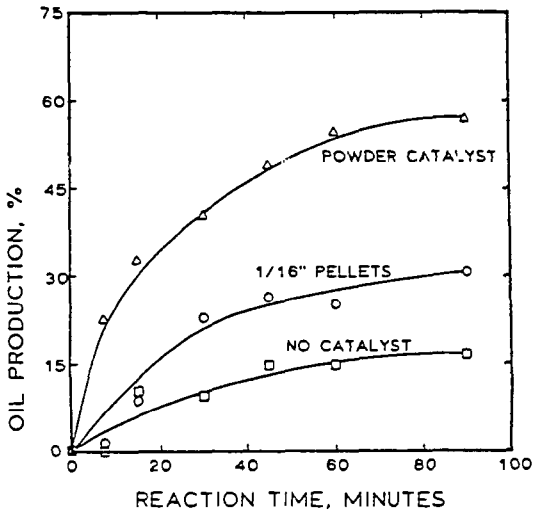

Figure 3. Effect of Time and Catalyst on Oil Production from Combined Processing of Illinois #6 Coal and Maya Crude.

PYROLYSIS MECHANISMS AND WEATHERING PHENOMENA IN ROCKY MOUNTAIN COALS

Henk L.C. Meuzelaar, William H. McClennen, Candace C. Cady, G. Steven Metcalf, Willem Windig, J. Rand Thurgood* and George R. Hill**

Biomaterials Profiling Center, University of Utah, 391 S. Chipeta Way, Suite F, Research Park, Salt Lake City, Utah 84108

*Utah Power & Light Company, Salt Lake City, Utah 84104
**Chemical Engineering Department, University of Utah, Salt Lake City, Utah 84108

INTRODUCTION

During the past decade coal scientists and technologists have become increasingly aware of the potentially dramatic effects of oxidation ("weathering") on the structure and reactivity of coals. Presently known effects range from autoignition in mines [1] and piles [2], changes in electrostatic charge, slurry pH and flotability [3] or loss of caking properties [4-7] and calorific value [3,4] to decreased tar [8,9] and volatile matter yields, increased char yields [9,10] and altered char properties [3,5,6]. An excellent overview of coal weathering effects can be found in a recent paper by Cox and Nelson [11].

Because of a lack of generally accepted and standardized procedures for determining the degree of weathering (the "weathering index") of a given coal sample, most data on structure and reactivity reported in the literature thus far were obtained on coal samples of uncertain weathering status and should therefore be interpreted with great caution.

Unfortunately, this situation is compounded by the difficulty of obtaining "non-weathered" coal samples for structure and reactivity tests since even reference samples available from coal sample banks have sometimes been found to exhibit signs of weathering. In the near future a new collection of standard coal samples, the Premium Coal Sample Program currently underway at Argonne National Laboratory under the most stringent anaerobic collection, preparation and storage conditions [12], may help solve the availability problem. In the coal weathering experiments reported here high volatile B bituminous coal samples obtained directly from freshly exposed seam facies in the Wasatch Plateau field (Hiawatha and Blind Canyon seams, Emery County, Utah) were used.

The present study was prompted by the discovery of FSI values as high as 4.0 in coals obtained directly from fresh mine cuts in the Hiawatha and Blind Canyon seams [4]. Until then, coals from these seams were generally considered to be noncaking. Since FSI values $\geq$ 2.0 could interfere with pyrolytic conversion schemes under consideration by Utah Power and Light Company [13], a systematic study of the influence of weathering on the reactivity and structure of selected Wasatch Plateau coals was undertaken.

EXPERIMENTAL

Several hundred pounds of samples were obtained from the top, middle and bottom of freshly exposed cross sections of the Hiawatha and Blind Canyon seams and immersed in water until being crushed and milled to < 60 mesh in a nitrogen atmosphere. All sample storage took place under nitrogen in hermetically closed glass bottles at -20°C in the dark. In the laboratory weathering experiments, 10-15 g aliquots of < 60 mesh coal were exposed to different temperatures and atmospheric conditions (N_2 or air; dry or H_2O saturated) for periods up to several weeks or months using a specially constructed bench scale weathering system [4].

FSI determinations were performed according to ASTM Standard D-720-67, whereas standard ASTM proximate analysis, calorific value and total sulfur determinations were carried out by Standard Laboratories (Huntington, Utah). TG/DTG analyses were performed with a Mettler I thermal analyzer under the following conditions: (initial pyrolysis run) sample weight approx. 10 mg, nitrogen flow 100 ml/min, heating rate 15°C/min, end temperature 790°C, (subsequent char combustion run; after cooling down) air flow 100 ml/min, heating rate 15°C/min, end temperature 990°C.

Curie-point pyrolysis mass spectrometry was performed with an Extranuclear 5000-1 instrument under the following conditions: sample weight 20 µg (deposited from a fine suspension in MeOH), heating rate approx. 100°C/s, end temperature 610°C, total heating time 10 s, electron energy 12 eV, mass range scanned m/z 20-260, total number of spectra summed 150, total scanning time 30 s. Computerized data analysis involved normalization of signal intensities by means of the NORMA program [14] followed by factor analysis, discriminant analysis and canonical variate analysis using the SPSS program package [15].

RESULTS AND DISCUSSION

The FSI was found to be a highly sensitive indicator of the weathering status of these coals with a slight, but measurable drop in FSI value occurring overnight upon exposure of fresh coals to air at room temperature. Typical FSI weathering profiles are shown in Figure 1. Since coal weathering is often accompanied by complex weight changes due to the interplay of fluctuations in moisture content and oxidative phenomena, a series of weathering experiments was carried out while carefully monitoring changes in sample weight, as shown in Figure 2. Weight corrected weathering trends of several conventional parameters are illustrated in Figure 3a and Table I showing how misleading results are obtained if the original weight of the non-weathered sample is unknown (as is usually the case). Note that the weight corrected change in calorific value is -1.1% after 96 hours at 80°C in air and -2.1% at 100°C in air.

Much more informative about changes in reactivity and structure are the Thermogravimetry (TG) and Derivative Thermogravimetry (DTG) data in Figures 4 and 5 and, in particular, the Pyrolysis Mass Spectrometry (Py-MS) data in Figures 6, 7, 8 and 9. The TG/DTG pyrolysis data in Figures 4a and 5a would seem to support a weathering mechanism dominated by the formation of crosslinks between coal molecules, thereby causing a widening of the temperature range of the pyrolysis process and a decrease in the maximum pyrolysis rate accompanied by increased char yields while having little or no influence the maximum rate temperature (~450°C). The results of the char combustion runs in Figures 4b and 5b indicate a similar kinetic trend (decreased reaction rate and increased temperature range) but are less definitive due to a lower level of reproducibility than in the pyrolysis runs.

Inspection of the pyrolysis mass spectra in Figure 6 shows the structural effects of weathering to be dominated by a decreased yield of phenolic and naphthalenic moieties and a relative increase in the yield of aliphatic carboxylic and carbonylic moieties, as further illustrated by the scatter plots of selected peak intensities in Figure 7. These findings are in excellent agreement with current views on chemical effects of coal weathering, according to which the process is characterized by the formation of ether bridges between aromatic nuclei with concurrent reduction in free phenolic hydroxyl groups [16], and by the oxidation of aliphatic moieties to carbonylic and carboxylic functional groups [17]. A more detailed picture of the complex changes in the pyrolysis mass spectra can be obtained by means of multivariate analysis techniques such as discriminant analysis, as illustrated in Figure 8. The application of these techniques to the evaluation of pyrolysis mass spectra of coal has been described elsewhere [14,18,19]. The discriminant analysis results in Figure 8 show that: (a) the first discriminant function exhibits no detectable changes in the coal spectra upon "weathering" at 80°C in a nitrogen atmosphere, (b)

weathering effects at 80°C and 100°C in air show strong quantitative differences, (c) several other series of aromatic, hydroaromatic and hydroxyaromatic compounds appear to decrease besides phenols and naphthalenes, and (d) the changes in aliphatic moieties are much more complex than the simple formation of carbonylic and carboxylic groups. Examination of the second discriminant function (not shown) confirmed the absence of detectable changes at 80°C in N_2 but revealed the presence of slight but significant qualitative differences between the 80°C and 100°C weathering trends, apparently reflecting transient chemical phenomena (peroxide formation?) during the weathering process.

Although, at first sight, the "classical" coal weathering concept of crosslinking through ether bridge formation between macromolecular chains appears to fit our observations quite well, modern views of vitrinite as a binary system consisting of a "mobile" phase and a macromolecular "network" phase necessitate a rethinking of the crosslinking concept. The binary phase model, recently summarized by Given [20], assumes that up to 50% or so of the bulk of the coal sample consists of relatively small, mobile molecules trapped in cages formed by a macromolecular network which makes up the remainder of the bulk. Direct evidence for the presence of a trapped mobile phase can be obtained by Time-resolved Py-MS, as shown in Figure 9. Approximately 50% of the C_2-alkylnaphthalene signal in Figure 9 is recorded well below typical pyrolysis temperatures for covalent bonds but far above the expected vacuum distillation point for these compounds. A crude attempt to visualize the proposed binary phase system is presented in Figure 10, demonstrating that, in principle, three possibilities for intermolecular bond formation exist in such a system: (1) "crosslinking" between network chains, (2) "condensation" between mobile phase constituents, and (3) "grafting" of mobile phase constituents onto the network chains.

To obtain a better insight into the behavior of the two phases, fresh and artificially weathered (212 hrs at 100°C in air) Hiawatha coal samples were submitted to vacuum distillation (30 hrs at 180°C and 10^{-3} Torr), pyridine extraction (24 hrs in Soxhlet extractor), short contact time (SCT) pyrolysis in a tubing bomb reactor (2.5 g coal in 5.0 g benzene, heating rate 20°C/s, end temperature 420°C, total heating time 40 s, H_2 pressure 1,000 psi initial to 1,700 psi final) and direct Curie-point Py-MS (1.5×10^{-5} g coal in vacuo, heating rate 100°C/s, end temperature 610°C, total heating time 10 s). Subsequently, the distillates, extracts or pyrolyzates, as well as the residues were analyzed by Py-MS. Preliminary results are shown in Table II and illustrate the dramatic effect of weathering on vacuum distillation yields, pyridine extraction yields and SCT tubing bomb reactor (TBR) pyrolysis yields. The yield of the small vacuum distillate fraction (4%, dominated by alkylnaphthalenes; see Figure 11a), shows a fourfold decrease upon weathering. The much larger pyridine-extractable fraction (22%, also dominated by alkylnaphthalenes but containing significant contributions from other aromatic moieties; see Figure 11b) decreases by a factor of five to six after weathering.

Hydroxyaromatics (e.g., phenols, dihydroxybenzenes), which are among the most abundant homologous ion series in pyrolysis mass spectra of fresh whole coals (see Figure 11d) are nearly absent in the vacuum distillate (Figure 11a) and relatively low in the pyridine extract (Figure 11b) but make a more prominent appearance among the SCT-TBR products shown in Figure 11c. Probably these hydroxyaromatics are partially produced through pyrolytic bond scissions and thus may represent the network phase. Additional support for this contention is provided by the much smaller reduction factor (2X) for the SCT-TBR yields from weathered coal.

A speculative interpretation of these findings might envisage a mobile phase representing 20-30% of the bulk of the fresh Hiawatha coal and undergoing a 4-6 fold reduction under the above weathering conditions. Presumably, this reduction is due to the formation of strong (diarylether?) bonds with hydroxyaromatic moieties in the network phase ("grafting"; see Figure 10). On this view, SCT pyrolysis results in

partial degradation of the network into hydroxyaromatic compounds and other small, mobile molecules. However, the pyrolysis conditions used appear to leave most of the new bonds formed in the weathering process intact, thus resulting in a marked decrease in overall pyrolysis yields from weathered coals.

Visual comparison of the four MS patterns in Figure 11 reveals an obvious trend towards increasing complexity from the vacuum distillate (Figure 11a) to the Curie-point pyrolyzate (Figure 11d). For the first three fractions this trend corresponds directly with increasing yields (from 4% for the vacuum distillate to 38% for the TBR pyrolyzate) and, if extrapolated, would indicate a yield of between 40-50% for the Curie-point pyrolyzate, which is in good agreement with previous estimates for hvb Utah coals [18].

At the same time, these observations highlight the fact that under SCT pyrolysis conditions some 50% of the (m.a.f.) coal forms a char. This char, which is difficult to analyze by most techniques currently available, might incorporate as much as 2/3 of the network phase. This leads to the question whether the pyrolysis products obtained from the network phase are representative for the overall chemical structure of the network. In his comprehensive discussion of the binary phase nature of coal, Given [20] concludes that in spite of all available data from sophisticated analytical methods, including FTIR and 13C NMR, the chemical nature of the network phase remains pretty much a mystery.

If the binary phase concept is valid indeed, much effort will have to be devoted to the elucidation of key structural features of the macromolecular network if a more comprehensive picture of the effects of weathering on the structure and reactivity of coals is to be obtained within the foreseeable future.

REFERENCES

1. Saranchuk, V.I., Khimiya Tverdogo Topliva, Solid Fuel Chemistry, 11, 63 (1977).
2. Bouwman, R. and Freriks, I.L.C., Fuel, 59, 315 (1980).
3. Gray, R.J., Rhoades, A.H. and King, D.T., AIME, Transactions, 260, 334 (1976).
4. Hill, G.R., Meuzelaar, H.L.C., "Free Swelling Index of Utah High Volatile Bituminous Coals", Report to UP&L Co., contract R&D 1003-83, Sept. 1982-Aug. 1983.
5. Crelling, J.C., Schrader, R.H. and Benedict, L.G., Fuel, 58, 542 (1979).
6. Habermehl, D., Orywal, F. and Byer, H.-D., "Chemistry of Coal Utilization, 2nd Supp. Vol., M.A. Elliot, Ed., Wiley-Interscience, New York, 1981.
7. Wachowska, H.M., Nandi, B.N. and Montgomery, D.S., Fuel, 53, 212 (1974).
8. Wachowska, H., Pawlak, W., Fuel, 56, 422 (1977).
9. Furmisky, E., MacPhee, J.A., Vancia, L., Ciavaglia, L.A., Nandi, B.N., Fuel, 62, 295 (1983).
10. Gromicko, F.N., Sarott, L., Gasior, S., Strakey, J., ACS, Div. Fuel Chem. Preprints, 23, 121 (1978).
11. Cox, J.L. and Nelson, C.R., ACS, Div. Fuel Chem. Preprints, 29, 102 (1984).
12. Premium Coal Sample Program Information obtained by Dr. K. Vorres, Argonne.
13. Thurgood, J.R., Presented Synfuels 3rd Worldwide Symp. Wash. D.C., Nov. 1983.
14. Harper, A.M., Meuzelaar, H.L.C., Metcalf, G.S., Pope. D.L., in "Analytical Pyrolysis Techniques & Applications", K.J. Voorhees, ed., Butterworth, in press.
15. Nie, N.H., Hull, C.H., Jenkins, J.G., Steinbrenner, K. & Bent, D.H. (eds.) Statistical Package for the Social Sciences (SPSS), McGraw Hill, NY, 1975.
16. R.C. Neavel, in "Coal Science", Gorbaty, Larsen, & Wender (eds) Academic Press, 1982.
17. Painter, P.C., Snyder, R.W., Pearson, D.R. and Kwong, J., Fuel, 59, 282 (1980).
18. Meuzelaar, H.L.C., Harper, A.M., Hill, G.H., Fuel, in press (1984).
19. Schenck, P.A., de Leeuw, J.W., Viets, T.C., Haverkamp, J., in Petroleum Geochemistry and Exploration of Europe, Brooks, J. (ed.), Blackwell, 267.
20. Given, P.H., in "Coal Science", M. Gorbaty, Larsen, J.L., Wender, I., Academic Press, NY 1984 (in press).

CREDIT

The work reported here was sponsored by research contracts from Utah Power and Light Company and the U.S. Department of Energy (contract #DE FG22-82-PC50970).

TABLE I

EFFECT OF WEATHERING ON CALORIFIC VALUE

Calorific Value (BTU)	Fresh	80°C in N_2 120 hours	Δ* (%)	80°C in air 96 hours	Δ* (%)	100°C in air 96 hours	Δ* (%)
- as received	12028	12556	+4.4	12299	+2.3	12063	+0.3
- dry	12457	12575	+0.9	12318	-1.1	12078	-3.0
- weight corrected	12028	12003	-0.2	11893	-1.1	11773	-2.1

* difference with corresponding "fresh" value.

TABLE II

WEATHERING EFFECTS ON HIAWATHA COAL PROCESS YIELDS

Process	% Yield	
	Fresh Coal	Weathered Coal
Vacuum Distillation	4	1*
Pyridine Extraction	22	4
SCT-TBR Pyrolysis	38	17

* Value from a single experiment; all other values averaged from two or more experiments.

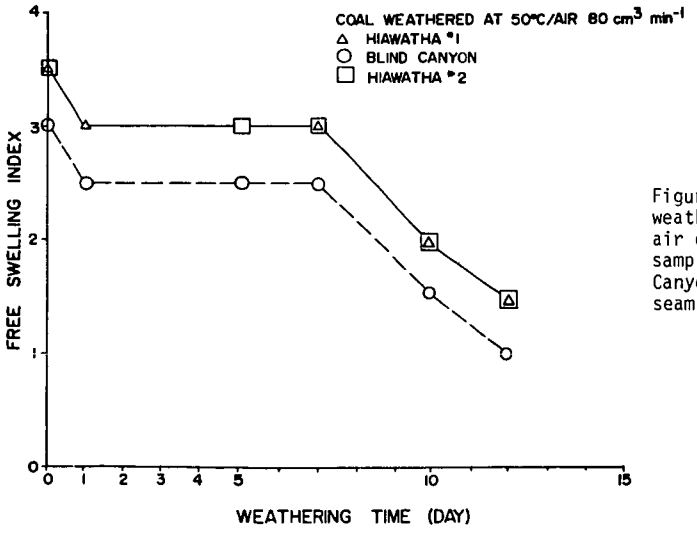

Figure 1. Effect of weathering at 50°C in air on FSI of coal samples from one Blind Canyon and two Hiawatha seam mines.

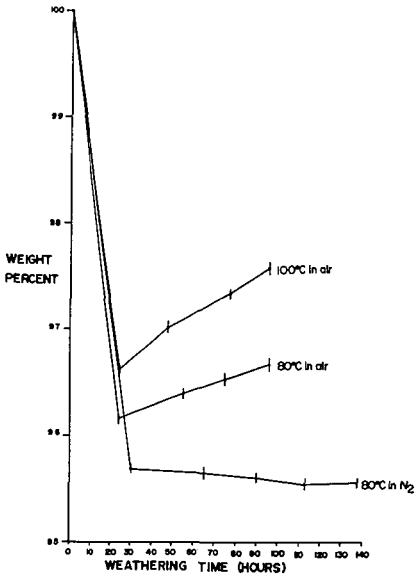

Figure 2. Effect of weathering on weight of Hiawatha seam coal. Note usefulness of control samples in N_2 for distinguishing effects of moisture loss (~4.4%) from effects of oxidative weight gain. Error bars represent range of values for three independently weathered aliquots.

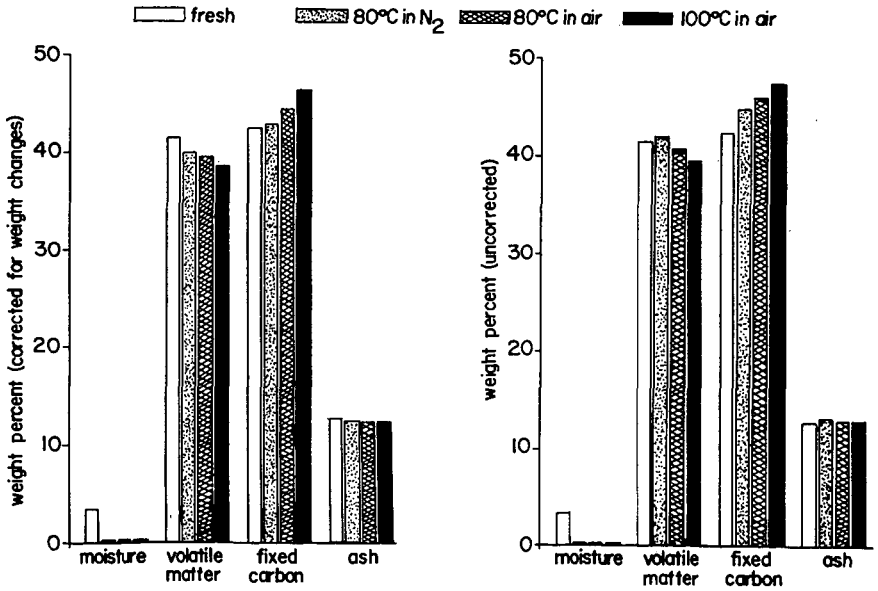

Figure 3. Effect of weathering on proximate analysis of Hiawatha coal.

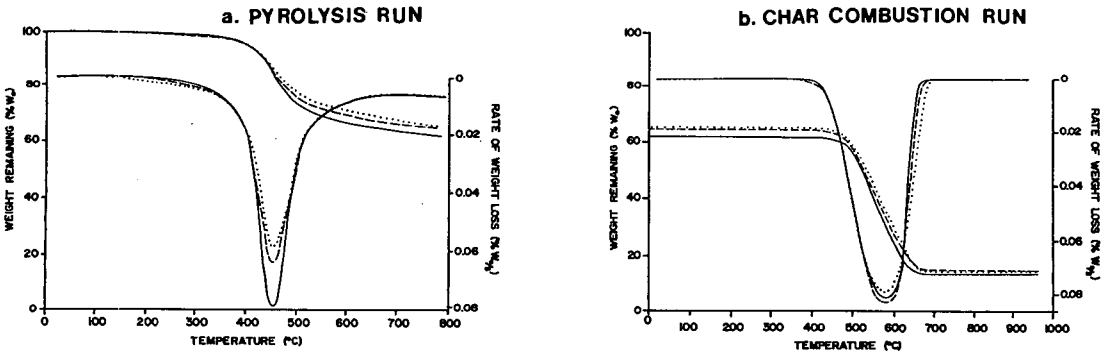

Figure 4a and b. Effects of weathering on TG/DTG profiles of Hiawatha coal. Each curve averaged from three replicate runs. W_o=original sample weight. —— fresh coal; ---- weathered at 80°C in air (96 hours); .... weathered at 100°C in air (96 hours).

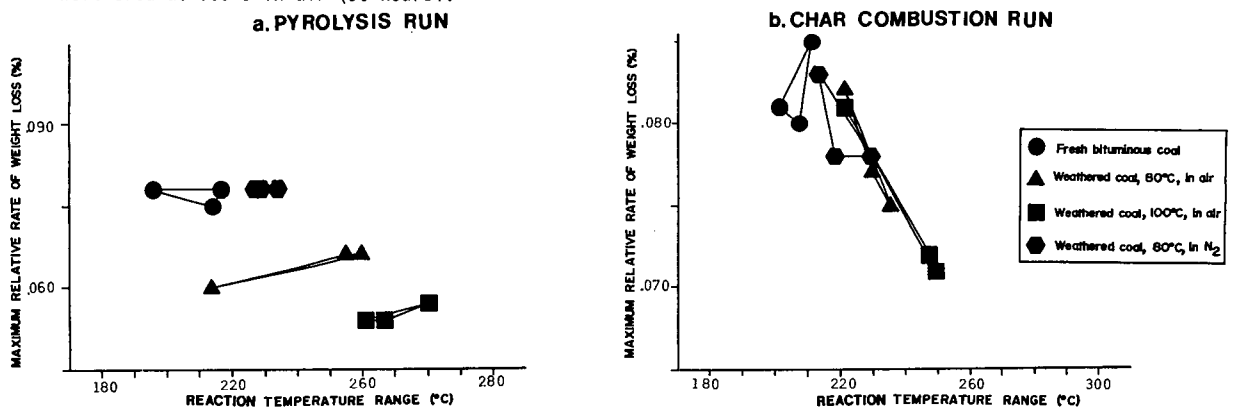

Figure 5a and b. Effects of weathering on selected TG/DTG parameters. The "Reaction Temperature Range" is defined as the temperature range over which the (pyrolysis or combustion) reaction rate is $\geq$3% of the maximum rate (compare with Figure 4). Data points on replicate weathering experiments connected by solid lines.

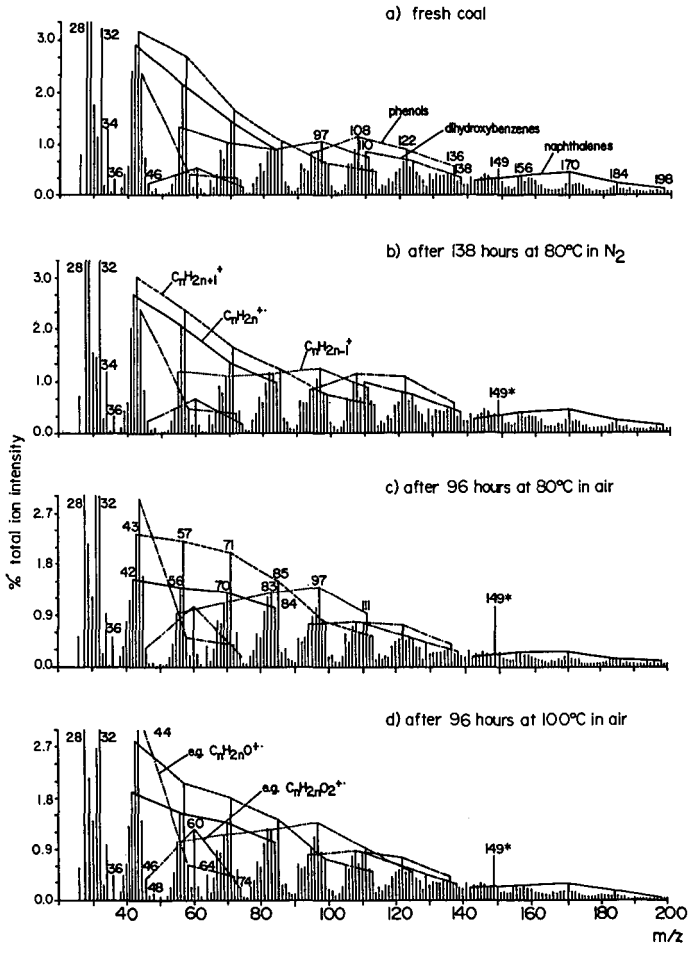

Figure 6. Curie-point pyrolysis mass spectra of fresh and weathered Hiawatha coal samples. Note high degree of similarity between spectra a) (fresh coal) and b) (80°C in N_2) and obvious changes in spectra c) (80°C in air) and d)(100°C in air). Overall weathering effects appear to be: decreased aromatic series; increased carbonylic ($C_nH_{2n}O$) and carboxylic ($C_nH_{2n}O_2$) series; decreased H_2S peak (m/z 34); increased CO_2 (m/z 44) and SO_2 (m/z 64) peaks; increased MeOH solvent retention (m/z 23); altered distribution of aliphatic hydrocarbon series. The phthalate fragment ion peak at m/z 149 may be due to contamination.

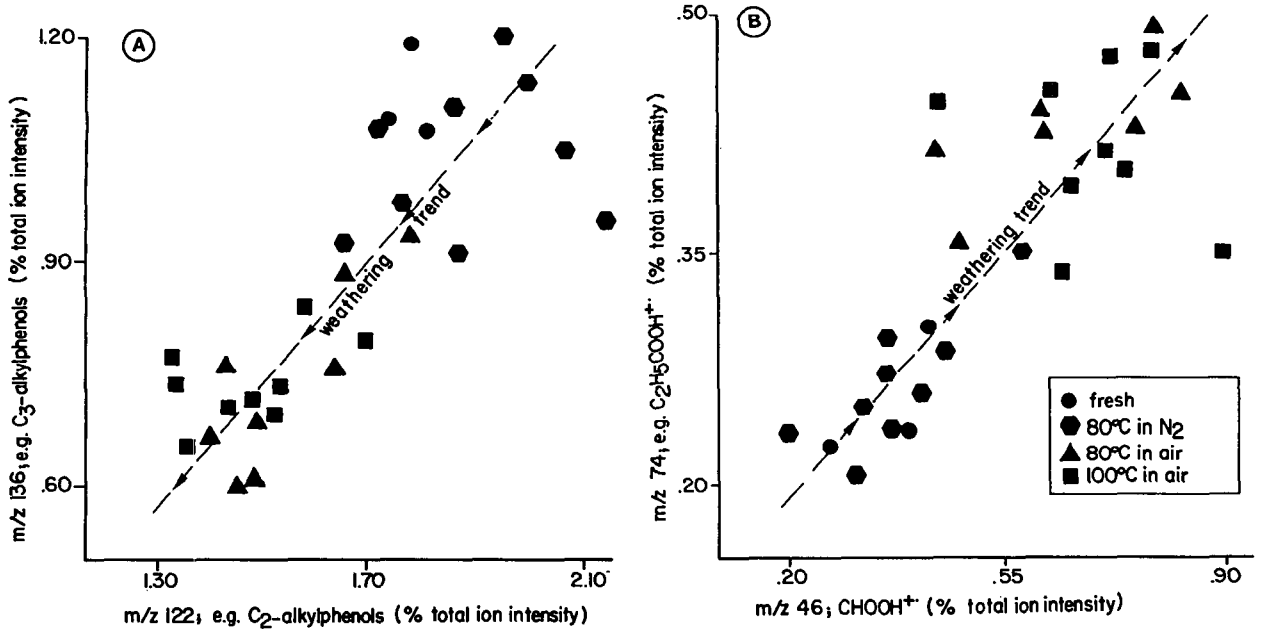

Figure 7 a and b. Scatter plots of selected ion intensities from the pyrolysis MS data set (compare with Figure 6) showing the effects of weathering on alkylphenol signals (strong decrease; see Figure 7a) and on short chain carboxylic acid signals (marked increase, see Figure 7b).

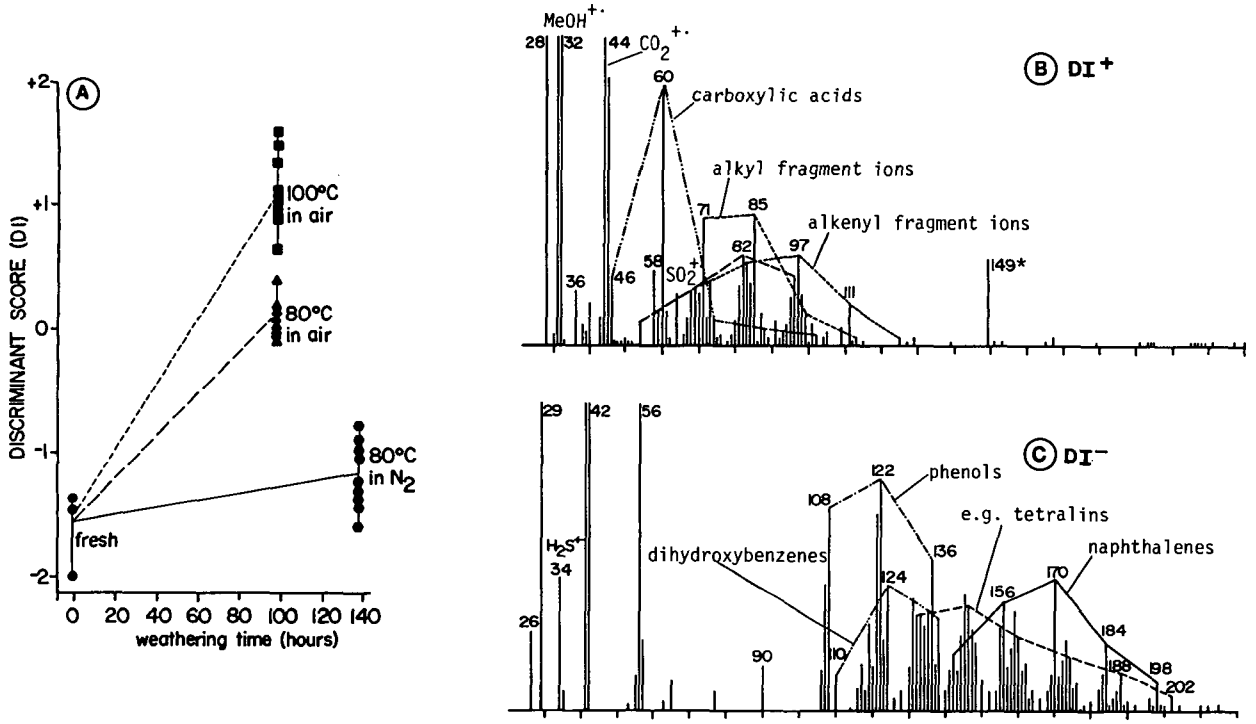

Figure 8. Discriminant score plot and associated "discriminant spectra" obtained on pyrolysis mass spectra of fresh and weathered Hiawatha coal samples (see Figure 6). Air and N_2 exposures were carried out with three different aliquots analyzed in triplicate, resulting in 27 spectra representing 3 categories (80°C in N_2, 80°C in air, 100°C in air). The triplicate spectra of the fresh coal sample were treated as "unknowns" in the discriminant analysis procedure. The two spectra correspond to the positive (DI^+) and negative (DI^-) components of the discriminant function.

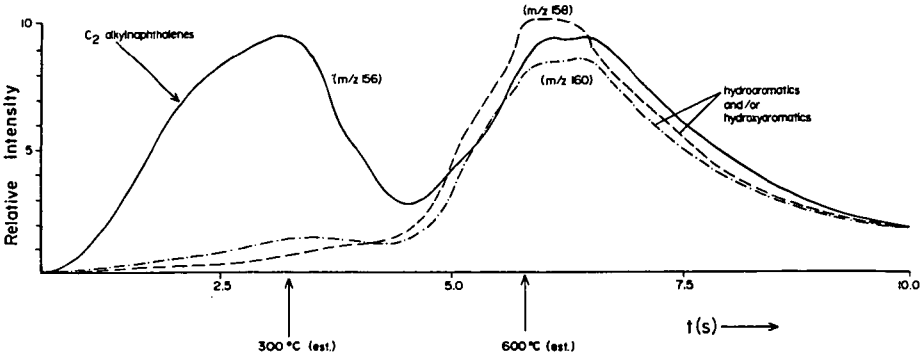

Figure 9. Time-resolved recording of the mass peaks at m/z 156 (mainly C_2-alkylnaphthalenes), m/z 158 (e.g., methylnapthol and/or C_2-alkyl dihydronaphthalenes) and m/z 160 (e.g., C_2-alkyl tetralins) during Curie-point pyrolysis of a 20 µg sample from a hvb Wasatch Plateau coal. Note bimodal character of the signal at m/z 156.

Figure 10. Highly schematized representation of all three possible types of weathering-induced bridge formations in a binary phase (mobile phase/network phase) coal model.

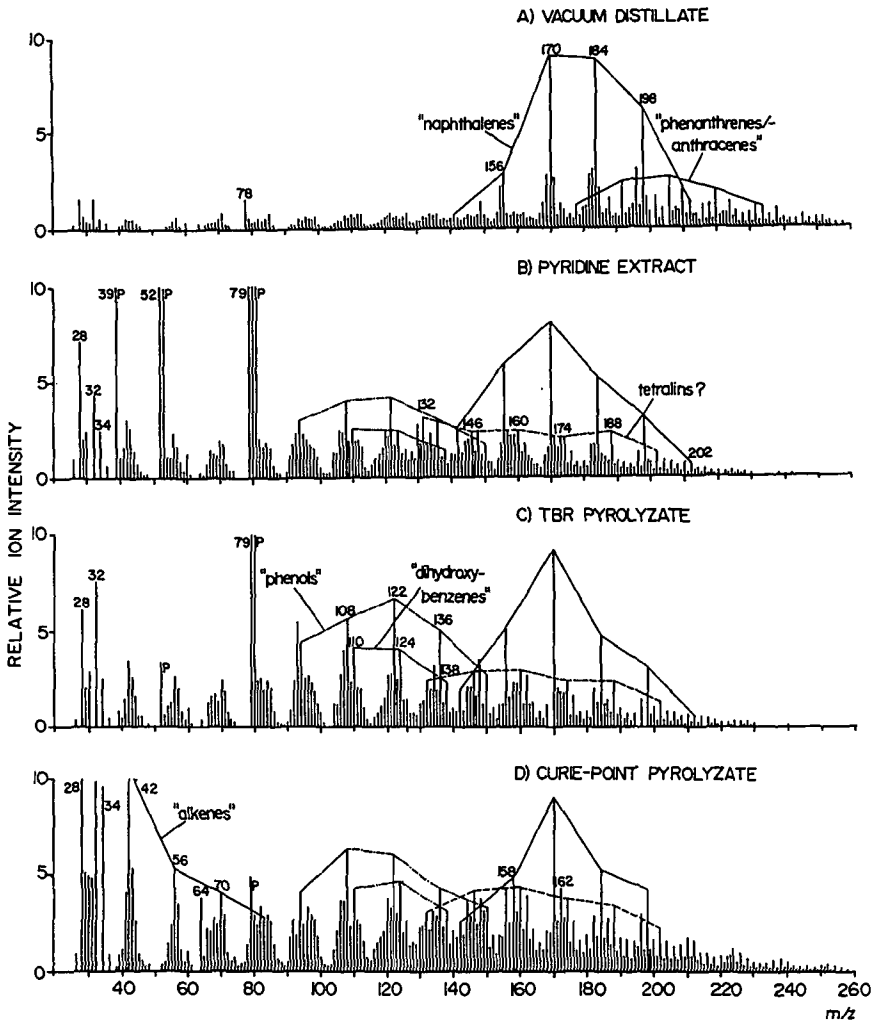

Figure 11. Curie-point desorption/pyrolysis mass spectra of tar fractions from a nonweathered ("fresh") Hiawatha coal obtained by different techniques. Compare with Table I. Note increasing complexity from a to d (exaggerated in d by the presence of gaseous, low molecular weight products, e.g., alkenes, lost during collection of a-c). Peaks labeled "P" represent pyridine residues and/or background signals.

THE ACTIVITY OF $Cu-ZnO-Al_2O_3$ METHANOL SYNTHESIS CATALYSTS

G C Chinchen, P J Denny, D G Parker, G D Short,
M S Spencer, K C Waugh‡ and D A Whan

Imperial Chemical Industries PLC, Agricultural Division,
PO Box No 1, Billingham. Cleveland, England

‡ ICI New Science Group, Runcorn Heath, Runcorn,
Cheshire, England

Methanol is made (1) with greater than 99% selectivity when a high pressure gas mixture of CO, CO_2 and H_2 is passed over a catalyst containing Cu, ZnO and Al_2O_3 at between 220°C and 300°C. Other than that the reaction is exothermic there seem to be few further facts about which complete agreement exists (2, 3). With increasing emphasis being placed worldwide on methanol synthesis processes because of the possible role which methanol may play in the future either as a feedstock or a fuel, there is now a considerable interest in the chemistry of the synthesis reaction. We have sought for many years to gain an understanding of the mechanism of methanol synthesis on $Cu-ZnO-Al_2O_3$ catalysts for the purely pragmatic reason that we hope thereby to discover ways of improving, still further, the already impressive performance characteristics of these catalysts.

Our approach has been to apply a wide range of techniques, particular emphasis being placed, where possible, on the use of practical catalysts under industrial working conditions, with the aim of answering the following questions:

(i) Is methanol synthesised from CO or CO_2?

(ii) What is the state of the copper in a working catalyst?

(iii) What roles are played by the ZnO and Al_2O_3 components in the commercial catalyst?

(iv) What is the mechanism and which reaction step is rate determining?

(v) What are the active sites for methanol synthesis on a $Cu/ZnO/Al_2O_3$ catalyst?

MEASUREMENT OF CATALYST ACTIVITY

Activity is determined under standard conditions of 250°C, 50 atms, SV 40,000 hrs^{-1}, gas composition 10% CO, 3% CO_2, 67% H_2, 20% N_2 in standardised pseudoisothermal reactors operating from a single large gas battery with a common purification system. Each catalyst sample is reduced under standard conditions (5% H_2 in N_2 at 1 atm for 15 hrs) and exposed to reaction gas for pre-set periods of time. To a first approximation, activity is proportional to methanol concentration in the outlet gases - an assumption reasonably defensible provided catalyst activity does not vary too widely between samples, and as long as equilibrium is not closely approached. The reproducibility of activity measurements is shown by the exit concentration of methanol (measured to 99% confidence limits) from 23 replicate runs with a standard industrial catalyst. An arbitrary activity of unity was assigned to this catalyst.

THE ROLE OF CARBON DIOXIDE

In 1975 Kagan et al[4] reported work with labelled carbon oxides which showed that methanol synthesis proceeds through carbon dioxide rather than carbon monoxide eg

$$CO + H_2O \rightarrow CO_2 + H_2 \rightarrow CH_3OH + H_2O \qquad (1)$$

This work has been repeated and confirmed by us. With $^{14}CO_2$ as a component, gas containing equal moles of CO and CO_2 has been reacted over the standard $Cu\text{-}ZnO\text{-}Al_2O_3$ catalyst under the standard conditions as described above. Space velocity was varied between 10,000 and 240,000 hrs^{-1} and the exit gases analysed for the separated components and their corresponding radioactivities measured. Results are shown in Figure 1 and reveal clearly that synthesis proceeds via carbon dioxide. 'Scrambling' of radioactivity via the shift reaction:

$$^{14}CO_2 + H_2 \rightleftharpoons {}^{14}CO + H_2O \qquad (2)$$

is negligible at high space velocities and indicates that under methanol synthesis conditions the reverse water gas shift reaction (ie left to right above) is slower than the methanol synthesis reaction. This coupled with the fact that methanol radioactivity is always higher than that of the CO_2 suggests there may be no intermediate common to the water gas shift and synthesis reaction.

THE STATE OF COPPER IN A WORKING CATALYST

Accurate measurement of the copper surface area of reduced Cu-ZnO-Al_2O_3 catalysts by the use of the reaction between nitrous oxide and surface copper atoms is now routine and reproducible.

The method has been described by previous authors (5, 6) and in its most convenient form the evolution of nitrogen following a pulse of nitrous oxide is measured. With this technique a number of Cu-ZnO-Al_2O_3 catalysts of different synthesis activity and covering a range of copper particle sizes has been examined. The results shown in Figure 2 illustrate a linear dependence of synthesis activity on total copper surface area.

In this work we have adhered to the standard reduction procedure because the resulting surface is representative of the initial state of the real catalyst surface in industrial use. Reduction, however with either CO or pure H_2 results in a 25% increase in copper surface area showing that some copper still remains oxidised after standard reduction treatment.

The available metal surface area associated with a working catalyst surface can be measured in a variation of the technique by sweeping the working system clean with inert gas and then switching in a pulse of nitrous oxide. The efficacy of this treatment can be measured by fully re-reducing the oxidised surface and redetermining the total surface area to ensure that no irreversible surface changes have occurred. Results shown in Table 1 reveal that about 30% of the initial copper surface of a typical industrial catalyst is unavailable for reaction with nitrous oxide under working conditions, ie is probably oxidised. The proportion of oxidised sites on the working surface will almost certainly be a function of the ratios of carbon dioxide to carbon monoxide and of steam to hydrogen as well as temperature. The catalyst surface is therefore in a dynamic state and it may be anticipated that the nature of the surface will vary in a fixed bed reactor from top to bottom, being a function of the ambient gas composition. This emphasises the uncertainties inherent in extrapolating from experimental results obtained under conditions differing significantly from those used practically.

The oxidised surface of the copper crystallites probably consist partly of $O_{(ads)}$ and $OH_{(ads)}$. The interchange of these species via hydrogen and water is well established (7-9) and likely to occur under methanol synthesis conditions.

THE ROLE OF SUPPORT OXIDES

The establishment of a correlation between copper surface area and methanol synthesis activity does not rule out a role for the supporting oxides in the detailed mechanism of synthesis. For example, some essential, but not rate-determining, steps in the reaction mechanism may occur on the support. Alternatively, if the surface/adsorbate complex involved in the rate determining step were a copper species, the presence of which was determined by juxtaposition with zinc oxide (zinc-copper contiguity) then the copper surface area correlation given above would still be obtained.

However, certain possible roles can be ruled out, for example, rate determining adsorption of any species onto a zinc or aluminium site.

One way in which evidence can be brought to bear on the role of zinc or aluminium oxides is to prepare high area catalysts in which one or the other oxide is omitted and to measure the activity/unit copper area compared with a standard copper-zinc-alumina catalyst. This has been done for a series of binary compositions containing copper allied respectively with the oxides of aluminium, manganese and magnesium. Results are shown in Figure 3 and compared with the standard $Cu-ZnO-Al_2O_3$ correlation. To a first approximation they reveal, surprisingly, no unique role for either zinc oxide or alumina in determining methanol synthesis activity. The copper surface areas of these catalysts under synthesis conditions are given in Table 1. As with the $Cu-ZnO-Al_2O_3$ catalysts, re-reduction gave an increase in copper area in all but one sample, but the proportion of copper surface covered by oxide was always much smaller. The high level of surface oxidation in copper/zinc catalysts may be a consequence of surface brass formation.

The area measurements therefore strongly suggest that only copper metal/copper oxide and probably only the copper metal surface is implicated in the rate determining step of synthesis and any oxide with appropriate basicity is substantially equally effective in promoting copper surface area and corresponding synthesis activity. Considerations of catalyst stability are, of course, not pertinent at this point.

MECHANISM OF METHANOL SYNTHESIS

The combination of temperature programmed desorption (TPD) and temperature programmed reaction spectroscopy (TPRS) has been used to examine the mechanism via adsorption, desorption and decomposition of reaction intermediates. These techniques have shown that on $Cu/ZnO/Al_2O_3$ catalysts, the observed intermediate on the surface of the Cu and ZnO components of the catalyst is the formate species. Methanol adsorption (Figure 4) at room temperature on to a catalyst in which the surface copper is about 25% oxidised (see above) was characterised by two main peaks in the desorption spectrum: (i) by the coincident desorption of H_2 and CO_2 at a peak maximum temperature of 440K - a fingerprint of the existence of a formate species adsorbed on the copper component (10) and (ii) by the coincident desorption of H_2 and CO at 580K - characteristic of a formate species adsorbed on zinc oxide (11, 12).

The same two formate species are observed after the adsorption of formaldehyde on this partially oxidised catalyst, in addition to which methanol itself is desorbed at 360 K. This latter is characteristic of desorption of methanol from copper 110 (13), suggesting that it has in fact been formed on the copper component of the catalyst in preference to the zinc oxide component.

A pointer to the rate determining step on the copper component of the catalyst and an indication of the role of the support in the mechanism is to be found in microreactor experiments (1 at) on a Cu/Al_2O_3 catalyst. Following CH_3OH synthesis, TPRS showed that the formate species existed on the surface of the copper under steady state methanol synthesis conditions (CO_2/H_2 feed, 220°C); the same formate species was observed after dosing the catalyst continuously with the same feed (CO_2/H_2), but at 100°C, when no detectable reaction occurred, ie neither methanol synthesis nor reverse shift. The rate determining step in the conversion of CO_2 and H_2 to methanol on the copper component of the catalyst occurs therefore after formation of the surface formate species - probably the hydrogenolysis of the adsorbed formate. TPD experiments on the Cu/Al_2O_3 catalyst and on Al_2O_3 alone showed the CO_2 to be adsorbed on the alumina itself, suggesting that a role of the basic support (both Al_2O_3 and ZnO) is the adsorption of the CO_2. This could then react at the support/copper interface with hydrogen atoms adsorbed on the copper, forming a formate species on the copper surface, the rate determining step probably being the hydrogenolysis of this adsorbed formate.

Alternatively, at working pressures (50-100 at), CO_2 may adsorb on the partially-oxidised copper surface and then react in the same way. Such adsorption of CO_2 has been reported by Stone and Tilley (14) for a copper surface, partially oxidised by molecular oxygen. It is clear from these results and those described above, that the adsorption of CO_2 is not rate determining.

The nature of the adsorbed CO_2 has been suggested in ab initio, self consistent field molecular orbital calculations (15) which showed that unlike other possible molecular interactions no energy barrier existed for the reaction of hydrogen atoms with CO_2^-.

The overall methanol synthesis mechanism from CO_2 and hydrogen can therefore be written as:

$$CO_{2(a)}^- + H_{(a)} \rightarrow HCO_{2(a)}^- \qquad (3)$$

$$HCO_{2(a)}^- + 3H_{(a)} \rightarrow CH_3OH_{(g)} + O_{(a)}^- \qquad (4)$$

where the subscript a and g relate to adsorbed and gas phase species respectively. The negative charge on the adsorbed CO_2 and formate species may be less than unity.

The mechanism does not specify which of the three hydrogenation steps represented by reaction 4 is rate determining, but it seems likely that it is the step which involves carbon-oxygen bond breakage, ie hydrogenolysis.

However, as reaction 4 shows, each copper site at which methanol is synthesised will become oxidised as a consequence of the synthesis reaction. These oxidised sites constitute in the steady state some 30% of the total surface available initially following reduction (see Table 1), the steady state being maintained by the reactions of CO (16) and H_2 (8) with $O_{(ads)}$.

Oxidation of CO on partially oxidised copper constitutes part of the shift reaction, while TPRS shows that CO is not a product of Cu(I) formate decomposition. The shift reaction, therefore, under methanol synthesis conditions on Cu-ZnO-Al_2O_3 catalysts does not involve the formate intermediate contrary to previous suggestions (18).

Thus:

$$CO_2 + H_2 \rightleftharpoons X \rightleftharpoons CH_3OH \qquad (5)$$

$$X \not\rightleftharpoons CO + H_2O$$

The mechanism proposed resembles that found (11, 12, 19) earlier for the synthesis of methanol from CO_2 and H_2 over zinc oxide. This reaction is several orders of magnitude slower than copper-catalysed synthesis and it plays no part in the reaction over $Cu/ZnO/Al_2O_3$ catalysts.

THE ACTIVE SITE

The experimental results indicate that the active site for methanol synthesis consists of a copper(0) surface atom in close proximity to an oxide surface site. These sites are formed in the first instance by reduction with H_2, the number of such sites being determined by the H_2:H_2O and CO:CO_2 ratios. This view is very similar to that proposed by Okamoto et al (17), following their study of reduced CuO-ZnO surfaces by XPS. From work by Habraken et al (16), and Mesters et al (8), CO reacts faster than H_2 with $O_{(a)}$, but with a significant activation energy, so it is possible that the CO:CO_2 ratio is the more important.

CONCLUSIONS

Methanol synthesis over $Cu-ZnO-Al_2O_3$ catalysts occurs via carbon dioxide hydrogenation on the partially oxidised copper surface. Oxide species may play a direct part in the synthesis by promoting absorption of CO_2 at the copper-oxide interface, reacted CO_2 being replenished via the shift reaction which occurs at different sites and by a different mechanism from methanol synthesis. Overall, CO can react at any oxidic or hydroxidic copper(I) site; methanol synthesis probably occurs at copper(0)/copper(I) sites.

Table 1

Total copper area, during use and copper area following use of a standard $Cu/Zn/Al_2O_3$ catalyst and various binary copper/metal oxide catalysts [m^2 per g catalyst charged]. Standard methanol synthesis conditions.

CATALYST		Cu AREA AFTER REDUCTION	RELATIVE INITIAL ACTIVITY PER g CATALYST	Cu AREA AFTER ACTIVITY TEST	Cu AREA AFTER RE-REDUCTION
$Cu-Zn-Al_2O_3$	60:30:10	32.2	1.0	19.6	29.2
Cu-MgO	60:40	9.0	0.15	7.5	8.6
Cu-MgO	20:80	22.6	0.21	23.4	-
Cu-MgO	40:60	5.9	0.13	6.1	6.4
Cu-MgO	60:40	14.9	0.27	13.0	13.7
$Cu-Al_2O_3$	20:80	11.7	0.45	10.6	-
$Cu-Al_2O_3$	40:60	19.9	0.5	17.2	20.5
$Cu-Al_2O_3$	60:40	12.7	0.40	12.2	11.6
Cu-MnO	20:80	15.6	0.30	14.1	16.0
Cu-MnO	40:60	15.7	0.28	15.4	16.8
Cu-MnO	60:40	23.9	0.38	24.7	26.2

19 March 1984
SM/L81A14

REFERENCES

1 UK Patent 1159035 (1965).

2 H. H. Kung, Catal. Rev. Sci. Eng., 22, 235 (1980)

3 K. Klier, Adv. Catal., 31, 243 (1982)

4 A. Ya Rozovskii, G. Lim, L. B. Liberov, E. V. Slivinskii, S. M. Loktev, Yu B. Kagan and A. N. Bashkirov., Kin i Kat 18 (3), 691, (1977) Eng. Trans.

5 R. M. Dell, F. S. Stone and P. F. Tiley, Trans. Farad. Soc., 49, 195 (1953).

6 J. J. F. Scholten and J. A. Konvalinka, Trans. Farad. Soc., 65, 2465 (1969).

7 C. T. Au, J. Breza and M. W. Roberts, Chem. Phys. Lett., 66, 340 (1979)

8 C. M. A. M. Mesters, T. J. Vink, O. L. J. Gijzeman and J. W. Geus, Surface Science, 135, 428 (1983)

9 K. Bauge, D. E. Grinder, T. W. Madey and J. K. Sass, Surface Science, 136, 38 (1984)

10 D. H. S. Ving and R. J. Madix, J. Catal. , 61, 48 (1980).

11 M. Bowker, H. Houghton and K. C. Waugh, J. Chem. Soc., Faraday Trans. 1, 77, 3023 (1981).

12 M. Bowker, H. Houghton and K. C. Waugh, J. Chem. Soc. Faraday Trans. 1, 72, 2573 (1982).

REFERENCES (Cont)

13 I. E. Wachs and R. J. Madix, J. Catal., 53, 208 (1978).

14 W. E. Garner, T. J. Gray and F. S. Stone, Disc. Farad. Soc., 8, 246 (1950).

15 E. A. Colbourn and W. C. Mackrodt, Unpublished Results

16 F. H. P. M. Habraken, C. M. A. M. Mesters and C. A. Bootsma, Surface Science 97 264 (1980)

17 Y. Okamoto, K. Fukino, T. Imanaka and S. Teranishi, J. Phys. Chem., 87, 3740 (1983).

18 T. van Herwijnen and W. A. de Jong, J. Catal., 63, 83 (1980).

19 M. Bowker, J. N. K. Hyland, H. D. Vandervell and K. C. Waugh, 8th Int., Congr. Catal., Berlin (1984).

Figure 1. C^{14} activity of outlet gas components as a function of reactant space velocity

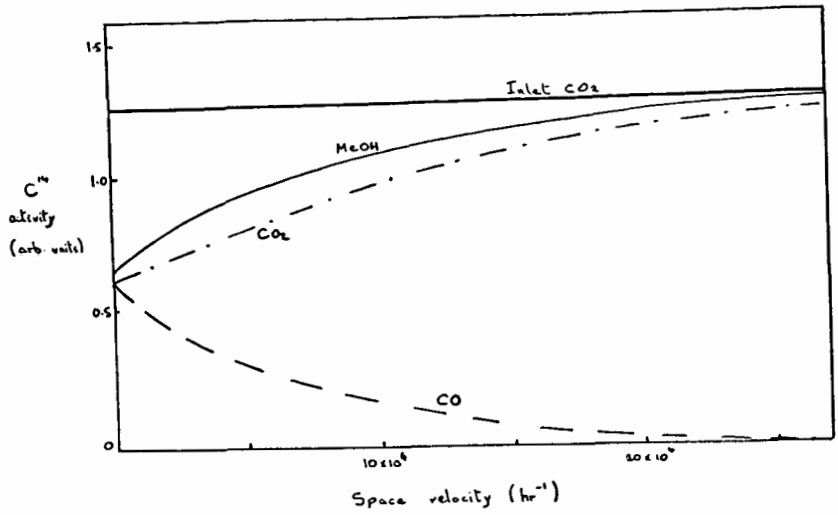

Figure 2. Linear correlation between activity and copper surface area (95% confidence limits) for $Cu-ZnO-Al_2O_3$

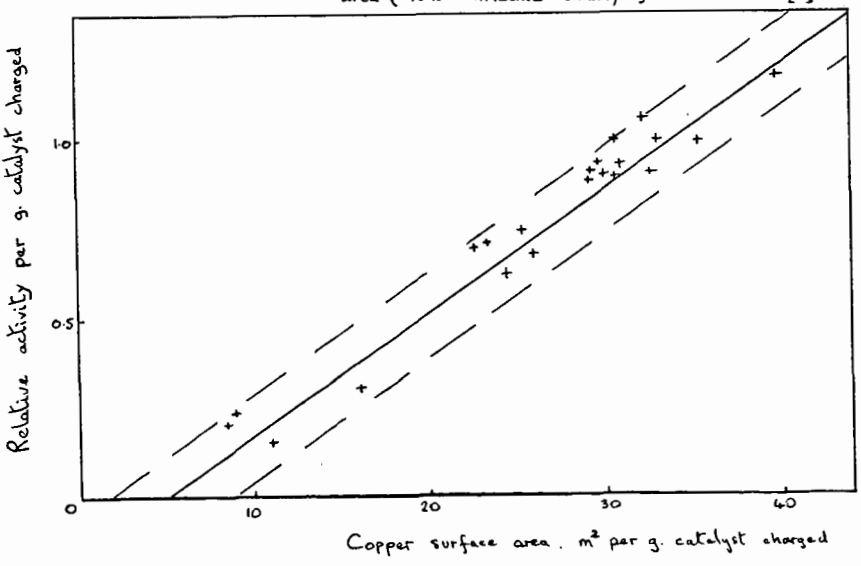

Figure 3 Initial activity of $Cu/Zn/Al_2O_3$ catalysts as a function of metallic copper surface area (solid line) compared with binary copper - metal oxide catalysts

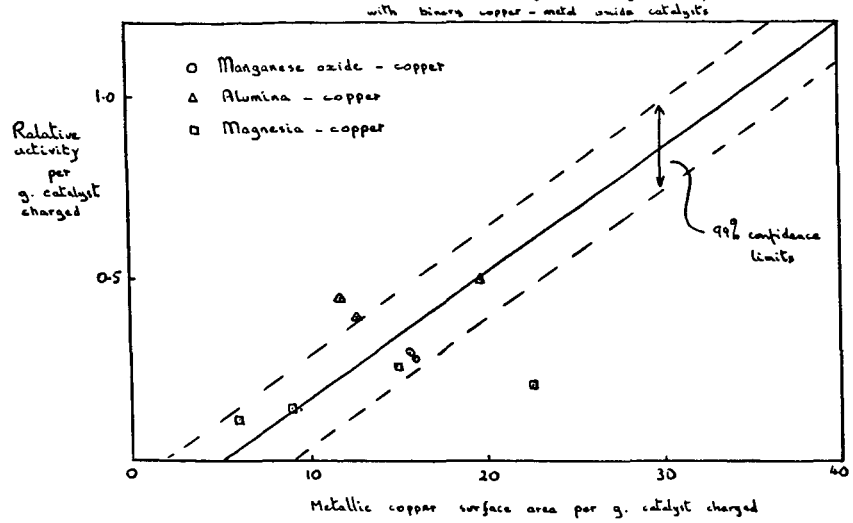

Figure 4

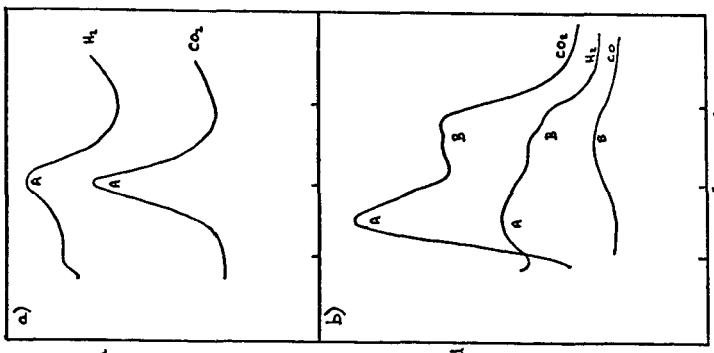

Methanol decomposition on a) unreduced and b) partially reduced $Cu-ZnO-Al_2O_3$ catalyst. Peaks A are associated with Cu(I) formate. Peaks B are associated with Zn formate.

Methanolization under pressure of carbon oxides and their mixture on Cu-ZnO-Al_2O_3 catalysts. Role of carbon dioxide.

*J. THIVOLLE-CAZAT, R. BARDET, Y. TRAMBOUZE.
Institut de Recherches sur la Catalyse
2, Av. A.Einstein 69626 VILLEURBANNE Cédex FRANCE

The hydrogenation of carbon oxides into methanol is a reaction known for a long time. Formely it was believed that methanolization of CO_2 proceeded via the intermediacy of CO (1). More recently, Bashkirov et Al.(2) have shown that reduction of CO_2 into CO and methanol could not be consecutive reactions since they both took place when contact time tended to zero; they reported as Temkin et Al.(3) that methanol formation from CO decreased dramatically if the presence of CO_2 or water was strictly eliminated from the reactive gases. Then it was concluded that methanolization of CO_2 proceeded through a direct pathway whereas that of CO involved the intermediacy of CO_2 through the water gas shift reaction. On the contrary, Klier et Al.(4) proposed that the role of CO_2 in a mixture of carbon oxides is to keep the catalyst in an oxidation state favourable to CO hydrogenation which was regarded as the main reagent leading to methanol. We report here some results which support the hypothesis of Bashkirov but do not exclude the oxidative role of CO_2.

EXPERIMENTAL

The CuO-ZnO-Al_2O_3 (65/25/10) catalyst used is an industrial one prepared by precipitation of nitrates mixture by potassium carbonate at pH 7. Its surface area is about 50 m^2/g. 5mg of this catalyst diluted in 500 mg of quartz powder are introduced in a 1/4" differential flow reactor and reduced for 12 hr at 300°C in a hydrogen stream (3l/hr; heating rate: 3°C/mn). Then the mixture of reactive gases (CO + $2H_2$, CO_2 + $3H_2$, or 23CO + 7CO_2 + 70H_2) kept in a pressurized steel container is passed through the catalytic bed (22bar, 2l/hr), depressurized downstream the reactor in a heated upstream pressure regulating valve and chromatographically analyzed on line.

Higher conversion experiments are performed in a 3/8" integral flow reactor (22bar, 2l/hr, 2,2g of catalyst); downstream the reactor, the products are partially trapped at ambient temperature and effluent gases are analyzed as above. All reactive gas mixtures are used with their residual moisture.

RESULTS AND DISCUSSION

The results obtained in the differential flow reactor (22bar, 2l/hr, 5mg of catalyst) are represented in the figure. As observed under atmospheric pressure (5), the formation of methanol under 22bar, from either CO or CO_2 shows a maximum versus temperature. The maximum obtained from CO_2 is higher and situated at a lower temperature than that from CO. Moreover the only significant by-product from CO_2 is CO, whereas hydrocarbons and higher alcohols are formed in important proportions

from CO. Thus the methanolization of CO_2 under the present conditions proves to be more active, more selective and to proceed at a lower temperature than that of CO. These results support the hypothesis of Bashkirov (2) according which CO_2 can be hydrogenated directly into methanol, without the intermediacy of CO; indeed the methanolization of CO_2 proceeds at a temperature which does not allow significant hydrogenation of CO. Thus the hydrogenation of CO and CO_2 must involve two distinct reaction pathways, the latter being more rapid. Nevertheless these results are in disagreement with those of Klier et Al. (4) who observed that hydrogenation of CO into methanol was more active and selective than that of CO_2 and concluded in the opposite way. The difference in catalyst composition and preparation may be the reason of such a divergence since Sneeden et Al. (6) observed that the ratio of methanol formation maxima from CO and CO_2 could be reversed by changing the nature of the catalyst.

Experiments were also performed in the integral reactor (22bar, 2l/hr; 2,2g of catalyst), whose results are reported in table 1.

Table 1: Conversion of carbon oxides into methanol(x%) and methanol concentrations measured(C%) or theoritical equilibrium values(Ceq) at determined temperatures.

Reagents	T °C	x%	C%	Ceq
$CO + 2H_2$	246	11,8	4,5	11
$CO_2 + 3H_2$	225	7,2	3,5	3,8
$23CO + 7CO_2 + 70H_2$	230	31,3	11,6	12

The theoritical equilibrium values of methanol concentrations were calculated from relations reported in reference 4.

It can be seen that the thermodynamic equilibrium is nearly reached in the case of CO_2 or CO, CO_2 mixture, but not with CO. These results confirm the high reactivity of CO_2 already observed in differential conditions which are governed by kinetics; in the integral reactor the CO_2 conversion is lower than that of CO because of thermodynamic limitations.

As was reported by Klier (5) and other workers (1), the CO,CO_2 mixture leads to the best results; according to the former the role of CO_2 in such a mixture is to keep the catalyst in an oxidized form Cu^I which would favour CO hydrogenation. In the light of our results we can propose a complementary explanation: taking into account its high reactivity, CO_2 may well be the main reagent leading to methanol. Each reduced CO_2 molecule leads to one of methanol and one of water; this latter can react in the presence of CO according to the water gas shift reaction which is kinetically and thermodynamically favoured under the present conditions. Thus, the equilibrium $CO_2 + 3H_2 = MeOH + H_2O$ can be displaced to the right and then the low thermodynamic limitations in the case of pure CO_2 can

be overstepped. In order to evaluate the realism of such a proposal, the influence of water content on the methanolization of CO was studied under atmospheric pressure (table 2).

Table 2: Influence of water content in CO + $2H_2$ mixture on CO hydrogenation at 220°C (1bar, 2l/hr, 175mg of catalyst).

Water content	.5ppm (a)	residual moisture	6000ppm	2%
Methanol concentration (ppm)	60	400	500	300

(a) dehydration of gas is performed by trapping in acetone-dry ice bath.

It must be pointed out that for each water content, CO_2 is obtained almost quantitatively from reaction of water and CO. Thus no kinetic limitation can restrict the conversion of CO into CO_2 during the hydrogenation of CO,CO_2 mixtures.

The results in table 2 show that methanolization rate of CO is very low in the absence of water; but traces of water are sufficient to reactivate the process; in this case the intermediacy of CO_2 is unlikely because of its low partial pressure. Higher water contents inhibit methanol formation probably for kinetic reasons.

These results support the mechanism already proposed by Sneeden et Al.(6), that is CO can be activated in two different ways:

- intermediacy of formyl $M\text{-}H + CO \longrightarrow M\text{-}CHO \xrightarrow{2H_2} MeOH + M\text{-}H$ 1)

This process may occur mainly in the absence of water and proves to be very slow; it may also lead to C-C bond formation.

- intermediacy of formate $M\text{-}OH + CO \longrightarrow M\text{-}OCHO \xrightarrow{2H_2} MeOH + M\text{-}OH$ 2)

The same formate intermediate shown by Deluzarche et Al.(7) by chemical trapping can be formed from CO_2:

$$M\text{-}H + CO_2 \longrightarrow M\text{-}OCHO \xrightarrow{2H_2} MeOH + M\text{-}OH \qquad 3)$$

The processes 2 and 3 prove to be rapid according to our results. The M-OH species which allows rapid activation of CO may be an oxidized form of copper as proposed by Klier (4); in agreement with these workers the conservation of such a species may involve the presence of CO_2 or water as can be illustrated by equations 3' and 4

$$M\text{-}H + H_2O = M\text{-}OH + H_2 \qquad 3')$$

$$M\text{-}H + CO_2 = M\text{-}OH + CO \qquad 4)$$

CONCLUSION

The comparative study of hydrogenation under pressure of CO and CO_2 has shown that CO_2 leads to methanol more rapidly, more selectively and at a lower temperature than CO. These results support the hypothesis of Bashkirov which suggests that methanolization of CO_2 proceed without the intermediacy of CO.

Moreover the hydrogenation of CO proves to be dramatically dependent of the presence of CO_2 or water; the role of these products may be to keep the catalyst in a suitable oxidized form. At high conversion the hydrogenation of CO in CO,CO_2 mixtures may also proceed at least partially through water gas shift reaction via the intermediacy of CO_2.

REFERENCES

1/ G. NATTA Catalysis,Emmett (Reinhold New-York) III,349,1955

2/ A.N. BASHKIROV et Al. Kinetics and Catal.16,704 and 706,1975, ibid 17,380 and 1132,1976

3/ V.D. KUZNETSOV, F.S. SHUB and M.I. TEMKIN ibid 23,788,1982

4/ K. KLIER et Al. J. Catal. 74,343,1982

5/ R. BARDET, J. THIVOLLE-CAZAT, Y. TRAMBOUZE J. Chim Phys 78,135,1981

6/ B. DENISE and R.P.A. SNEEDEN J. Mol. Catal. 17,359,1982

7/ A. DELUZARCHE et Al. React. Kinet. Catal. Lett 16,207,1981

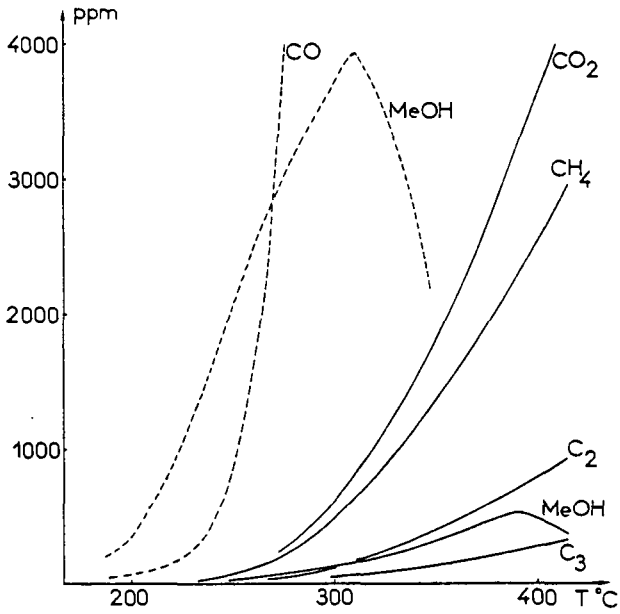

Figure: Evolution of products concentration versus temperature, during CO (——) or CO_2 (----) hydrogenation (22bar, 2l/hr, 5mg of Cu-ZnO-Al_2O_3 catalyst).

The Effect of CO_2 and H_2O in the Methanol Synthesis Reaction on Cu-Zn-O

Harold H. Kung, George Liu, and Dave Willcox

Chemical Engineering Department, Northwestern University, Evanston IL 60201

Introduction:

Methanol production over a copper-zinc oxide catalyst has been extensively investigated recently. With regard to the effect of the feed composition, Klier et al. reported a detailed measurement of the rate of methanol production as a function of the CO/CO_2 ratio (1). They observed a sharp maximum at a CO/CO_2 of about 28/2. Later, they also reported the effect of H_2O in the feed. Again, an optimum H_2O partial pressure was observed (2). The data were interpreted with the change in the active site concentration on varying feed composition, and competition of the active site by CO_2 and water.

Since these data indicated a strong dependence of the kinetics on the gas composition, it became interesting to try to determine the kinetics at well-controlled gas compositions. This can be achieved either by using a differential flow reactor, or by using a batch reactor and performing initial rate measurements. This paper describes results of the latter approach.

Experimental and Results:

Briefly, the experiments were conducted in a batch well-stirred reactor at about 200°C. The total pressure was about 17 atm. The catalyst was prepared according to Herman et al. (3). It has a CuO/ZnO of 30/70. All the data were obtained in the absence of diffusional effect. The catalyst was first reduced by H_2/N_2, and then preconditioned by a mixture of CO_2, CO, H_2 and CH_3OH, which was also used to calibrate the mass spectrometer. The rate of methanol production was measured by monitoring the gas composition with the mass spectrometer.

Table 1 shows the initial rates of methanol production as a function of the feed gas composition.

Table 1.

	Initial Gas Composition (%)				CH_3OH rate	H_2O rate
T°C	H_2	CO	CO_2	H_2O	10^{-5} moles/min-g	10^{-5} moles/min-g
228	70.05	27.74	2.21	0	1.27	1.30
	70.25	20.95	8.80	0	1.50	3.30
	70.02	16.22	13.76	0	1.70	4.57
	69.73	12.24	18.03	0	2.00	9.88
	69.99	0	30.01	0	2.49	11.24
220	71.13	26.3	1.66	0.90	0.118	-
	69.62	25.8	3.76	0.82	0.155	-
	70.45	19.80	7.23	2.52	0.138	-
	69.44	20.11	9.45	1.00	0.225	-
	69.57	11.40	18.16	0.87	0.410	-
	69.70	0	28.80	1.50	0.469	-

It can be seen from the data in the table that unlike previous results, the initial rates of methanol production increase with increasing CO_2/CO ratio, and the addition of water greatly suppresses the rate. Parallel to the methanol production, the rate of water production also increases with increasing CO_2/CO ratio. Similar trend was observed at a lower temperature of 197°C.

The effect of water can be explained by the competitive adsorption of water at the active site. The effect of CO_2, however, must indicate other reasons. Since these were initial rate measurements, the catalyst can be assumed to be in an identical state for all the measurements, (except for a slow deactivation which did not change the dependence on the feed composition), the positive effect of CO_2 may indicate that the hydrogenation of CO_2 is faster than that of CO, or that the hydrogenation of CO is enhanced by coadsorption of CO_2 which may facilitate the formation of some unstable intermediates.

To investigate the rate of hydrogenation of CO_2 in the feed mixture, $C^{18}O_2$ was used. Using conditions similar to those used in Table 1 with a CO/CO_2 ratio of about 4/1, it was found that the initial rate of production of CH_3OH-^{16}O was about as fast as the rate of production of CH_3OH-^{18}O. The results indicated clearly the importance of the hydrogenation of CO_2 in methanol production.

Another interesting result is on the rate of the isotope exchange reaction of CO_2:

$$C^{18}O_2 + [^{16}O] \rightleftharpoons C^{16}O^{18}O + [^{18}O]$$

$$C^{16}O^{18}O + [^{16}O] \rightleftharpoons C^{16}O_2 + [^{18}O]$$

This exchange reaction proceeds at a reasonable rate in a mixture of CO_2 and He, and CO_2 and CO. The rate is greatly enhanced in a mixture of H_2, CO, and CO_2 with the rapid production of $C^{18}O$. This result can be explained by the rapid reversible water gas shift reaction, which scrambles the oxygen in CO and CO_2, presumably via a formate intermediate.

References:

(1) K. Klier, V. Chatikavanij, R.G. Herman, and G.W. Simmons, J. Catal., 74, 343 (1982).
(2) K. Kiler, presented in the Materials Research Society Conference, Boston MA, November 1983.
(3) R.G. Herman, K. Klier, G.W. Simmons, B.P. Finn, J.B. Balko, and T.P. Kobylinski, J. Catal., 56, 407 (1979).

Acknowledgement:

This work was supported by the Department of Energy, contract no. DE-FG22-80PC30239.

MECHANISM AND INTERMEDIATES OF METHANOL SYNTHESIS OVER THE Cu/ZnO CATALYST IN THE PRESENCE OF WATER AND CARBON DIOXIDE

G. A. Vedage, R. Pitchai, R. G. Herman and K. Klier

Department of Chemistry and Center for Surface and Coatings Research
Lehigh University, Bethlehem, PA 18015

INTRODUCTION

Since Sabatier's first experiments on heterogeneously catalyzed methanol decomposition (1), many studies have been devoted to the mechanism of both the decomposition and the synthesis of methanol, and surface intermediates such as formyl (2,3), formate (4-6), and methoxide (4,5) have been identified by IR spectroscopy and chemical trapping techniques. In a previously reported (7) study from our laboratory, it was found that the methanol synthesis rate over Cu/ZnO catalyst is greatly enhanced by small additions of water to the synthesis gas while large additions of water resulted in a decrease in synthesis rate. Comparison of the water effect with that of CO_2 on the synthesis rate (8) showed that water behaved as a more effective promoter at low concentrations and a more severe retardant at higher concentrations than did equimolar carbon dioxide at the same experimental conditions. Further, injection of a 65/35 mole % mixture of $H_2{}^{18}O/H_2{}^{16}O$ to synthesis gas resulted in ^{18}O incorporation, the % ^{18}O in CH_3OH, CO and CO_2 in the exit stream being 3.41, 0.60 and 3.56, respectively. These results indicated that H_2O and/or CO_2 participate in methanol synthesis as reactants. D_2O addition to the synthesis gas was employed to further determine the kinetic and mechanistic role of water, and it was observed that a significant portion of the synthesized methanol occurred as CH_2DOH. No CHD_2OH or CD_3OH was detected, and these results indicated that water was involved in the formation of an intermediate with one single hydrogen atom. This observation was further supported by the promotion of isotopic scrambling between $^{12}C^{18}O$ and $^{13}C^{16}O$ by water preadsorption on the catalysts.

Chemical trapping experiments were also used (7) in identifying reactive intermediates involved in methanol synthesis. When diethylamine was continuously injected along with the synthesis gas, methylated tertiary amine was selectively obtained by the reaction:

$$(C_2H_5)_2NH + CO + 2H_2 \longrightarrow (C_2H_5)_2NCH_3 + H_2O \quad . \qquad 1)$$

At 215°C, H_2:CO = 70:30, 75 atm and a molar feed rate of diethylamine = 14.5 mmol/2.45 g cat/hr, the yield of methyldiethylamine was 11.2 mmol/2.45 g cat/hr and 97% of the water formed during methylation of diethylamine was converted to carbon dioxide by the water gas shift reaction. Amine addition, however, was not found to affect the water gas shift reaction. The intermediate trapped by amine behaved chemically as formyl, formaldehyde or hydroxycarbene. The evidence for an aldehydic intermediate was further corroborated by utilizing it for aldol addition with propanaldehyde followed by hydrogenation to give 2-methyl-1-propanol. Although both the above trapping reactions allowed a fairly complete mechanism to be formulated, it was still deemed necessary to address some alternative trapping and side reactions, particularly those of amines with surface formates.

It is known that (9) amines react with carboxylic acids to give acid amides, which could be hydrogenated to the corresponding amines (10). In order to determine whether the added diethylamine reacted more rapidly with surface formyl or formate, the hydrogenation of N,N-diethylformamide, a suspected intermediate of the reaction of surface formate with diethylamine, was studied. It is reported herein that non-dissociative hydrogenation of N,N-diethylformamide occurs at a lower rate than the addition of synthesis gas to diethylamine 1), indicating that the amine trapped the aldehydic and not the formate intermediate under the synthesis conditions.

EXPERIMENTAL

The Cu/ZnO = 30/70 mol % catalysts were coprecipitated from nitrate solution by Na_2CO_3, calcined, pelletized, and reduced with 2% hydrogen in nitrogen, according to a procedure previously described in detail (11,12). A schematic of the catalytic reactor system has been presented (11), but a high pressure unit for pumping liquids into the synthesis gas stream at the reactor pressure of 75 atm has been added at the top of the reactor preheater section. The exit gas was reduced to atmospheric pressure and was sampled by an on-line Hewlett-Packard 5730A GC, coupled with a Model 3388A integrator/controller.

RESULTS AND DISCUSSION

The results of N,N-diethylformamide hydrogenation at 215°C and 75 atm are given in Table I. When the flow rate of N,N-diethylformamide was 10.8 mmol/2.45 g cat/hr, 62% of it was converted to diethylmethylamine and the remaining 38% was distributed among other products. When the flow rate of N,N-diethylformamide and hydrogen was doubled and tripled at 215°C and 75 atm, the yields of diethylamine and methanol increased while the yield of all other products decreased (Table I).

As indicated in Table I, the N,N-diethylformamide was completely converted to diethylmethylamine (Eqn. 2), methanol (Eqn. 3), diethylamine (Eqn. 3), methylethylamine (Eqn. 4), triethylamine (Eqn. 4), and ethanol (Eqn. 5).

$$(C_2H_5)_2N-\overset{O}{\overset{\|}{C}}-H + 2H_2 \longrightarrow (C_2H_5)_2NCH_3 + H_2O \qquad 2)$$

$$(C_2H_5)_2N-\overset{O}{\overset{\|}{C}}-H + 2H_2 \longrightarrow (C_2H_5)_2NH + CH_3OH \qquad 3)$$

$$(C_2H_5)_2NCH_3 + (C_2H_5)_2NH \longrightarrow C_2H_5NHCH_3 + (C_2H_5)_3N \qquad 4)$$

$$(C_2H_5)_3N + H_2O \longrightarrow (C_2H_5)_2NH + C_2H_5OH \qquad 5)$$

The reactions given by Eqn. 4) and 5) were formulated by CH_3, C_2H_5 and H_2O balancing. Hence, a part of diethylmethylamine and

TABLE I

HYDROGENATION OF N,N-DIETHYLFORMAMIDE (NNDEF) AT 215°C, 75 atm OVER 2.45 g OF Cu/ZnO (30/70) CATALYST

Flow Rate of Substrate	Flow Rate of Hydrogen		H_2O	CH_3OH	C_2H_5OH	MEA	DEA	DEMA	TEA	NNDEF	CO	CO_2
Experiment (A)												
20 µl/min of NNDEF	10.5 ℓ (STP)/hr	mmol/hr In	--	--	--	--	--	--	--	10.8	--	--
		mmol/hr Out	7.6	2.9	0.5	1.4	1.9	6.7	0.9	<0.02	<0.02	<0.02
		Exit gas composition[a] (mol %)	34.70	13.24	2.28	6.39	8.68	30.59	4.11	<0.01	<0.01	<0.01
Experiment (B)												
40 µl/min of NNDEF	21.0 ℓ (STP)/hr	mmol/hr In	--	--	--	--	--	--	--	21.6	--	--
		mmol/hr Out	13.0	7.6	0.7	1.7	6.2	12.6	1.0	<0.02	<0.02	<0.02
		Exit gas composition[a] (mol %)	30.37	17.76	1.64	3.97	14.49	29.44	2.34	<0.01	<0.01	<0.01
Experiment (C)												
60 µl/min of NNDEF	31.5 ℓ (STP)/hr	mmol/hr In	--	--	--	--	--	--	--	32.4	--	--
		mmol/hr Out	19.1	13.0	0.8	2.0	11.0	18.3	1.1	<0.02	<0.02	<0.02
		Exit gas composition[a] (mol %)	29.25	19.91	1.23	3.06	16.85	28.02	1.68	<0.01	<0.01	<0.01

[a] Exit gas composition excluding hydrogen.

MEA = methylethylamine DEMA = diethylmethylamine
DEA = diethylamine TEA = triethylamine

diethylamine produced by reactions 2) and 3) was consumed by reactions 4) and 5) to produce ethylmethylamine, triethylamine and ethanol. In Figure 1, the amount of diethylmethylamine produced by reaction 2), diethylamine produced by reaction 3), methanol and water are plotted as a function of the reciprocal flow rate of hydrogen (flow rate N,N-diethylformamide = 0.025 x flow rate hydrogen). When these curves are extrapolated to infinite flow rate of hydrogen, the amounts of diethylmethylamine, diethylamine, methanol and water were 20%, 30%, 30% and 20%, respectively. This flow rate dependence study shows that there are two kinds of reactions occurring on the catalyst surface during the hydrogenation of N,N-diethylformamide: one giving rise to diethylmethylamine, and the other giving rise to diethylamine and methanol. Diethylmethylamine could be synthesized via two routes: one as in Eqn. 2) and the other by the condensation of diethylamine and methanol, produced by Eqn. 3). The results in Figure 1 indicate that the maximum amount of diethylmethylamine formed by direct hydrogenation (Eqn. 2)) was 40%.

In the following paragraphs the results of the hydrogenation of N,N-diethylformamide will be compared to the results of the methylation of diethylamine by synthesis gas (discussed in the Introduction section). This comparison is done to determine whether N,N-diethylformamide is an intermediate in methyldiethylamine synthesis from synthesis gas and diethylamine. Over Cu/ZnO catalyst, 14.5 mmol/2.45 g cat/hr of diethylamine reacted with synthesis gas to produce 11.2 mmol/2.45 g cat/hr of methyldiethylamine. When 10.8 mmol/2.45 g cat/hr of N,N-diethylformamide, approximately equal to the methyldiethylamine produced, was hydrogenated under conditions similar to methyldiethylamine synthesis, the conversion to methyldiethylamine was 62%. A comparison of these two experiments indicated that the rate of hydrogenation of N,N-diethylformamide to methyldiethylamine was lower than the rate of production of methyldiethylamine from synthesis gas and diethylamine. Hence, the synthesis gas and diethylamine reaction does not proceed exclusively via a N,N-diethylformamide intermediate. However, the participation of this intermediate to a lesser extent cannot be ruled out. The following path is suggested for the synthesis of methyldiethylamine from synthesis gas and diethylamine, which proceeds via a N,N-diethylformamide intermediate.

$$H_2O \rightleftharpoons OH^- + H^+ \qquad 6)$$

$$CO + OH^- \rightleftharpoons HCOO^- \qquad 7)$$

$$(C_2H_5)_2NH + H^+ + HCOO^- \rightleftharpoons (C_2H_5)_2\overset{+}{N}H_2HCOO^- \qquad 8)$$

$$(C_2H_5)_2\overset{+}{N}H_2HCOO^- \longrightarrow (C_2H_5)_2N\overset{O}{\overset{\|}{C}}H + H_2O \qquad 9)$$

$$(C_2H_5)_2N\overset{O}{\overset{\|}{C}}H + 2H_2 \longrightarrow (C_2H_5)_2NCH_3 + H_2O \qquad 10)$$

According to this scheme, the surface formate produced by the interaction of CO and surface hydroxyls will react with diethylamine (Eqn 8)) to form an amine salt (9). Upon heating, the amine salt will be converted to N,N-diethylformamide (9), and upon hydrogenation methyldiethylamine and water are produced (10). The flow rate

dependence study established that there are two basic pathways for the hydrogenation of N,N-diethylformamide. One gives rise to methanol and diethylamine (Eqn. 3)) and the other gives rise to the direct hydrogenation product, methyldiethylamine (Eqn. 2)). At zero contact time, the contribution of the latter path is 40%. At other conditions, e.g. when 10.8 mmol/2.45 g cat/hr of N,N-diethylformamide was hydrogenated with 10.5 ℓ(STP)/2.45 g cat/hr of hydrogen (Table I(A)), only 50% of the methyldiethylamine would be produced by reaction 2). The remaining 50% was produced by the secondary reaction in which diethylamine and methanol would undergo condensation probably via a formaldehyde intermediate.

If all the diethylamine injected (14.5 mmol/2.45 g cat/hr) during the methylation of diethylamine with synthesis gas was converted to N,N-diethylformamide intermediate, only 5.8 mmol/2.45 g cat/hr of methyldiethylamine would be produced by the direct hydrogenation path (Eqn. 2)). The remainder would be converted back to the reactants, diethylamine and methanol. During the methylation of diethylamine with synthesis gas, 11.2 mmol/2.45 g cat/hr of methyldiethylamine was produced. Hence, the rate of hydrogenation of N,N-diethylformamide does not account for the rate of the overall synthesis of methyldiethylamine by synthesis gas and diethylamine. The flow rate dependence study showed that at most, 50% of the methyldiethylamine would arise by the reaction of diethylamine with surface formate, followed by the reaction sequence given by Eqns. 9),10). The evidence against such a participation can be summarized in the following manner. It has been shown before that surface formate was a common intermediate for both methanol synthesis and the water gas shift (WGS) reaction (7). If surface formate underwent amination, one would expect the rate of the WGS reaction to be lowered as compared with the WGS reaction rates in the absence of amine but with an equivalent amount of water. Vedage et al. (7) showed that the WGS reaction rates were unaffected by the methylation of diethylamine with synthesis gas. Therefore, the C_1 intermediate undergoing amination is not formate or a precursor of formate but an intermediate formed subsequent to the surface formate in methanol synthesis. This intermediate can be deduced as an aldehydic type intermediate by the process of elimination. This intermediate which can take the form formyl, formaldehyde or hydroxycarbene is therefore a kinetically significant intermediate in methanol synthesis.

ACKNOWLEDGMENTS

This research was supported by the U.S. Department of Energy through the Pittsburgh Energy Technology Center (Grant No. DE-FG22-80PC30265) and the Solar Energy Research Institute (Grant No. XX-2-02173-01).

REFERENCES

(1) P. Sabatier and J. B. Senderens, Ann. Chim. Phys. 4, 418 (1905); P. Sabatier and A. Mailhe, C.R. 146, 1376 (1908).

(2) J. C. Lavalley, J. Saussey and T. Rais, J. Mol. Catal. 17, 289 (1982).

(3) J. Saussey, J. C. Lavalley, J. Lamotte and T. Rais, J. Chem. Soc. Chem. Commun., 278 (1982).

(4) A. Ueno, T. Onishi and K. Tamaru, Trans. Faraday Soc. 67, 3585 (1971).

(5) A. Deluzarche, R. Kieffer and A. Muth, Tetrahedron Lett. 38, 3357 (1977).

(6) M. Bowker, H. Houghton and K. C. Waugh, J. Chem. Soc., Faraday Trans. 1, 77, 3023 (1981).

(7) G. A. Vedage, R. Pitchai, R. G. Herman and K. Klier, 8th Intern. Congr. Catal., Berlin (1984).

(8) K. Klier, V. Chatikavanij, R. G. Herman and G. W. Simmons, J. Catal. 74, 343 (1982).

(9) I. L. Finar, "Organic Chemistry - The Fundamental Principles," Longman Group Limited, London, 1973.

(10) H. Adkins and B. Wojcik, J. Am. Chem. Soc. 56, 247 (1934).

(11) R. G. Herman, K. Klier, G. W. Simmons, B. P. Finn, J. B. Bulko and T. P. Kobylinski, J. Catal. 56, 407 (1979).

(12) J. B. Bulko, R. G. Herman, K. Klier and G. W. Simmons, J. Phys. Chem. 83, 3118 (1979).

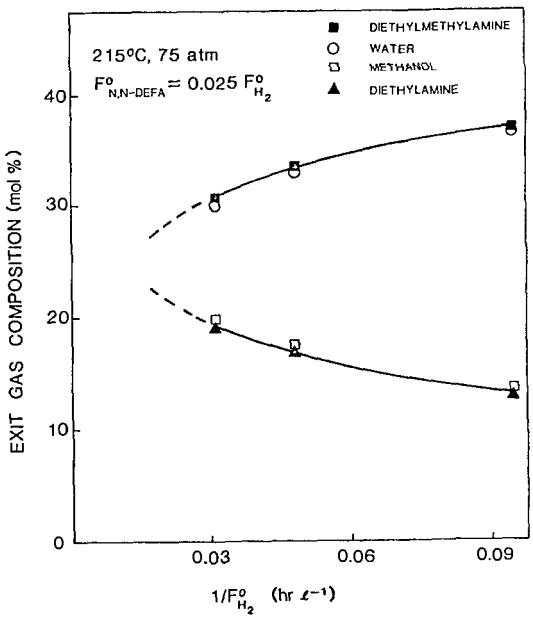

Figure 1. Diethylmethylamine, diethylamine, methanol and water produced by Eqns. 2) and 3) as a function of the reciprocal flow rate of hydrogen at 215°C, 75 atm and over 2.45 g Cu/ZnO (30/70) catalyst.

Periodic Dosing of Methanol Synthesis Over a Copper Zinc Mixed Oxide Catalyst

L. Fabbricino, R.R. Hudgins and P.L. Silveston

Department of Chemical Engineering
University of Waterloo
Waterloo, Ontario, Canada N2L 3G1

INTRODUCTION

Transient operations of reactor systems have been used for many years in kinetic studies as a means of elucidating kinetic mechanisms. In the last two decades, however, interest has grown in using intentional transient operation as a means of improving the performance of chemical reactors. The requirement of maintaining a uniform level of production at unsteady state can be achieved through cyclic operations in which one of the variables in the reaction system is periodically shifted between two values. When viewed on a larger time scale than that of the periodic shifts, the system exhibits uniform production. Figure 1 illustrates how periodic operation may be performed. In the LHS of the diagram the normal steady state operation is shown. A feed of fixed composition is fed to the reactor and once steady state has been achieved, one expects a constant stream of product to flow from this unit, as illustrated in the upper LHS. In the cyclic mode, however, the partial pressure or concentration of both the reactants making up the feed are changed periodically between two levels (in the simplest case). Before a new steady state is achieved after this switch, a second switch is made back to the original levels. The operation is characterized by a period t. It can be seen from the diagram that it is not necessary for the length of time at the two different concentrations to be the same. This can be changed as well so that the system may be exposed to a short period in which there is a high concentration of one component and a much longer period in which that same component is at a much lower level. This introduces a new variable referred to as the cycle split. Additional variables are, of course, the amplitudes of the individual changes. The result of periodic changes in composition, as illustrated in the diagram, is a constantly varying product composition at the exit of the reactor. This variation occurs around a mean value which we will refer to hereafter as the time-average product concentration, and from this value we can obtain a time-average reaction rate.

There is a growing body of literature suggesting that this mode of operation can cause substantial improvements in catalyst activity (Unni et al., 1973; Asfour et al., 1983; Jain et al., 1982; Jain et al., 1980; Wilson and Rinker, 1981; Kenny and Cutlip, 1976; Lynch, 1982. For CO oxidation of platinum, the system most extensively explored, Lynch (1982) suggests that periodic operation is exploiting the existence of multiple steady states at low CO_2/oxygen ratios in the feed.

Apart from those reactions which exhibit multiple steady states, the explanation frequently advanced for the improvement found with cyclic operation is that redox reactions are involved in which periodic operation involves changes in the coordination of metal atoms in the surface oxide structures which can interact with the bulk of the system through diffusional processes. This gives rise to a storage phenomena in the bulk of the catalyst that is not attainable in steady state operation. The stored reactant becomes available through pulsing.

Methanol synthesis over the copper zinc oxide system appears as an interesting candidate for this new mode of reactor operation because it probably proceeds via a redox mechanism. The use of cyclic operation can be implemented in two ways. The first of these is to periodically change the hydrogen to carbon monoxide ratio in the feed just as has been done in most of the other studies given above. The use of carbon dioxide dosing of this system suggests an alternate mode which might be explored. It has been found with the copper-zinc oxide-alumina system, which forms the basis for many of the commercial methanol synthesis catalysts, that the catalyst undergoes slow deactivation unless a low concentration of carbon dioxide is maintained in the feed. In place of maintaining CO_2 at a constant level, it can be pulsed in the feed.

In an earlier paper (Nappi et al., 1984) we examined the performance of a reactor operating under cyclic variations of the hydrogen-to-CO ratio in the feed. Even though nonlinear transient behaviour was observed, periodic forcing of this system failed to improve the yield to methanol. Indeed, the main effect was to roughly double the production rate of methane in the system. We speculated that the surprising lack of improvement was due to rather small changes in the reducing power of the feed gas in switching from hydrogen-rich to carbon-rich mixtures. When maximum amplitude experiments were carried out in which the feed varied between pure carbon monoxide and pure hydrogen, performance was significantly better, but still failed to attain the levels possible with steady-state operation. Thus, in this paper, we examine periodic forcing with carbon dioxide.

EXPERIMENTAL

The question addressed in our experimental program was whether periodic pulsing of the reaction system with carbon dioxide could increase the production rate of methanol to a greater extent than maintaining a small bleed of the same gas into the system. Only exploratory experiments were carried out. These employed the stoichiometric hydrogen-carbon monoxide mixture for methanol synthesis of 2:1. In one of the source gases, carbon dioxide was added to a level of 2% by volume. The experiments were then carried out by periodically switching the feed from the source containing carbon dioxide to the source free of CO_2. Referring to Figure 1, the variables explored were period and the length of exposure to the gas containing carbon dioxide, referred to earlier as the cycle split. All experiments were carried out at a pressure of 2.52 MPa and 250°C. The catalyst used was a commercial low temperature water gas shift catalyst with the following formulation: Cu/Zn/Al = 29/47/24. BET surface area of this catalyst was 80.0 m^2/g and its pore volume was measured as 0.470 mL/g. Thus, the mean pore diameter was 240 Å. Auger spectroscopy showed the presence of copper as Cu^+ on the surface. Transmission electron microscopy indicated the catalyst was a finely dispersed mixture of various phases.

Measurements were carried out using a Berty reactor. This reactor behaves as totally backmixed which simplifies experimentation, as well as interpretation of the results. It has the disadvantage, however, that the reactor contains a significant dead volume which limits the switching frequency in cyclic operation. If this frequency is too high, the well stirred dead volume smooths out the concentration pulse so that the catalyst phase sees no change in composition with time. The arrangement of the experimental equipment is shown schematically in Figure 2. Details of the experimental equipment are available elsewhere (Jain et al., 1983; Nappi et al., 1984). The only change made from the reactor described in these publication is that the interior has been electroplated with copper in an attempt to reduce the methanation activity.

Blank runs were performed to check methanation activity. It was found that a very small amount of methane was produced; however, it is not certain whether this methane was produced on the reactor walls or in the low temperature, catalytic oxygen scavenging unit located upstream from the reactor. Methane found in the blank runs, in any case, was well below the methane contained in the source cylinders feeding the reactor. Corrections were made for both methane sources.

Analyses were performed by gas chromatogrphy using a 3-m Porapak Q column and a hot wire detector in series with a flame ionization detector.

It was found experimentally that a cyclic stationary state was achieved after about two cycles between the CO_2 containing and CO_2 free synthesis gas mixtures. In most cases the experiment was carried out over a time frame of many hours so that up to 20 complete cycles were run. Sampling was done intermittently, but sufficient measurements were made to characterize completely the time-varying methanol and methane yields.

EXPERIMENTAL RESULTS

Table 1 summarizes the experimental results for methanol production. Of the two variables that were explored in these measurements, the period was only examined at 12 and 30 minutes. Decreasing the period effected a small improvement. Reactor dead space and mixing rendered experiments much below 12 minutes unproductive. As the cycle split is decreased, however, the effect is the opposite, the rate of methanol production decreases. This is, of course, expected because it has been demonstrated that at low levels of carbon dioxide in the feed, methanol production becomes proportional to the concentration of this component. Thus, as the cycle split is decreased, the quantity of carbon

Table 1

Time-Average Rate of Methanol Production as a Function of Period and Cycle-Split With CO_2 Dosing

τ(min)	Cycle Split	Quasi-Steady-State Rate (10^{-7} mol/g cat·s)	Transient Average Rate (10^{-7} mol/g cat·s)	*Normalized Rate
12	0.05	7.10	8.25	1.16
12	0.10	7.38	9.34	1.27
12	0.25	8.22	9.89	1.20
12	0.50	9.61	10.1	1.05
12	0.75	11.0	11.4	1.03
30	0.50	9.61	9.97	1.04

* The transient rate was normalized with respect to the quasi-steady-state rate.

dioxide the catalyst sees within a cycle falls. It is incorrect, therefore, to compare the measurements from the cyclic operation to the steady state measurements with CO_2 free synthesis gas. The proper comparison is with the steady state results at the same mean level of CO_2 used in a complete cycle in the

periodic forcing experiments. For example, if the cycle split were 0.5 and the two source gases contained 2% and 0% CO_2, the mean level would have been 1%. Unfortunately, a complete set of steady-state experiments at different CO_2 levels was not made. However, it is possible to estimate these steady state rates by assuming a linear relationship between the mole % CO_2 in the gas and the rate of methanol formation. If this is done, and the estimated steady state value is divided into the measurements shown in Table 1, the normalized rate is obtained. These are found in the last column of the table. Normalized results reflect the improvement in methanol yield over the comparable steady state through periodic forcing.

Adding 2% CO_2 by volume to the stoichiometric mixture increases the steady-state methanol formation from 6.8×10^{-7} to 12.4×10^{-7} mol/g cat•s. Evidentally, periodic forcing is capable of further increasing the methanol production rate by about 25%. Worth noting is that the measurement reported in this paper are of a screening nature and no attempt has been made to optimize the periodic dosing sequence.

Table 2 shows our methane production results. Introduction of a steady stream of CO_2 into the feed gas dramatically suppresses the steady-state rate of formation of methane in this reaction system from 3.4×10^{-8} to 5.4×10^{-9} g mol/g cat•s. Although the methane formation rate for this catalyst in the absence of carbon dioxide is only about 5% of the formation rate for methanol, the introduction of CO_2 suppresses this rate to just 0.4% of the methanol rate. Table 2 shows that cycle period has a much stronger effect on methane than on methanol production. Unlike methanol production however, periodic pulsing with CO_2 reduces methane formation substantially and shortening the pulse length exerts just a small effect on the rate of formation.

Table 2

Time-Average Rate of Methane Production as a Function of Period and Cycle-Split With CO_2 Dosing

τ(mins)	Cycle Split	Quasi-Steady-State Rate (10^{-9} mol/g cat•s)	Transient Average Rate (10^{-9} mol/g cat•s)	*Normalized Rate
12	0.05	32.6	3.10	0.095
12	0.10	31.2	3.42	0.11
12	0.25	26.9	3.39	0.13
12	0.50	19.7	2.98	0.15
12	0.75	12.6	5.83	0.46
30	0.50	19.7	5.87	0.30

* The transient rate was normalized with respect to the quasi-steady-state rate.

If the rate of formation of methane is proportional to the carbon dioxide concentration, the rate of formation at quasi-steady-state will be a close estimate of the steady state for CO_2 levels between 0 and 2 vol%. These values are appropriate for comparison with the time-average rates of methane formation under periodic pulsing. We have assumed appropiateness and the last

column in Table 2 compares the time-average cyclic rates with the assumed steady-state ones. These results indicate the large influence of dosing time on methane formation.

Periodic sampling through the gas chromatograph permits a reconstruction of the change of rate with time inside a dosing cycle. These reconstructions are shown in Figures 3 and 4 for two quite different cycling conditions: the first is for a short pulse of CO_2 containing feed while the second figure considered a relatively long pulse. Immediately upon introduction of the CO_2-containing gas, methane production falls to a level which cannot be detected with our analytical equipment. In Figure 4, when the CO_2-free gas stream is introduced, the methane concentration builds up to about one. The measurements have been normalized with exit concentration measured at steady state with the CO_2-containing gas. If a short CO_2 pulse is used, Figure 3 shows the normalized concentration rising to about 2.4. In both cases, these values are well below the steady state values expected for a CO_2-free synthesis.

In both figures, methanol production changes very little. Although it is shown in the figures, the CO_2 detected in the stream leaving the reactor changed very little within the dosing cycle.

DISCUSSION

The failure of the methanol production rate to follow the changes in the CO_2 content of the gas coupled with the dramatic 20 to 25% improvement in production rate with respect to steady state strongly suggests that the introduction of CO_2 causes a restructuring of the surface and/or reoxidation of the sites in the system. These sites, or surfaces, however, are not corrected immediately back to their starting condition when CO_2 is removed. Restructuring or reductions appears to be very slow. A long-term decay of the copper/zinc oxide catalyst activity in the absence of CO_2 in the feed gas is observed, of course, in steady state operation. If a massive reoxidation of copper in the catalyst were occurring on the introduction of CO_2, methanol production would have changed much more sharply then what can be seen in the data shown in Figures 3 or 4.

A sharp change in production rate does appear, however, for methane. It seems likely that the explanation for this is a wholesale destruction of the sites responsible for methane production by the introduction of CO_2. Evidentally, these sites must be quite different from those for methanol formation judging from the sharply different behaviour when CO_2 is either introduced or removed from the system. Substantial adsorption of CO_2 accounts for the lack of change in CO_2 levels in the exit stream. The presence of CO_2 when the feed is CO_2-free seems to result from methane formation. Methane formation is favoured thermodynamically at the operating conditions employed so that CO_2 suppression cannot occur through a equilibrium interaction because the reaction system operates so far away from equilibrium.

ACKNOWLEDGEMENTS

Support of a Strategic Grant form the Natural Sciences and Engineering Research Council of Canada to Professors Hudgins and Silveston is gratefully acknowledged.

REFERENCES

Jain, A.K., P.L. Silveston, and R.R. Hudgins, "Forced Composition Cycling Experiments in a Fixed Bed Ammonia Synthesis Reactor", Proc. Seventh Internat. Sympos. Chem. Reaction Engg., Boston, Mass., ACS Sympos., Ser. 196, 97-107 (1982).

Jain, A.K., P.L. Silveston, and R.R. Hudgins, "Influence of Forced-Feed Composition Cycling on the Rate of Ammonia Synthesis Over an Industrial Iron Catalyst: Part I - Effect of Cycling Parameters and Mean Composition", Can. J. Chem. Eng., 61, 824-831 (1983).

Unni, M.P., R.R. Hudgins and P.L. Silveston, "Influence of Cycling of the Rate of Oxidation of SO_2 over a V_2O_5 Catalyst," Can. J. Chem. Eng. 31, 623-9 (1973).

Asfour, H., P.L. Silveston, and R.R. Hudgins, "Effect of Forced Concentration Cycling of the Claus Reaction", Paper presented at the 66th Can. Chem. Conf., Calgary, Canada (1982).

Cutlip, M.B. and Kenny, C.N., Paper presented at the 15th Int. Symp. on Chemical Reaction Engineering, Houston, Texas, March (1978).

Lynch, D.T., Can. J. Chem. Eng. 61, 183, 1983.

Nappi, A., R.R. Hudgins, and P.L. Silveston, "Influence of Forced Feed Composition Cycling on Catalytic Methanol Synthesis", Preprints, 9th ISCRE Meeting, Edinborough, U.K. (1984).

Wilson, H.D. and Rinker, "Concentration Forcing in Ammonia Synthesis - I Controlled Cyclic Operation", Chem. Eng. Sci., 37, 343-355 (1982).

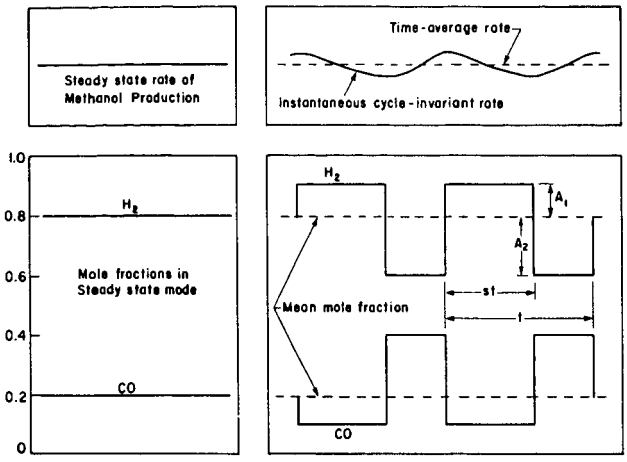

Figure 1 Schematic of the Periodic Operation of a Catalytic Reactor.

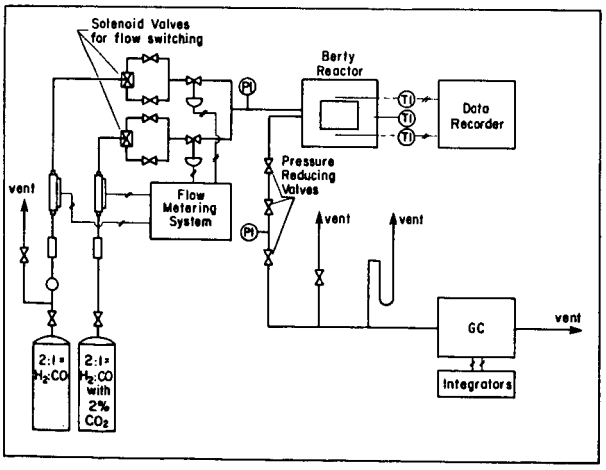

Figure 2 Schematic of the Experimental Apparatus (PI = pressure gauge, TI = thermocouple, GC = gas chromatograph)

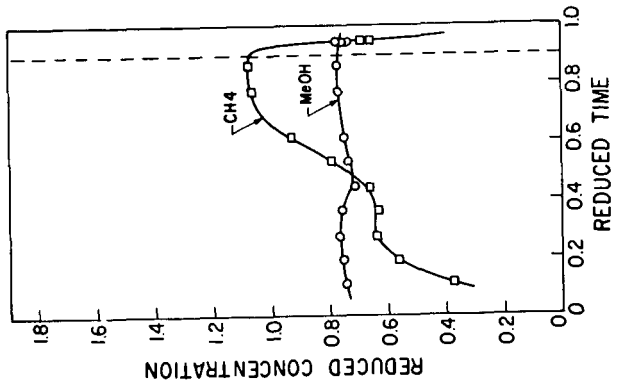

Figure 3 Time Variation of Product Concentrations Under Periodic Dosing with 2 vol. % CO_2 for τ=12 Minutes, *s=0.10 (Concentrations Normalized With Steady State Product Concentration Using 2 vol.% CO_2 in Feed, 250°C 2.513 MPA).

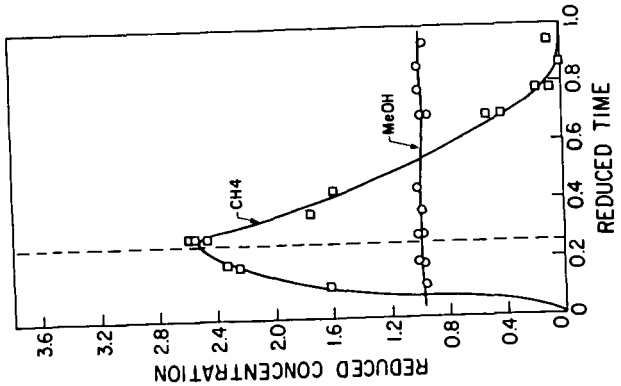

Figure 4 Time Variation of Product Concentrations Under Periodic Dosing with 2 vol. % CO_2 for τ=12 Minutes, *s=0.75 (Concentrations Normalized With Steady State Product Concentration Using 2 vol.% CO_2 in Feed, 250°C 2.513 MPA).

*s, defined as the ratio of the CO_2-rich portion of the cycle to the cycle period.

An Investigation of the Chemical States of Copper in Methanol Catalysts and Their Relevance to Activity Maintenance

E. J. Karwacki, Jr., M. R. Anewalt, and D. M. Brown

Air Products and Chemicals, Inc.
Box 538, Allentown, PA 18105

Summary

Information on the chemical states of a catalyst surface is obtainable by X-Ray Photoelectron Spectroscopy (XPS). Copper-zinc oxide catalysts from the DOE sponsored Liquid Phase Methanol (LPMeOH) project have been studied to ascertain the oxidation states of copper on fresh, reduced, and spent catalyst samples. Using the Auger parameter to differentiate valence levels it is shown that Cu^{+1} must be maintained on the surface for continued catalyst activity to methanol. Unusually strong shifts, due to matrix effects, in the $Cu2p_{3/2}$ binding energy for reduced/active catalysts indicate that Cu^{+1} is stabilized by incorporation within the ZnO lattice. Energy Dispersive X-Ray Spectrometry (EDS) and XPS show that while the bulk Cu/Zn ratio is maintained at a value near 2.1 the surface Cu/Zn ratio decreases in use to well below unity. The effects of metal and halogen poisoning have also been studied by the additions of iron (as iron carbonyl) and chlorine, and are observed to deactivate the catalyst by reduction of Cu^{+1} to Cu^{0}. These results suggest a relationship between the copper state needed to maintain activity and the reducing/oxidizing potential of the reactant gases.

Introduction

Determination of the active copper state in copper/zinc/alumina catalysts, used for methanol synthesis, has been of recent interest (1-5). Klier and coworkers, using optical spectroscopy, have presented evidence indicating Cu^{+1}, dissolved in the ZnO lattice(1,2), as the catalytically active state. X-Ray Photoelectron Spectroscopy (XPS) has been employed by Okamato et al.(3,4) to show that CuO-ZnO samples containing less than 10% copper, upon reduction, do exhibit weak Cu(LMM) x-ray induced Auger lines suggestive of the presence of Cu^{+1}. The Okamato studies, unfortunately, do not present supporting data regarding activity of the catalysts to methanol synthesis. Himelfarb et al.(5) have presented evidence, by X-Ray Diffraction (XRD), for the existence of an intermediate Cu^{+1} phase during reduction of copper-zinc oxide catalysts. Since XRD is a bulk sensitive technique the chemical state of the surface is, however, still in doubt.

In conjunction with the current DOE sponsored Liquid Phase Methanol Project (LPMeOH) we have undertaken studies of commercially available copper-zinc oxide catalysts which have demonstrated actual activity to methanol synthesis in both the gas and liquid phases. Here we present XPS results which confirm that Cu^{+1} is indeed the active state. Poisoning by metal and/or halogens has also been investigated by XPS and Energy Dispersive X-Ray Spectrometry (EDS). Deactivation apparently occurs via reduction of Cu^{+1} to Cu^{0}.

Because the chemical shifts observed in the XPS spectrum for copper are limited it is necessary to employ the Auger parameter to follow the three valence states Cu^{0}, Cu^{+1}, and Cu^{+2}. The Auger parameter (α), proposed by Wagner(6) and later modified by Gaarenstrom and Winograd(7) is defined as:

$$\alpha + h\nu = BE_P + KE_A = \alpha' \qquad 1)$$

where $h\nu$ is the photon energy, BE_p the binding energy of the photoelectron peak, and KE_A the kinetic energy of the x-ray induced Auger line which is also observed in the spectrum. The addition of $h\nu$ to α is defined as α', the modified parameter(7), and is independent of the excitation energy.

From Equation 1 a plot of α' vs the corrected BE_p can be generated. This plot or Auger map, as it is referred, enables one, through analyses of standards, to assign regions to a particular elemental oxidation state or chemical environment.

Experimental

A commercially available copper-zinc oxide catalyst, in powdered form (2-7μm), has been used in these studies. Gas phase and in situ liquid phase reductions were performed by suitable laboratory adaptation of the commercial gas phase technique. Catalysts from liquid phase studies were prepared for surface analysis by stripping the inert oil via a series of cyclohexane washings in a nitrogen filled glove box. Upon drying, the samples were transported to an argon filled glove box. The catalyst samples were applied to a piece of double-sided adhesive tape attached to a sample mount. The mounts were then sealed in a vessel for transportation to the spectrometer. Under vacuum the vessels were reopened and the mounts attached to the transfer rod assembly.

XPS has been performed on a Physical Electronics 560 spectrometer equipped to perform XPS, Scanning Auger Microscopy (SAM), Ion Scattering Spectroscopy (ISS), and Secondary Ion Mass Spectrometry (SIMS). Mg Kα radiation (1253.6eV) at 15 keV and 20mA was used as the excitation source. Charge correction was performed by referencing to the $Zn2p_{3/2}$ line at 1021.7eV and C1s, for residual oil, at 284.7eV. Both lines were found to agree to within $\pm$ 0.2eV.

EDS was performed on an Amray 1000 Scanning Electron Microscope (SEM) equipped with a Kevex 7000 spectrometer. Quantitative analysis was accomplished using ZAF corrections.

Copper oxide standards were prepared in situ by mounting a cleaned and polished (to 1μm alumina) copper foil to a probe that could be heated and cooled. After repeated cycles of ion sputtering and annealing at 300°C, a clean surface was obtained as verified by Auger Electron Spectroscopy (AES) and XPS. A thin film of CuO was then produced on the surface by heating the foil to 250°C under a stream of air. Larson(8) has reported that Cu_2O can be produced by reheating the CuO surface film to 250°C in vacuum. The advantage of this preparation is that surface charging is negligible due to the conduction of the thin oxide films produced on the surface.

Results and Discussion

Because of discrepancies in the literature(6,8), regarding the binding energy of the $Cu2p_{3/2}$ line, a study to determine α' for Cu, Cu_2O, and CuO was undertaken. The results of this investigation are listed in Table 1. The $Cu2p_{3/2}$ line is not observed to shift as copper metal is oxidized to Cu_2O, however, the Cu(LMM) line is found to move from 334.8eV to 336.8eV. This change causes a shift in α' from 1850.9eV, for copper metal, to 1848.9eV for Cu_2O. Further oxidation to CuO results in the $Cu2p_{3/2}$ line shifting to 933.2eV as well as the Cu(LMM) line to 335.6eV. The net result is a reshifting of α' back to 1851.2eV. These movements in α' are better illustrated by the Auger map, shown in Figure 1, which indicates the regions occupied by copper metal and its oxides. Though CuO and Cu metal possess the same α' value, the shift in the $Cu2p_{3/2}$ line, as well as the observation of satellites due to the paramagnetic nature of Cu^{+2} in the Cu2p spectrum, permits these chemical states to be distinguished.

The fresh, as received catalyst is found to be comprised of copper primarily as CuO. This is indicated by the observation of strong satellite peaks and an α' of 1851.0eV. Upon reduction, the Cu2p spectrum is observed to undergo a loss in satellite structure and a shift in the $Cu2p_{3/2}$ binding energy. Also, as shown in Table 1, the $Cu2p_{3/2}$ line is found to move from 933.6eV to 931.7eV. The x-ray induced Auger line, however, remains at 336.2eV. Calculating α' shows that the Cu^{+2} has been reduced to Cu^{+1}. To better illustrate these observed changes the Auger map is depicted in Figure 2. The region occupied by the reduced catalyst is in good agreement with the coordinates for Cu_2O in Figure 1. Thus it appears that Cu^{+1} is present on the surface after reduction. The binding energy shift observed for the $Cu2p_{3/2}$ line as the copper is reduced is observed to be significantly greater than expected for Cu^{+2} being reduced to the Cu^{+1} state. For Cu_2O, the $Cu2p_{3/2}$ line is found to be at 932.1eV while for the reduced sample a shift to 931.7eV is observed. This larger than anticipated chemical shift is believed to be attributable to matrix effects, similar to those observed by Kim and Winograd for Au implanted in SiO_2(9). The Cu^{+1} is apparently stabilized on the surface by its incorporation within ZnO lattice defects.(2) The electron rich environment offered by these sites is thus believed responsible for the large shift in the $Cu2p_{3/2}$ binding energy. In as received form (oxide), elemental analysis shows a Cu/Zn ratio of approximately 2 to 1. XPS measurements, however, clearly and reproducibly show a surface Cu/Zn ratio of almost unity.

After reduction the catalysts are used to produce methanol in either gas or liquid phase operations. Upon demonstration of satisfactory activity, samples of the catalysts are removed for analysis. In Table 1 and Figure 2 the results of studies on these active catalysts are also shown. The copper present on the surface is observed to exist as Cu^{+1} by the fact that α' remains at 1849.0eV. The surface Cu/Zn ratio, calculated by XPS, is found to decrease to approximately 0.7 to 1 upon reduction. This ratio becomes even smaller (0.3 - 0.1) after use in the reactor.

Upon an observed loss in activity a catalyst sample was again removed for analysis. The data, shown in Table 1 and Figure 2, indicates that Cu^{+1} has been reduced to Cu^0 by the observation of a shift in α' to 1851.0eV. It is our contention that deactivation is occurring by the reduction of Cu^{+1} to Cu^0 on the surface. this suggests that the continued presence of Cu^{+1} is important in maintaining catalytic activity.

The small particle size (2-7μm) of the catalyst powder used in liquid phase operations has permitted the use of EDS to rapidly determine a bulk Cu/Zn ratio for comparison with the surface ratio obtained by XPS. The results indicate that while the bulk Cu/Zn ratio remains at 2.1, a decrease in the surface Cu/Zn ratio, calculated by XPS, is observed upon reduction and use. Catalyst reduction decreases the surface Cu/Zn ratio from 1.0 to ~0.7. After use in methanol synthesis this ratio is found to further decrease to values approaching 0.3. This data fits well with proposals by Klier and coworkers(2) regarding specific site stabilization of Cu^{+1}. Since only a finite number of defect sites are anticipated within the ZnO lattice near the surface the Cu/Zn ratio is expected to decrease as Cu^{+1} dissolves within the ZnO lattice. Therefore recrystallization, due to excessive heat, is expected to severely effect the surface's ability to synthesize methanol. A requirement, for tight temperature control, thus is necessary to prevent surface recrystallization which suggests that the LPMeOH process offers significant advantages, as a result more efficient heat transfer, over gas phase synthesis.

Poisoning and its effects upon surface copper have also been investigated. The injection of a very low level of $Fe(CO)_5$ to the feed stream is observed to cause

a rapid deactivation of the catalyst. XPS indicates that no iron is apparently present on the surface of these samples. EDS analysis, however, shows that iron is present in the bulk of the poisoned samples. By XPS changes in the Cu(LMM) spectrum are observed. In Figure 3, the Cu(LMM) spectra for a fresh-reduced catalyst is compared with that obtained after iron poisoning. The observation of a second peak near 334.6eV is attributed to the presence of Cu^0 on the surface. Using Equation 1, α' is found to be equal to 1851.0eV for this new line. This region has been earlier determined, in the oxide study, to be occupied by metallic copper (Fig. 1). Thus upon contact with iron the Cu^{+1} is reduced to Cu^0, thereby deactivating the catalyst. Chlorine poisoning has also been investigated and the chlorine, likewise, appears to deactivate by reducing the surface Cu^{+1} to Cu^0. Unlike iron poisoning, XPS and EDS are both able to detect the presence of chlorine on the surface as well as a reduction in the Cu/Zn ratio at the catalyst surface. The mechanisms of deactivation are not well understood at this time and are currently the subject of continued research.

Conclusion

From this study it has been determined, using the Auger parameter, that Cu^{+1} is the active chemical state of copper on the surface, and is apparently stabilized by its incorporation within the ZnO lattice. Deactivation is believed to occur by the reduction of Cu^{+1} to Cu^0. Poisoning by either Fe or Cl is observed to also proceed through a mechanism by which the Cu^{+1} is reduced to Cu^0.

References

1. K. Klier, Adv. in Catalysis, 31, 243 (1982).

2. R. G. Herman, K. Klier, G. W. Simmons, B. P. Finn, and J. B. Bulko, J. of Catalysis, 56, 407 (1979).

3. Y. Okamato, K. Fukino, T. Imanaku, and S. Teranishi, J. Chem. Soc., Chem. Commun., 1405 (1982).

4. Y. Okamato, K. Fukino, T. Imanaku, and S. Teranishi, J. Phys. Chem., 87, 3747 (1983).

5. P. B. Himelfarb, F. E. Wawner, Jr., A. Bieser, Jr., and S. N. Vines, J. of Catalysis, 83, 469 (1983).

6. C. D. Wagner, L. H. Gale, and R. H. Raymond, Anal. Chem., 51, 466 (1979).

7. S. W. Gaarenstrom and N. Winograd, J. Chem. Phys., 67, 3500 (1977).

8. P. E. Larson, J. of Electron Spectr. and Rel. Phen., 4, 213 (1974).

9. K. S. Kim and N. Winograd, Chem. Phys. Lett., 30, 91 (1975).

1040A

Table 1

Results of Copper Auger Parameter
Determination for Copper Oxide Standards and
Catalyst Samples Analyzed by XPS

Sample	$Cu2p_{3/2}$(ev)[1]	Cu(LMM)(eV)[2]	α'(ev)
Clean Cu	932.1	334.8	1850.9
Cu_2O	932.1	336.8	1848.9
CuO	933.2	335.6	1851.2
Fresh-Unreduced Catalyst	933.6	336.2	1851.0
Fresh-Reduced Catalyst	931.7	336.2	1849.1
Spent-Active Catalyst	931.9	336.5	1849.0
Spent-Deactivated Catalyst	932.0	336.6	1849.0
	932.0	334.6	1851.0

1 $Cu2p_{3/2}$ energies presented as binding energies.
2 Cu(LMM) energies presented in this study as binding energies for consistency.

1040A

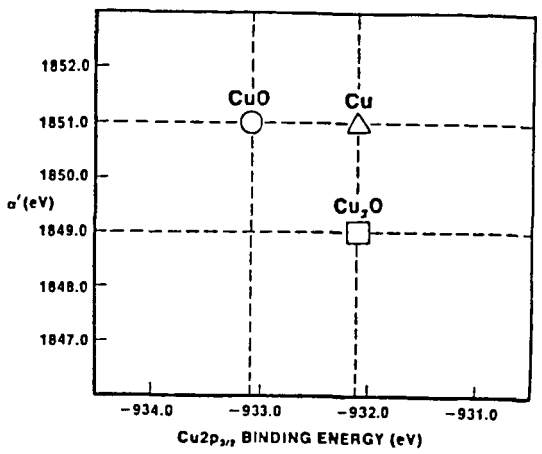

Figure 1: Auger map depicting results of in situ copper oxide study.

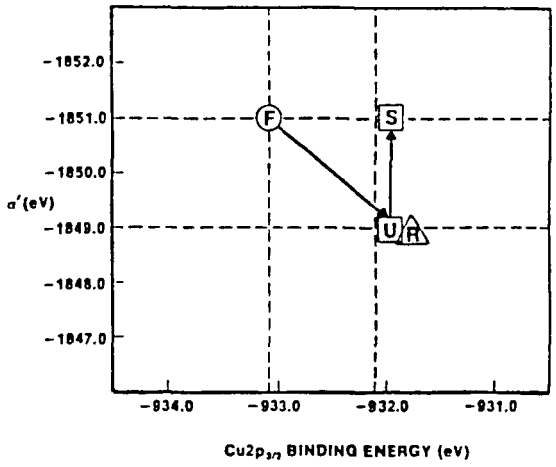

Figure 2: Auger map illustrating the observed changes in the surface copper oxidation state for: (F) fresh-as received catalyst, (R) fresh-reduced catalyst, (U) methanol-active catalyst, and (S) spent catalyst.

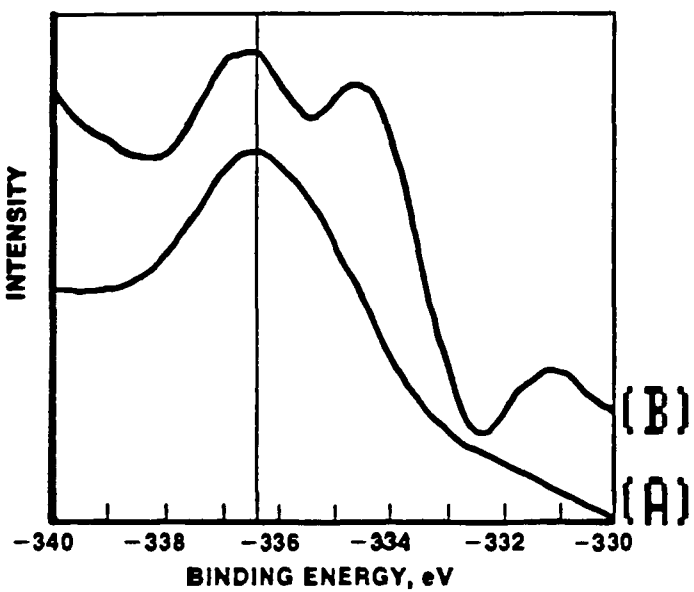

Figure 3: Cu(LMM) X-ray induced Auger spectra for (A) fresh, methanol-active catalyst and (B) spent catalyst.

RELATIONSHIP BETWEEN SURFACE STABILIZED Cu^+ IN COPPER-CHROMIA CATALYSTS AND ACTIVITY FOR METHANOL FORMATION.

G. Apai, J. R. Monnier, M. J. Hanrahan, Research Laboratories, Eastman Kodak, Rochester, New York 14650.

Recent evidence suggests that in Cu-ZnO, the Cu^+ species may be the component responsible for methanol formation. Copper-chromium oxide catalysts also have similar selectivity for methanol synthesis under reaction conditions like those used for Cu-ZnO catalysts. X-ray photoelectron spectroscopy and x-ray diffraction studies of the Cu-Cr oxide catalyst indicate that the activity for methanol formation is associated with a crystalline cuprous chromite phase. The concentration of surface Cu^+ species, stable under H_2 reduction or syngas reaction conditions, is correlated with the activity for methanol formation. Bulk stabilization of $CuCrO_2$ (Cu^+) appears to be responsible for the surface stabilized Cu^+ species. The concentration of surface Cu^+ is dependent upon the Cu/Cr ratio, the calcination temperature, and the nature of the catalyst pretreatment. Comparisons will be made between real and model catalysts. In addition the concentration of these Cu^+ sites is independent of CO_2 addition to the synthesis gas feedstream. The associated decrease in catalytic activity is attributed to the non-catalytic, competitive adsorption of CO_2 on sites active for CH_3OH formation. These results for Cu-Cr oxide provide some interesting similarities and differences in comparison to the Cu-ZnO catalyst.

CHEMISORPTION OF CO, CO_2, O_2 AND H_2 ON THE Cu/ZnO METHANOL SYNTHESIS CATALYSTS

By

G. E. Parris
Air Products & Chemicals, Trexlertown, Pennsylvania

and

K. Klier
Department of Chemistry, Lehigh University, Bethlehem, Pennsylvania

INTRODUCTION

Historically the successful catalysts for methanol synthesis from synthesis gas have always utilized zinc oxide. The addition of chromia, Cr_2O_3, or alumina, Al_2O_3 to the zinc oxide based catalysts were found to be beneficial as supports for extending catalyst life and as promoters to enhance the catalytic activity for synthesis of methanol. These catalysts operate at high pressures (>200 atm) and temperatures (573-623 K), however. The addition of copper oxide to these catalysts resulted in much higher methanol synthesis activity at lower pressures (75 atm) and temperatures (523 K) than observed with the pure components only, or with the ZnO/Cr_2O_3 and ZuO/Al_2O_3 catalysts, (1,2). In addition, the method of preparation of copper catalysts was found to be an extremely important factor(3).

These observations implied that the final state of copper in the mixed $Cu/ZnO/M_2O_3$ catalysts critically determined their high activity and selectivity for the production of methanol. The present work was undertaken to determine the chemisorption properties of CO, CO_2, O_2 and H_2 for a series of binary copper-zinc oxide methanol synthesis catalysts and thereby clarify the reason for the observed mutual promotion effect between Cu and ZnO by identifying the nature of the reactive centers in methanol synthesis catalysts based on copper.

EXPERIMENTAL

The Cu/AnO = 0/100-100/0 catalysts were coprecipitated from nitrate solution by Na_2CO_3, calcined and reduced with H_2/N_2 = 2/98 vol according to a procedure previously described in detail (3,4). The adsorption experiments were conducted in a glass high vacuum volumetric adsorption apparatus with a stationary background vacuum of 10^{-4} Pa. The catalysts were reduced on the adsorption system without exposure to air.

The CO and H_2 isotherms were measured at 293 K up to a final pressure of approximately 16 kPa. The weak and strong capacities were determined as follows: (1) run an adsorption isotherm on a reduced and activated sample, (2) evacuate the sample for 10 minutes then run a second isotherm, and (3) this second isotherm corresponds to the weakly adsorbed gas and the difference between the first and second isotherms is the strongly adsorbed gas. Oxygen chemisorption experiments were conducted at 78 K according to the procedure of Zettlemoyer et al (6). Surface area measurements were made using the BET method with argon as adsorbate.

Carbon dioxide isotherms were studied at 523 K and 293 K on pure ZnO and on the Cu/ZnO = 30/70 catalyst sample. For analysis of the gas phase composition in mixed gas CO/CO_2 redox studies a Varian VGA-100 quadrapole gas analyzer was installed on the chemisorption apparatus. The full details of these experiments are reported elsewhere (5).

RESULTS AND DISCUSSION

CO, O_2 and H_2 Chemisorption

The total CO capacities plotted in Figure 1 are seen to increase with increasing copper content in the binary Cu/ZnO catalysts, with maximum coverage obtained for pure copper. While no adsorption of CO was observed on pure ZnO at 293 K, the saturated coverage obtained for CO on copper is Θ = 0.15-0.18 using the range of site densities estimated for copper surfaces. The strong CO fraction however, shows a double humped feature with broad maxima at the Cu/ZnO = 30/70 and 67/33 compositions. In Figure 2 is shown a comparison between the weak CO and irreversible O_2 chemisorption data. It can be seen from the figure that weak CO capacities show good linearity with irreversible O_2 adsorption, has zero intercept and correctly predicts the observed CO capacity on pure copper.

The series of binary Cu/ZnO catalysts studied here may be divided into two groups, Cu/ZnO = 0/100-30/70 and 40/60-67/33 compositions, which are distinguishable by their crystallite sizes and morphological constitutions as reported earlier (7). Also, a substantial portion of copper was found to be X-ray amorphous (8) and scanning transmission electron microscopy analyses showed this amorphous copper to be in the ZnO phase (7). In an attempt to correlate the chemisorption behavior determined here, with the microstructure and distribution of elements reported earlier in the catalyst particles, four models are proposed below to describe the adsorption behavior of oxygen and carbon monoxide. They are as follows:

Model I — Irreversible O_2 and weak and strong CO adsorption occurs on copper crystallites only.

Model II — Irreversible O_2 and weak CO are adsorbed on copper crystallites; strong CO adsorbs on solute copper.

Model III — Irreversible O_2 is adsorbed on copper crystallites and solute copper. Weak and strong CO are on copper crystallites.

Model IV — Irreversible O_2 is adsorbed on copper crystallites and solute copper. Weak CO on copper crystallites, strong CO on solute copper.

It is apparent from Figure 2 that the sites for weak CO and irreversible O_2 are the same and can readily be attributed to the crystalline copper phase. Further, the strong CO capacities cannot be correlated directly with irreversible O_2 capacities and Models I, III and IV are therefore discarded. On this basis, using the specific adsorption of O_2 on pure copper as well as the measured total surface areas the copper and zinc oxide surface areas in the composite catalysts were determined and the results are shown in Table 1. The methanol synthesis activity does not correlate with either the ZnO or Cu surface areas in the individual catalysts.

With the zinc oxide surface areas available a test can be made of the dependence of strong CO capacities on the surface concentration of solute copper assuming the surface concentration to be proportional to the bulk concentration reported by Bulko et al (8). The plot of surface coverage by strong CO against the concentration of copper solute shown in Figure 3 has a linear portion for each morphology. Therefore, if the strongly bound CO molecules titrate the surface copper solute sites, then the basal (0001) ZnO planes tend to accomodate more solute copper atoms than the prism (10$\bar{1}$0) planes, which predominate in the compositional ranges Cu/ZnO = 40/60-67/33 and 0/100-30/70 respectively. Since the basal plane of ZnO is formally electrostatically charged while the prism plane is not, its higher accomodation of copper is consistent with the idea that the solute copper species are also charged. These solute copper sites are therefore considered to be the active centers for strong carbon monoxide adsorption and the adsorption characteristics of CO and O_2 are adequately described by Model II.

The amounts of weakly adsorbed hydrogen is proportional to that of irreversibly adsorbed O_2 but the relationship is not linear. Further, the weak H_2 capacities lie above the capacities predicted by pure copper metal and cannot be accounted for by total H_2 coverage on metallic copper surface. Without further evidence therefore, adsorption of H_2 on copper solute sites on the ZnO phase, created by the Cu-ZnO interactions, cannot be excluded.

Redox Behavior with CO/CO_2 Mixtures

The studies on the redox behavior of the Cu/ZnO catalysts were done on, and are of particular interest for the Cu/ZnO = 30/70 catalyst since it is the most active one and was used by Chatikavanij (9) in CO_2 kinetic studies.

The CO_2 isotherms at 523K on a freshly reduced (2% H_2 in N_2) show that there is a very strong interaction of this gas with the Cu/ZnO = 30/70 catalyst, this interaction being stronger but apparently less extensive than with pure ZnO. No carbon monoxide was found in the gas phase when pure CO_2 was added. Upon addition of CO at 523 K to a freshly reduced catalyst, however, a build up of CO_2 in the gas phase was detected. The time dependence of the partial pressure of desorbed CO_2 is shown in Figure 4 for pure ZnO as well as Cu/ZnO = 30/70 samples. There was no preexposure to CO_2 in the samples of Figure 4 and the ZnO areas used in all samples were similar. Also, addition of CO_2 to CO-reduced then outgassed samples gave CO in the gas phase, and as Figure 5 shows, irrespective of whether or not CO_2 is initially present on the surface, the amount of CO_2 desorbed upon CO addition depends only upon the mole fraction of CO in the gas phase.

The redox equilibrium can be represented using the defect notation of Kofstad (12) by the equation

$$CO_{2(g)} + V_o \overset{Kg}{\rightleftharpoons} CO_{(g)} + O_o \qquad 1)$$

where the subscript g denotes gas phase O_o is a lattice oxygen anion and V_o is a lattice oxygen anion vacancy. Adsorption equilibrium for CO and CO_2 on the catalyst surface are given by equations (2) and (3)

$$CO_{2(g)} \overset{K_{CO_2}}{\rightleftharpoons} CO_{2(s)} \qquad 2)$$

$$CO_{(g)} \overset{K_{CO}}{\rightleftharpoons} CO_{(s)} \qquad 3)$$

where subscript s denotes surface.

Using equations (1)-(3) a model equation was developed (5) for the redox equilibria data shown in Figure 5. It was estimated from fitting the data that

$$\frac{K_{CO}}{K_{CO_2}} = 1.3$$

and

$$Kg = 40$$

The value obtained for Kg is neither that for the redox equilibrium of pure ZnO nor pure Cu_2O. This result points to the presence of a compound of intermediate composition such as might be realized from a disolution of copper in zinc oxide as proposed earlier (4). Klier et al (10), in a quantitative study of the kinetics of methanol synthesis for the Cu/ZnO = 30/70 catalyst in the presence of CO_2, reported three sets of constants with which best fits were obtained for three cases involving competitive adsorption schemes of CO, CO_2 and H_2. The values given above for Kg and K_{CO}/K_{CO_2} are consistent with the values they report for the scheme wherein CO_2 competes with both CO and H_2, but CO and H_2 are adsorbed on different sites.

The solubility limit of copper (II) oxide in zinc oxide is 4-6% (11,12) whereas Bulko et al (8) measured up to 16.8%. Since it was earlier concluded that the copper solute species is a charged entity it appears substantiated that the solute copper species exist as copper (I) in zinc oxide.

CONCLUSIONS

The following important conclusions emerge from this work:

1. The sites for weak CO and irreversible O_2 adsorption are the same and readily attributable to the crystalline copper phase.
2. The methanol synthesis activity does not correlate with either the ZnO or Cu surface areas in the composite catalysts.
3. Strong CO chemisorption is associated with the surface copper solute sites which are preferentially accommodated on the electrostatically charged basal plane of ZnO.
4. The ZnO phase in the composite catalyst undergoes redox equilibria in CO/CO_2 mixtures at 523 K with an equilibrium constant that is different from those for pure ZnO or Cu_2O.
5. The solute copper species exist as copper (I) in zinc oxide and are probably the reactive centers in methanol synthesis from synthesis gas.

LITERATURE CITED

(1) M. Patart, French Patent 540,343 (August, 1921).
(2) Brocker, F. J., German Patent 2,116,949 (October 19, 1972); assigned to BASF.
(3) Audibert, Q, and Raineau, A., Ind. Eng. Chem., 20, 1105 (1928).
(4) Herman, R. G., Klier, K., Simmons, G. W., Finn, B. P., Bulko, J. B., and Katylinski, T. P., J. Catal., 56, 407 (1979).
(5) Parris, G. E., Ph.D. Thesis, Lehigh University, Bethlehem, Pa. (1982).
(6) Zettlemoyer, A. C., Yu, Y. F., Chessick, J. J. and Healey, F. H., J. Phys. Chem., 61, 1319 (1957).
(7) Mehta, S., Simmons, G. W., Herman, R. G. and Klier, K., J. Catal., 57, 339 (1979).
(8) Bulko, J. B., Herman, R. G., Simmons, G. W., and Klier, K., J. Phys. Chem., 83, 3118 (1979).
(9) Chatikavanij, V., M. S. Thesis, Lehigh University, 1980.
(10) Klier, K., Chatikavanij, V., Herman, R. G. and Simmons, G. W., J. Catal., 74, 343 (1982).
(11) Chapple, F. H. and Stowe, F. S., Proc. Brit. Ceram. Soc., 1, 45 (1964).
(12) Schiavello, M., Pepe, F. and DeRossi, S., J. Phys. Chem., 92, 109 (1974).

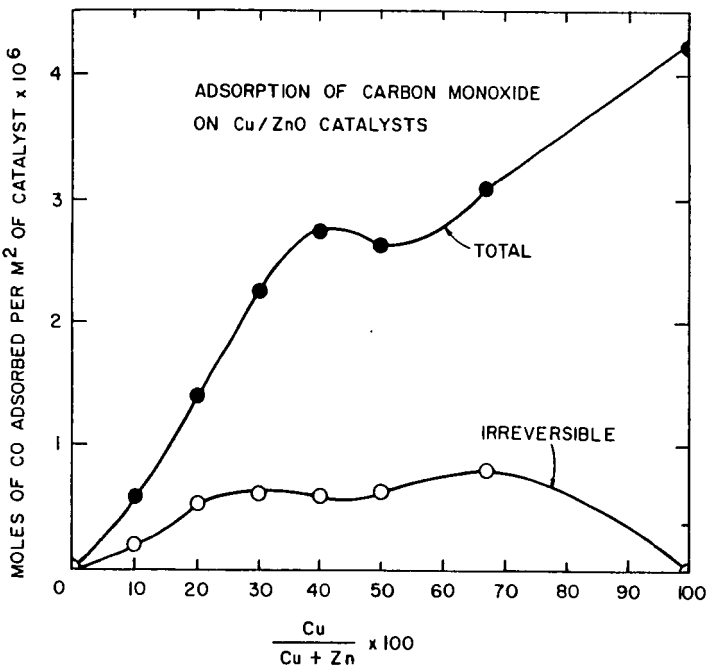

Figure 1. The dependence of the carbon monoxide saturation adsorption (total) and irreversible adsorption (irreversible) on the Cu/ZnO ratio in the binary copper-zinc oxide catalysts.

Table 1

Surface Area of Copper Metal and Zinc Oxide in the Binary Cu/ZnO Catalysts

Catalyst Composition Cu/ZnO	Cu Surface Area m^2/g Catalyst	ZnO Surface Area m^2/g Catalyst	Total Surface Area m^2/g Catalyst
0/100	--	24.1	24.1
10/90	4.9	30.1	35.0
20/80	8.9	27.6	36.5
30/70	16.0	23.3	39.3
40/60	6.5	8.5	15.0
50/50	5.7	5.4	11.1
67/33	3.9	3.5	7.4
100/0	0.62	--	0.62

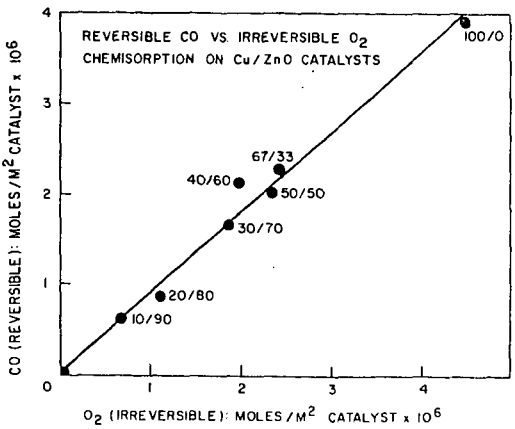

Figure 2. The relation between the amounts of weakly chemisorbed carbon monoxide and irreversibly chemisorbed oxygen indicating that these two adsorbates are a measure of copper metal surface area.

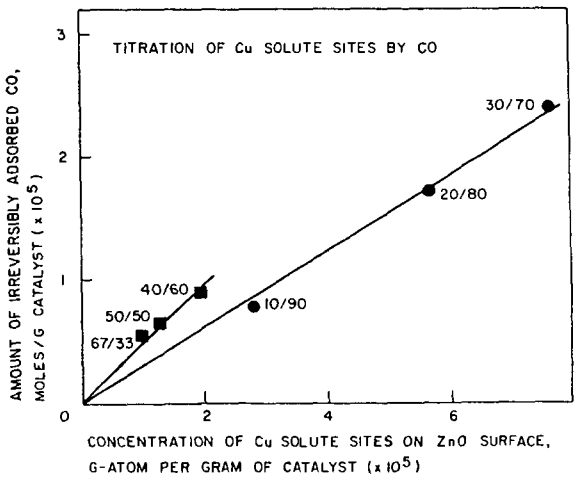

Figure 3. The dependence of the amount of irreversibly chemisorbed carbon monoxide on the concentration of amorphous copper found by X-ray diffraction and by STEM. The (1010) prism planes of zinc oxide are exposed in the Cu/ZnO = 10/90, 20/80, and 30/70 catalysts and the (0001) basal planes of ZnO are exposed in the Cu/ZnO = 40/60, 50/50, and 67/33 catalysts.

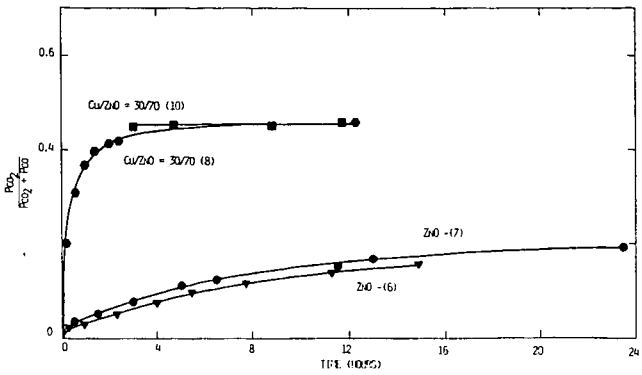

Figure 4. The time dependence of CO_2 partial pressure over ZnO and Cu/ZnO catalysts after CO is admitted to catalyst prereduced in H_2/N_2 = 2/98 vol. % at 523K.

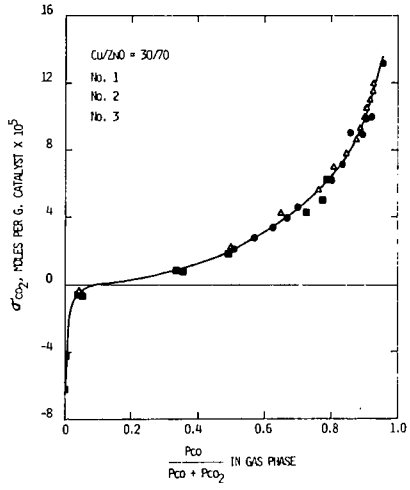

Figure 5. The dependence of σ_{CO_2}, defined as the cummulative amount of CO_2 desorbed from the catalyst surface less the initial amount of CO_2 adsorbed prior to the addition of CO, on the mole fraction of CO in the gas phase.

Nature of H_2 Adsorption Sites in Cu/ZnO Synthesis Catalysts

D. L. Roberts and G. L. Griffin

Department of Chemical Engineering and Materials Science
University of Minnesota, Minneapolis, MN 55455

Abstract

For a co-precipitated Cu/ZnO mixture that is representative of methanol synthesis catalysts, we observe that H_2 adsorption occurs at isolated Cu sites on the catalyst surface. These H_2 adsorption sites differ from those previously observed on pure ZnO samples in two respects: The range of H_2 desorption energies is significantly higher (21-30 kcal/mole for the 10:90 Cu:ZnO mixture, vs. 16-21 kcal/mole for pure ZnO), and the pretreatment temperature needed to activate the sites is lower (523 K for the Cu/ZnO mixture, vs. 673 K for pure ZnO). This suggests that the enhanced activity of Cu/ZnO catalysts, relative to ZnO catalysts, is due to Cu sites that adsorb H_2 more strongly and which maintain their activity at lower temperatures.

Introduction

Catalysts for the direct synthesis of alcohols from $CO:H_2$ mixtures must satisfy two functional requirements. They must activate the CO molecule for reduction without directly dissociating the C-O bond, and they must activate the H_2 molecule to perform the reduction. These two functions are combined quite effectively in the Cu/ZnO catalysts for methanol synthesis (1,2), which hydrogenate CO to CH_3OH with better than 99% selectivity (3).

Understanding the hydrogenation mechanism on these ZnO-based catalysts is important, not only for selecting the optimum operating conditions for methanol catalysts but also for designing catalysts to perform higher alcohol synthesis or other hydrogenation reactions. As a prerequisite for understanding the hydrogenation mechanism itself, in this paper we discuss our current knowledge of the H_2 adsorption sites on ZnO and Cu/ZnO mixtures.

H_2 Adsorption on ZnO

The distinguishing feature of H_2 adsorption on oxide catalysts is that adsorption occurs via heterolytic dissociation of the H_2 molecule at polar surface sites consisting of co-ordinatively unsaturated cation-anion pairs. On ZnO, this adsorption process has been conclusively shown to occur at so-called Type I sites (4-7):

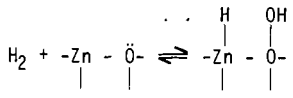

1)

Reaction 1 is demonstrated by bands in the IR spectrum of H_2-saturated catalysts at 1710 cm-1 and 3490 cm-1, assigned to Zn-H and O-H stretching vibrations respectively (4-7).

The energetics of the Type I adsorption sites are fairly complex. Adsorption is activated but reversible at room temperature. A range of adsorption and desorption energies are observed, suggesting that more than one kind of Type I site exists. The equilibrium adsorption energy is 12-13 kcal/mole, the activation barrier for adsorption is 3-8 kcal/mole, and the desorption energy is 16-21 kcal/mole (7).

A second type of H_2 adsorption state has also been identified that is irreversible at room temperature (5). This so-called Type II state is not IR active, and consequently has not been studied as intensively as the Type I state. Dent et al. (8) have shown that Type II hydrogen is not involved in hydrogenation reactions, at least for the case of ethylene hydrogenation. The authors go on to speculate that Type II hydrogen may be bound in sub-surface sites, and therefore is non-reactive. While this remains to be proven conclusively, we will restrict the remaining discussion to Type I sites.

The geometry of the Type I sites has been partially determined. Temperature programmed desorption experiments show that H_2 molecules are adsorbed at spatially discrete sites: The coverage dependence of the TPD spectra indicate that desorption obeys first-order kinetics (cf. Fig. 1 below). Also, co-adsorbed H_2-D_2 mixtures retain most of their isotopic identity when desorbed. Both results are in marked contrast to the second order desorption kinetics and isotopic scrambling seen in TPD spectra of H_2 and D_2 on metals, where H atoms may interact with any of several neighbors during desorption.

The Type I sites are located within next-nearest neighbor proximity of each other. This is shown by the shifts of the ZnH and OH vibrational frequencies that occur as H_2 coverage increases. These shifts can be explained on the basis of electrodynamic and inductive interactions between oscillating ZnH and OH dipoles, provided that H_2 molecules adsorbed at different sites are within two lattice spacings of each other (9). (The shifts do not appear to be caused by long range electronic interactions involving the ZnO conduction band electrons, because the background transmission of the sample, and hence the Fermi level, remains unchanged during H_2 adsorption). Further evidence that the sites are spatially proximate is given by the observation that scrambling of H_2-D_2 mixtures does occur readily over ZnO at room temperature, where adsorption is reversible (5). This shows that migration and exchange between Type I sites does occur, albeit with a modest activation barrier.

Additional information about the nearest-neighbor geometry of the sites is provided by spectroscopic measurements of co-adsorbed CO:H_2 mixtures (10,11). These results show that the ZnH vibrational band undergoes two sequential, discrete frequency shifts as the CO coverage is increased. In contrast, the OH vibration shows only a continuous frequency shift with increasing CO coverage. Thus the Zn cation of the Type I sites appears to have two nearest neighbor sites that can adsorb CO, while the O anion of the Type I site has no such neighbors. Since the CO adsorption state that is occupied under the conditions of these experiments is known to occur at coordinately unsaturated Zn cations (12), this leads to the perhaps surprising conclusion that the Zn cation of the Type I site has two unsaturated Zn cations as neighbors, while the O anion has no unsaturated cations as neighbors (other

than its own Type I cation partner). However, such a "triad" of unsaturated Zn cations would be expected at an $O^=$ vacancy produced when a three-fold co-ordinated surface O anion is removed from the surface layer (10). Moreover, if this anion vacancy is produced by a dehydration reaction with the proton of a neighboring surface OH group, then the unsaturated O anion that remains after proton removal can serve as the anion partner in the Type I site.

Such oxygen vacancies can be most easily imaged on the basal $(000\bar{1})$ oxygen plane (10). This is supported by the fact that Type I sites are most easily observed on powdered samples that contain a large fraction of polar planes in their crystal morphology (13), and also by the fact that sublimation occurs more readily on the basal oxygen face (14). However, recent studies of ZnO single crystal surfaces have raised the possibility that such vacancies might also be produced at step defects on the $(10\bar{1}0)$ prism planes (15,16).

One other important feature of the Type I sites is their strong poisoning by adsorbed H_2O or CH_3OH (5):

2)

Reaction 2 is irreversible at room temperature, indicating that the desorption energy of these adsorbates is much greater than for H_2. Quantitative measurements of the desorption energies are still needed.

It is generally believed that the activation mechanism for producing the Type I site is dehydration to produce a cation-anion pair site. While this is certainly a necessary condition, experience in our laboratory has shown that it is not sufficient. Heating ZnO samples to less than 673K produces highly dehydrated surfaces, as indicated both by a sharp decrease in the IR bands due to residual OH species on the sample, and by the ability of the sample to re-adsorb H_2O. However, these surfaces are not active for the adsorption of H_2. In light of the discussion above, this suggests that an additional requirement for activating the Type I sites is that the dehydration step must also produce an $O^=$ anion vacancy. Adsorption of H_2O or CH_3OH thus represents a strong poisoning reaction, because these species re-occupy the $O^=$ vacancy.

H_2 Adsorption on Cu/ZnO

The results discussed above have been obtained for pure ZnO. While the ZnO Type I sites have been suggested as the source of the hydrogenation activity in Cu/ZnO synthesis catalysts (3), their presence has not been conclusively demonstrated on Cu/ZnO mixtures. As a first test for their presence, we therefore examined the H_2 adsorption behavior of a Cu/ZnO mixture with a 10:90 Cu:Zn ratio, prepared using the co-precipitation technique described by Hermann et al. (3).

In figures 1 and 2 we compare the H_2 desorption spectra of pure ZnO and the Cu/ZnO mixture. After outgassing each sample at the necessary temperature, the spectra were obtained by admitting the indicated pressure

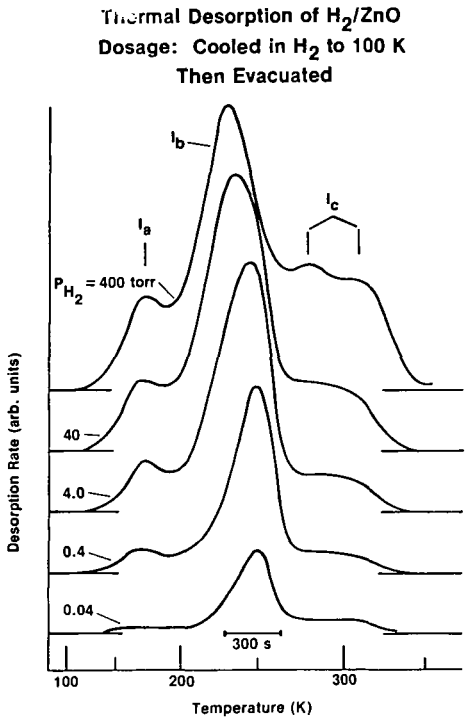

FIGURE 1

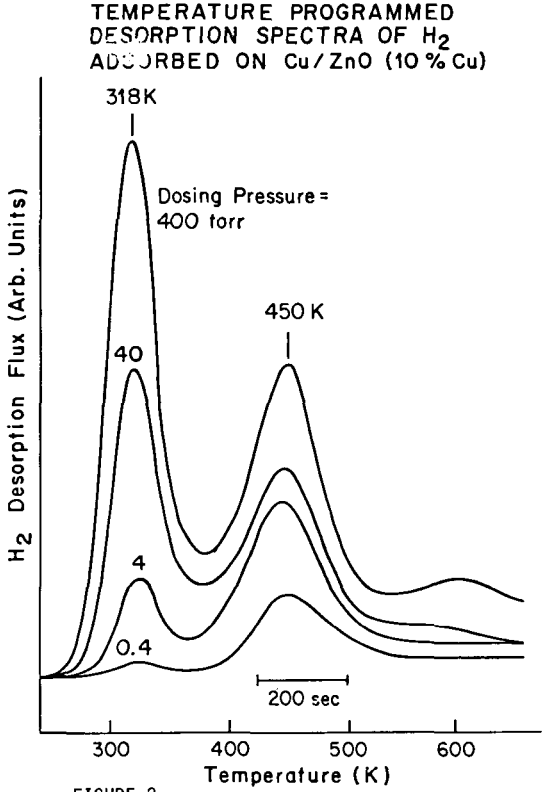

FIGURE 2

of H_2 to the sample cell at room temperature, cooling the sample to 100K, evacuating the non-adsorbed gas, and then warming the sample (heating rate = 1.5 K/sec) while monitoring the flux of desorbing H_2. This dosing procedure was required to overcome the activation barrier for adsorption noted above.

The results for pure ZnO (Figure 1) have been discussed elsewhere in more detail (7). First we note that the spectra are quite complex, suggesting the presence of multiple binding states. The amount of H_2 adsorbed increases with dosing pressure, indicating that the activation barrier for adsorption increases with coverage. The peak temperatures are only weakly dependent on coverage, indicating first order kinetics. (First order kinetics are also indicated by the absence of isotopic scrambling, as noted above). The peak temperatures occur at 170, 240, 270, and 310 K, corresponding to desorption energies of 12, 16, 18, and 21 kcal/mole, respectively. No additional information about the individual states corresponding to each peak is available, except that the state at 170 K has a unique OH vibrational frequency and a small enough desorption energy that it is not occupied at room temperature. Finally, we note that it is necessary to outgas the sample at 673 K or above in order to observe any of these H_2 adsorption states.

The spectra for the Cu/ZnO samples are shown in Fig. 2. As was the case with pure ZnO, we see that the amount adsorbed increases with dosing pressure, indicating that adsorption is an activated process and that the activation barrier increases with coverage. The peak temperatures are again independent of H_2 coverage, suggesting first order desorption kinetics. However, two differences from the results for ZnO are observed: The peak temperatures are 310 K and 450 K, corresponding to desorption energies of 21 and 30 kcal/mole. These are higher than the range of energies found for ZnO. In addition, these experiments were performed using samples outgassed at 523 K, instead of the 673 K needed for ZnO. As mentioned above, pretreating ZnO at the lower temperature results in a surface with negligible H_2 adsorption capacity.

Discussion

We first consider what these results indicate about chemical bonding at the adsorption sites on Cu/ZnO catalysts. The fact that H_2 adsorption is observed after pretreatment at much lower temperature for the Cu/ZnO mixture than for pure ZnO indicates either that Cu species make it easier for the Type I ZnO sites to be activated, or else that Cu species themselves can function as the cations in Type I sites that have a much lower activation temperature. Competitive adsorption experiments with $CO:H_2$ mixtures described elsewhere (17) indicate that the latter explanation is correct; that is, the Cu species themselves participate as the cations in Type I sites analogous to those found on pure ZnO. The lower temperature required to activate the Cu sites suggests that the $O^=$ vacancy needed at a Type I site is more easily produced at a Cu neighbor, which is consistent with the lower enthalpy of decomposition of bulk CuO (36 kcal/mole for CuO, vs. 81 kcal/mole for ZnO (18)).

The higher desorption energy for H_2 may be the result of the d-electron vacancy on a divalent Cu cation, which would stabilize the CuH hydride bond (19).

Finally, we consider the implication of these results for the hydrogenation

mechanism on Cu/ZnO catalysts. The lower pretreatment temperature needed to activate the Cu Type I sites is remarkably consistent with the lower operating temperature required for Cu/ZnO synthesis catalysts, relative to the high pressure ZnO catalysts. The stronger H_2 adsorption energy may also contribute to the improved activity of the Cu/ZnO catalysts, although more detailed knowledge of the energetics of the subsequent reaction steps is needed before this conclusion can be stated with certainty. Finally, it is interesting to note that this H_2 adsorption behavior has not been reported for Cu species prepared on other supports. This suggests that the basicity and/or the tetrahedral coordination geometry of the ZnO lattice may be necessary to generate Type I cation-anion sites. This last point suggests that the potential of ZnO as a support material for hydrogenation catalysts should be more fully explored.

Acknowledgment: One of us (DLR) acknowledges fellowship support from Chevron Research Company, Standard Oil Company of California. This research was supported by the National Science Foundation, grant no. CPE-8105823.

References

1) G. Natta; in Catalysis (P. H. Emmett, ed., Reinhold, 1955) Vol. 3, p. 349

2) K. Klier; Adv. in Catal. 31 243 (1982)

3) R. G. Herman, K. Klier, G. W. Simmons, B. P. Finn, J. B. Bulko, and T. P. Kobylinski; J. Catal. 56 407 (1979)

4) R. P. Eischens, W. A. Pliskin, and M. J. D. Low; J. Catal. 1 180 (1962)

5) R. J. Kokes, A. L. Dent, C. C. Chang, and L. T. Dixon; JACS 94 4429 (1972)

6) F. Boccuzzi, E. Borello, A. Zecchina, A. Bossi, and M. Camia; J. Catal. 51 150 (1978)

7) G. L. Griffin and J. T. Yates, Jr.; J. Catal. 73 396 (1982)

8) A. L. Dent and R. J. Kokes; J. Phys. Chem. 73 3781 (1969)

9) G. L. Griffin and J. T. Yates, Jr.; J. Chem. Phys. 7 3744 (1982)

10) F. Boccuzzi, E. Garrone, A. Zecchina, A. Bossi, and M. Camia; J. Catal. 51 160 (1978)

11) G. L. Griffin and J. T. Yates, Jr.; J. Chem. Phys. 77 3751 (1982)

12) R. R. Gay, M. H. Nodine, V. E. Henrich, H. J. Zeiger, and E. I. Solomon; JACS 102 6752 (1980)

13) M. Grunze, W. Hirschwald, and D. Hofmann; J. Crystal Growth 52 241 (1981)

14) D. Kohl, M. Henzler, and G. Heiland; Surf. Sci. 41 403 (1974)

15) W. H. Cheng, S. Akhter, and H. H. Kung; J. Catal. 82 341 (1983)

16) L. Chan and G. L. Griffin (to be submitted)

17) Handbook of Chemistry and Physics (52nd ed., Chem. Rubber Co., Cleveland, 1972) Table D-61

18) B. Kunz; in Theory of Chemisorption (Topics in Current Physics, Vol. 19, Springer Verlag, 1980) p. 115

MICROSTRUCTURE OF $Cu/ZnO/Al_2O_3$ METHANOL SYNTHESIS CATALYSTS STUDIED BY SCANNING AND TRANSMISSION ELECTRON MICROSCOPY AND DIFFRACTION METHODS

P. B. Himelfarb, G. W. Simmons, and K. Klier

Department of Metallurgy and Materials Engineering,
Department of Chemistry, and Center for Surface and
Coatings Research, Lehigh University,
Bethlehem, PA 18015

INTRODUCTION

Catalysts containing Cu/Zn/Al are well known active catalysts in methanol synthesis and the water-gas shift reaction, and have been described extensively in the literature (1-6). However, limited information is available on the elemental distributions in the various morphologies present in the many preparative variants of these catalysts. The understanding of these material properties and their relationship to synthesis activity is a primary goal in catalyst characterization. In the present work, transmission electron microscopy coupled with diffraction and elemental analysis was used to compare the chemical structure, morphology and elemental distribution in three different preparations of active Cu/Zn/Al catalysts.

EXPERIMENTAL

Two catalysts were prepared from Zn(II), Cu(II) and Al(III) acetate solution by coprecipitation with sodium carbonate at 90°C until a pH of 6.9 was reached to produce the compositions, Cu/Zn/Al equal to 54.4/24.3/23.3 and 27.3/63.6/9.0 at.% (prepared at Lehigh University). Another catalyst was similarly prepared from nitrate solution at 30°C to produce Cu/Zn/Al equal to 60.0/30.0/10.0 at.% (prepared at the University of Virginia). In all preparations, the precipitates were washed extensively, calcined in air at 350°C, and reduced at 250°C in a 60-70 cc/min 2% H_2/N_2 mixture for the time required for the stoichiometric reduction of CuO to Cu. Methanol synthesis activities were determined in a tubular fixed bed flow reactor equipped with pressure, temperature and flow rate controls (7,8). Methanol yields were determined by gas chromatography.

A Philips EM 400T transmission electron microscope (TEM) which included a scanning transmission mode (STEM) was used in the characterization studies. Samples were prepared by dispersing the catalyst powders in ethanol and placing a drop of the dispersion on a carbon coated titanium grid. Exposure time to air was minimized by preparing and transporting specimens in a N_2 filled glove bag. Energy dispersive X-ray analysis (EDS) for elemental identification and quantification was obtained in the manner described in references (4) and (9).

RESULTS

Methanol yields and respective surface areas for the catalysts studied are given in Table I. Data published for catalysts of similar

TABLE I

ACTIVITIES OF Cu/Zn/Al CATALYSTS

#	Catalyst Cu/Zn/Al at.%	Surface Area m^2/g	MeOH Yield g/g cat/hr
1	60.0/30.0/10.0[a]	54.2	1.35
2	52.4/24.3/23.3[b]	26.0	1.37
3	27.3/63.6/9.0[c]	61.8	1.55
4	67.0/33.0/0.0 (7)	7.4	0.41
5	30.0/70.0/0.0 (7)	39.3	1.35

[a]Prepared from nitrate solution, tested at 80 atm, 255°C, GHSV = 5600 hr^{-1}, $H_2/CO/CO_2$ = 69/27/4 (8).

[b]Prepared from acetate solution, tested at 75 atm, 250°C, GHSV = 5000 hr^{-1}, $H_2/CO/CO_2$ = 70/24/6 (10).

[c]Prepared from acetate solution, tested at 75 atm, 250°C, GHSV = 3750 hr^{-1}, $H_2/CO/CO_2$ = 70/24/6.

Cu/Zn compositions prepared without Al are given for comparison (7). As shown, high yields are maintained within a large variation in elemental composition. Elemental distribution, morphology, and chemical structure were determined for catalysts 1 and 3 (cf. Table I), and the results were compared with previously published data on catalyst 2 (10).

Two distinctly different morphologies were observed in both catalysts 1 and 3. One morphology was a platelet structure containing all three metals (Cu/Zn/Al) which gave a ZnO (0001) electron diffraction pattern, and appeared similar to the platelet morphology reported in catalyst 2 (10). The other morphology was lacelike and contained two metals (Cu/Zn) in the form of Cu and ZnO as determined by selected area diffraction (SAD). The lace-like morphology appeared similar to that found in an active Cu/ZnO (30/70 at.%) methanol catalyst (4,11). Micrographs of the ternary platelet and binary lace-like morphologies with corresponding dark field images from ZnO are given in Figures 1 and 2, respectively. The dark field micrographs show that the ZnO is more highly dispersed in the ternary platelet morphology. An SAD pattern of a platelet is given in Figure 3 which shows that the ZnO (0001) and Cu($\bar{1}$11) planes are parallel to the surface of the platelet. The epitaxial relationship between the Cu and ZnO shows that the Cu[0$\bar{2}$2] axis is parallel to the ZnO[1$\bar{2}$10] axis, which was similarly found in catalyst 2 (10) and in the Cu/ZnO (30/70 at.%) catalyst (4). Although the spot patterns appear to have been produced by single crystals, they originate from highly dispersed Cu and ZnO crystallites in crystallographic registry.

Crystal sizes of ZnO determined from TEM dark field images in the ternary platelet and binary lace-like morphologies, and Cu and ZnO crystallite sizes determined by X-ray diffraction line broadening are given in Table II for catalysts 1 and 3. Published data for catalyst 2 is also given for comparison (10). The microstructural similarities

TABLE II

MORPHOLOGIES AND CRYSTALLITE SIZES OF Cu/Zn/Al CATALYSTS

Catalyst #	Bulk Composition Cu/Zn/Al at.%	Abundance[a] of Platelets	ZnO by TEM (nm)[b]		XRD (nm)[c]	
			Platelet	Binary	ZnO	Cu
1	60.0/30.0/10.0	≅ 10%	2.6	9.1	7.0	12.4
2	52.4/24.3/23.3	≅100%	2-4	d	--	--
3	27.3/63.6/9.0	≅ 20%	2.6	11.9	12.3	8.9

[a]Given as the percent abundance of the ternary platelet morphology compared to the binary lace-like morphology.

[b]ZnO crystal sizes are an average of 100 measurements from TEM dark field measurements produced from the ZnO{10$\bar{1}$0}, {0002}, and {10$\bar{1}$1} reflections for the binary morphology, and from the ZnO(1$\bar{1}$00) diffraction spot for the platelet morphology.

[c]Crystallite sizes determined by X-ray diffraction line broadening using the Scherrer equation corrected for instrumental broadening (12); the Cu{111} and an average from the ZnO{10$\bar{1}$0}, {0002}, and {10$\bar{1}$1} reflections were used.

[d]Lace-like binary phase not present.

are striking in the platelet morphology in that the ZnO crystal sizes are essentially identical in catalysts 1, 2 and 3, and the epitaxial relation between Cu and ZnO was commonly observed. The higher average ZnO crystal sizes, determined by X-ray diffraction, reflect the higher concentration of the binary lace-like morphology which has larger ZnO crystallite sizes than the platelet morphology. In contrast to catalysts 1 and 3, catalyst 2 had large (greater than 0.1 μm) Cu particles and the binary lace-like morphology was not detected (10).

Elemental distributions in the platelets determined by EDS were: Catalyst 1 had the composition 4.5 ± 3.8 at.% Cu, 75.5 ± 2.8 at.% Zn, and 20.0 ± 1.9 at.% Al from 27 measurements, and catalyst 3 platelets contained 24.5 ± 7.9 at.% Cu, 56.6 ± 5.8 at.% Zn, and 18.9 ± 7.8 at.% Al from 23 measurements. No Al was detected in the binary lace-like morphology in catalyst 3, and in catalyst 1 a weak Al peak was sometimes observed which corresponded to less than 1 wt.% in the binary morphology. No evidence of crystalline Al-containing compounds was found by either X-ray or electron diffraction analysis. EDS analysis of platelets in catalyst 2 resulted in 8 ± 2 at.% Cu, 50 ± 5 at.% Zn, and 42 ± 4 at.% Al (10).

DISCUSSION

Comparison of the methanol yields for the three Al-containing catalysts studied shows that active catalysts can be prepared from either acetate or nitrate solutions, and that high concentrations of

Cu are not necessary for high activity.

The activity of catalyst 2 has been attributed to the platelet morphology because the only other morphology present was large inactive Cu particles, as reported earlier (10). Since methanol yields for catalysts 1, 2 and 3 are similar, and the relative abundance of the platelet and lace-like morphologies varied significantly (see Table II), the activity of the platelet and lace-like morphologies must be comparable. Binary Cu/ZnO catalysts have been prepared with high methanol synthesis activity (see catalyst 5 in Table I). The activity of the binary lace-like morphology in catalysts 1 and 3, which contains little or no Al, supports the view that an Al_2O_3 component serves basically as a structural promoter (2).

A comparison of catalysts 2 and 3 (which have similar activities but dramatically different Cu/Zn ratios) to catalysts of similar Cu/Zn ratios prepared without Al (see catalysts 4 and 5 in Table I) shows that the addition of Al widens the Cu/Zn compositional range which can be used to produce an active catalyst. This is a result of the increased dispersion of Cu and ZnO occurring in the Al-containing catalysts.

In summary, active Cu/Zn/Al methanol synthesis catalysts do not require high concentrations of copper. Three basic morphologies — large Cu particles (greater than 0.1 μm), Cu/Zn/Al polycrystalline platelets, and a binary Cu/ZnO morphology can be produced in different amounts by variations in the initial elemental concentrations and preparation conditions. The ternary platelet and binary lace-like morphologies are active in methanol synthesis, which is believed to be a result of the intimate dispersion of the Cu and ZnO crystallites in both morphologies. The Al component, which appears amorphous, is a structural support in the platelets, and widens the Cu/Zn ratio range for which high dispersion of Cu and ZnO can be obtained.

ACKNOWLEDGMENTS

This research was supported by the U.S. Department of Energy through the Pittsburgh Energy Technology Center (Grant No. DE-FG22-80PC30265).

REFERENCES

(1) Kung, H. H., Catal. Rev. - Sci. Eng. 22(2), 235 (1980).

(2) Klier, K., Adv. Cat. 31, 243 (1982).

(3) Shimomura, K., Ogawa, K., Oba, M, Kotera, Y., J. Catal. 52, 191 (1978).

(4) Mehta, S., Simmons, G. W., Klier, K., Herman, R. G., J. Catal. 57, 339 (1979).

(5) Natta, G., (Emmett, P. H., ed.) "Catalysis Volume III," Reinhold Publishing Corp., New York, 1955, p.349.

(6) Imperial Chemical Industries, "Catalyst Handbook," Springer-Verlag, New York, Billing and Sons Ltd., 1970.

(7) Herman, R. G., Klier, K., Simmons, G. W., Finn, B. P., Bulko, S. B., J. Catal. 56, 407 (1979).

(8) Bieser Jr., A. L., Ph.D. Thesis, University of Virginia, Charlottesville, VA (1983).

(9) Himelfarb, P. B., Master's Thesis, University of Virginia, Charlottesville, VA (1983).

(10) Herman, R. G., Simmons, G. W., Klier, K., Proceedings of the 7th International Congress on Catalysis, Tokyo, June 30 - July 4, 1980 (1981).

(11) Cullity, B. D., "Elements of X-Ray Diffraction," 2nd edition, Addison-Wesley Publishing Co., Inc. 1978, p.284.

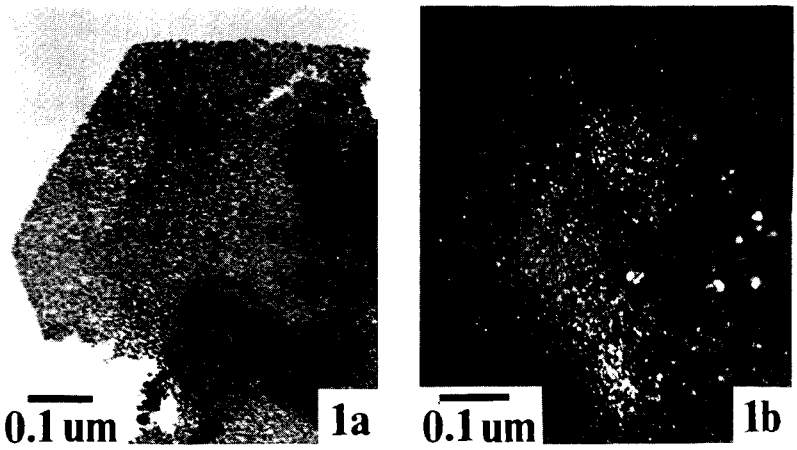

Figure 1. Electron micrographs of ternary platelet morphology in catalyst 3 (Cu/Zn/Al at.% = 27.3/63.6/9.0). (a) Bright field image, (b) dark field image from a ZnO($1\bar{1}00$) diffraction spot (see Fig. 3).

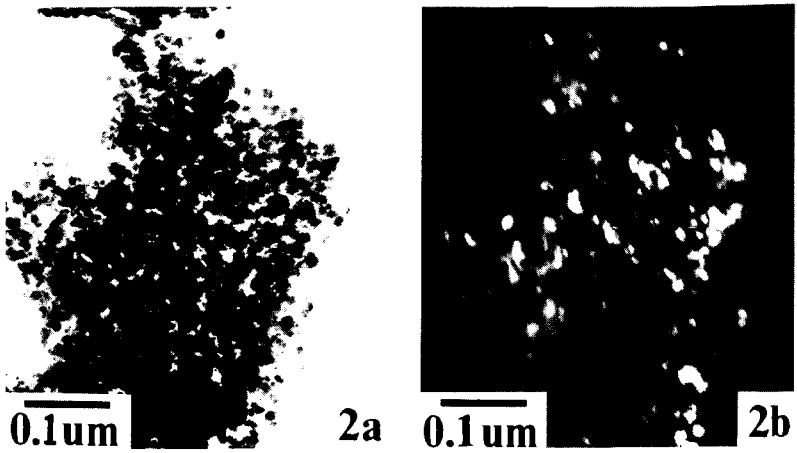

Figure 2. Electron micrograph of binary lace-like morphology in catalyst 3 (Cu/Zn/Al at.% = 27.3/63.6/9.0). (a) Bright field image, (b) dark field image from ZnO{$10\bar{1}0$}, {0002}, and {$10\bar{1}1$} diffraction rings.

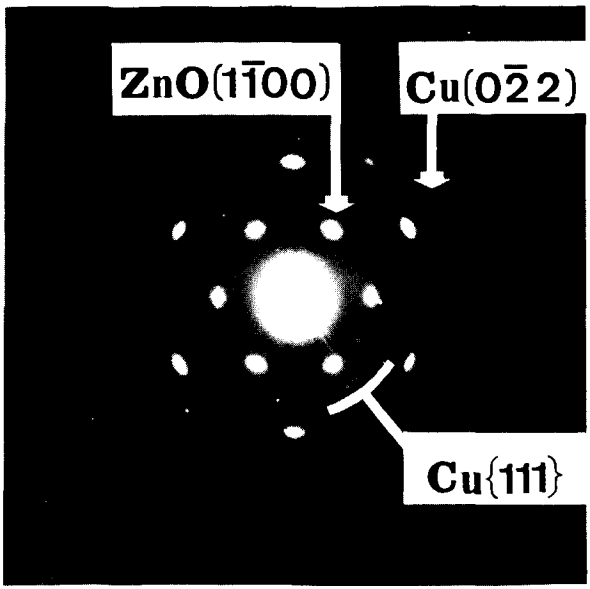

Figure 3. Selected area diffraction pattern of the ternary platelet morphology in catalyst 3 (Cu/Zn/Al at.% = 27.3/63.6/9.0) showing randomly oriented Cu, from the Cu{111} ring pattern, and single crystal patterns of Cu($\bar{1}$11) and ZnO(0001), defined by the Cu(0$\bar{2}$2) and ZnO(1$\bar{1}$00) diffraction spots.

CRYSTAL AND CATALYTIC CHEMISTRY OF METHANOL SYNTHESIS

William R. Moser, Randy Lo, Edward G. DeMattia and John A. Willard

Department of Chemical Engineering, Worcester Polytechnic Institute,
Worcester, MA 01609

Solid solutions of mixed metal oxides in the perovskite (ABO_3) and scheelite (ABO_4) families of crystals were used as host materials for the preparation of methanol synthesis catalysts. These materials contain a partial substitution of a copper (1+) ion in the A-sites of their structures and a Zn(2+) ion in their B-sites as homogeneous solid solutions in a host lattice containing at least two other metal oxides.

$A_xCu_{1-x}B_yZn_{1-y}O_3$ perovskite

$A_xCu_{1-x}B_yZn_{1-y}O_4$ scheelite

The synthesis of these unusual materials was accomplished by recognizing that copper oxides exist as an equilibrium mixture of Cu(1+) and Cu(2+) ions at temperatures in the range of 1100 C in air. Utilizing high temperature synthesis techniques, copper was disproportionated to a mixture of copper(2+) and copper(1+) oxides under oxidizing conditions. When this equilibrium mixture was exposed at high temperatures to a metal oxide composition containing a substoichiometric amount of the A-site cation, the equilibrium was shifted to copper(1+) which was incorporated into the A-site of the host. Due to the removal of Cu(1+) from the equilibrating system by its location in the stable A-site, all of the copper was converted to Cu(1+).

$$4Cu(2+)O \xrightarrow{1100C} 2Cu_2(1+)O + O_2$$

$$xSrCO_3 + ySnO_2 \xrightarrow{1100\ C} Sr_x^{2+}\square_{1-x}Sn_y^{4+}\square_{1-y}O_3$$

$$(1-x)CuO + (1-y)Zn(NO_3)_2 \xrightarrow{1100\ C} (1-x)Cu_2O + (1-y)ZnO$$

$$Sr_x^{2+}Cu^{1+}_{1-x}Sn_y^{4+}Zn_{1-y}^{2+}O_n$$

Support for the structure for these compounds was gained from an analysis of their magnetic susceptibility data, photoelectron spectra, x-ray diffraction data, and analytical analysis. The compounds were shown by the magnetic susceptibility data to be diamagnetic which was consistent with a d-10 copper(1+) ion. The absence of any shake-up structure in their ESCA spectra was

consistent only with a copper (1+) ion incorporated in the A-site of the solid state mixed metal oxide. Copper (2+) ions demonstrated large shakeup satellites in their ESCA spectra.

The objective of the synthesis of these novel materials was to provide a homogeneous solid solution of both the copper(1+) and zinc(2+) ions in the lattices of metal oxides which have unusual thermal and structural stability under reducing conditions. Using these materials which were then further modified by other ions substituted in the A- or B-sites, gradual electronic changes may be made in the copper(1+) ion. The solid solution, ion modified compounds will be subsequently used to understand the activation of carbon monoxide in methanol synthesis.

The activities of these materials as methanol synthesis catalysts were studied at 75 atm. and 230 C. The stabilities of the copper(1+) ions in the host lattices were examined between 200 C to 450 C in separate studies using diluted hydrogen in nitrogen. The methanol synthesis activities of these compounds when compared on a unit surface area basis were generally a bit lower than the copper modified zinc oxide catalysts prepared by coprecipitation. Their surface areas were substantially smaller than the Cu-Zn-O catalyst. In only a few cases was the stability of these solid state solutions toward reduction to copper(0) superior to that of the copper modified zinc oxide catalyst. This finding was surprising since one would expect the Cu(1+) atom of about 0.96 atomic radius to be configurationally stable from purely structural considerations. However, location of the mono-cation in a substantially greater electronegative lattice position contrasted to its solution in pure ZnO, may account for the observation of accelerated reduction in most examples using the complex solid state inorganics. A comparison of the relative rates of reduction of the solid state inorganic solutions to the coprecipitated standard Cu-Zn-O catalyst is shown in Figure 1. These data show that the metal ion composition may be used to regulate stability.

A study of the ease of reduction to metallic copper in a series of 10% metal ion modified copper zinc (25%/65%) oxide catalysts was performed. In addition a newly developed attrition test was used to examine the attrition resistance of these catalysts to mechanical wear. Ten percent concentrations of lanthanum, aluminum, magnesium,strontium, zirconium, tin, tungsten, molybdenum and chromium oxides were prepared with 25% copper oxide and 65% zinc oxide by coprecipitation. These modified compositions were found to be of superior mechanical strength when compared to unmodified 30% copper oxide-70% zinc oxide. In most cases the unmodified catalyst was reduced in hydrogen more easily than the modified ones. The solid state inorganic solutions of copper in the perovskite or scheelite crystals classes were substantially more attrition resistant than the modified copper zinc oxide systems.

FIGURE I RELATIVE DEGREES OF REDUCTION OF

$La_{.8}Cu_{.2}Nb_{.8}Zn_{.2}O_{3.5}$, $Cu_{.73}Zn_{.27}O_{x}$, and $Sr_{.8}Cu_{.2}Mo_{.8}Zn_{.2}O_{3.5}$

to copper zero at temperatures of 150°C to 450°C by 2% hydrogen in nitrogen

at a gas hourly space velocity (GHSV) of 3500 hr^{-1}.

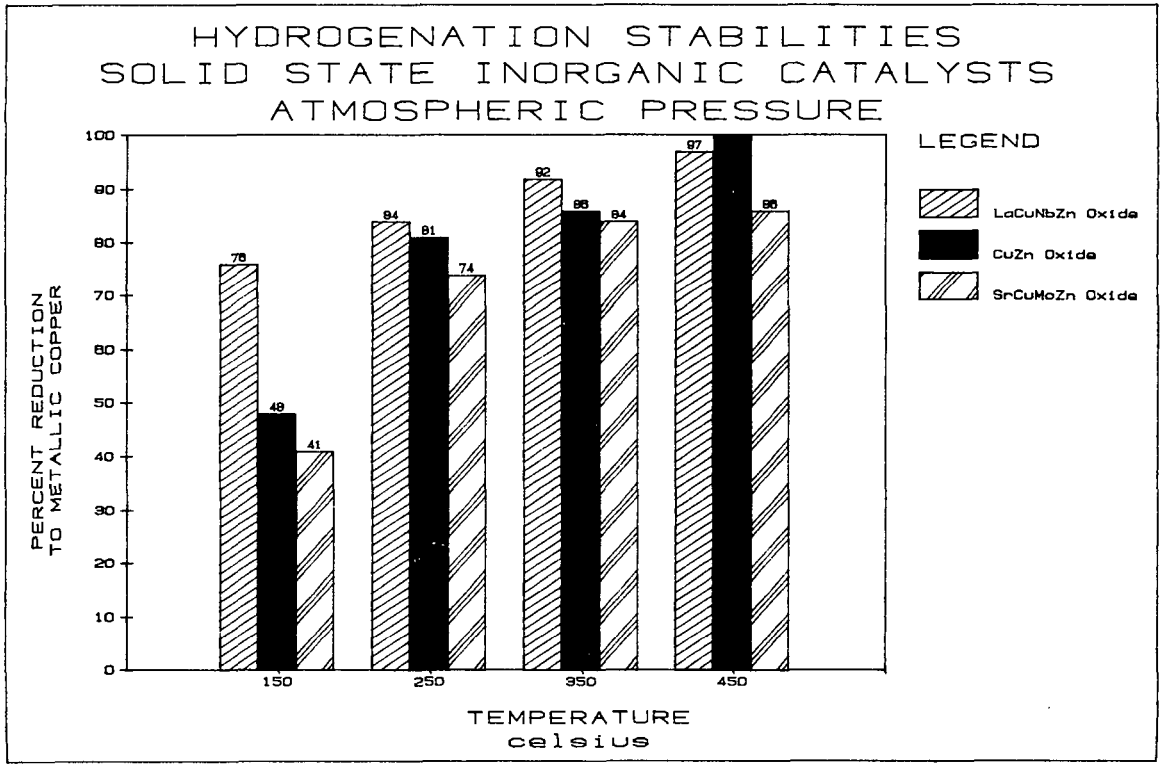

POSSIBLE RELATIONSHIPS OF SITES FOR CO ADSORPTION WITH METHANOL SYNTHESIS ACTIVITY OF SUPPORTED Pd CATALYSTS

H. Deligianni, R. L. Mieville, and J. B. Peri

Amoco Oil Company, P.O. Box 400, Naperville, Illinois 60555

Pd/SiO_2 catalysts with and without promoters for methanol synthesis have been previously studied (1-6), with partially contradictory conclusions. Lunsford, et al. (3), concluded that Pd structural effects play an important role in the activity of the catalyst, since catalysts with small Pd crystallites produce methanol while larger crystallites produce methane. Such structural effects can be induced by different grades of silica support. On the other hand, Ponec, et al. (1,6) believe that electronic factors are more important and Pd II "ions" are the centers for CO activation. The number of such sites is presumably increased by the presence of alkali metals. The effect of alkali metals such as Li appears to be more complex (1,5). Whatever the nature of the active centers, the addition of basic metals as well as the use of basic supports (4) promotes reactivity.

EXPERIMENTAL

The reactor used in testing the methanol synthesis catalyst was a vertical 1/2" stainless steel tube enclosed in a hinged furnace. Cylinder CO and H_2 were fed into the system via pressure regulators and Brook's mass flow controllers. The desired pressure was maintained at the reactor outlet by a pneumatically operated research control valve. Outlet flows were measured by a wet test meter.

Four grams of vacuum-dried catalyst (14-20 mesh) were diluted (if necessary) to a 10 cc volume with α-alumina particles and placed centrally in the reactor. The catalyst was pretreated in situ by passing N_2 at 150°C for 30 minutes, and then passing H_2 at 340°C for 1 hour. Activities were measured after two hours running in a H_2/CO feed of mole ratio 2/1.

Infrared analysis were performed on a computerized IR Beckman 4260 as previously described (7). Corrections were applied for changes in background bands (arising from the support) caused by cooling of the sample when CO was admitted to the cell. Some spectra were recorded with a Perkin-Elmer 1550 FTIR spectrometer.

The catalysts were prepared using two different batches of Davison silica gel, 57 and 59.

Impregnated catalysts were prepared by the incipient wetness technique. Pd ion exchanged catalysts were prepared by the following procedure: The required amount of Pd $(NH_3)_4(NO_3)_2$ solution was added to a slurry of the mixture gel and water. The water was alkalized by adding a few drops of NH_4OH to make the pH ~9.5. After mixing for 1 hour, the silica was washed and filtered and, finally, calcined at 300°C for 2 hours. For the Li doped samples, Li was added as the hydroxide prior to the Pd impregnations.

RESULTS AND DISCUSSION

Activity Measurements

The reproducibility of activity measurements by the reactor was tested and found to be about ±20% of the absolute value in terms of CO converted.

Some preliminary results on pretreatment variations indicated that the initial activity of the unreduced Pd catalysts was half that of the fully reduced catalyst, but that on increasing time on stream, the activity approached that of the fully pretreated catalyst.

Two different batches of Davison silica, #57 and #59, were used in preparing the catalysts. Although specifications for the two were the same, there were some differences in the results observed, as shown in Table I.

Table I. Variation in Silica Support

Conditions: 500 psig, SV = 900 hr^{-1}, 275°C and H_2:CO = 68.2:31.8

Catalyst	Method of Pd Addition	% CO Converted to MeOH
5% Pd/SiO_2 57	Impregnated	0.8
5% Pd/SiO_2 59	with $PdCl_2$ solution	2.5
5% Pd/SiO_2 57	Ion exchanged with	1.2
5% Pd/SiO_2 59	$Pd(NH_3)_4(NO_3)_2$	3.0
5% Pd/1.6% Li/SiO_2 57	Impregnated with	4.6
5% Pd/1.6% Li/SiO_2 59	$PdCl_2$ solution	6.0

In all cases, Davison 59 showed an increase in activity over Davison 57. However, the increase was smallest with the Li promoted catalyst, suggesting the differences in activity may arise out of differences in the amount of residual alkali metal contaminant.

Differences in the mode of adding Pd to the support evidently made little difference in the activity of the catalyst as shown by the data of Table II.

Table II. Variation in Pd Addition
Conditions: As in Table I

Catalyst	Method of Pd Addition	% CO Converted to MeOH
5% Pd/SiO_2 59	Impregnated with $PdCl_2$	2.5
5% Pd/SiO_2 59	Impregnated with $Pd(NO_3)_2$	2.0
5% Pd/SiO_2 59	Ion Exchanged with $Pd(NH_3)_4(NO_3)_2$	2.0
1.5% Pd/SiO_2 57	Impregnated with $PdCl_2$	0.9
1.5% Pd/SiO_2 57	Impregnated with $Pd(NO_3)_2$	0.8

These data were obtained on catalysts ion-exchanged with amino nitrate complex or impregnated with either the nitrate or chloride salt.

Significant differences were observed when Li was added as a promoter.

Table III. Effect of Lithium Promotion
Conditions: As in Table I

Catalyst	Method of Pd Addition	% CO Converted to MeOH
5% Pd/SiO_2 57	Impregnated with	0.8
5% Pd/SiO_2 57 + 1.6% Li	$PdCl_2$	4.6
5% Pd/SiO_2 59	Impregnated with	2.5
5% Pd/SiO_2 59 + 1.6% Li	$PdCl_2$	6.0
5% Pd/SiO_2 59	Impregnated with	2.0
5% Pd/SiO_2 59 + 1.6% Li	$Pd(NO_3)_2$	5.0
1.5% Pd/SiO_2 59	Ion exchanged with	3.0
1.5% Pd/SiO_2 59 + 1.6% Li	$Pd(NH_3)_4(NO_3)_2$	4.3

Table III shows that Li always increased the activity for every catalyst type used. The increase, however, was smallest for the Pd ion exchanged on silica 59 possibly since without Li this catalyst had a higher activity, but, also, this smaller increase could be a result of the absence of residual alkali in the support.

Infrared Spectra

Figures 1 to 5 represent IR spectra of CO adsorbed on some of the catalyst samples whose activities were measured in attempting to relate catalyst performance to catalyst surface properties. Each spectrum is characterized by bands near ~2075 and 1975 cm^{-1} corresponding to weakly-held CO previously assigned to linear and bridged bonding of CO on Pd, respectively (8). The spectra after evacuation and therefore representing strongly held CO, typically show less intense bands near 2060 and 1900 cm^{-1}, again reflecting linear and bridged CO. Additional bands can also be seen. These probably reflect various bridged CO species held on different crystal faces (8).

Figures 1 and 2 show spectra of CO on 5% Pd/SiO_2 made by impregnation of the chloride and nitrate salt respectively. Although the general features are similar, some differences are observed in relative intensities of the bands near 2075 and 1975 cm^{-1} corresponding to a weakly-held linear and bridge bonded CO. Differences can also be seen in the frequencies of bands caused by strongly-held CO remaining after evacuation. No difference was observed in the relative activities of the two catalysts, however.

Figure 3 shows spectra of CO on 1.5% Pd/SiO_2 (ex. $PdCl_2$) which was run on the FTIR. This was the only case where a band at 2165 cm^{-1} was detected.

Figure 4 shows the effect of Li on the CO/Pd spectra obtained for 1.5% Pd ion-exchanged on Davison 59 silica. (Note change in absorbance scale.) The spectrum of CO on the catalyst shows significant differences from those on the impregnated catalysts. A much more intense linear CO band is observed and a relatively weaker bridge-bonded CO band. No difference is seen in the linear CO bands (2060 and 2090 cm^{-1}) when Li is present. Only a slight difference exists between the bridged CO bands, yet a small increase in activity was noted. The strongly-held bridged CO bands in the 1850-1950 cm^{-1} appear to be progressively decreased in intensity and shifted to lower frequencies as Li content increases.

Figure 5 shows spectra of CO on the catalysts of Figures 1 and 2, respectively, after the addition of Li. Comparison with Figures 1 and 2 shows very little effect of Li on the CO spectra in the region above 1950 cm^{-1}. In the region below 1950 cm^{-1}, however, there was a significant increase in both weakly and strongly held bridged CO. There was a large corresponding increase in activity, by factors of 6 and 3, respectively, when Li was present.

DISCUSSION

Spectra of CO on Pd have been thoroughly discussed elsewhere (9). It was initially hoped, and expected, that among the variety of different types of bands observed for CO adsorbed on silica-supported Pd some correlation would be found with methanol synthesis activity. No obvious correlation was, in fact, apparent. Some previous speculation appears to have been excluded by the evidence, however, and possible explanations for Li promotion can be offered.

Careful attention was paid to possible adsorption of CO on Pd^{2+} ions, which would have been expected to give bands above 2100 cm^{-1}, and even, by analogy with Ni^{2+}, as high as 2195 cm^{-1} (9). A band suggestive of Pd^{2+} adsorption sites was seen in only one instance. This was observed with the 1.5% Pd/SiO_2 (ex. $PdCl_2$) sample (Figure 3). After prereduction at 300°C and addition of CO, this catalyst showed a

very weak band at 2165 cm^{-1} which probably reflects CO held on Pd^{2+} ions. This catalyst was, however, one of the least active (see Table II). Unreduced Pd would not be expected under reaction conditions in any case, but the fact that activity was found to increase with increasing prereduction of the catalysts and, initially, with increasing time on stream strongly argues that Pd^{2+} sites are not, as postulated by Ponec, et al. (2,6), the active sites.

The infrared spectra show that Li addition has a small but definite effect on the bridged bonding of CO to Pd. Such bonding presumably occurs mainly on exposed faces of Pd crystallites. The effect could be either electronic or structural in nature. The Li, in a partial overlayer on a Pd surface, could affect the electronic properties of adjacent Pd atoms, changing their subsequent adsorption of CO. Alternatively, Li might promote exposure of crystal faces different from those normally present. The existence of an effect of Li on bridge bonding of CO does not, of course, mean that this is the factor responsible for activity promotion by Li. The data generally show no obvious correlation of activity with any particular type of CO bonding as revealed by the frequency and intensity of infrared bands arising from adsorbed CO.

The fact that wide differences in the types of CO adsorption on reduced Pd made so little difference in catalyst activity while marked differences in activity were observed on catalysts with generally similar CO adsorption sites suggests that some factor other than CO binding could well be of major importance. This could be the ability of the support to heterolytically dissociate hydrogen to form hydroxyl and hydride species on the surface. Zinc oxide is well-known for its ability to do this and evidence has also been presented that MgO and La_2O_3 can similarly dissociate hydrogen. Work in this laboratory has shown that alumina possesses a few sites which exhibit this behavior. The ability to form surface hydride may be the essential feature needed for methanol synthesis in addition to the non-dissociative adsorption of CO. The effect of Li may be to provide surface sites on silica on which such dissociation can occur more readily. Further work is planned to investigate these possibilities. Obviously, the types of sites available for CO and H_2 adsorption under reaction conditions may differ from those seen on fresh or used catalysts. In situ IR studies under reaction conditions could shed additional light on this subject. Such studies are also planned.

LITERATURE CITED

1. Kikuzono, Y., Kagami, S., Naito, S., Onishi, T., and Tamaru, K., Faraday Gen. Discuss., 72, 135, 1982.
2. Ponec, V., Proc. Int. Cong. and Catal., 7th Tokyo 1980, p. 925, 1981.
3. Fajula, F., Anthony, R. G., and Lunsford, J. H., J. Catal., 73, 237, 1982.
4. Ryndin, Yu A., Hicks, R. F., Bell, A. T., and Yermakov, Yu. I., J. Catal., 70, 287, 1981.
5. Tatsumi, T., Uematsu, T., and Lunsford, J. H., Paper Presented at 8th N. American Meeting of Catal. Soc., Philadelphia, May 1-4, 1983.
6. Driessen, J. M., Poels, E. K., Hindermann, J. P., and Ponec, V., J. Catal., 82, 26, 1983.
7. Peri, J. B., J. Phys Chem., 86, 1615, 1982.
8. Sheppard, N., and Nguyen, T. T., "The Vibrational Spectra of Carbon Monoxide Chemisorbed on the Surfaces of Metal Catalysts--A Suggested Scheme of Interpretation," in Adv. Infrared Raman Spectros, 5, 67-148, 1978.
9. Peri, J. B., Discuss. Faraday Soc., 41, 121, 1966.

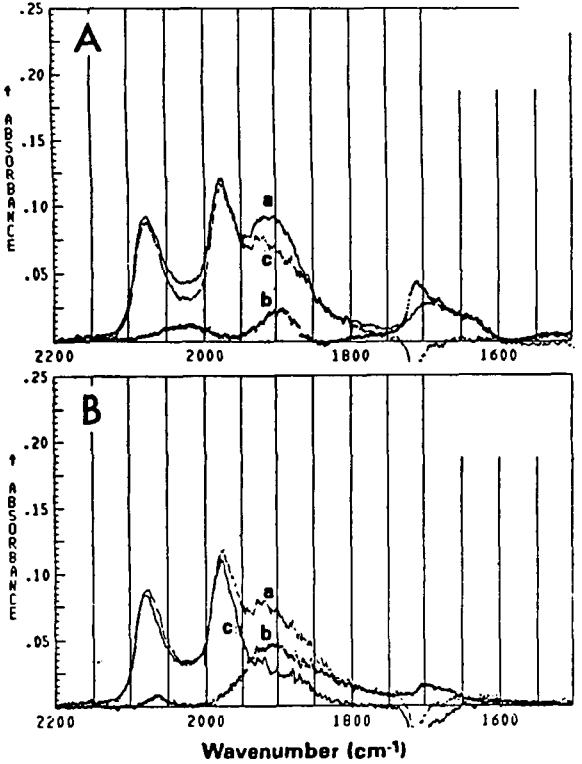

Figure 1. Spectra of CO adsorbed on 5% Pd/Davison 57 silica (ex $PdCl_2$).

A. Spectra showing "cooling" correction
a) CO (2.3 Torr); b) N_2; c) (a-b)

B. Spectra showing strongly and weakly-held CO.
a) "corrected" CO spectrum = C above
b) CO held after 5 min. evac. c, (a-b) = weakly-held CO.

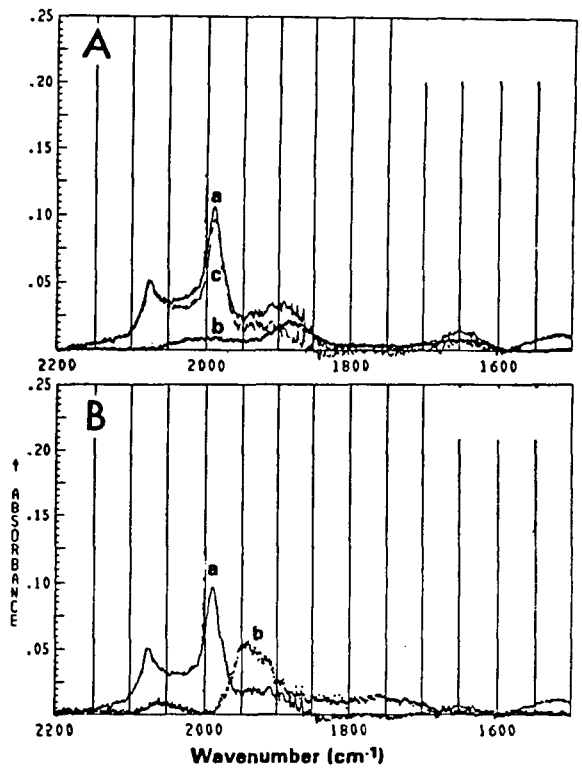

Figure 2. Spectra of CO adsorbed on 5% Pd/Davison 59 silica (ex $Pd(NO_3)_2$)

A. Spectra showing "cooling" correction
a) CO (2.3 Torr); b) N_2; c) (a-b)

B. Separation into strongly and weakly-held CO
a) weakly-held CO; b) strongly-held CO

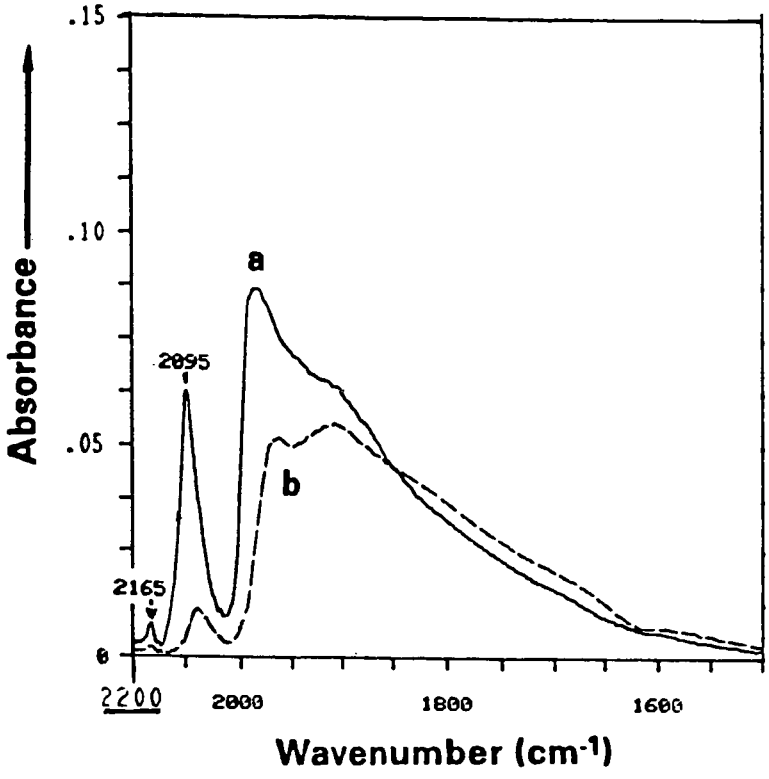

Figure 3. FTIR Spectrum of CO Adsorbed on 1.5% Pd/Davison 57 silica (ex $PdCl_2$)

A. CO (2.0 Torr);

B. After 5 min. evacuation.

(The background was subtracted, but no corrections were applied.)

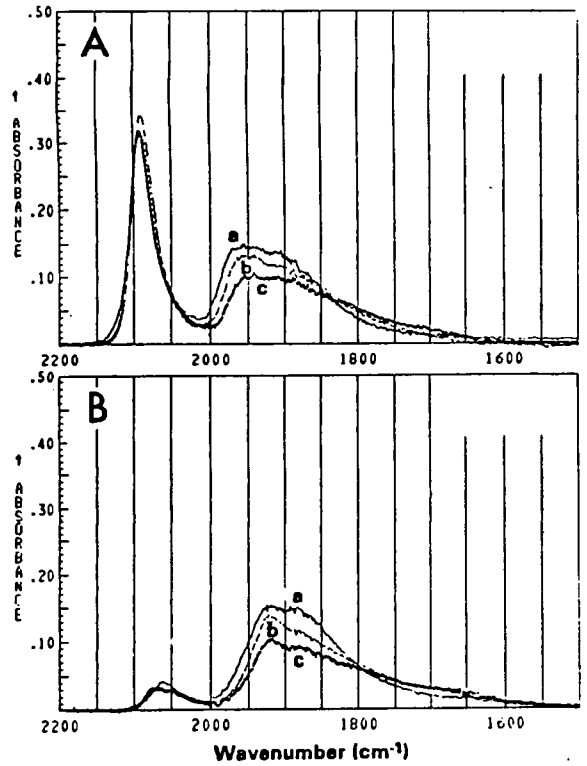

Figure 4. Effects of Li on 1.5% Pd/Davison 59 silica (ion exchanged)

A. Spectra of CO (2.1 Torr-corrected for "cooling") on catalysts containing the following Li contents:
a) 0%; b) 0.7%; c) 1.6%

B. Spectra of CO retained after 5 min. evacuation on the same catalysts (a, b and c above).

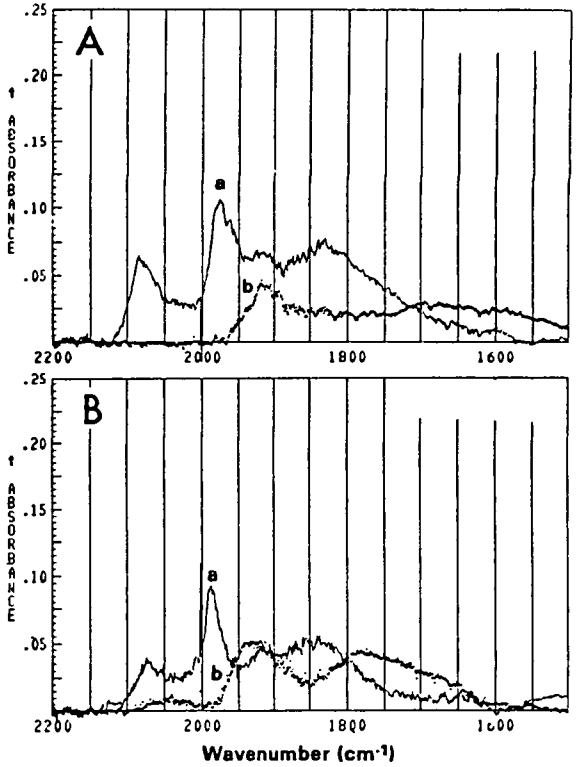

Figure 5. Effects of Li on 5% Pd/SiO_2

A. CO/5% Pd/1.6% Li/SiO_2 57
a) CO (2.2 Torr-corrected); b) after 5 min. evacuation.

B. CO/5% Pd/1.6%Li/SiO_2 59
a) CO (2.1 Torr-corrected); b) after 5 min. evacuation.

THE EFFECT OF ALKALI PROMOTION ON ALCOHOL SYNTHESIS OVER Rh/TiO_2

S.C. Chuang, J.G. Goodwin, Jr., and I.Wender

Chemical and Petroleum Engineering Department
University of Pittsburgh
Pittsburgh, PA 15261

I. INTRODUCTION

The importance of the direct synthesis of higher (C_2-C_6) alcohols from synthesis gas as a promising route for providing clean fuels and petrochemical feedstocks is generally recognized. It is known that the addition of alkali salts to methanol synthesis catalysts often results in greater yields of higher alcohols. However, little is known about how various alkali species affect the catalyst component and alcohol synthesis reaction. Rh catalysts are simple yet model systems for studying the effect of alkali promoters on CO hydrocondensation. Depending on the oxide support used, the product catalyzed by Rh may be primarily hydrocarbons or alcohols (1, 2). This paper reports on an investigation of the effect of various alkali species (Li, K, and Cs) on CO hydrocondensation over Rh/TiO_2. Rh/TiO_2 was an attractive catalyst to study since both hydrocarbons and oxygenated compounds are formed in significant quantities during CO hydrogenation. This provided the possibility to investigate simultaneously the effect of alkali promotion on the formation of these two types of products.

II. EXPERIMENTAL

The alkali-promoted rhodium catalysts were prepared by the impregnation of TiO_2 using $RhCl_3.3H_2O$ and an alkali nitrate (Li, K, Cs) in aqueous solution having a pH of 3-3.5. The catalysts were prepared in such a way so that the Rh loading was 3 wt% and the atom ratio of alkali promoter to Rh was 1/2. After impregnation, the samples were dried overnight in air at 40°C and reduced in flowing H_2 on heating in 50°C steps (30 min.) to 400°C and holding for 16 hr. Prior to reaction, the TiO_2-supported catalysts were again reduced in flowing hydrogen at 500°C for 3 hr. to induce strong metal-support interaction (SMSI) (3). The study was carried out in a differential reactor at reaction conditions of 250-330°C, 10 atm, and CO/H_2=2. A small amount of ethylene (2.3 mole%) was added to the reactant mixture to study the specific reactions of this synthesis.

III. RESULTS AND DISCUSSION

The activity of CO conversion was observed to decrease in the order: unpromoted > Li > K > Cs. The rates of formation for all the products decreased upon alkali promotion but the oxygenate selectivities were enhanced as shown in Fig. 1. This clearly indicated that there was less suppression in the rate of oxygenate formation than in that of hydrocarbon formation. It may suggest that alkali promoters have a different effect on the formation of oxygenates than on that of hydrocarbons. The selectivity of acetone paralleled that of acetaldehyde suggesting that the acetone may be formed by the combination of the acetaldehyde intermediate and a surface methyl species as proposed by Schulz and Zein El Deen (4). The decrease in mole ratio of [MeCHO]/[EtOH] and (olefin)/(paraffin) as shown in Table I may be attributed to the suppression of hydrogenation as a result of alkali promotion. Hydrogenation suppression has been identified as a major

effect of alkali promoters on CO hydrogenation over transition metal catalysts (5, 6).

Although oxygenate selectivities were enhanced upon alkali promotion, the chain growth probability based on carbon number of both oxygenates and hydrocarbons was only increased slightly by alkali promotion. Less deviation of the ethylene fraction from the Schulz-Flory distribution was also observed on alkali-promoted catalysts, indicating that the effect of ethylene incorporation was less pronounced in the presence of alkali promoters.

In order to verify the above findings, a small amount of ethylene [2.3 mole %] was added to the reactant mixture. The results of ethylene addition are essentially consistent with the above findings.

IV. CONCLUSIONS

1. The rate of CO conversion decreased in the order: unpromoted > Li > K > Cs.
2. The hydrogenation ability also decreases in the order: unpromoted > Li > K > Cs.
3. The alkali promoters had different effects on the formation of oxygenates than on that of hydrocarbons.
4. The active sites for oxygenate formation during CO hydrogenation over Rh/TiO_2 appeared not to be sensitive to the chemical nature of the alkali promoter.

ACKNOWLEDGMENT

Funding for this research was provided by the U.S. Department of Energy, Office of Fossil Energy, under grant no. DE-FG22-82PC50810.

REFERENCES

1. Katzer, J.R., Sleight, A.W., Gajardo, P., Michel, J.B., Gleason, E.F., and McMillan, S., Faraday Discussions, 72-72/8 (1979).

2. Ichikawa, M., CHEMTECH, 674 (1982).

3. Tauster, S.J., and Fung, S.C., J. Catal. 55, 29 (1979).

4. Schulz, H., and Zein El Deen, A., Fuel Processing Technology 1, 45 (1977).

5. Gonzalez, R.D., and Miura, H., J. Catal 77, 338 (1982).

6. Campbell, C.T., and Goodman, D.W., Surf. Sci. 123, 413 (1982).

TABLE I The Effect of Alkali Promoter on [MeCHO]/[EtOH] and [olefin]/[paraffin] Ratios

	Rh/TiO_2	$Li-Rh/TiO_2$	$K-Rh/TiO_2$	$Cs-Rh/TiO_2$
$\frac{[MeCHO]}{[EtOH]}$	0.3	0.6	2.7	10.4
$\frac{[C_3-C_5 \text{olefins}]}{[C_3-C_5 \text{ paraffins}]}$	2.7	5.8	4.6	4.2

Reaction conditions: CO/H_2 = 2, 300°C, 10 atm

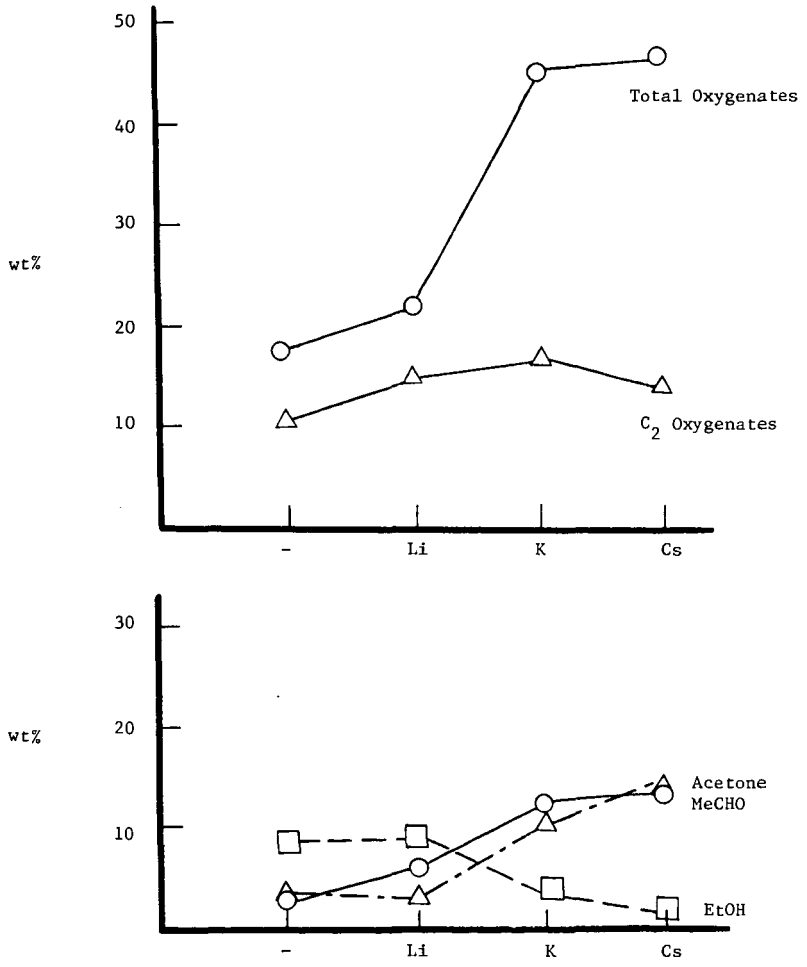

Figure 1: The Effect of Alkali Promotion on Oxygenate Selectivity for Rh/TiO_2 (CO/H_2 = 2, 300°C, 10 atm)

Heteropoly Compounds and Their Properties as Catalysts, in Oxidation Reactions and Methanol to Hydrocarbon Process.

J.B. Moffat*, J.G. Highfield, and B.K. Hodnett

Department of Chemistry and
Guelph-Waterloo Centre for Graduate Work in Chemistry
University of Waterloo
Waterloo, Ontario CANADA
N2L 3G1

INTRODUCTION

Heteropoly compounds are ionic solids with complex, high molecular weight anions, the latter possessing a minimum of three elements. Although heteropoly compounds possess a variety of structures, those of interest in the present work have anions with cagelike structures, often referred to as Keggin units (Fig. 1). These have a central metal atom contained within a tetrahedron of oxygen atoms which is itself surrounded by twelve octahedra of oxygen atoms with a second metal atom at each of their centres. The octahedra overlap and share a portion of their oxygen atoms with each other and with those of the central tetrahedron. The central metal atom is typically P, Si, As, while the peripheral metal atoms are commonly W, Mo, V, and Ti.

Fortunately, detailed structural information for some of the heteropoly compounds is beginning to become available. One of the most detailed studies was that performed by Brown, Noe-Spirlet, Busing and Levy (1) with X-ray crystallography and neutron diffraction on 12-tungstophosphoric acid ($H_3PW_{12}O_{40}\cdot nH_2O$). Their work showed that the proton in this heteropoly acid is surrounded by four water molecules only two of which are hydrogen-bonded to the proton at a given time. The water molecules are, in turn, hydrogen-bonded through their hydrogen atoms to the outer or terminal oxygen atoms of the anions (Fig. 2).

Heteropoly compounds have gained increasing interest in the last few years, largely as heterogeneous catalysts, but also in homogeneous catalysis (for example, refs. 2-6). One of the sources of the interest in the catalytic properties of these solids undoubtedly lies in their multifunctional capabilities. As a result of variation in their elemental composition, virtually a continuous change in catalytic functions can be achieved, ranging from that associated with Bronsted acidity to that with oxidation catalysis, while the Keggin structure is retained.

While the cation can be shown to influence the catalytic properties in various ways, but principally through changes in both the bulk and surface properties of the heteropoly compound, the present work is primarily concerned with the effect of the anion on the bulk, surface and catalytic properties of heteropoly compounds. The influence of the anion, and in particular the nature of both the central heteroatom and the peripheral metal atoms, can be seen from the results of a variety of experiments. Hayashi and Moffat (2) have shown that 12-tungstophosphoric acid catalyzes the gas phase conversion of methanol to hydrocarbons at 350°C, for example, while with 12-molybdophosphoric acid ($H_3PMo_{12}O_{40}$), oxidation predominates. Pretreatment of the former catalyst with air at 400°C reduces the conversion to hydrocarbons, while the use of helium or hydrogen in the calcination is beneficial to the conversion process.

The dehydration of propanol is catalyzed by a variety of heteropoly acids as $H_3PW_{12}O_{40}$ $H_4SiW_{12}O_{40}$ $H_5PW_{10}V_2O_{40}$ $H_3PMo_{12}O_{40}$ $H_5PMo_{10}V_2O_{40}$ $H_4SiMo_{12}O_{40}$

(5). In the oxidation of methacrolein heteropoly acids $H_3PMo_{12}O_{40}$ and $H_4SiMo_{12}O_{40}$ have been shown to be more active and selective than $H_3PW_{12}O_{40}$ and $H_4SiW_{12}O_{40}$ (6). In the oxidation of acrolein, methacrolein, and isobutyric acid by $H_3PW_xMo_{12-x}O_{40}$, the conversion increases as the value of x decreases, that is as the molybdenum content increases (6). Finally it should be noted that in many of the reactions catalyzed by heteropoly compounds, the existence of the Keggin structure of the anion appears to be a necessary although not a sufficient condition for the efficacy of the heteropoly compounds as heterogeneous catalysts (7).

Although the anion structure and composition are quite evidently of particular importance to the activity of the heteropoly compounds, the nature of the cations cannot be disregarded. Hayashi and Moffat (3) have compared the activity and selectivity of a number of salts of 12-tungstophosphoric acid in the conversion of methanol to hydrocarbons. Of the metal salts employed, Na, Zr, Zn, B, Mg, and Al, the first and the last produced the lowest and highest yields, respectively, of hydrocarbons. The yield of hydrocarbons was shown to increase with decreasing magnitude of charge on the peripheral oxygen atoms of the anion. The ammonium salt of 12-tungstophosphoric acid was found by Hayashi and Moffat (4) to produce significantly higher yields of paraffinic hydrocarbons, as contrasted with the largely olefinic products from both the parent acid and its metal salts.

In the present paper the results from temperature programmed desorption (TPD), photoacoustic spectroscopy in the infrared region (PAS), and semi-empirical (extended Hückel) calculations are presented to demonstrate the relationship between the cation, the anion and catalytic properties of the heteropoly compounds.

METHODS

To conserve space only the briefest description of procedures will be presented. The TPD experiments were carried out on a standard apparatus, described elsewhere (8,9). Both a thermal conductivity detector and a C.E.C. mass spectrometer, the latter attached to the system via a variable leak valve, were used as detectors. PAS-FTIR spectra from 4000-550 cm^{-1} were recorded at 5 cm^{-1} resolution on a Bomem DA3.02 Fourier Transform using a globar source and KBr beamsplitter. The photoacoustic detector module, supplied as a standard accessory by the manufacturer, was used with minor modifications (10).

RESULTS AND DISCUSSION

The TPD of 12-tungstophosphoric acid exhibits two peaks (Fig. 3), one centred at 473°K (Peak 1) with an unresolved shoulder on the high temperature side, the other a very broad asymmetrical peak centred around 773°K (Peak 2), both due entirely to water as shown from mass spectrometry. The magnitudes of peaks 1 and 2 corresponded to 1.3-1.4 and 6.5 water molecules per Keggin Unit (KU), respectively. Outgassing at 463 or 593°K essentially removed peak 1 but had no effect on peak 2. No peaks were observed after outgassing at 723°K. It should be noted that copious quantities of water were evolved from the unpretreated HPW at room temperature when a stream of helium was passed through the sample. Water desorbed during outgassing at 463 or 593°K could be replaced by contacting the acid with water vapour at 298°K, but after outgassing at 723°K it was not possible to restore the original TPD behaviour.

The heteropoly acids, 12-molybdophosphoric acid and 12-tungstosilicic acid, as with HPW, displayed two peaks (1 and 2) both due to water (not shown). In addition a very sharp peak (peak 3) was evident on the high temperature side of

peak 2. While the positions of the peaks for HSiW were similar to those with HPW, those for HPMo were found at approximately 373, 673, and 723°K, for peaks 1, 2, and 3, respectively. The importance of the peripheral metallic element of the anion in determining the TPD behaviour is evident.

The position of peak 1 for each of the acids reported here is consistent with the type of multiple hydrogen bonding interactions between the acid and molecular water, as found by Brown et al (1). Since the position of peak 1 depended strongly on the peripheral element of the anion, it appears that such interactions occur externally to the Keggin Unit, consequently largely shielded from influence by the central atom of the anion. It appears the peak 2 must be associated with a deprotonation of the catalyst, the protons combining with anionic oxygen to emerge as molecular water. X-ray diffraction analysis of HPW, which had been pretreated at 723°K suggested that decomposition of the structure had not occurred, in spite of the loss of anionic oxygen.

The PAS spectrum of HPW after pumping at room temperature displays a featureless background absorption which extends across the range from approximately 2000 to 4000 cm^{-1} (Fig. 4). The broad band at 3200 cm^{-1} and the more intense and narrow band at 1710 cm^{-1} may be attributed to molecular water and protonated water. The bands below 1100 cm^{-1} are characteristic of the Keggin Unit. After heating with evacuation at various temperatures up to 450°C, the band at 1710 cm^{-1} decreases and shifts to 1640 cm^{-1}, the bending vibration of lattice water. The band at 1080 cm^{-1} is assigned to the triply-degenerate asymmetric stretching vibration of the central phosphate tetrahedron, while that at 980 cm^{-1} may be attributed to a stretching vibration of the bonds between tungsten and the outer oxygen atoms. Although at 450°C bands associated with the anion structure have diminished somewhat in intensity it is apparent that the structure remains essentially intact.

The twelve octahedra surrounding the central tetrahedron in the Keggin unit can be divided into four compact tritungstate groups, $W_3O_3^{-8}$, resulting from the edge sharing of three WO_6 octahedra (11) (Fig. 5b). The three octahedra in each such group have one common oxygen atom, which is also part of the inner tetrahedron in the heteropoly anion, and three other oxygen atoms are each shared by two octahedra to form the edge-shared unit. In $W_3O_{13}^{-8}$ there are three terminal and three bridging oxygen atoms on the outer surface of the unit, when viewed as a fragment of the heteropoly anion. The central tetrahedron may then be attached to produce the $XM_3O_{16}^{-n}$ species (Fig. 5a), where X refers to the central atom and M the peripheral metal atom. The use of this fragment to simulate the heteropoly anion in semi-empirical extended Hückel calculations provided a convenient means of evaluating the effect of charges in both the central and the peripheral atom.

The effect of changes in the central atom and the peripheral atoms of the Keggin structure may be observed from calculations on $PW_3O_{16}^{-9}$(PW), $SiW_3O_{16}^{-10}$ (SiW) and $PMo_3O_{16}^{-9}$ (PMo) (Fig. 6). The net atomic charges on the outer atoms of the former two species are similar, while those on the fragment containing molybdenum are considerably more negative. In addition, the partitioned energies for the M-O (outer) bond on PW and SiW are approximately the same, that on PMo is considerably smaller. Evidently, a change in the central atom has little effect on either the atomic charges of the outer oxygen atoms or the partitioned energies of the bonds formed by these atoms with the peripheral metal atoms. In contrast, substitution of the peripheral atoms, with the central atom fixed, produces substantial changes in the two properties.

The results of these calculations together with the available experimental data are consistent with the conclusion that Bronsted acidity increases as the

magnitude of the negative charges on the outer oxygen atoms of the heteropoly fragment decreases, while the activity in oxidation reactions can be correlated with the energy associated with the bond between the outer oxygen atom and the peripheral metal atom.

It appears reasonable as a first approximation to assume that the protons in the heteropoly compounds are interacting primarily with the outer oxygen atoms of the anion structure. The acid strength, being directly dependent on the mobility of the protons, should then be inversely proportional to the magnitude of the negative charge on these oxygen atoms. In the oxidation processes involving heteropoly compounds, it may be reasonably assumed, again as a first approximation, that the activity of these catalysts is related to the case with which the most immediately available oxygen atom can be removed from the anion. The partitioned energy of the bond associated with the peripheral metal atoms and the outer oxygen atoms of the anion would therefore appear to fill this role.

ACKNOWLEDGEMENTS

The financial support of the Natural Sciences and Engineering Research Council of Canada is gratefully acknowledged.

REFERENCES

1. G.M. Brown, M.-R. Noe-Spirlet, W.R. Busing, and H.A. Levy, Acta Cryst. B33, 1038 (1977).
2. H. Hayashi and J.B. Moffat, J. Catal. 77, 473 (1982).
3. H. Hayashi and J.B. Moffat, J. Catal. 81, 61 (1983).
4. H. Hayashi and J.B. Moffat, J. Catal. 83, 192 (1983).
5. M. Misono, K. Sakata, Y. Yoneda, and W.Y. Lee, Intern. Congr. Catal., p. 1047, Tokyo 1980, Kodanska, Tokyo, and Elsevier, Amsterdam, 1981.
6. M. Misono, T. Komaya, H. Sekiguchi, and Y. Yoneda, Chem. Letts. 53 (1982).
7. H. Hayashi and J.B. Moffat, unpublished.
8. J.B. Moffat, E.E. Chao, and B. Nott, J. Coll. Interf. Sci. 67, 240 (1978).
9. B.K. Hodnett and J.B. Moffat, J. Catal. (in press).
10. J.G. Highfield and J.B. Moffat, J. Catal. (in press).
11. D.L. Kepert, in Comprehensive Inorganic Chemistry, J.C. Bailar (Ed.) Vol. 4, Chapt. 51, Pergamon, New York, 1973.

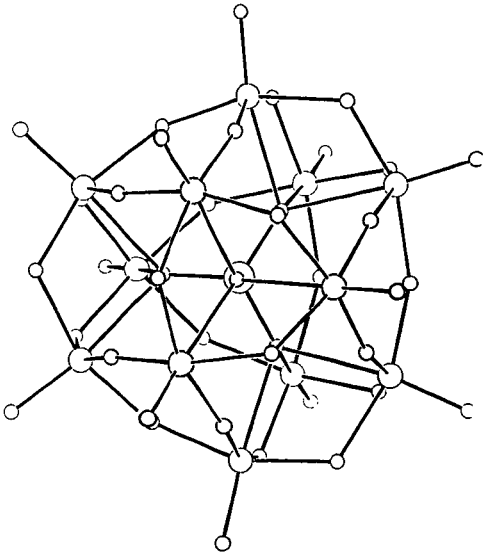

Figure 1 *Anion of* $SiMo_{12}O_{40}^{-4}$

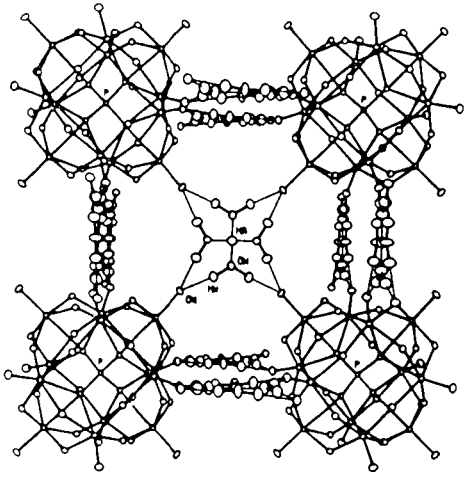

Figure 2 *Arrangement of cations, water, and anions in 12-tungstophosphoric acid.*

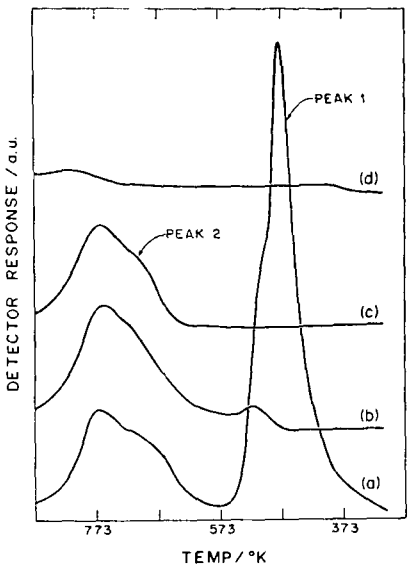

Figure 3 *Temperature Programmed Desorption spectra of 12-tungstophosphoric acid after pretreatment temperatures of (a) 298°K, (b) 463°K, (c) 593°K, (d) 723°K (9).*

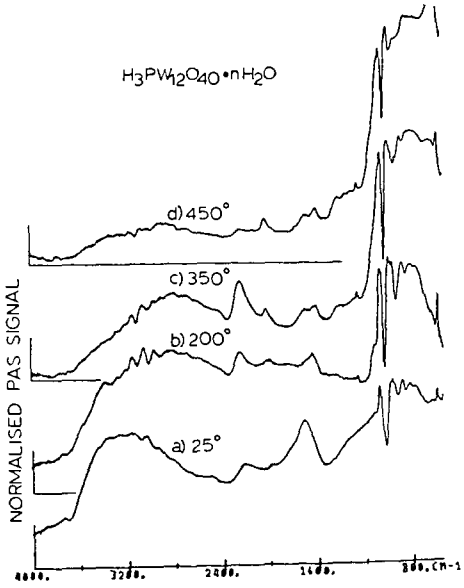

Figure 4 *Photoacoustic spectra of 12-tungstophosphoric acid after heating with evacuation at various temperatures (10).*

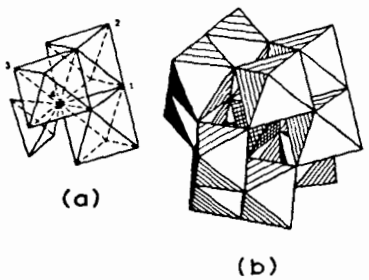

Figure 5 (a) Fragment $XM_3O_{16}^{-n}$ of heteropoly anion.
(b) Heteropoly anion showing position of fragment.

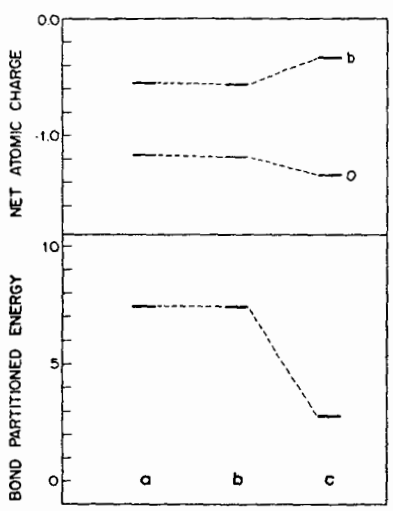

Figure 6 Results of extended Hückel calculations of net atomic charges on bridging (b) and outer (o) oxygen atoms and partitioned energies for the M-O (outer) bond.

ALCOHOL SYNTHESIS OVER Fe/Cu/ZnO CATALYSTS

J. A. Sibilia, J. M. Dominguez, R. G. Herman, and K. Klier

Center for Surface and Coatings Research
and Department of Chemistry
Lehigh University
Bethlehem, PA 18015

INTRODUCTION

In the attempt to produce higher molecular weight oxygenated compounds from synthesis gas (H_2 + CO) for utilization as fuels and intermediate chemicals, an approach to catalytically forming higher alcohols is to combine an alkyl-forming agent with a methanol synthesis catalyst. It is well-known that copper-based catalysts are very selective for the synthesis of methanol (1-3). On the other hand, cobalt- and iron-based catalysts promote the Fischer-Tropsch synthesis (4,5) of hydrocarbons. The Fischer-Tropsch process converts synthesis gas to a mixture of predominantly linear alkanes and alkenes rather non-selectively but in such a manner that the product distribution with respect to carbon chain length displays a recognizable pattern (6-8), commonly referred to as the Schulz-Flory distribution (9,10). This distribution arises from the stepwise catalytic polymerization and hydrogenation of CO by processes whose reaction mechanisms have not been fully established (11-13).

Utilizing mixed copper/cobalt catalysts has led to enhanced selectivities for the synthesis of higher alcohols (14-19). However, the quantity of hydrocarbons formed were greater than the quantity of higher alcohols formed (18,19), methane was the dominant product (15,16), or methanol was the most selectively formed product (14,17,18). It appears that the copper/cobalt catalysts that contain small amounts of cobalt (<8 wt%) are principally methanol synthesis catalysts in which the cobalt has suppressed the catalytic activity while shifting the selectivity toward higher molecular weight products (19). The distribution of products, which are linear, indicates that they are formed by a Fischer-Tropsch mechanism.

Iron-based Fischer-Tropsch catalysts are usually promoted with copper, e.g. 20% Cu relative to Fe (20-23), where the copper increases the activity of the catalysts via its redox properties during the preparation of the catalysts (20,22). Oxygenates are often observed as products over these catalysts, but the yields of these products are inversely proportional to the reactant stream space velocity, e.g. more oxygenates are formed at lower gas hourly space velocities (GHSV) (21). The linear products that are synthesized over these catalyst follow the Schulz-Flory distribution.

The present work has utilized a well-characterized Cu/ZnO = 30/70 mol% methanol synthesis catalyst (2,24-27) into which small amounts of iron have been introduced. It is shown that the incorporation of the latter alkyl-forming agent caused the production of higher molecular weight compounds, both paraffins and olefins, as well as alcohols.

EXPERIMENTAL

The Fe/Cu/ZnO catalysts were coprecipitated from heated nitrate solution by sodium carbonate, calcined, pelletized, and reduced with H_2/N_2 = 2/98 vol% at 250°C according to a procedure previously described in detail for the binary Cu/ZnO catalysts (2,25). A schematic of the catalytic reactor system has been presented (2), but a high pressure unit for pumping liquids into the synthesis gas stream at a reactor pressure of 75 atm has been added at the top of the reactor preheater sec-

tion (28). The exit gas was reduced to ambient pressure and was sampled approximate-every hr using a heated automatic sampling valve and analyzed using an on-line Hewlett-Packard 5730A gas chromatograph coupled with a H-P Model 3388A Integrator/ Controller. Condensables (at 0°C) were collected and further analyzed by direct liquid injection into the H-P GC and a Finnigan 4021 GC/MS/Nova system. The analyses resulted in less than 2% error in the carbon atom balance.

The catalysts were characterized by BET surface area determination using argon and by electron microscopy using a Philips 400T electron microscope fitted with a STEM unit and an X-ray energy dispersive spectrometer.

RESULTS

The influence of iron concentration on the catalytic activity of the Fe/Cu/ZnO catalysts was determined for the usual testing conditions employed for methanol synthesis catalysts. The results are given in Table 1, and it is evident that the activities of the catalysts decrease with increasing iron content. These conversions can be compared with the 55 ± 5% carbon conversion observed with the undoped Cu/ZnO = 30/70 methanol catalyst (26). The catalyst containing the lowest iron content produced predominantly methanol, while the catalyst containing 9.0 mol% iron produced an appreciable quantity of waxes. Therefore, the Fe/Cu/ZnO = 1.2/31.8/67.0 catalyst was chosen for further study.

In examining the effect of CO_2 concentration in the synthesis gas on the activity and selectivity of the catalyst, it was observed that the maximum conversion to products (12.0 mol%) and the greatest selectivity to C_2-C_7 hydrocarbons (60.7 C atom %) occurred with a $H_2/CO/CO_2$ = 70/28/2 vol% synthesis gas. However, the highest selectivities toward methanol and methane were produced by the $H_2/CO/CO_2$ = 70/24/6 vol% synthesis gas (see Table 1). On the other hand, the highest selectivity toward the C_2-C_5 alcohols (17.1%) was achieved with CO_2-free H_2/CO = 70/30 synthesis gas to yield a C_2-C_5/C_1 alcohol molar ratio of 0.61.

Using the binary H_2/CO synthesis gas, the effect of the partial pressure of the reactants on the higher alcohol synthesis was investigated. The results are presented in Table 2, and it is evident that as the H_2/CO ratio decreased, the % carbon conversion to products also decreased. However, the water gas shift reaction became more efficient at the same time so that the selectivity of CO conversion to CO_2 increased as the H_2/CO ratio decreased. As the latter ratio decreased, the selectivity toward the higher alcohols relative to methanol increased. Analyses of the condensable liquids collected from the reactions with the low H_2/CO ratio synthesis gases showed that traces of 2-methyl-1-propanol and 2-methyl-1-butanol were present. It was estimated that these trace compounds were each less than 5 wt% of the total C_4 and C_5 alcohol product.

In studying the effects of the synthesis gas feed rate on alcohol synthesis, the inlet GHSV was varied in four steps from 2500 to 6250 hr^{-1} (contact time = 1.44 to 0.58 sec, respectively) with the H_2/CO = 50/50 gas mixture. As the contact time increased, the carbon conversion to alcohols and hydrocarbons increased in a directly proportional manner. The carbon atom ratio of higher alcohols to methanol remained relatively constant at 2.1 ± 0.1, while the alcohol/hydrocarbon molar ratio decreased with increasing contact time. Thus, longer contact times favored hydrocarbon synthesis, while shorter contact times shifted the selectivity towards the alcohols. This indicates that both alcohols and hydrocarbons are primary products.

This was further supported by injecting liquid isopropylamine into the inlet synthesis gas stream under the experimental conditions given in Table 3. The small quantity of isopropylamine pumped into the system had little effect on the carbon conversion. However, the production of alcohols was completely suppressed, while the synthesis of hydrocarbons was only partially inhibited, particularly the forma-

TABLE 1

Conversion of $H_2/CO/CO_2$ = 70/24/6 vol% Synthesis Gas to Products at 250°C, 75 atm, and GHSV = 5000 hr^{-1} over Fe/Cu/ZnO Catalysts

Fe/Cu/Zn (mol%)	0.3/32.1/67.6	1.2/31.8/67.0	9.0/31.4/59.6
Catalyst Charge (g)	2.4547	2.4556	2.6971
Total Conversion			
CO + CO_2 (mol%)	23.1	10.6	8.3
(mol/kg cat/hr)	17.0	8.0	6.3
Selectivity (C atom%)			
Methanol	95.2	16.0	5.1
Ethanol	0.4	4.2	7.8
1-Propanol	0.0	2.4	2.8
2-Propanol	0.0	0.2	0.2
1-Butanol	0.0	1.4	2.2
1-Pentanol	0.0	0.7	1.2
Methane	1.4	24.3	17.9
Ethane	0.7	9.0	10.2
Ethylene	0.0	1.0	1.0
Propane	0.1	12.4	7.3
Propylene	0.0	1.0	7.6
C_4-C_7 Hydrocarbons	2.2	23.3	24.5
C_5^+ Alcohols and C_8^+ Hydrocarbons	0.0	4.1	11.2
Group Mole Ratios			
C_2-C_5 Alcohols/Methanol	0.002	0.22	1.12
C_1-C_5 Alcohols/C_1-C_7 Hydrocarbons	38.9	0.51	0.31
C_2-C_3 Olefins/C_2-C_3 Paraffins	0.0	0.10	0.47
Yields (g/kg cat/hr)			
Methanol	518	41.0	10.3
C_2-C_5 Alcohols	1.6	15.6	18.3

tion of methane and ethane. Thus, the hydrocarbon distribution was shifted slightly toward longer chain molecules and, as indicated in Table 3, from paraffins to olefins. It is evident from the data for the amines that the injected isopropylamine principally trapped methyl and ethyl groups.

A reduced Fe/Cu/ZnO = 1.2/31.8/67.0 catalyst was examined by electron microscopy after being ultrasonically dispersed from an ethanol suspension onto a carbon-coated titanium grid. Metallic copper crystallites, predominantly with a diameter of about 5.0 nm, were supported on the ZnO matrix. Electron diffraction showed that Cu ($\bar{1}11$) planes. Using a 5 nm electron probe, energy dispersive X-ray analysis of the ZnO phase indicated that it contained about 15% Cu and 0.8% Fe. A few bimetallic Fe-Cu particles were observed that contained more iron than copper. However, in general the iron was homogeneously dispersed over the catalyst.

Analysis of a tested catalyst by Auger spectroscopy indicated that the atomic composition of the surface was Cu/Zn/O/C = 15.0/9.9/6.2/68.9 %. No Fe was detected by Auger or X-ray photoelectron spectroscopy. Thus, it appears that carbon covered the iron and most of the ZnO surface, but much of the copper phase was left exposed. The BET surface area of the used catalyst, as removed from the reactor under a

TABLE 2

Reactant Concentration Effects on Alcohol Synthesis over the 1.2% Iron Catalyst at 250°C, 75 atm, 5000 hr^{-1} and $H_2/CO/CO_2$ = 30/70/0 to 70/30/0. Catalyst Charge = 2.4524g.

$H_2/CO/CO_2$ (vol%)	30/70/0	40/60/0	50/50/0	60/40/0	70/30/0
Conversion					
CO (mol%)	1.5	2.8	4.3	6.5	8.2
(mol/kg cat/hr)	2.7	4.1	5.4	6.5	6.1
Yields (g/kg cat/hr)					
Methanol	4.1	9.2	15.1	18.2	17.7
Ethanol	3.2	6.5	9.4	10.6	9.0
1-Propanol	1.8	3.9	5.4	5.6	4.9
2-Propanol	0.2	0.4	0.5	0.4	0.4
1-Butanol	0.9	2.0	2.9	2.9	2.7
1-Pentanol	0.4	1.0	1.5	1.5	1.3
Selectivity (C atom%)					
Carbon Dioxide	41.5	30.5	23.9	19.6	16.8
Methanol	4.8	6.9	8.7	8.8	8.9
C_2-C_5 Alcohols	11.4	15.9	17.4	15.4	14.2
C_1-C_7 Hydrocarbons	42.3	46.7	50.0	56.2	60.1

nitrogen atmosphere, was 0.4 m^2/g, and this contrasts with the surface area of 37-40 m^2/g for tested binary Cu/ZnO = 30/70 catalysts (25,26). After washing the tested ternary catalyst with cyclohexane, the surface area was found to be 15 m^2/g.

DISCUSSION

The composition of the synthesis gas mixture has a pronounced effect on the selectivity observed over the Fe/Cu/ZnO catalyst. The presence of CO_2 in the synthesis gas tends to favor the formation of low molecular weight products, i.e. methanol and methane. When CO_2 is removed from the reactant stream, carbon chain growth is promoted, apparently due to exposure of sites active in the transfer of alkyl groups. In the absence of CO_2, the percentage of CO converted to carbon dioxide, alcohols, and hydrocarbons increased as the H_2/CO ratio was increased from 0.43 to 2.33. Similar behavior has been observed with other iron catalysts, for which the rate of synthesis increased as the hydrogen content of the feed increased (6).

The carbon chain growth reactions that occurred over these iron-containing catalysts can be treated as a polymerization process in which the molecular weight distribution of products is determined by the chain propagation and chain transfer steps. The Schulz-Flory molecular weight distribution can be derived to give the following equation:

$$N_x = N_o(1-\alpha)^2\alpha^{x-1}, \qquad 1)$$

where N_x is the total number of molecules containing x carbon atoms, N_o is the total number of monomer units ($-CH_2-$) in the system, and α is the probability of chain growth (28). Equation 1 can be expressed in logarithmic form as

TABLE 3

Effects of Isopropylamine on Product Distributions over a 1.2% Fe Containing Cu/ZnO Catalyst at 235°C, 75 atm, 5000 hr^{-1}, and $H_2/CO/CO_2$ = 70/30/0 vol%. Catalyst Charge = 2.414 g. (R = isopropyl).

Isopropylamine in Feed (μl/min)	0	20
$H_2/CO/RNH_2$ (molar ratio)	2.33/1.00/0	2.33/1.00/0.08
CO Conversion (mol%)	4.45	4.38
(mol/kg/hr)	3.4	3.3
Products ($x10^{+4}$ mol/hr)		
C_1-C_5 Alcohols	7.03	0
C_1-C_7 Hydrocarbons	38.43	23.01
Amines:		
R-NH-CH_3	0	1.01
R-N-$(CH_3)_2$	0	1.34
R-NH-C_2H_5	0	0.70
R-N-(CH_3, C_2H_5)	0	7.71
R-N-$(C_2H_5)_2$	0	0.35
R-NH-(n-C_3H_7)	0	0.38
Certain Molar Ratios		
Alcohols/Hydrocarbons	0.2	0
Olefins/Paraffins	0.1	1.4

$$\log (N_x/N_o) = \log [(1-\alpha)^2/\alpha] + x\log\alpha. \qquad 2)$$

If the graphical representation of $\log (N_x/N_o)$ vs x gives a straight line, and the values of α determined from the intercept and the slope are in good agreement, then the molecular weight distribution follows the Schulz-Flory law.

Figure 1 demonstrates that both the alcohols and the hydrocarbons produced over the Fe/Cu/ZnO catalyst follow the Schulz-Flory law. The propagation constant (α) is 0.32 for the alcohols, while it is equal to 0.55 for the hydrocarbons. This distinct difference in α values again suggests that the alcohols and the hydrocarbons are formed by different pathways over this catalyst. In the absence of CO_2 and at a lower temperature of 235°C, the distributions for alcohols and hydrocarbons yield α values of 0.47 and 0.53, respectively. Upon addition of isopropylamine to the reactor feed gas (Table 3), the production of alcohols was stopped, while the hydrocarbon distribution was shifted toward longer chain products to give $\alpha = 0.58$. The distribution of alkyl groups on the product amines (excluding the isopropyl group) yielded a non-linear plot, showing that the formation of these alkyl groups do not follow the Schulz-Flory distribution. This indicates that the amines primarily attack the alcohol precursor. If the amines had reacted with the alcohols after they formed, the Schulz-Flory distribution of the alkyl groups would have produced the same distribution as that of the alcohols with $\alpha = 0.47$.

The yield of C_2 substituted amines lies above the expected value found for the alcohol distribution, while the quantities of C_1 and C_3 alkylated amines fall below the expected values. This could be due to a methyl transfer reaction, as reported previously (29), to form a C_2 oxygenated species that is readily attacked by the amine. The results of the present amine trapping experiments are in contrast to those obtained with ammonia and synthesis gas over other iron catalysts (30). In the latter work, exclusively primary amines were formed that obeyed the Schulz-Flory distribution to give $\alpha = 0.69$. It was proposed that ammonia attacked ($-CH_x$) inter-

mediates. However, in the presence work, it is evident that the amines reacted with the oxygenated intermediates and that the hydrocarbon intermediate was left essentially undisturbed.

CONCLUSIONS

While a complete mechanistic reaction scheme has not been verified for this catalyst system, the following conclusions have been deduced from the experimental data:

(a) both alcohols and hydrocarbons are primary products formed over the Fe/Cu/ZnO catalysts,

(b) two polymerization processes are indicated, one with short carbon chain length for alcohols and one with the usual chain length for hydrocarbons,

(c) the alcohols are formed by interaction of methanol precursors and iron-bound intermediates, with the methanol precursor behaving as a monomer in the alcohol synthesis,

(d) the optimum catalysts for the synthesis of C_2-C_5 alcohols contain small amounts of iron (~1%), which is homogeneously dispersed throughout the catalyst, and

(e) hydrocarbon growth appears to occur very actively over Fe-Cu intermetallic particles.

ACKNOWLEDGMENT

This research was supported by the U.S. Department of Energy through the Pittsburgh Energy Technology Center (Grant No. DE-FG22-80PC30265) and the Solar Energy Research Institute (Grant No. XX-2-02173-01).

REFERENCES

1. Natta, G., in "Catalysis," Vol. 3, ed. by P. H. Emmett, Reinhold, New York, 349 (1955).

2. Herman, R. G., Klier, K., Simmons, G. W., Finn, B. P., Bulko, J. B., and Kobylinski, T. P., J. Catal. (1979), 56, 407.

3. Klier, K., Adv. Catal. (1982), 31, 252.

4. Fischer, F. and Tropsch, H., Chem. Ber. (1926), 59, 830.

5. Fischer, F. and Tropsch, H., Brennst. Chem. (1926), 7, 97.

6. Storch, H. H., Golumbic, N., and Anderson, R. B., "The Fischer-Tropsch and Related Synthesis," John Wiley and Sons, New York (1951).

7. Pichler, H., Adv. Catal. (1952), 4, 271.

8. Anderson, R. B., in "Catalysis," Vol. 4, ed. by P. H. Emmett, Reinhold, New York (1956).

9. Schulz, G. V., Z. physik Chem. (1940), B47, 155; and references contained therein.

10. Flory, P. J., J. Am. Chem. Soc. (1940), 62, 2261; and references contained therein.

11. Biloen, P. and Sachter, W. M. H., Adv. Catal. (1981), 30, 165.

12. Rofer-DePoorter, C. K., Chem. Rev. (1981), 81, 447.

13. Bell, A. T., Catal. Rev.-Sci. Eng. (1981), 23, 203.

14. Morgan, G. T. and Taylor, R., Proc. Roy. Soc. (1931), A131, 533.

15. Taylor, R., J. Chem. Soc. (London) (1934), 1429.

16. Yang, C. H., Zaman Khan, M. K., Massoth, F. E., and Oblad, A. G., Preprints, Div. Fuel Sci., ACS (1977), 22(2), 148.

17. Sugier, A. and Freund, E. , U.S. Patent 4,122,110 (Oct. 24, 1978) and German Offen. 2,748,097 (Nov. 5, 1978); assigned to Institut Francais du Petrole.

18. Courty, P., Durand, D., Freund, E., and Sugier, A., J. Mol. Catal. (1982), 17, 241.

19. Lin, F. N. and Pennella, F., in "Catalytic Conversions of Synthesis Gas and Alcohols to Chemicals," ed. by R. G. Herman, Plenum Press, New York, 53 (1984).

20. Madon, R. J., Bucker, E. R., and Taylor, W. F., "Development of Improved Fischer-Tropsch Catalyst for Production of Liquid Fuels," Report E(46-1)-8008 to the U.S. Department of Energy (July 1977).

21. Zaman Khan, M. K., Yang, C. H., and Oblad, A. G., Preprints, Div. Fuel Sci., ACS (1977), 22(2), 138.

22. Kölbel, H. and Ralek, M., Catal. Rev.-Sci. Eng. (1980), 21(2), 225.

23. Amelse, J. A., Schwartz, L. H., and Butt, J. B., J. Catal. (1981), 72, 95.

24. Mehta, S., Simmons, G. W. Klier, K., and Herman, R. G., J. Catal. (1979), 57, 339.

25. Bulko, J. B., Herman, R. G., Klier, K., and Simmons, G. W., J. Phys. Chem., (1979), 83, 3118.

26. Klier, K., Chatikavanij, V., Herman, R. G., and Simmons, G. W., J. Catal., (1982), 74, 343.

27. Dominguez, J. M. Simmons, G. W., and Klier, K., J. Mol. Catal. (1983), 20, 369.

28. Sibilia, J. A., M.S. Thesis, Department of Chemical Engineering, Lehigh University (1983).

29. Chen, M. J. and Feder, H. M., in "Catalysis of Organic Reactions," ed. by W. Moser, Marcel Dekker, New York, 273 (1981).

30. Olivé, H. and Olivé, S., Angew. Chem., Int. Ed. Engl. (1976), 15, 136.

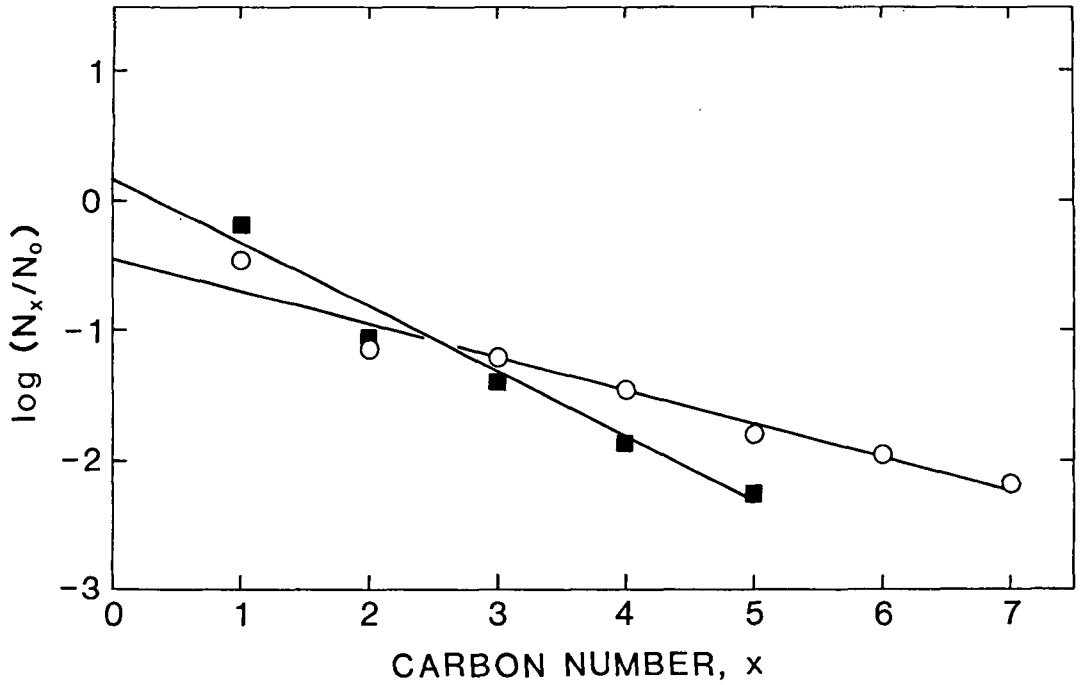

FIGURE 1. The Schulz-Flory Distribution of Alcohols (■) and Hydrocarbons (O) Produced over the Fe/Cu/ZnO = 1.2/31.8/67.0 mol% Catalyst from $H_2/CO/CO_2$ = 70/24/6 vol% Synthesis Gas at 75 atm, GHSV = 5000 hr^{-1}, and 250°C.

THE SYNTHESIS OF HIGHER ALCOHOLS ON Cu/ZnO CATALYSTS PROMOTED WITH K_2CO_3

by Kevin J. Smith* and Robert B. Anderson

Department of Chemical Engineering and Institute for Materials Research

McMaster University, Hamilton, Ontario, Canada L8S 4L7

Alkali oxides added to methanol catalysts increase the formation of ethanol, n-propanol and isobutyl alcohol. This result has been known for many years, yet few quantitative studies have been reported in the literature. Data obtained on a commercial copper-zinc oxide catalyst promoted with K_2CO_3 are presented and compared with published work. Catalyst particles with a mean diameter of about 0.9 mm were used. The catalyst was initially reduced in $2H_2$ + 1CO gas at 300°C and atmospheric pressure for 12-15 hours. Most of the synthesis tests were made at 285°C and 13.2 MPa of $1H_2$ + 2CO gas. The alkali concentration varied from 0-10 wt % K_2CO_3; the optimum amount was about 0.5% by weight, as shown in Table 1. The H_2 to CO feed ratio was important in determining the higher alcohol selectivity. The rate of production of isobutyl alcohol varied as $p_{H2}^{-0.7}\ p_{CO}^{2.2}$ while for methanol, ethanol and n-propanol both exponents were positive and less than 1.6. Decreasing the hydrogen to carbon monoxide ratio from 2 to 0.5 more than doubled the isobutyl alcohol selectivity.

* Present address: Research Department, SASOL 1, Sasolburg 9570, South Africa.

TABLE 1: PROMOTER CONCENTRATION EFFECTS

Pressure = 13.2 MPa. Temperature = 285°C

Wt.% K_2CO_3	0	0.5	1.0	2.0	3.0	10.0
Inlet space velocity (h^{-1})	4300	3300	3800	4300	4600	2900
H_2:CO in feed	0.44	0.47	0.52	0.49	0.48	0.44
Alcohol selectivities(1)						
methanol	65.8	48.6	61.4	75.7	82.4	81.8
ethanol	6.4	4.8	4.8	3.7	2.6	1.6
2-propanol	1.7	0.8	1.8	1.8	1.4	0.3
1-propanol	5.3	6.7	9.2	8.1	7.0	5.2
1-butanol	2.1	4.0	2.5	1.3	1.1	2.2
2-butanol	0.8	1.5	1.7	1.0	1.3	0.9
2-methyl-1-propanol	10.1	18.8	13.8	7.1	3.8	4.6
pentanols	8.0	14.8	4.8	1.2	0.5	3.4
(H_2+CO) consumption						
$mmol.g_{-2}^{-1}.h^{-1}$	50.5	58.5	68.5	41.5	54.3	16.0
$mmol.m^{-2}.h^{-1}$	1.19	1.61	1.76	1.18	1.66	0.89

(1) selectivity = $\frac{\text{C atoms in alcohol i}}{\text{total C atoms in alcohols}} \times 100\%$

A chain growth scheme for the synthesis of alcohols from carbon monoxide and hydrogen is proposed. The scheme describes the alcohol product distribution, assuming one or two carbon addition at the α- or β-carbon atom of the growing alcohol. Estimates of the distribution parameters were obtained from selectivities measured for a range of operating conditions on a Cu/ZnO catalyst promoted with 0.5% K_2CO_3. Typical data showing the values of growth parameters and the comparison of observed and predicted alcohol yields are given in Table 2. The α-addition is a slow step with a large activation energy (140 kJ/mol) while β-addition is faster and has a smaller activation energy (66 kJ/mol). Large methanol selectivities result from the slow initial α-addition, and large 2-methyl-1-propanol selectivities from α-addition being the only growth step of the 2-methyl-1-propanol intermediate. The rate of chain growth is approximately proportional to the CO partial pressure and the rate of chain termination proportional to the H_2 partial pressure. Addition of alcohols to the synthesis gas resulted in significant increases in the yields of some of the alcohols, consistent with the chain growth scheme.

Two papers have been published on this work, Can. J. Chem. Eng., 61, 40 (1983) and J. Catal., 85, 428 (1984).

Table 2: Predicted and Measured Product Distributions

Pressure 10.4 MPa Temperature 285°C

Feed H_2/CO	0.49	0.93	2.01
Space Velocity (h^{-1})	2900	8200	32000
Conversion %			
(H_2+CO)	39	41	23
CO	28	34	27

Alcohols(1)	measured	predicted	measured	predicted	measured	predicted
methanol	0.6177	0.6313	0.8530	0.8572	0.9610	0.9649
ethanol	0.0536	0.0575	0.0505	0.0512	0.0227	0.0227
2-propanol	0.0046	0.0040	0.0022	0.0022	0.0021	0.0003
1-propanol	0.0643	0.0574	0.0378	0.0357	0.0076	0.0071
1-butanol	0.0224	0.0077	0.0062	0.0007	0.0027	0.0008
2-butanol	0.0111	0.0065	0.0043	0.0029	0.0027	0.0004
2-methyl-1-propanol	0.1484	0.1519	0.0402	0.0414	0.0012	0.0024
pentanols	0.0780	0.0838	0.0059	0.0086	0	0.0015

Estimated growth scheme parameters:

Rate constants:			
α	0.136	0.056	0.015
β	1.986	0.870	0.254
γ	0.170	0.013	0.022

Probabilities:			
h	0.136	0.056	0.015
k	0.665	0.465	0.203
ℓ	0.057	0.007	0.018

(1) selectivity = $\frac{\text{C atoms in alcohol i}}{\text{total C atoms in alcohols}}$

DIRECT SYNTHESIS OF 2-METHYL-1-PROPANOL

K. Klier, R. G. Herman, and C. W. Young

Department of Chemistry and Center for Surface
and Coatings Research, Lehigh University, Bethlehem, PA 18015

INTRODUCTION

The hydrogenation of carbon monoxide to aliphatic alcohols follows the general equations

$$2nH_2 + nCO \longrightarrow C_nH_{2n+1}OH + (n-1)H_2O \qquad 1)$$

and

$$(n+1)H_2 + (2n-1)CO \longrightarrow C_nH_{2n+1}OH + (n-1)CO_2 \qquad 2)$$

The isomer distribution in the $C_nH_{2n+1}OH$ involves linear primary, branched primary, or branched secondary alcohols depending on the catalysts used. It is well known that linear alcohols are co-products of hydrocarbon synthesis over Group VIII metals, primarily iron (1), while both linear and branched alcohols are products of CO hydrogenation over methanol synthesis catalysts modified with alkali promoters (2). It is this second class of catalysts that has been shown to produce 2-methyl-1-propanol in relatively high yields. The conditions utilized in the early work (3-7) were rather severe, however, exemplified by the pressure range 300-400 atm and temperatures above 400°C. The catalysts were in general alkali-promoted oxides of zinc and manganese with structural promoters such as chromia or alumina. Only recently Smith and Anderson (8) have demonstrated that the low pressure copper-zinc oxide-alumina methanol synthesis catalysts could be promoted by potassium carbonate to enhance the yields of higher alcohols, optimized the K_2CO_3 concentration, and developed a mathematical model for the chain growth that accounted for high degree of branching. The synthesis was carried out at temperatures below 300°C and pressures 100 - 130 atm over the $K_2CO_3/Cu/ZnO/Al_2O_3$ catalysts. Further study of alkali and alkaline earth promoted copper-based catalysts demonstrated that alkali hydroxide promotion enhances higher alcohol yields at pressures as low as 75 atm in the temperature range 250-310°C (9). Cesium was found to be the most effective promoter and its surface concentration optimized in the binary Cu/ZnO catalysts.

In the present work we report an investigation of the effect of reaction conditions on the yields of higher alcohols, particularly 2-methyl-1-propanol (isobutanol), over the Cs/Cu/ZnO = 0.4/30/70 catalyst (9). High selectivities for direct synthesis of isobutanol are demonstrated herein.

RESULTS AND DISCUSSION

The selectivity patterns have been studied at 75 atm, temperature range 288-325°C, $H_2/CO = 0.45$, and contact time range 1-5 sec in an apparatus described earlier (10). The catalyst preparation was that of ref. 9 with the cesium compound being CsOH. The products of the synthesis were, in the order of abundance, alcohols, esters, ketones, and aldehydes.

Figures 1-4 and Tables 1-2 describe the product composition under various conditions used. These results can be summarized as follows:

1. The general Smith-Anderson pattern for alcohols (8) is confirmed. However, secondary alcohols are very minor products over the Cs/Cu/ZnO catalyst. This is a result that differs from all previous reports (2-8) and is interpreted as due to the absence of an acid component in the Cs/Cu/ZnO catalyst.
2. The selectivity to isobutanol increases with increasing temperature and contact time.
3. Esters are minor products with methyl esters of C_1-C_3 carboxylic acids dominating. The selectivity to esters decreases with increasing temperature and goes through a maximum with increasing contact time. This is consistent with the ability of the Cs/Cu/ZnO catalyst to hydrogenate esters to the corresponding alcohols (11).

The mechanism of the alcohol and ester forming reactions has been discussed elsewhere (9). We point out that the selectivity pattern is such that the formation of isobutanol can be maximized and that of esters suppressed by the choice of conditions and of recycling schemes. The utility of isobutanol rests in its high energy density compared to methanol, in its high octane number (12), and in its being a convenient source of isobutene via catalytic dehydration.

ACKNOWLEDGEMENT

This work was partially supported by DOE - SERI Contract DE-AC02-80CS83001.

REFERENCES

(1) H. H. Storch, N. Golumbic, and R. B. Anderson, "The Fischer-Tropsch and Related Syntheses", John Wiley & Sons, 1951, N.Y.
(2) G. Natta, U. Colombo, and I. Pasquon, in: "Catalysis" (ed. P. H. Emmett) Volume V, Chapter 3, Reinhold Publishing Corp., N.Y. 1957.
(3) P. K. Frolich and D. S. Cryder, Ind. Eng. Chem. 22, 1051 (1930).
(4) G. D. Graves, Inc. Eng. Chem. 23, 1381 (1931).
(5) G. T. Morgan, D. V. N. Hardy, and R. H. Procter, J. Soc. Chem. Ind. Trans. Comm. 51, 1T (1932).
(6) R. Taylor, J. Chem. Soc. (London), 1429 (1934).
(7) G. Natta and R. Rigamonti, Chimica e industria 18, 623 (1936).
(8) K. Smith and R. B. Anderson, Canad. J. Chem. Eng. 61, 40 (1983).
(9) G. A. Vedage, P. Himelfarb, G. W. Simmons, and K. Klier, Preprints, ACS Division of Petroleum Chemistry, Washington, DC 1983, Vol. 28, No. 5, pp. 1261-1271.
(10) K. Klier, V. Chatikavanij, R. G. Herman, and G. W. Simmons, J. Catal. 74, 343 (1982).
(11) G. Vedage, Thesis, Lehigh University, 1984.
(12) F. W. Cox, "Physical Properties of Gasoline/Alcohol Blends", DOE Report BETC/RI-79/4, September 1979.

Table I

Product distribution over Cu/ZnO = 30/70 catalysts with varying concentrations of cesium salts at 288°C, 75 atm, H_2/CO = 0.45
Total flow rate = 8 l/hr Yield in gm/kg cat/hr,
Selectivity in carbon atom percent

	Cu/ZnO		CsOH/Cu/ZnO (0.4/30/70)		CsOH/Cu/ZnO (0.8/30/70)		CsOOCH/Cu/ZnO (0.4/30/70)	
	Yield	Selec-tivity	Yield	Selec-tivity	Yield	Selec-tivity	Yield	Selec-tivity
CO	2136.65	-	1757.35	-	2110.69	-	2015.85	-
CO_2	124.38	-	96.17	-	78.83	-	97.67	-
H_2O	-	-	-	-	-	-	0.32	-
CH_4	3.93	2.06	3.46	1.54	3.89	1.92	3.47	1.72
C_2H_6	1.90	1.06	0.54	0.26	0.37	0.19	0.57	0.30
CH_3OH	283.73	74.31	322.11	71.88	318.66	78.86	303.58	75.31
$HCOOCH_3$	6.16	1.72	7.94	1.89	8.74	2.31	8.04	2.13
C_2H_5OH	20.83	7.59	17.90	5.56	12.92	4.45	15.01	5.18
CH_3COOCH_3	11.13	3.78	8.04	2.33	4.45	1.43	6.68	2.15
C_3H_7OH	12.11	5.07	24.29	8.67	14.95	5.92	17.55	6.97
$(CH_3)_2CHCH_2OH$	5.33	2.41	14.82	5.72	9.01	3.86	12.11	5.20
C_4H_9OH	3.67	1.66	5.59	2.16	2.47	1.06	2.44	1.05
$C_2H_5COOCH_3$	0.55	0.21	-	-	-	-	-	-
$CH_3COOC_2H_5$	0.30	0.12	-	-	-	-	-	-
CO conversion %	14.11		17.54		14.27		14.89	

Table II

Product distribution over the 0.4% CsOH doped Cu/ZnO (=30/70) catalyst at 325°C, 75 atm H_2/CO = 0.45, 0.75, 1, and 2.33 Yield in gm/kg cat/hr

H_2/CO ratio =	2.33	1			0.75			0.45		
Flow Rate =	15 l/hr	3 l/hr	2 l/hr	1 l/hr	3 l/hr	2 l/hr	1 l/hr	12 l/hr	8 l/hr	3 l/hr
CO	1284.28	391.79	245.62	119.43	513.94	315.33	141.92	3281.8	1991.57	640.53
CO_2	152.86	175.76	134.22	75.26	163.35	132.76	82.39	316.42	327.48	217.17
H_2O	3.44	1.47	1.03	0.44	1.02	0.75	0.47	1.02	1.08	0.68
CH_4	9.81	7.49	5.83	3.79	6.70	5.52	3.60	13.42	11.47	6.80
C_2H_6	1.59	1.55	1.12	0.56	1.31	1.05	0.62	3.73	3.52	2.25
CH_3OH	683.53	62.18	33.47	9.74	53.42	29.17	10.24	211.73	135.69	27.91
$HCOOCH_3$	3.36	0.73	0.49	0.29	0.61	0.43	0.31	3.01	1.90	0.74
C_2H_5OH	33.53	5.59	2.97	0.84	4.84	2.52	0.90	22.07	14.19	2.60
C_2H_5CHO	-	0.36	0.23	0.075	0.50	0.25	0.094	1.58	1.32	0.33
CH_3COOCH_3	2.91	1.18	0.68	0.31	1.24	0.75	0.37	5.46	3.97	0.85
C_3H_7OH	36.31	17.82	10.21	3.12	16.90	9.21	3.51	48.55	39.39	8.92
$(CH_3)_2CHCHO$	-	1.05	1.02	0.81	2.23	2.27	1.15	1.93	3.70	2.40
$C_2H_5(CO)CH_3$	-	1.28	0.60	0.54	1.90	1.74	0.80	4.03	4.47	1.46
$C_2H_5CHOHCH_3$	3.47	1.71	1.56	0.80	2.02	2.46	1.25	4.10	3.57	1.50
$(CH_3)_2CHCH_2OH$	18.13	41.45	27.92	14.51	41.02	29.85	16.18	60.22	75.15	42.07
C_4H_9OH	4.78	3.90	2.45	0.91	3.53	2.20	0.94	9.41	9.27	2.78
$C_3H_7(CO)CH_3$	-	0.15	0.30	0.32	0.58	0.98	0.24	0.91	1.25	0.56
$C_2H_5(CH_3)CHCH_2OH$	3.35	6.91	4.73	3.15	7.32	5.61	3.28	9.31	12.88	9.30
$C_5H_{11}OH$	-	1.18	0.67	0.45	1.43	2.17	0.47	3.19	2.63	0.59
C_5^+	-	9.71	8.21	6.25	14.50	12.31	6.93	6.99	13.95	15.11
CO Conversion %	35.32	29.05	29.86	29.30	23.64	25.82	28.10	11.86	15.62	20.25

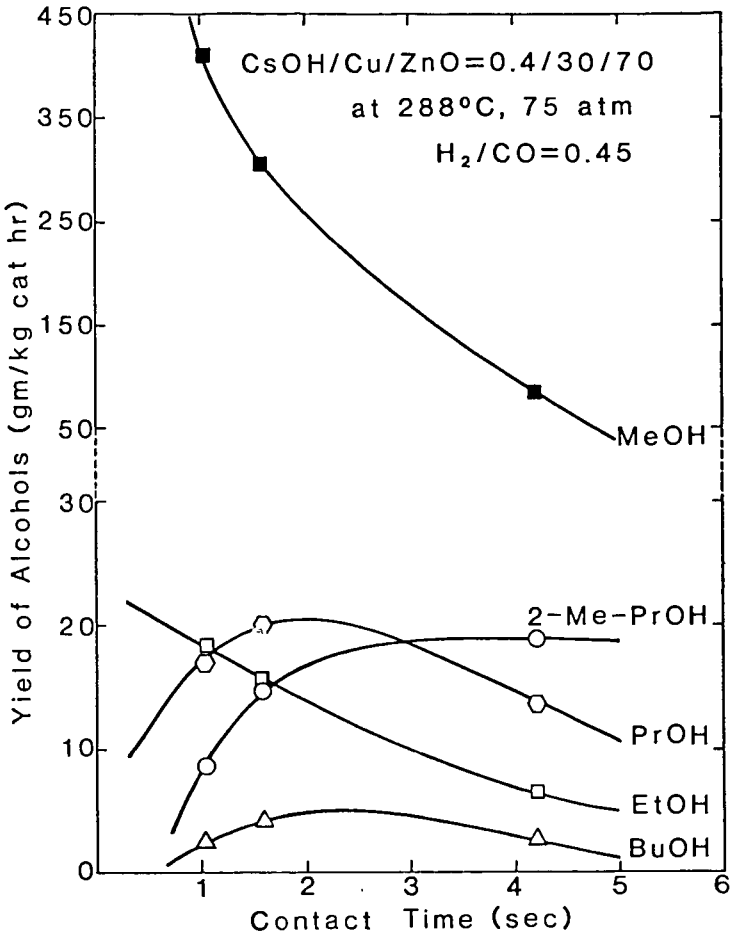

Figure 1. The contact time dependence of alcohol yields at 75 atm, 288°C, $H_2/CO = 0.45$ over the CsOH /Cu/ZnO = 0.4/30/70 catalyst.

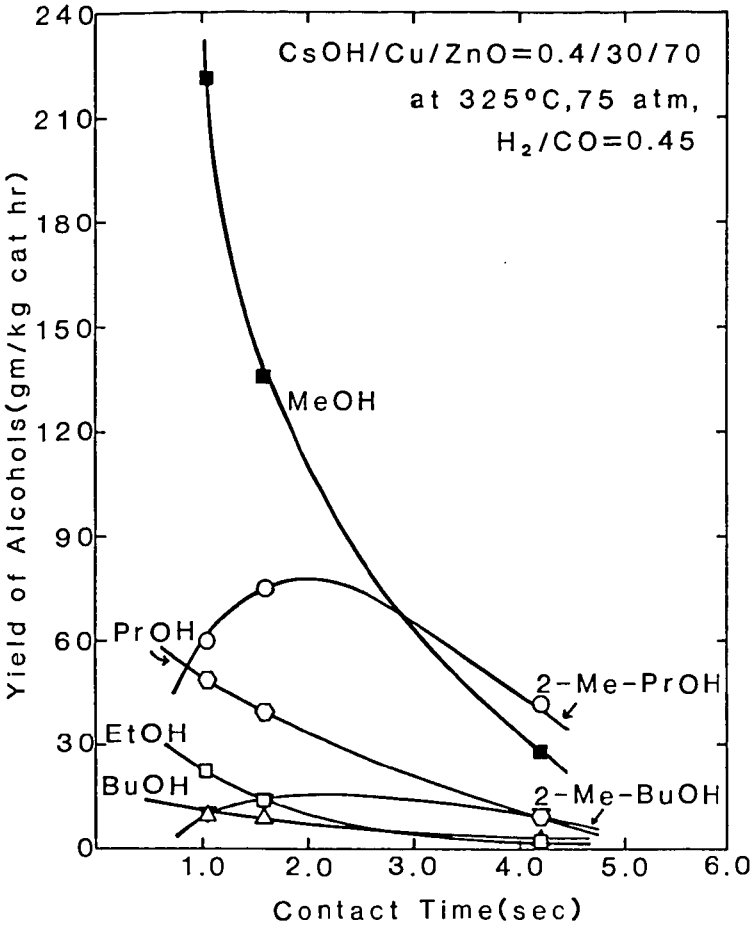

Figure 2. The contact time dependence of alcohol yields at 75 atm, 325°C, H_2/CO = 0.45 over the CsOH/Cu/ZnO = 0.4/30/70 catalyst.

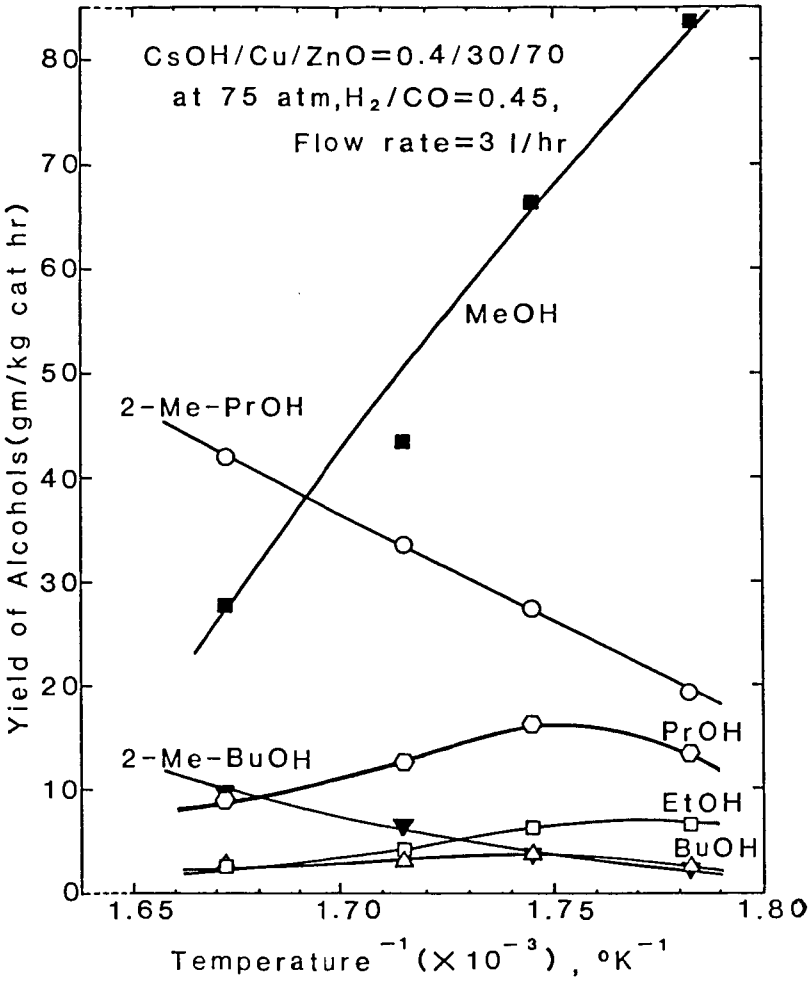

Figure 3. The temperature dependence of alcohol yields at 75 atm, H_2/CO = 0.45 at GHSV = 1200 over the CsOH /Cu/ZnO = 0.4/30/70 catalyst.

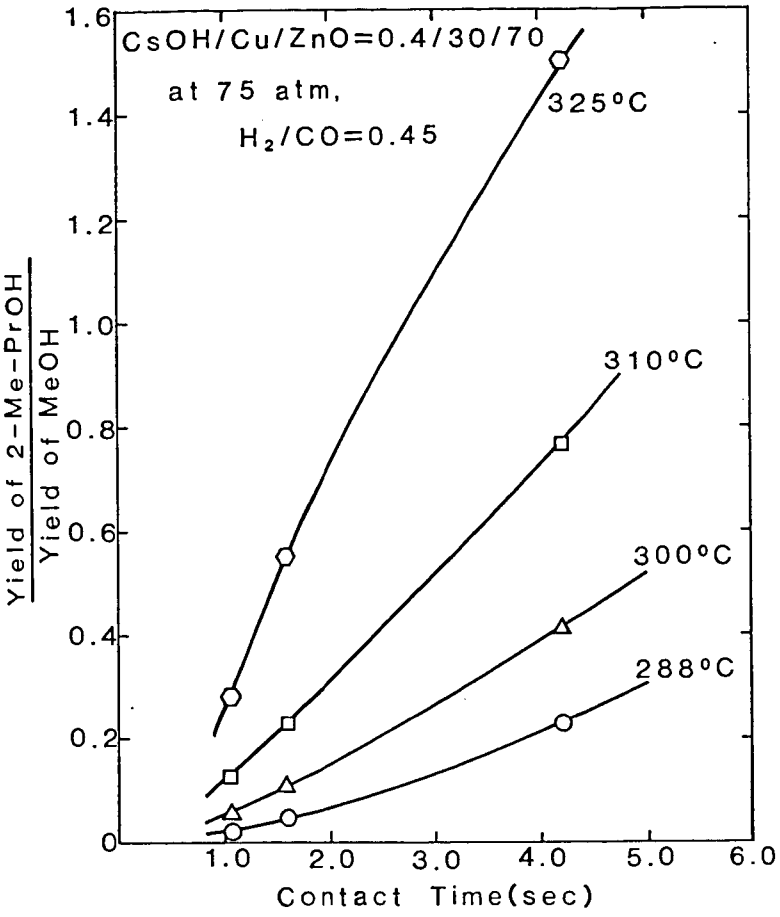

Figure 4. Selectivity to 2-methyl-1-propanol expressed as the ratio of yields of 2-methyl-1-propanol and methanol at 75 atm, H_2/CO = 0.45, as a function of contact time and temperature.